

**Ursolic acid and oleanolic acid as novel
therapeutic agents in breast cancer**

Candidate

Emhemed Mohamed Abukhattala

**Submitted in partial fulfillment for the degree
Philosophiae Doctor (PhD)**

Supervisor

Prof. M. de Kock

Dr. Sahar Abdul-Rasool

**Department Biosciences
University of the Western Cape**



November

2015

DECLARATION

I, the undersigned, declare that **Ursolic acid and oleanolic acid as novel therapeutic agents in breast cancer** is my own work and has not previously in its entirety, or in part, been submitted at any university. All the sources that I have used or quoted have been indicated and acknowledged by complete references.

Abukhattala E. M

Date



DEDICATION

I dedicate my dissertation work to my family and many friends. My uncle Muhamod, and my mother Fatma have never left my side and are very special.



ACKNOWLEDGEMENTS

This study was performed in the Department of Medical Biosciences at the University of the Western Cape and was funded by the Libyan Embassy.

Firstly, I'd like to give my sincere thanks to my supervisors, prof. M. de Kock and Dr. Sahar Abdul-Rasool, that they accepted me as their Ph.D. student without any hesitation when I presented my project research proposal for them. After that, they gave me so a lot advice, patiently supervising me, and always guiding me in the right direction. I've learned a lot from them, without them help I could not have finished my dissertation successfully.

Special thanks are also given to

Prof. Dr. Mervin Meyer, Department of Biotechnology, the University of the Western Cape, for using the western blot equipment.

Mr, Ronald Dreyer, Department of Immunology, Medical School, University of Cape Town for using the flow cytometer.

A special thanks to my family. Words cannot express how grateful I am to my mother-in law, father-in-law, my mother, and father for all of the sacrifices that you've made on my behalf. Your prayers for me was what sustained me thus far. I would also like to thank all of my friends who supported me in writing, and incented me to strive towards my goal. At the end I would like express appreciation to my family who was always my support in the moments when there was no one to answer my queries.

TABLE OF CONTENTS

DECLARATION.....	I
DEDICATION.....	II
ACKNOWLEDGEMENTS	III
TABLE OF CONTENTS	IV
ABSTRACT	X
List of abbreviation	XII
List of Figures.....	XVI
List of Tables	XX
1 Literature Review.....	1
1.1 Breast Cancer: An insight into incidence and survival.....	1
1.2 Cell cycle	4
1.2.1 Cyclins	6
1.3 Control of the cell cycle	8
1.3.1 Cell cycle progression through phosphorylation/dephosphorylation	8
1.3.2 Cell cycle checkpoints	8
1.3.2.1 DNA damage response pathways of G ₁ phase	9
1.3.2.2 The P53 response to DNA damage.....	9
1.3.2.3 The Cdc25A pathway.....	11
1.3.3 S phase DNA damage checkpoints.....	11
1.3.3.1 The intra-S phase checkpoint.....	11
1.3.3.2 The DNA replication (S/M) checkpoint.....	12
1.3.4 G ₂ (G ₂ /M) checkpoint.....	12
1.3.5 The spindle assembly checkpoint	13
1.4 Cell death	15

1.4.1	Apoptosis	15
1.4.1.1	The intrinsic pathway	16
1.4.1.2	The extrinsic pathway	18
1.4.1.3	Endoplasmic reticulum-mediated (ER) pathway	21
1.4.1.4	The caspase independent pathway(s).....	22
1.4.1.5	The role of Tumour suppressor p53 in apoptosis	23
1.4.2	Autophagy.....	23
1.4.2.1	Molecular regulation of autophagy (Figs. 1.6 and 1.7)	26
1.4.2.2	Signalling pathways regulating autophagy.....	29
1.4.2.2.1	Lkb1-Ampk-Autophagy-Axis	29
1.5	Crosstalk between autophagy and apoptosis in mammalian cells (Fig. 1.8).....	30
1.5.1	The role of Beclin-1 in apoptosis and autophagy	30
1.6	Terpenoids	32
1.6.1	Triterpenes.....	34
1.6.1.1	Uroslic Acid.....	34
1.6.1.2	Biosynthesis of uroslic acid	37
1.6.1.3	Oleanolic Acid.....	38
1.6.1.4	Biosynthesis of OA.....	41
1.7	Objectives	42
Chapter II.....		44
2	Materials and Methods.....	44
2.1	Materials.....	44
2.2	Cell Lines.....	46
2.3	Culture medium	47
2.4	Supplements	47
2.4.1	Oleanolic acid and ursolic acid.....	47
2.5	Cell treatments for experimental techniques.....	48
2.5.1	Estradiol proliferative assay.....	48
2.5.2	ER status of MCF-10A cells	48

2.5.3	Cell Viability	49
2.5.4	Morphological effects	50
2.5.4.1	Light microscopy: Haematoxylin and Eosin staining	50
2.5.5	Fluorescent microscopy	50
2.5.5.1	Apoptosis, autophagy and necrosis detection	50
2.5.5.2	Triple Fluorescence staining: Hoechst, Propidium iodide and Acridine Orange stain.	51
2.5.6	Apoptosis and necrosis detection using the Tali® Apoptosis Kit - Annexin V Alexa Fluor® 488 and Propidium Iodide.....	52
2.5.7	Determination of Reactive oxygen species (ROS) using the Cell ROX	53
2.5.8	Flow cytometry	54
2.5.8.1	Cell cycle progression	54
2.5.9	Western Blotting.....	55
2.5.9.1	Protein Extraction	55
2.5.9.2	Determination of protein concentration.....	55
2.5.9.3	SDS-PAGE and electrophoresis.....	55
2.5.9.4	Immuno-detection	56
2.5.10	Quantitative PCR.....	56
2.5.10.1	RNA extractions	56
2.5.10.2	Quality control of RNA samples.....	57
2.5.10.3	cDNA synthesis	57
2.5.10.4	qPCR analysis	57
2.6	Statistical analysis.....	58
 CHAPTER III.....		 59
3	Results	59
3.1	Determining the influence of 17β-Estradiol on cellular proliferation as a parameter of ERα antagonistic properties	59
3.1.1	ER status of MCF-10A cells	60
3.2	Cell viability studies.....	60

3.2.1	The effect of OA on the viability of MCF-7 and MCF-10A cells.....	60
3.2.2	The effect of UA on the viability of MCF-7 and MCF-10A cells.....	63
3.3	Morphological studies: Haematoxylin and Eosin (H&E) staining.....	65
3.3.1	The effect of OA on MCF-7 and MCF-10A cells after 6h.....	65
3.3.2	Mitotic index the effect of OA on MCF-7 and MCF-10A cells after 6h.	65
3.3.3	The effect of OA on MCF-7 and MCF-10A cells after 12h.....	68
3.3.4	Mitotic index: effect of OA on MCF-7 and MCF-10A cells after 12h.....	68
3.3.5	The effect of OA on MCF-7 and MCF-10A cells after 24h.....	71
3.3.6	Mitotic index: MCF-7 and MCF-10A cells after 24h OA exposure	71
3.3.7	The effect of OA on MCF-7 and MCF-10A cells after 48h	74
3.3.8	Mitotic index: MCF-7 and MCF-10A cells after 48h exposure to OA	74
3.3.9	The effect of OA on MCF-7 and MCF-10A cells after 72h	77
3.3.10	Mitotic index effect of OA on MCF-7 and MCF-10A cells after 72h.....	77
3.3.11	Effect OA: Comparison between MCF-7 and MCF-10A cell lines.....	80
3.3.12	The effect of UA on MCF-7 and MCF-10A cells after 6h	81
3.3.13	Mitotic index: the effect of UA on MCF-7 and MCF-10A cells after 6h.....	81
3.3.14	The effect of UA on MCF-7 and MCF-10A cells after 12h	84
3.3.15	Mitotic index: effect of UA on MCF-7 and MCF-10A cells after 12h.....	84
3.3.16	The effect of UA on MCF-7 and MCF-10A cells after 24h	87
3.3.17	Mitotic index: effect of UA on MCF-7 and MCF-10A cells after 24h.....	87
3.3.18	The effect of UA on MCF-7 and MCF-10A cells after 48h	90
3.3.19	Mitotic index: effect of UA on MCF-7 and MCF-10A cells after 48h.....	90
3.3.20	The effect of UA on MCF-7 and MCF-10A cells after 72h	93
3.3.21	Mitotic index: effect of UA on MCF-7 and MCF-10A cells after 72h.....	93
3.3.22	Mitotic index: effect of UA on MCF-7 and MCF-10A cells.....	96
3.3.23	Contrasting proliferative effects between MCF-7 and MCF-10A.....	96
3.4	Hoechst 33342 staining (HOC)	99
3.4.1	Effect of OA and UA on MCF-7 and MCF-10A cells after 6h	99
3.4.2	Effect of OA and UA on MCF-7 and MCF-10A cells after 12h	101
3.4.3	Effect of OA and UA on MCF-7 and MCF-10A cells after 24h	103
3.4.4	Effect of OA and UA on MCF-7 and MCF-10A cells after 48h	105
3.4.5	Effect of OA and UA on MCF-7 and MCF-10A cells after 72h	107
3.5	Apoptosis, autophagy and necrosis detection using triple staining: Hoechst (HOC), acridine orange (AO) and propidium iodide (PI) staining.....	109

3.5.1	The effect of OA and UA on apoptosis, autophagy and necrosis induction in MCF-7 and MCF-10A cells after 6h.....	109
3.5.2	The effect of OA and UA on apoptosis, autophagy and induction in MCF-7 and MCF-10A cells after 12h.....	112
3.5.3	The effect of OA and UA on apoptosis, autophagy and induction in MCF-7 and MCF-10A cells after 24h.....	114
3.5.4	The effect of OA and UA on apoptosis, autophagy and induction in MCF-7 and MCF-10A cells after 48h.....	116
3.5.5	The effect of OA and UA on apoptosis, autophagy and induction in MCF-7 and MCF-10A cells after 72h.....	118
3.6	Quantification of apoptosis using the Tali® Image Cytometer	120
3.6.1	The effect of OA and UA after 6h on apoptosis induction in MCF-7 and MCF-10A cells as quantified by the Tali® Image Cytometer	120
3.6.2	The effect of OA and UA after 12h on apoptosis induction in MCF-7 and MCF-10A cells as quantified using the Tali® Image Cytometer.....	121
3.6.3	The effect of OA and UA after 24h on apoptosis induction in MCF-7 and MCF-10A cells as quantified by the Tali® Image Cytometer	123
3.6.4	The effect of OA and UA after 48h on apoptosis induction in MCF-7 and MCF-10A cells as quantified by the Tali® Image Cytometer	124
3.6.5	The effect of OA and UA after 72h on apoptosis induction in MCF-7 and MCF-10A cells as quantified by the Tali® Image Cytometer	125
3.7	Cell cycle progression	127
3.7.1	Effect of OA on MCF-7 and MCF-10A cell cycle progression	127
3.7.2	Effect of UA on MCF-7 and MCF-10A cell cycle progression	131
3.8	Reactive oxygen species (ROS)	135
3.8.1	Effects of OA on ROS in MCF-7 cells after 6, 12, 24, 48 and 72h	135
3.8.2	Effects of OA on ROS in MCF-10A cells after 6, 12, 24, 48 and 72h.....	136
3.8.3	Effects of UA on ROS in MCF-7 cells after 6, 12, 24, 48 and 72h	137
3.8.4	Effects of UA on ROS in MCF-10A cells after 6, 12, 24, 48 and 72h.....	138
3.9	Western blot	140
3.9.1	LC3 and Beclin-1 expression in MCF-7 and MCF-10A after OA and UA exposure for 6h.	140
3.9.2	LC3 and Beclin-1 expression in MCF-7 and MCF-10A after OA and UA exposure for 12h	141
3.9.3	LC3 and Beclin-1 expression in MCF-7 and MCF-10A affected by OA and UA for 24h	141

3.9.4	LC3 and Beclin-1 expression in MCF-7 and MCF-10A affected by OA and UA for 28h	142
3.9.5	LC3 and Beclin-1 expression in MCF-7 and MCF-10A after OA and UA for 72h	143
3.10	Analysis of gene expression	144
Chapter IV.....		148
4	Discussion.....	148
4.1	Proliferation studies.....	151
4.2	Morphological studies.....	154
4.3	Apoptosis and cell death detection	156
4.4	OA and UA effect on cell cycle progression in MCF-7 and MCF-10A cells.....	158
4.5	Autophagy detection.....	163
4.6	QPCR	166
4.7	Conclusion.....	167
5	Reference	170
6	Appendix I (WESTERN BLOT RECIPES)	192
7	Appendix II (QPCR).....	194



ABSTRACT

Breast cancer is one of the most common cancers among women in South Africa and the second leading cause of cancer death after lung cancer. According to the American Cancer Society 2015, women have a 12% chance of developing invasive breast cancer and a 3% chance of dying from it. Despite the wide variety of breast cancers e.g. lobular carcinoma in situ (LCIS) and ductal carcinoma in situ (DCIS), many share the same etiology and target tissue. Estrogen related carcinogenesis with regard to breast cancer typically results from the activation of distinct signalling pathways. These pathways are not mutually exclusive and are often constituted by receptor mediated stimulation of cell proliferation caused by specific transcriptional gene activation, reactive oxygen species (ROS) formation causing DNA damage and consequently mutations. The molecular pathways that cause drug resistance are not fully understood and the search continues to find novel targets for treatment. The effects of non-toxic triterpenes, oleanolic acid and ursolic acid and the role of autophagy and apoptosis as mechanisms to overcome drug resistance in breast cancer were studied in vitro in MCF-7 breast cancer cells and MCF10A breast cells. In this study the first aim was to establish the influence of OA and UA on cell growth and to see if opposing proliferation patterns could be observed between the presumably ER α negative (ER α / β -/+) MCF-10A and ER α positive (ER α / β +/+) MCF-7 cells. This was followed by morphology studies to establish the possible presence of cytotoxicity and examination of molecular pathways contributing to the anti-cancerous properties of UA and OA and their validity as therapeutic agents. The MCF-7 breast cancer cell line and the immortalized normal mammary cell line, MCF-10A were treated with different concentrations of UA and OA for 6hrs, 12hrs, 24hrs, 48hrs, and 72hrs respectively. Cell morphology was studied in hematoxylin and eosin as well as Hoechst and acridine orange stained cells and viability was measured using crystal violet staining. Molecular techniques employed included the Tali® Apoptosis - and the cellROX assays, flow cytometry and western blotting. Morphological, viability and apoptotic studies have shown that at their lowest concentration, both UA and OA have anti-proliferative and apoptotic effects on MCF-7 and to a lesser extent on MCF-10A. Flow cytometric analysis of treated cells has demonstrated cell arrest in the S- and G2/M phase. The

MCF-7 and MCF-10A cells growth inhibition effect may be due to increased autophagy and apoptosis as an alternative to decreased proliferation in MCF-7 cells. This possibility should be evaluated in further studies. The results showed that UA was more effective OA in decreasing cell numbers and it may be applied as treatment for breast cancer. Our observation has shown the treatment with OA and UA increased cell death in MCF-7 cells.

The opposing proliferation patterns observed between the presumably ER α negative (ER α/β -/+) MCF-10A and ER α positive (ER α/β +/+) MCF-7 cells could possibly be ascribed to ER β forming homodimers that may facilitate proliferation, whereas ER α/β heterodimers (expressed in 59% of breast cancers) are frequently associated with the ER α antagonising actions of ER β .

The results indicate a trend towards biphasic and anti- proliferative effects of the reactants in breast cancer cells which may contribute towards the development of anti-cancer therapies. However, further work is must be done to identify the OA and UA mechanism(s) responsible for anticancer activity.

Key words: Breast cancer, OA, UA, MCF-7, MCF-10A, autophagy, apoptosis

List of abbreviation

°C	Degrees celsius/centigrade
µM	Micrometre
53 kDa	53 kilo Dalton
AIF	Apoptosis initiation factor
AKT	Protein Kinase B (PKB)
AMP/ATP	Adenosine monophosphate/ Adenosine-5'-triphosphate
AMPK	AMP-activated protein kinase
AO	Acridine orange
APAF-1	apoptotic protease activating factor-1
APC	Anphase-promoting complex
APS	Ammonium persulphate
Atg12	Autophagy-related protein 12
Atg7	Autophagy Related 7
Atg9/mAtg9	Two transmembrane proteins
Atgs	Autophagy-related genes
ATM	Ataxia telangiectasia mutated
ATR	ATM and rad 3-related
B 16F-10 cells	Melanoma cell lines
Bax, Puma, Noxa, and Bid	Bcl-2 family members
BC	Breast carcinoma
Bcl-2 Bcl-XL	Apoptotic factor
BCL-2 family	B-cell lymphoma 2
Bcl-XL and Bcl2 proteins	Atg18/WIPI-1 and VMP1
bcl-xl, bcl-w, bfl-1, and mcl-1	Anti-apoptotic BCL-2 family
BH1, BH2, BH3 and BH4	BH domains
BH3	The Bcl-2 homology domain 3-proteins
Bid	A BH3 domain-only death agonist protein
C5H8	Derivatives of isoprene, a five- carbon acyclic chain
CaCl₂	Calcium chloride
CAMKKβ	Calmodulin-dependent protein kinase kinase β
CARDs	Caspase activation and recruitment domains
Cdc25A	Cell division cycle 25A
Cdc25B	Cell division cycle 25B
Cdc25C	Cell division cycle 25C
CDK	Cyclin-dependent kinase
CDK4	Cyclin-dependent kinase 4
CDKI	CDKI inhibitor
CDKs	Cyclin dependent kinase
CH₃COOH	Acetic acid
Chk1	Checkpoint kinase 1
Chk2	Checkpoint kinase 2
cIAP-1 and cIAP-2	Cellular inhibitor of apoptosis protein 1 and 2
CICD	Caspase independent cell death
CIP	Cdk inhibitor protein
CKIs	Cyclin dependent kinase inhibitors
c-Myc	Avian myelocytomatosis virus oncogene cellular homolog
CVS	Crystal violet stain

Cys572	CYSTINE 572
Cyt C	Cytochrome C
Cytokines IL-6	Cytokines Interleukin 6
DAPK	Death-associated protein kinase
DCIS	Ductal carcinoma in situ
DcR2	Death cytoplasmic domain
DISC	Death Inducing Signaling Complex
DMAPP	Dimethylallyl pyrophosphate
DMEM	Dulbecco's modified eagles medium
DMSO	Dimethyl sulphoxide
DNA	Deoxyribonucleic acid
dNTP mix	A solution of high purity deoxynucleotide triphosphates (dATP, dGTP, dCTP, dTTP)
DR	Death receptors
DR4 and DR5	Death receptor 4 and 5
DSBs	Double-strand DNA breaks
DU-145 cells	Prostate tumor cell lines
E2F 1	E2F transcription factor 1
EGF	Epidermal growth factor
EndoG	Endonuclease G
ER	Endoplasmic reticulum
EtOH	Ethanol
FADD	Fas-associated death domain
Fas	CD95 or APO-1
FasL	Fas ligand
FBS	Fetal bovine serum
FLIP	FLICE (Caspase-8) inhibitory protein
GPP	Geranyl pyrophosphate
h	hour(s)
H&E	Haematoxylin and eosin
H2ax	H2A histone family, member X
HepG2 Hepatoma cells	Hepatocellular carcinoma hepg2 cell line
HIF-1α	Hypoxia inducible factor 1 α
HL 60 cells	Human promyelocytic leukemia cells
HOC 33342	Hoechst 33342
HT-29 cells	Human colon cancer cell line
HtrA2 or Omi	High temperature requirement A2
IAP	Inhibitor of apoptosis
INK4	Inhibitor of CDK4
IPP	Isopentyl diphosphate
IPP and DMAPP	The isomer dimethylallyl diphosphate
IR	Ionizing radiation
KCL	Potassium chloride
KIP	kinase inhibitor protein
LAMP-2A	Lysosomal associated membrane type 2A
LC3	Light chain 3
LCIS	lobular carcinoma in situ and
M	Mitosis
M4Beu cells	Melanoma cells
Mapk	Mitogen-activated protein kinase (MAPK)

MAPK	Mitogen activated protein kinase
M-CDK	Mitotic Cyclin-dependent kinase
MCF-10 cell	MCF-10A non-tumorigenic human breast epithelial cells
MCF-7	MCF-7 human breast cancer cell line
MCM2, 3 and 7	Mini-chromosome maintenance proteins 2, 3 and 7
MDM2	Mouse double minute 2 homolog
MDMX	Mammalian cells also express an MDM2 homolog
MEOH	Methanol
MEP	2C-methyl-D-erythritol 4-phosphate
min	Minutes
MOMP	mitochondrial outer membrane permeabilization
mTOR	Mammalian Target of Rapamycin
MTORC1	Mechanistic TOR complex 1
MVA	The Mevalonic acid
Myt1	Protein kinase, membrane associated tyrosine/threonine 1)
NaCl	Sodium chloride
NF-κB	Nuclear factor kappa-light-chain-enhancer of activated B cells
NOXA	Damage protein, a pro-apoptotic BH3-containing protein
OA	Oleanolic acid
P110	Phosphatase 110
P15ink4b	Cyclin-dependent kinase 4 inhibitor B
P16ink4a	Tumor suppressor protein functions as an inhibitor of CDK4 and CDK6
P18ink4c	Tumor suppressor protein functions as an inhibitor of CDK4 family
P21, Cip1	CDKN1A cyclin-dependent kinase inhibitor 1A
P53	Tumour suppressor gene
p53AIP	P53-regulated apoptosis-inducing protein 1
p57, Kip2	Cyclin-dependent kinase inhibitor 1C
P62/SQSTM1	The p62 protein, also called sequestosome 1
P75NTR	P75 neurotrophin receptor
PAS	Phagophore assembly site
PBS	Phosphate buffer saline
PCNA	Proliferating-cell nuclear antigen
PE	Phosphatidylethanolamine
PI	Propidium iodide
PI3K	Phosphoinositide-3 kinase/ Phosphatidylinositol 3-kinase
PIK3C3/VPS34, BECN1	Mammalian homolog of yeast Vps30
PIK3R4/p150	Homolog of Vps15
PP1	Protein phosphatase 1
PP2a	Protein phosphatase2a
Primer dimer	A secondary structure resulting from the covalent bond between a primer pair. This usually occurs from poor primer design or when no template is present in a reaction.
PtdIns3K/Vps34 complex I	Class III phosphatidylinositol 3-kinase
PUMA	P53 upregulated modulator of apoptosis
R2 value	Another critical parameter to evaluating PCR efficiency is R2, which is a statistical term that indicates how good one value is at predicting another. When R2 is 1, the value of Y (Ct) can be used to accurately predict the value of X. If R2 is 0, the value of X cannot be predicted from the value of Y. An R2 value >0.99 provides good confidence in correlating two values.

RB	Retinoblastoma
RFBs	Replication fork barriers
Rheb	Ras Homolog Enriched in Brain
RIP	Receptor interacting protein
RNA	Ribonucleic acid
RNase	Ribonuclease
ROS	Reactive oxygen species
S367	Serine 367
SDS	Sodium Dodecyl Sulfate
ser/thr	Serine/threonine
Slope	To properly evaluate PCR efficiency, a minimum of 3 replicates and a minimum of 5 logs of template concentration are necessary. To accurately determine the efficiency of a PCR reaction, a 5-log dilution series must be performed. A slope of $-3.3 \pm 10\%$ reflects an efficiency of $100\% \pm 10\%$. A PCR reaction with lower efficiency will have lower sensitivity.
smARF	Small mitochondrial isoform of this protein
SNG-II cells	Uterine endometrial cancer cell line
SQSTM1	Sequestosome-1
The Caco-2 cell line	Caco-2 colon cancer cells
TNF	Tumor necrosis factor
TNF family	Tumor necrosis factor family
TNFR	Tumor necrosis factor receptor
TOR	Target of rapamycin
TRADD	TNF receptor-1-associated death domain protein
TRAF	TNF receptor-associated factor
TRAIL	TNF-related apoptosis-inducing ligand
TRAIL-R	TNF-related apoptosis inducing ligand receptor
TSC1/TSC2	Tuberous Sclerosis Complex1/2
Tyr-15 and 14	Tyrosin-15 and 14
UA	Ursolic acid
ULK1/2	The mammalian ULK1/2 complex contains a component, C12orf44
UPR	Unfolded protein response
UV	Ultraviolet
UVRAG	UV radiation resistance-associated gene
Vps38	Vacuolar protein sorting 38
Wee1	WEE1 G2 checkpoint kinase
XYL	Xylene

List of Figures

Figure 1.1: Progression of the cell cycle is regulated by cyclin-cyclin-dependent kinase (CDK) complexes which are primary targets of mitogenic signals	7
Figure 1.2: Control of late mitotic events by the APC M-Cdk activity promotes the events of early mitosis, resulting in the metaphase alignment of sister chromatin on the spindle	14
Figure 1.3: Three pathways of cell death.....	15
Figure 1.4: Overview of the intrinsic and extrinsic apoptotic pathways.....	20
Figure 1.5: Apoptosis mediated by the unfolded protein response signaling.....	21
Figure 1.6: Stages of autophagy.....	25
Figure 1.7: Regulation ULK1/2 complex in mammals.....	27
Figure 1.8: Crosstalk between autophagy and apoptosis in mammalian cells.....	31
Figure 1.9: Simplified scheme of the origin of the diverse biosynthetic plant terpene classes.....	33
Figure 1.10: The biosynthesis of terpenes from isopentyl diphosphate (IPP) and dimethylallyl diphosphate (DMAPP) to form geranyl pyrophosphate (GPP).....	34
Figure 1.11: Molecular structure of UA.....	35
Figure 1.12: Biosynthesis of dammarenyl cation (I), oleanyl cation, lupenyl cation and lupeol (1).....	37
Figure 1.13: Biosynthesis of ursolic acid (4) and oleanolic acid (5) from oleanyl cation.....	38
Figure 1.14: Molecular structure of OA.....	39
Figure 1.15: OA biosynthetic pathway. BAS = b-amyrin synthase, CAS = cycloartenol synthase, IPP = isopentenyl pyrophosphate.....	42
Figure 3.1: SDS-PAGE gel of MCF-10A whole cell lysates after combination treatment.....	60
Figure 3.2: Cell viability percentage of A: MCF-7 and B: MCF-10A cells as determined by crystal violet assay in 96-well plates following 6, 12, 24, 48 and 72-hour exposure to OA.....	62
Figure 3.3: Cell viability percentage of (A); MCF-7 and (B); MCF-10A cells as determined by crystal violet assay in 96-well plates following 6, 12, 24, 48 and 72-hour exposure to UA	64
Figure 3.4: MCF-7 and MCF-10A cell morphology. MCF-7 (A, B, C, D, E) and MCF-10A (F, G, H, I, J) cells were treated with OA for 6h and stained with haematoxylin-eosin.....	66
Figure 3.5: MCF-7: quantification of the effects of OA on dividing and pycnotic and apoptotic cells after 6h exposure.....	67
Figure 3.6: MCF-10A: quantification of the effects of OA on dividing pycnotic and apoptotic cells after 6h exposure.....	67
Figure 3.7: Haematoxylin and eosin stained. MCF-7 (A, B, C, D, E) and MCF-10A (F, G, H, I, J) cells were treated with OA after 12h is shown.....	69
Figure 3.8: MCF-7: quantification of the effects of OA on dividing pycnotic and apoptotic cells after 12h exposure	70
Figure 3.9: MCF-10A quantification of the effects of OA on dividing pycnotic and apoptotic cells after 12h exposure.....	70
Figure 3.10: MCF-7 and MCF-10A cell morphology. MCF-7 (A, B, C, D, E) and MC-F10A (F, G, H, I, J) cells were treated with OA after 24h and stained with haematoxylin and eosin.....	72
Figure 3.11: The quantification of the effects of OA on dividing pycnotic and apoptotic MCF-7 cells after 24h exposure.....	73

Figure 3.12: The MCF-7 quantification of the effects of OA on dividing pycnotic and apoptotic MCF-10A cells after 24h exposure.....	73
Figure 3.13: Shows H and E stained. MCF-7 (A, B, C, D, E) and MCF-10A (F, G, H, I, J) cells were treated with OA after 48h using haematoxylin-eosin staining.....	75
Figure 3.14: The quantification of the effects of OA on dividing pycnotic and apoptotic MCF-7 cells after 48h exposure.....	76
Figure 3.15: The quantification of the effects of OA on dividing pycnotic and apoptotic MCF-10A cells after 48h exposure.....	76
Figure 3.16: MCF-7 (A, B, C, D, E) and MCF-10A (F, G, H, I, J) cells were treated with OA after 72h and stained with haematoxylin eosin are shown.....	78
Figure 3.17: The quantification of the effects of OA on dividing, pycnotic and apoptotic MCF-7 cells after 72h exposure.....	79
Figure 3.18: The quantification of the effects of OA on dividing, pycnotic and apoptotic MCF-10A cells after 72h exposure.....	79
Figure 3.19: MCF-7 and MCF-10A cell morphology. MCF-7 (A, B, C, D, E) and MCF-10A (F, G, H, I, J) cells were treated with UA after 6h using haematoxylin-eosin staining.....	82
Figure 3.20: The quantification of the effects of UA on dividing pycnotic and apoptotic MCF-7 cells after 6h exposure.....	83
Figure 3.21: The quantification of the effects of UA on dividing pycnotic and apoptotic MCF-10A cells after 6h exposure.....	83
Figure 3.22: MCF-7 and MCF-10A cell morphology. MCF-7 (A, B, C, D, E) and MCF-10A (F, G, H, I, J) cells were treated with UA after 12h using haematoxylin-eosin staining.....	85
Figure 3.23: The MCF-7 quantification of the effects of UA on dividing and pycnotic and apoptotic cells after 12h exposure.....	86
Figure 3.24: The MCF-10A quantification of the effects of UA on dividing and pycnotic and apoptotic cells after 12h exposure.....	86
Figure 3.25: MCF-7 and MCF-10A cell morphology. MCF-7 (A, B, C, D, E) and MCF-10A (F, G, H, I, J) cells were treated with UA after 24h using haematoxylin-eosin staining.....	88
Figure 3.26: The quantification of the effects of UA on dividing pycnotic and apoptotic MCF-7 cells after 24h exposure.....	89
Figure 3.27: The quantification of the effects of UA on dividing pycnotic and apoptotic MCF-7 cells after 24h exposure.....	89
Figure 3.28: MCF-7 and MCF-10A cell morphology. MCF-7 (A, B, C, D, E) and MCF-10A (F, G, H, I, J) cells were treated with UA after 48h using haematoxylin-eosin staining.....	91
Figure 3.29: The MCF-7 quantification of the effects of UA on dividing and pycnotic and apoptotic cells after 48h exposure.....	92
Figure 3.30: The MCF-10A quantification of the effects of UA on dividing and pycnotic and apoptotic cells after 48h exposure.....	92
Figure 3.31: MCF-7 and MCF-10A cell morphology. MCF-7 (A, B, C, D, and E) and MCF-10A (F, G, H, P, and Q) cells were treated with UA after 72 h stained with haematoxylin-eosin.....	94
Figure 3.32: The MCF-7 quantification of the effects of UA on dividing and pycnotic and apoptotic cells after 72h exposure.....	95
Figure 3.33: The MCF-10A quantification of the effects of UA on dividing and pycnotic and apoptotic cells after 72h exposure.....	95
Figure 3.34: Show the percentage mitotic – and dead cells in MCF-7 and MCF-10A cells exposed to 10µg/ml for the different time periods.....	97

Figure 3.35: Show the percentage mitotic – and dead cells in MCF-7 and MCF-10A cells exposed to 20µg/ml for the different time periods.....	97
Figure 3.36: Show the percentage mitotic – and dead cells in MCF-7 and MCF-10A cells exposed to 50µg/ml for the different time periods.....	98
Figure 3.37: Show the percentage mitotic – and dead cells in MCF-7 and MCF-10A cells exposed to 100µg/ml for the different time periods.....	98
Figure 3.38: Show MCF-7 (A, B, C, D, and E) and MCF-10A (F, G, H, I, and J) cells treated with OA and MCF-7 (K, L, M, N, and O) and MCF-10A (P, Q, R, S, and T) cells treated with UA for 6h and stained with Hoechst.....	100
Figure 3.39: Show MCF-7 (A, B, C, D, and E) and MCF-10A (F, G, H, I, and J) cells treated with OA and MCF-7 (K, L, M, N, and O) and MCF-10A (P, Q, R, S, and T) cells treated with UA for 12h and stained with Hoechst.....	102
Figure 3.40: Show MCF-7 (A, B, C, D, and E) and MCF-10A (F, G, H, I, and P) cells treated with OA and MCF-7 (K, L, M, N, and O) and MCF-10A (P, Q, R, S, and T) cells treated with UA for 12h and stained with Hoechst.....	104
Figure 3.41: Show MCF-7 (A, B, C, D, and E) and MCF-10A (F, G, H, I, and J) cells treated with OA and MCF-7 (K, L, M, N, and O) and MCF-10A (P, Q, R, S, and T) cells treated with UA for 48h and stained with Hoechst.....	106
Figure 3.42: show MCF-7 (A, B, C, D, and E) and MCF-10A (F, G, H, I, and J) cells treated with OA and MCF-7 (K, L, M, N, and O) and MCF-10A (P, Q, R, S, and T) cells treated with UA for 72h and stained with Hoechst.....	108
Figure 3.43: MCF-7 and MCF-10A cell morphology. MCF-7 (A, B, C, D and E) and MCF-10A (F, G, H, I and J) cells were treated with OA and MCF-7 (K, L, M, N and O) and MCF-10A (P, Q, R, S and T), cells treated with UA for 6h.....	111
Figure 3.44: MCF-7 and MCF-10A cell morphology. MCF-7 (A, B, C, D and E) and MCF-10A (F, G, H, I, J) cells were treated with OA and MCF-7 (K, L, M, N and O) and MCF-10A (P, Q, R, S and T), cells treated with UA for 12h.....	113
Figure 3.45: MCF-7 and MCF-10A cell morphology. MCF-7 (A, B, C, D and E) and MCF-10A (F, G, H, I and J) cells were treated with OA and MCF-7 (K, L, M, N and O) and MCF-10A (P, Q, R, S and T), cells treated with UA for 24h.....	115
Figure 3.46: MCF-7 and MCF-10A cell morphology. MCF-7 (A, B, C, D and E) and MCF-10A (F, G, H, I and J) cells were treated with OA and MCF-7 (K, L, M, N and O) and MCF-10A (P, Q, R, S and T), cells treated with UA for 48h.....	117
Figure 3.47: MCF-7 and MCF-10A cell morphology. MCF-7 (A, B, C, D and E) and MCF-10A (F, G, H, I and J) cells were treated with OA and MCF-7 (K, L, M, N and O) and MCF-10A (P, Q, R, S and T), cells treated with UA for 72h.....	119
Figure 3.48: Comparison of live, dead and apoptotic cells as analyzed by the Tali® Image Cytometer after exposure to OA and UA for 6h.....	121
Figure 3.49: Comparison of live, dead and apoptotic cells as analyzed by the Tali® Image Cytometer after exposure to OA and UA for 12h.....	122
Figure 3.50: Comparison of live, dead and apoptotic cells as analysed by the Tali® Image Cytometer after exposure to OA and UA for 24h.....	124
Figure 3.51: Comparison of live, dead and apoptotic cells as analysed by the Tali® Image Cytometer after exposure to OA and UA for 48h.....	125
Figure 3.52: Comparison of live, dead and apoptotic cells as analysed by the Tali® Image Cytometer after exposure to OA and UA for 72h.....	126
Figure 3.53: Beclin-1 and LC3 Expression in MCF-7 and (B): MCF-10A in cells exposed OA and UA for 6h.....	140

Figure 3.54: Beclin-1 and LC3 expression in MCF-7 and MCF-10A cells following OA and UA exposure for 12h	141
Figure 3.55: Beclin-1 and LC3 expression in MCF-7 and MCF-10A cells following OA and UA exposure for 24h	142
Figure 3.56: Beclin-1 and LC3 expression in MCF-7 and MCF-10A cells after OA and UA exposure for 48h.....	143
Figure 3.57: Beclin-1 and LC3 expression in MCF-7 and MCF-10A cells following OA and UA exposure for 72h	144
Figure 3.58: The relative quantity of ATG6 in MCF-7 cell lines treated with various concentrations of OA	145
Figure 3.59: The relative quantity of ATG6 in MCF-7 cell lines treated with various concentrations of UA	146
Figure 3.60: The relative quantity of ATG6 in MCF-10A cell lines treated with various concentrations of OA.	146
Figure 3.61: The relative quantity of ATG6 in MCF-10A cell lines treated with various concentrations of UA.	147



List of Tables

Table 1.1: The basic molecular structure of terpenes	32
Table 2.1: cDNA synthesis cycling parameters	57
Table 2.2: qPCR cycling parameters.....	58
Table 3.1: The quantification of the effects of 17 β -Estradiol on the proliferation of MCF-7 and MCF-10A cells after 48- and 72 hours. Significant differences between treated and control samples are indicated by *P \leq 0.05 compared to respective controls (Two-way ANOVA followed by Tukey's multiple comparisons test).	59
Table 3.2: Shows the percentage distribution for control and OA treated MCF-7 cells. As the OA concentration increased, the percentage of cells that arrested in the phase of the cell cycle also increases.	129
Table 3.2: Shows the percentage distribution for control and OA treated on MCF-10A cells. As the OA concentration increased, the percent of cells that arrested in the S phase of the cell cycle also increases.	130
Table 3.3: Shows the percentage distribution for control and UA treated MCF-7 cells. As the UA concentration increased, the percentage of cells that arrested in the S phase of the cell cycle also increased.	133
Table 3.4: Shows the percentage distribution for control and UA treated on MCF-10A cells. As the UA concentration increased, the percentage of cells that arrested in the S phase of the cell cycle also increased.	134
Table 3.5: Show the percentage oxidative stress in MCF-7 cells treated with OA concentrations (10, 20, 50, and 100 μ g/ml) respectively, and at different times of exposure. A consecutive increase in the percentage of cells that stained positive with CellRox orange after exposure to OA, is seen.	136
Table 3.6: Show MCF-10A cells ROS levels induced by OA (10, 20, 50, and 100 μ g/ml) for the different times of exposure. A dosed dependent increase in ROS is observed for all the different tome periods.	137
Table 3.7: Show oxidative stress in MCF-7 cells treated with UA concentrations, 10, 20, 50, and 100 μ g/ml respectively, and at different time of exposure. A consecutive increase in the % of cells that stained positive with CellRox orange was observed after exposure to increasing concentrations of UA, excluding 10 μ g/ml. ROS is shown as percentage.	138
Table 3.8: Show oxidative stress in MCF-10A cells treated with UA after 10, 20, 50, and 100 μ g/ml respectively for 6-, 12-, 24-, 48-, and 72 hours. A dose dependent increase in the % of cells that stained positive with CellRox orange after exposure to increasing concentration of UA was seen. ROS is shown as percentage.....	139
Table 3.9: Primer efficiency (E), slope and R ² value for each primer pair as calculated using qbase software. An E value of 2 indicates 100% primer efficiency and an R ² value of 0.99 indicates a good correlation between Ct and sample concentration.	145

Chapter I

1 Literature Review

1.1 Breast Cancer: An insight into incidence and survival

Breast cancer is the most frequent type of cancer and the leading cause of death among females (Li et al., 2014) accounting for 23% (1.38 million) of the total new cancer cases and 14% (458,400) of the total cancer deaths in 2008. The life-time risk of breast cancer among American women continues to remain at an astonishing one in eight, and the breast cancer incidence (26%) and mortality rate (15%) remain very high when compared to other cancers in women. Many factors are believed to contribute to this high burden of breast cancer, including lifestyle, environmental, genetic, and biological factors (Cummings et al., 2009; McTiernan et al., 2008).

It is a fact that breast cancer is one of the most common cancers in women in both developed and undeveloped countries. The American Cancer Society has shown that in 2011 an estimated 230,480 new cases of invasive breast cancer have been diagnosed among women, as well as an estimated 57,650 additional cases of in situ breast cancer (Jemal et al. 2011; DeSantis et al. 2011). The previous report had indicated that approximately 39,520 women are expected to die from breast cancer and that only lung cancer accounts for more cancer deaths in women.

Despite the fact that breast cancer is a recognized disease of the developed world, and more frequently observed in industrialized western countries, about 50% of breast cancer cases and as many as 58% of deaths arise in less developed countries (Ferlay et al., 2010). A report has stated that worldwide almost 460,000 people died of the disease in 2008 and about half of these breast cancer cases and 60% of the deaths had occurred in economically less developing countries (Jemal et al., 2011).

According to the World Cancer Report 2000, the incidence of cancer at any localization would increase by 50 % by the year 2020, in which there would be 15

million new cases. In 2000, malignant tumors were the cause of 12 % of nearly 56 million deaths that were produced throughout the world; in many countries, more than one-quarter of these deaths were attributable to breast cancer. In that same year, there were 6.2 million cancer-related deaths. Considering the fact that breast cancer incidence is already staggering, this increment means that breast cancer will continue to be a global threat in the future.

Moreover, the disease is no more a “female illness”, in 2011, about 2,140 cases of breast cancer were expected to occur among men, accounting for about 1% of all breast cancers, and approximately 450 men would die from breast cancer (DeSantis et al., 2011). This low percentage might be attributed to the fact that men are not routinely screened for breast cancer, thus the diagnosis is often delayed. The most common clinical manifestation of male breast cancer is a painless, firm, subareolar breast mass. Once detected, any suspicious breast mass in a male is subjected to a diagnostic biopsy and if a malignancy is diagnosed, the common treatment is mastectomy with assessment of the axillary nodes.

Breast cancer survival rates differ seriously worldwide. It is estimated that survival rates range from 80% or over in North America, Sweden and Japan to around 60% in middle-income countries and below 40% in low-income countries (Coleman et al., 2008). On the whole, survival rates are high in Western and Northern Europe, Australia/New Zealand, and North America; intermediate in South America, the Caribbean, and Northern Africa; and low in sub-Saharan Africa and Asia. This might be attributed to the availability of medical services and the high standards of living where patients can get access to proper screening and follow-up. However, the reasons behind such variations are currently under vigorous evaluation.

In the African continent, breast cancer has shown to be the most diagnosed cancer in women in a number of Sub-Saharan African countries. This presents a shift from previous decades where cervical cancer was the most commonly diagnosed cancer in many of these countries. This might be attributed to the increased awareness of breast cancer, the education regarding self-examination of the breast, and the fact that

mammography has become more accessible with the advent of medical services. Breast cancer is currently considered as the second leading cause of cancer death among women (92,600 cases, 50,000 deaths). The number of cases varied enormously from 19.3 per 100,000 women in Eastern Africa to 89.7 per 100,000 women in Western Africa. This percentage is quite elevated when compared to the majority of the developed countries where the incidence rates are below 40 per 100,000 (Ferlay et al., 2010). The incidence rates are rising in many African countries previously known to have low incidence of the disease. In addition, the high mortality rates in Africa have called for more research into the etiology of breast cancer. It is well documented that women diagnosed with breast cancer in Africa generally have a poorer prognosis than those in more developed. Moreover, race differences in incidence are very apparent. For example, the female breast cancer incidence rate in Harare (Zimbabwe) in 1990-1992 was 6 times higher in white population (129.0) than in African Blacks (20.0) (Bassett et al., 1995).

Cancer in South Africa is a rising health problem, with breast cancer being one of the leading cancers in women, following similar worldwide statistics (Vorobiof et al., 2001). Breast cancer is the most common cancer affecting South African women – 1 in 33 women in South Africa are diagnosed with Breast Cancer across all race groups (Schlebusch et al., 2010). It is generally estimated that White South African women have the highest risk with one in twelve diagnosed positive, whereas the lifetime factor risk for colored and Asian women is one in eighteen and the risk factor for black women is one in forty-nine thus showing the lowest incidence rates of all population groups. However, survival rates varies among groups with black females having the worst survival rate; as only 22% of black female patients present with early stages of the cancer (I and II) in contrast to nearly 69% of the non-black patients who are diagnosed at their early stages of the disease (Vorobiof et al., 2001).

Despite the complex etiology, breast cancer is of moderate aggressiveness, meaning that most cancers grow from small size with low metastatic potential to large size and greater metastatic potential over several years (Gonzalez-Angulo et al., 2007; Pagani et al., 2010). Southern African women have the highest breast cancer incidence rates

of all African regions, in part because of a higher prevalence of reproductive risk factors for breast cancer, including early menarche and late childbearing among the more affluent predominantly white population (Vorobiof et al., 2001).

Currently, Tamoxifen, a powerful estrogen antagonist is an accepted treatment and prevention therapy for breast cancer in both early and late stage cancer patients (Pagani et al., 2010). Tamoxifen exerts its effects on breast cancer cells by binding to the ER receptors thereby displacing estrogen (Musgrove et al., 1998). Taking into account that ER positive breast cancers utilize estrogen for proliferation, it is clear that Tamoxifen is a highly effective treatment to prevent tumour proliferation through ER antagonistic action. However, studies have indicated that while Tamoxifen inhibits the proliferation of breast cancer cells, it has been associated with uterotrophic effects such as, hyperplasia, polyps and the development of uterine cancer. Therefore, alternatives to the use of Tamoxifen require exploration.

Genes that participate in oncogenesis are the result of the transformation of the genes that normally control cell cycle, damaged-DNA repair and cellular adherence. Cell transformation into a cancer one requires at least of two mutations: a) a mutation in a tumor suppressor gene and b) a mutation in a proto-oncogene that give rise to an oncogene. When these DNA changes cannot be repaired, cell falls into the first steps of malignant transformation (Vogelstein and Kinzler, 2004).

1.2 Cell cycle

Cell cycle checkpoints preserve genome integrity by monitoring the fidelity of DNA replication and segregation. The cell cycle consists of five phases, the Gap1 (G_1), Synthesis (S), Gap2 (G_2), Mitosis (M) and Quiescence (G_0) phases, which are intimately linked to proliferation, differentiation, apoptosis and other important cellular processes. The cell cycle progression is controlled by a biochemical reaction system consisting of genes and proteins (Kohn, 1999).

The cell cycle is a coordinated process controlled by a complex network of signaling pathways molecules. Cell cycle progression is governed by the activity of cyclin dependent kinase (CDKs) in complex with their activating partner cyclin (Lim and Kaldis, 2013). This process is essential to the survival of cell, which involves the detection and repair of DNA damage and the avoidance of uncontrolled cell division (Fig. 1.1) (Keaton, 2007).

The cell cycles length varies in time from one cell type to another. Fly embryos have the shortest known cell cycles, as little as 8 minutes. Whereas the cell cycle of liver cells of the mammalian could last longer than a year (Kohn, 1999). The cell cycle in culture, typically occupies a 16 to 24 hour period (Kohn, 1999). The G₁ phase is highly variable, ranging from almost non-existent in rapidly dividing cells to days, weeks or years. The length of the S phase differs between species and between different development stages within a species, but within any particular type of cell the S phase is remarkably constant in length and is usually 8 hours (Lara-Gonzalez et al., 2012). The G₂ period was estimated to be 3 to 4 hours or even as long as 6 hours while the M phase takes approximately an hour (Keaton, 2007).

Checkpoints serve to monitor the order of events in the cell cycle and ensure that a cell cycle event occurs only after the completion of a prior event (Langerak & Russell 2011). Different DNA damage checkpoints can be activated in response to DNA damage (Langerak & Russell 2011). DNA damage checkpoint is one such example that is activated upon various kinds of external or internal stimuli that induce DNA damage, either programmed or accidental, and thus helps integrate DNA repair with cell cycle progression (Jones and Petermann, 2012).

Cells have systems which transduces DNA-damage signals to regulatory mechanisms of the cell cycle and arrests cell cycle progression, thus contributing to maintain the stability of the cell cycle (Dasika et al., 1999).

1.2.1 Cyclins

Cyclins were described in 1982 by Timothy Hunt, (Jackson, 2008) as a diverse family of proteins whose defining feature is to bind and activate members of the CDK family. 29 Cyclins and more than 20 CDKs have been identified in mammalian cells (Lim and Kaldis, 2013). Cyclin levels are regulated by cyclin gene expression and destruction of cyclins via proteolysis, and in a tightly controlled manner during distinct phases of the cell cycle (Bloom and Cross, 2007).

All cyclins contain a highly conserved region of 100-150 amino acid residues called the “cyclin box”, which is required for their interaction with CDKs (Mikolcevic et al., 2012). Four major cyclins (D, E, A, and B1) are required for cell cycle progression (Lim and Kaldis, 2013). Cyclins and CDKs are both subject to post-translational regulation by phosphorylation (Lim and Kaldis, 2013). There are three major amino acid sites of phosphorylation namely threonine (Thr 160 of CDK2, Thr 161 of CDK1, and Thr 172 of CDK4/6), tyrosine (Tyr 15 of CDK2 and CDK2 and Tyr 17 of CDK4 and CDK6) and threonine 14 (Thr 14). The phosphorylation of threonine (160, 161 or 172) activates the cyclin-CDK complex whereas tyrosine (15 or 17) and threonine 14 phosphorylations are dominant and inactivate the complex (Bloom and Cross, 2007).

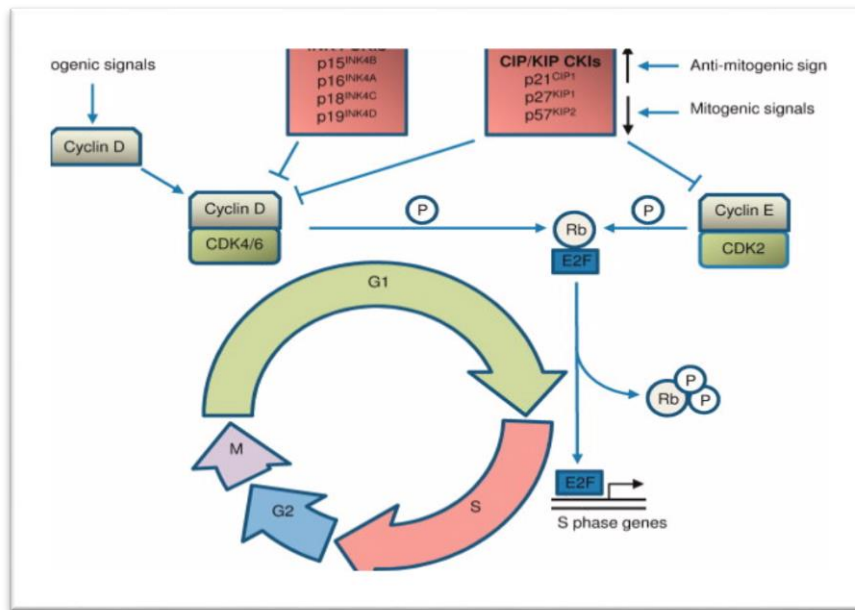


Figure 1.1: Progression of the cell cycle is regulated by cyclin-cyclin-dependent kinase (CDK) complexes which are primary targets of mitogenic signals. During G1 phase, cyclin D-CDK4/6 and cyclin E-CDK2 phosphorylate the protein Rb, releasing transcription factors including E2F. Free E2F activates the transcription of genes necessary for DNA synthesis, resulting in S phase entry. Activities of cyclin-CDK complexes are inhibited by CDK inhibitory proteins (CKIs). CKIs are divided into two families: the INK4 proteins (p15^{INK4B}, p16^{INK4A}, p18^{INK4C}, and p19^{INK4D}) and CIP/KIP proteins (p21^{CIP1}, p27^{KIP1}, and p57^{KIP2}). While INK4 CKIs inhibit specifically cyclin D-CDK4/6 complexes, CIP/KIP proteins bind and inhibit a broad range of cyclin/CDK complexes including cyclin E-CDK2. CIP/KIP proteins are regulated by mitogenic and anti-mitogenic extracellular signals.

Source (Tury et al., 2012)

The cyclin-CDK inhibitors namely the Cip/Kip family p21^{Cip1}, p27^{Kip1}, and p57^{Kip2} control not only the cell cycle progression but also have additional roles such as apoptosis induction (Sherr and Roberts, 1999), transcriptional regulation, cell migration and cytoskeletal dynamics (Romagosa et al. 2011; Besson et al. 2008).

The Cip/Kip CDK inhibitor p21^{Cip1}/WAF1 has a critical role in the nucleus to limit cell proliferation by inhibiting CDK-cyclin complexes. In response to DNA damage or anti-mitogenic signals, p21^{Cip1} and p27^{Kip1} can induce a cell cycle block mediating chemotherapeutic results (Besson et al., 2008; Scorah and McGowan, 2010). P21 mediates the P53-dependent G1/S checkpoint, which may be considered to be a key

requirement to preserve genomic stability when DNA damage occurs (Roque et al., 2012; Starostina et al., 2010). P27Kip1 regulates cell proliferation, cell motility and apoptosis. P57Kip2 inhibits CDK2, CDK3, and CDK1 and belongs to the CDK interacting protein/kinase interacting protein (CIP/KIP) family of CKIs (Jayapal & Kaldis 2014).

1.3 Control of the cell cycle

1.3.1 Cell cycle progression through phosphorylation/dephosphorylation

The phosphorylation of proteins on serine, threonine and tyrosine residues by protein kinases is a basic post-translational modification which regulate protein activation/deactivation in cell proliferation and differentiation, cell mobility and motility, metabolism and apoptosis (Bononi et al. 2011). Three major cellular phosphatases have been characterized as retinoblastoma (RB) or RB-like protein phosphatases and the Ser/Thr phosphatases protein phosphatase (PP1 and PP2A), are the major cellular phosphates (Virshup and Shenolikar, 2009).

Phosphorylation of the (RB) in the G₁-phase of the mammalian cell division cycle is a controlling element regulating the passage of cells into S-phase (Henley and Dick, 2012). Substrates are the p110 retinoblastoma (RB) protein as well as Cdc25 phosphatase. The catalytic subunit of PP1 associates with RB in mitosis and G₁ and is a positive regulator of its function (Durfee et al., 1993). PP1 dephosphorylate and inactivate Cdc25 phosphatase that stimulates CDK1 kinase through dephosphorylating Tyr-15 and Thr14 for the beginning of mitosis.

1.3.2 Cell cycle checkpoints

The following checkpoints have been identified, in the cell cycle: (I) the restriction point (mammalian) or START (yeast), which integrates internal and environmental signals early in G₁ and decides if the cell will replicate, (II) the DNA damage checkpoint, which arrests cells after DNA damage, to allow repair to occur before

DNA is replicated in the S phase (Langerak & Russell 2011), (III) a DNA damage-independent, p53-mediated G₁ checkpoint (Langerak & Russell 2011), (IV) S phase DNA damage checkpoint, which prevents initiation at DNA replication forks following DNA damage, without affecting the DNA synthesis which has already started, (V) S/M DNA replication checkpoint which ensures that cells do not enter mitosis if all chromosomes are not replicated fully, (VI) activated Ras G₂ checkpoint, which arrests some type of cells when activated Ras is present, (VII) the G₂ DNA repair checkpoint, which surveys DNA replication for faults and (VIII) the mitotic spindle assembly checkpoint, which prevents chromosome segregation before spindle formation and chromosomal attachment have been accomplished (Medema and Macurek, 2012)

1.3.2.1 DNA damage response pathways of G₁ phase

The G₁ arrest due to DNA damage causes a delay in cell cycle progression to facilitate DNA repair, thus preventing mutations. Entrance into S-phase is regulated by either a p53 dependent– or P53 independent pathway (Chao et al., 2006). The p53 independent pathway is known as Cdc25A pathway. These pathways share the same key upstream regulators, ataxia-telangiectasia mutated/ATM and Rad3-related (ATM/ATR) and checkpoint kinases 1 and 2 (Chk1/Chk2) and target Cdc25A, a dual specificity phosphatase and p53 simultaneously within minutes after DNA damage. However, not all DNA damage leads to the activation of both pathways, thus it would relay information to activate both or either one or the other (Chao et al., 2006). ATM is mainly activated in response to double-strand DNA breaks (DSBs) whilst ATR is primarily activated following replicative errors that result in single-stranded DNA (Beckerman and Prives, 2010; Takahashi et al., 2011).

1.3.2.2 The P53 response to DNA damage

Wild type p53 demonstrated that its anti-proliferative effect is mediated by stimulation of a CKI the P21^{Waf1/Cip1} (P21) that inhibits CDK activity (Jossen and Bermejo, 2013). For p53 to become active, cellular levels must be stabilized by blocking the antagonist protein, murine double minute 2 (MDM2) (Chao et al., 2006). Activation of

ATM/ATR leads to phosphorylation of p53 at Ser20 causing inhibition of the p53/MDM2 interaction, preventing ubiquitin-mediated p53 degradation and thereby enhancing p53 stabilization (Hustedt et al., 2013). After modification, p53 translocate to the nucleus where it forms a homo-tetramer complex that can regulate the transcription of a wide variety of genes including p21 (Shangary and Wang, 2008). ATM can also phosphorylate the Mdm2 related protein, MdmX at S367. MdmX also inhibits p53 activity through binding to the p53 N-terminal domain and reducing acetylation of p53 (Okamoto et al., 2005).

The activation of p21 by p53 regulates the transition between G1 and S-phase by interacting with CDK2, repressing the kinase activity of cyclinD-CDK4, cyclinE-CDK2, and cyclinA-CDK2 (Takahashi et al., 2011). In cells with unrepaired DNA that are already in S-phase, p21 binds to the complex composed of replication factor C, DNA polymerase- δ , and proliferating-cell nuclear antigen (PCNA), causing their dissociation from the replication fork, which blocks synthesis of DNA (Takahashi et al., 2011). This cell cycle checkpoint may be further prolonged by the gradual accumulation of p16, a protein that can selectively disrupt the cyclin D-CDK4/6 complexes and by this means release the existing pool of p21 (Hustedt et al., 2013). When the threshold level of p21 is achieved, p21 can bind and inhibit the S phase promoting cyclin E-CDK2 complexes, and thereby secure the maintenance of the G₁ arrest. The inhibition of both the cyclin-CDK complexes leads to the dephosphorylation of RB which therefore cause the inhibition of the E2F dependent transcription of S phase genes. P21 is also involved in G₂ arrest by interacting with CDK1 (Takahashi et al., 2011).

On the other hand, phosphorylation of p53 at Ser46 has been shown to mediate the selectivity of p53 (Jossen and Bermejo, 2013) in favor of promoters which enhance apoptotic signaling, such as the p53-regulated apoptosis-inducing protein 1 (P53AIP) (Beckerman and Prives, 2010; Takahashi et al., 2011).

1.3.2.3 The Cdc25A pathway

The Cdc25 family consists of Cdc25A, Cdc25B and Cdc25C. Cdc25A promotes entry into S phase by acting on cyclin A-CDK2 and cyclin E-CDK2, both Cdc25B and Cdc25C play a role in the commencement of mitosis (Polager and Ginsberg, 2009).

A p53 independent pathway is activated by ATM phosphorylation. Chk2 phosphorylates the Cdc25A phosphatase in several serine residues, which stimulates ubiquitination and proteasome mediated degradation of Cdc25A leading to cell cycle arrest (Lee et al., 2000). Degradation of Cdc25A inhibits CDK2 activity thus preventing recruitment of DNA polymerase α and initiation of DNA synthesis. This mechanism induces cell cycle arrest at the intra S Phase and G1/S Phase interface in response to DNA damage (Polager and Ginsberg, 2009). This pathway, targeting Cdc25A, is implemented rapidly and operates independently of the p53 status, and it is relatively transient and able of delaying cell cycle progression for a few hours.

1.3.3 S phase DNA damage checkpoints

Replication fork barriers (RFBs) slow down or stall fork progression. Examples of RFBs include; (1) DNA protein complexes that lead to natural “pause sites” that are active in every S phase, (2) alternative DNA metabolism, (3) secondary DNA structure, (4) DNA damage which could be produced by endogenous metabolism or induced by exogenous carcinogens and inter strand cross linking agents, and (5) replication inhibitors which competitively inhibits pol α (Lambert and Carr, 2005). Because of the genetic instability caused by the RFB, the nature of the cellular response could lead to DNA structure checkpoint pathways.

1.3.3.1 The intra-S phase checkpoint

The intra-S phase checkpoint prevents the firing of new replication forks by inhibiting initiation at licensed but unfired origins (Shibata et al., 2010), thus resulting in a reduction in the rate of progression through the S phase rather than an arrest. Unlike

the G₁ or G₂/M checkpoints, the intra-S phase response to DNA damage is independent of p53 (Cortez et al., 2004). The initial pathway is the ATM/ATR–Chk1/Chk2–Cdc25A–cyclin E (A)/Cdk2–Cdc45 cascade (Shibata et al., 2010) (see section 1.3.2.3). Inhibition of CDK2 activity through Cdc25A degradation leads to a several-hour delay of S phase progression, a timing that correlates well with the transient intra-S phase checkpoint response (Boutros et al., 2013).

1.3.3.2 The DNA replication (S/M) checkpoint

Disturbance of replication elicits four definable cellular responses. (1) The inhibition of late origin firing, (2) stabilization of active replication forks, (3) a delay into mitotic entry and (4) slowing down of replication fork progression on damaged templates. The first three responses are fully dependent on the S phase checkpoint proteins whereas the latter is not (Timofeev et al., 2010). Most of the proteins involved in the S phase checkpoints are also essential for the G₁ and the G₂/M DNA damage checkpoints.

Chk1 has a role in the maintenance of fork stability and claspin binding to the fork (Shibata et al., 2010). As a result of blocked replication or repair of lesions on DNA, the S phase checkpoint is activated and the signal finally arrives to the replicating fork. This results in slowing down of DNA replication. The different rate at which synthesis in the leading and lagging strands occur results in fork asymmetry (Boutros et al., 2013; Timofeev et al., 2010). Chk 1 and 2 and mediators are recruited to sites of damage and are phosphorylated within nuclear foci. Chk kinases that are activated are released from foci and phosphorylate Cdc25 (Boutros et al., 2013; Timofeev et al., 2010).

1.3.4 G₂ (G₂/M) checkpoint

The biochemical pathways involved in the DNA damage induced G₂ checkpoints are signaling cascades that unite to inhibit the activation of CDK1. This checkpoint is very similar to the G₁/S checkpoint. DNA double-strand breaks activate the ATM-Chk2-Cdc25 pathway and DNA lesions such as UV light activate the ATR-Chk1-Cdc25

pathway. Down regulation of Cdc25A, Chk1, Chk2 and WEE1 regulates CDK1 activity and consequently G2 arrest together with p53/p21, which is distinct from the G1/M checkpoint activities (Reinhardt et al., 2007). After ATM dependent activation, Chk1 and Chk2 furthermore phosphorylate Cdc25C on Ser216 creating a binding site for 14-3-3 proteins. Binding of 14-3-3 proteins to Cdc25C, results in the nuclear export of Cdc25C to the cytoplasm thus inhibiting CDK1 activity (Reinhardt et al., 2007).

1.3.5 The spindle assembly checkpoint

Making sure that segregation does not occur before all chromosomes make proper attachments, the spindle assembly checkpoint (also known as the spindle checkpoint or mitotic checkpoint) acts in mitosis by delaying the onset of anaphase when chromosomes fail to align completely at the metaphase plate.

The anaphase-promoting complex (APC) is an ubiquitin protein ligase that triggers the metaphase-to-anaphase transition (Keaton, 2007) and ensures sister chromatid separation by destruction of securin. Fig. 1.2 illustrates the destruction of securin by the 26S proteasome causing exit from mitosis (Peters, 2006). The APC/C consists of 12 core subunits and cofactors the Cdc20 and Cdh1. Cdc20 stimulates APC/C in the beginning mitosis and Cdh1 stimulates APC/C activity from late mitosis to the G1–S transition (Peters, 2006). The dependency of APC phosphorylation on Cdc20 binding ensures that APC-Cdc20 is only active while in mitosis.

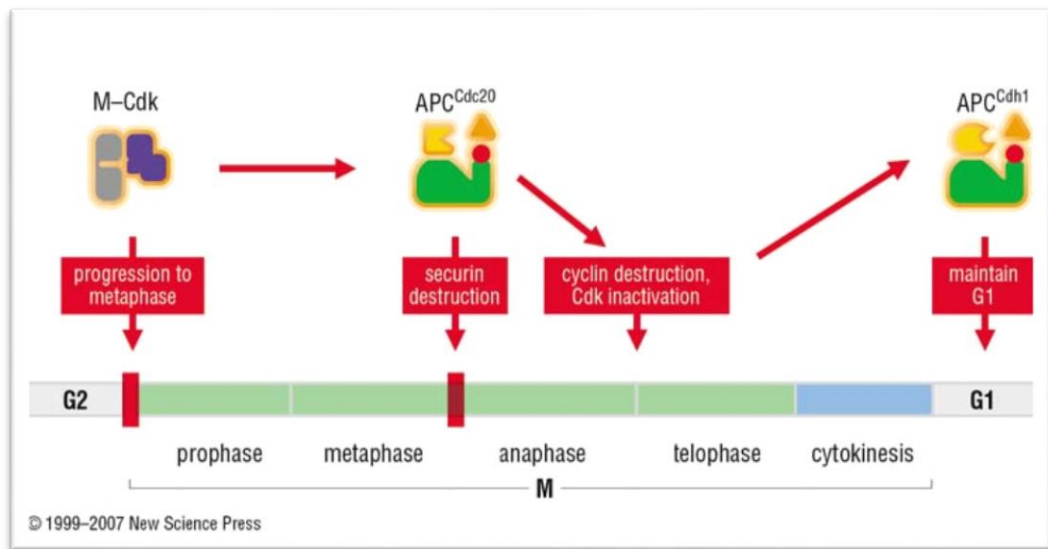


Figure 1.2: Control of late mitotic events by the APC M-Cdk activity promotes the events of early mitosis, resulting in the metaphase alignment of sister chromatin on the spindle. CDK1 activity also promotes the activation of APC^{Cdc20}, which triggers anaphase and mitotic exit by stimulating the destruction of regulatory proteins, such as securin and cyclins, which govern these events.

Source (Keaton, 2007)

Kinetochores assist as assembly points for active Mad2 protein. Mad2 binds to Cdc20 and inhibits APC activity (Kim et al., 2010). When most kinetochores are attached and chromosomes are aligned on the metaphase plate, Mad2 inhibition of APC-Cdc20 activity is ended. Non-phosphorylated Cdh1 then initialize the APC (Rodier et al., 2008). The active complex then ubiquitinates securin and allows the activation of separase, which cleaves cohesion. Loss of cohesion triggers chromosome segregation and the onset of anaphase.

When the spindle assembly checkpoint is satisfied, APCs become active and ubiquitinate several proteins, including cyclin B (Kim et al., 2010). The destruction of securin allows the chromatids to separate, while proteolysis of cyclin B allows the cell to exit the mitotic state (Kim et al., 2010). The ubiquitin proteolysis of cyclin B is associated with the inactivation of CDK1, initiation of telophase, chromosome decondensation, nuclear envelope reformation, and cytokinesis (Rodier et al., 2008).

1.4 Cell death

In vitro cellular stress studies, using morphology and biochemical criteria display three categories of cell death: apoptosis, autophagy and necrosis (Fig. 1.3).

1.4.1 Apoptosis

Apoptosis is a natural process of self-destruction in certain cells that are genetically programmed to have a limited life span or are damaged. Outspoken apoptosis can cause atrophy, while decreased apoptosis leads to uncontrolled cell proliferation, such as cancer (Kerr et al., 1972).

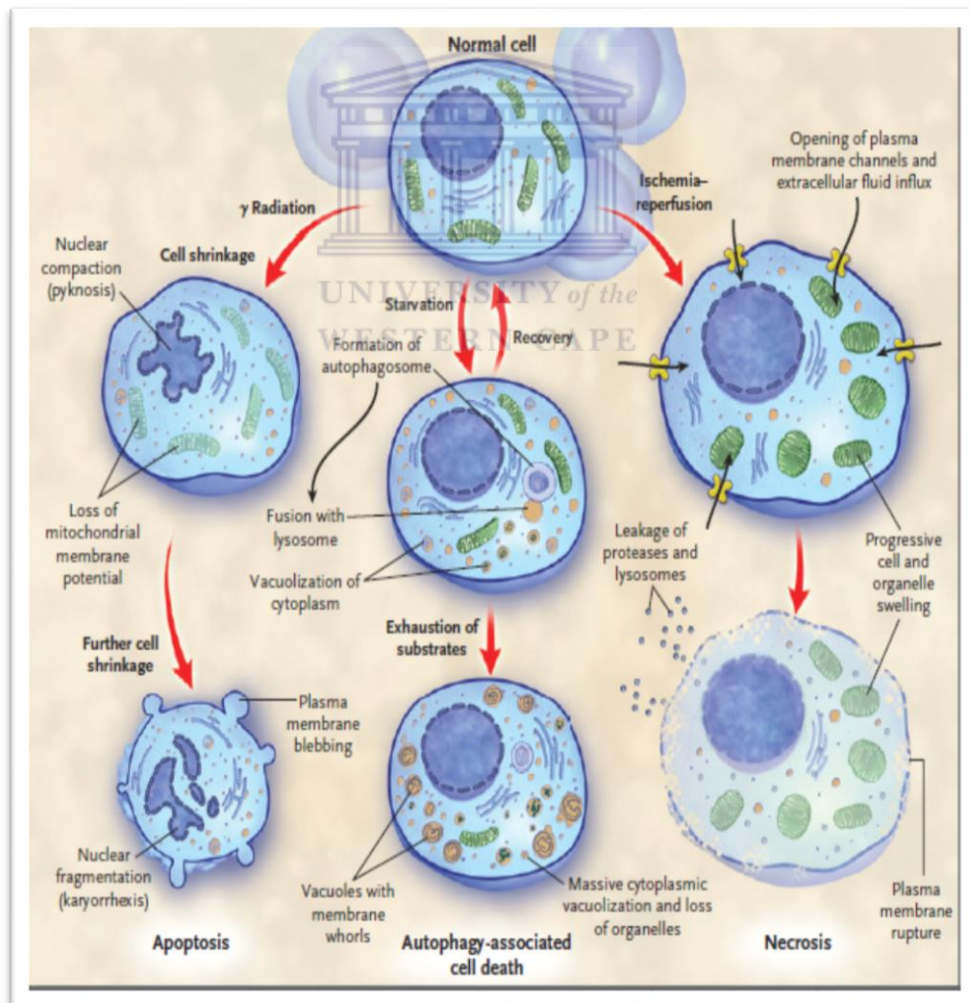


Figure 1.3: Three pathways of cell death

Source (Hotchkiss et al., 2009)

Morphologically, apoptosis involves a series of structural changes in dying cells characterized by degradation of cytoskeletal filaments, cell shrinkage, membrane blebbing and cellular fragmentation, nuclear condensation and DNA fragmentation, the formation of apoptotic bodies and loss of its ability to make contact with neighboring cells (Doonan and Cotter, 2008).

Caspases are cysteine aspartyl proteases that are central regulators of apoptosis. Initiator caspases (caspase-2, -8, -9, -10, -11, and -12) are closely coupled to pro-apoptotic signals. Once activated, these caspases cleave and activate downstream effector caspases (including caspase-3, -6, and -7), which in turn execute apoptosis by cleaving cellular proteins (Ola et al., 2011).

Three distinct apoptotic pathways exist that both end in caspase activation. The first is under the control of the Bcl-2 (B-cell lymphoma 2) family of genes and its proteins (Brentnall et al., 2013).

The second pathway of apoptotic signaling is called the "death receptor pathway", which is initiated by extracellular ligands such as Death receptors DR that are members of the tumor necrosis factor (TNF) receptor gene superfamily that consists of more than 20 proteins with a broad range of biological functions, including regulation of cell death and survival, differentiation or immune regulation (Ashkenazi and Salvesen, 2014; Mahmood and Shukla, 2010). The third pathway is endoplasmic reticulum-mediated apoptosis.

1.4.1.1 The intrinsic pathway

The intrinsic pathway is induced by DNA damage and cytotoxic insults (Surova and Zhivotovsky, 2013). It acts through the mitochondria Bcl-2. Under normal conditions, the anti-apoptotic Bcl-2 family (Bcl-XL, Bcl-W, Bfl-1, and Mcl-1) maintains mitochondrial integrity by inhibiting the pro-apoptotic Bax, Bak, Bad, Bcl Xs, Bid, Bik, Bim, and Hrk (Fig. 1.4A) (Zhai et al., 2008). Under stress conditions such as DNA damage or UV irradiation, Bcl-2-homology 3 (BH3) proteins are stimulated to stop the

action of the Bcl-2 family (Kook et al., 2014). This results in the upregulation of Bax and Bak leading to their oligomerization and the formation of a channel through which cytochrome C (Cyt C) will be released into the cytosol. The channel formation is influenced by mitochondrial outer membrane permeabilization (MOMP) that leads to the release of cytochrome c and other proteins from the mitochondrial intermembrane space (Czabotar et al., 2014) and is required for activation of the caspases that cause apoptosis or progressive mitochondrial malfunction, which causes energy depletion and cell death (Tait and Green, 2012).

The Bcl-2 family proteins are characterized by the presence of Bcl-2 homology (BH) domains (Frenzel et al., 2009). There are four important Bcl-2 structural homology (BH domains) BH1, BH2, BH3 and BH4. The pro-apoptotic proteins are classified into two subgroups: the Bax-subfamily consisting of Bax, Bak, and Bok that all possess the domains BH1, BH2, and BH3, whereas the BH3-only proteins (Bid, Bim, Bik, Bad, Bmf, Hrk, Noxa, Puma, Blk, BNIP3, and Spike) have only the short BH3 motif, an interaction domain that is both necessary and sufficient for their killing action (Frenzel et al., 2009). Cyt C, released from the mitochondrial space binds to apoptosis protease activating factor (Apaf-1) and dATP in the cytosol to form a heptameric complex, the apoptosome, in which each Apaf-1 subunit is bound non-covalently to a procaspase-9 subunit by their respective Caspase activation and recruitment domains (CARDs) domains (Shalaeva et al., 2015). Active caspase-9 cleaves and activates downstream executioner caspases, caspase-3, -6 and -7 which are important for the execution of apoptosis (Shalaeva et al., 2015). The 'inhibitor of apoptosis' (IAP) proteins are negative regulators of apoptosis that function by inhibiting the executioners of cell death (caspases) including caspase 3. Endonuclease G (EndoG) triggers DNA degradation and cell death upon translocation from mitochondria to the nucleus (Büttner et al., 2013). Endo G cleaves chromatin DNA into nucleosomal fragments independently of caspases thus representing a caspase-independent apoptotic pathway initiated from the mitochondria (Büttner et al., 2013).

1.4.1.2 The extrinsic pathway

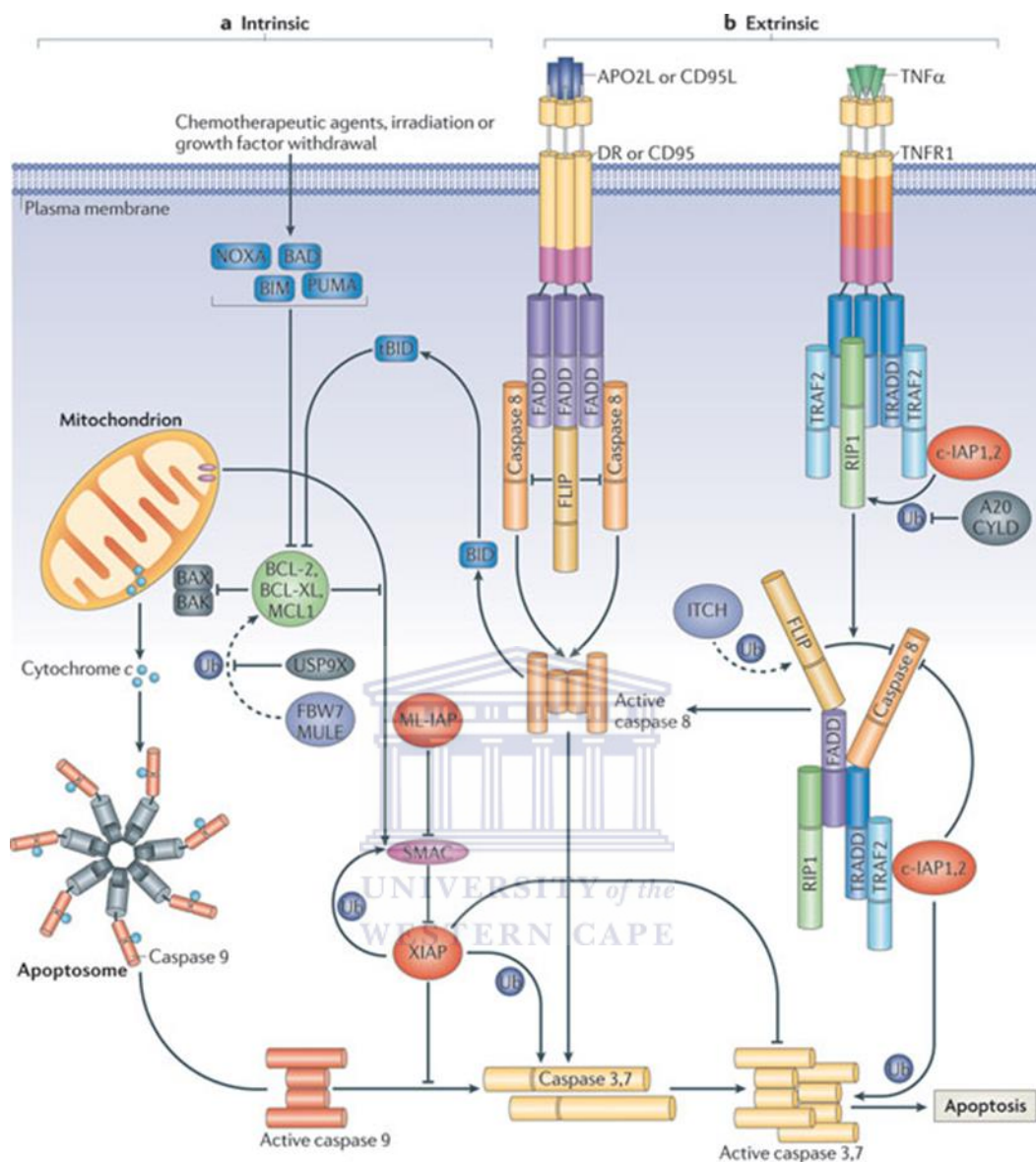
The extrinsic pathway of apoptosis is activated after stimulation of death receptors (DR) that belong to the tumor necrosis receptor (TNFR) family like Fas, TNF-related apoptosis inducing ligand receptor (TRAIL-R) (Nair et al., 2014). TRAIL-R has strong antitumor activity in a wide variety of cancer cells and minimal cytotoxicity in most normal cells (Fig. 1.4B).

DRs mediate a wide-range of physiological processes ranging from non-apoptotic responses that protect cells and regulate tissue regeneration to proliferation and migration. DRs have been classified into two groups: the first group contains EDAR, P75NTR and DR6 and members of this group all play a role in developmental processes (Büttner et al., 2013). The second group includes DR3, DR4, DR5, FAS and TNFR1 which function primarily in different aspects of the immune response (Jiang, 2011).

TRAIL can signal both apoptosis in transformed tumor cells and non-apoptotic signaling cascades. TRAIL initiates extrinsic apoptosis by binding to two related receptors, TRAIL-R1 (DR4) and TRAIL-R2 (DR5). Clustering and oligomerization of DR4 and DR5 by TRAIL leads to the recruitment of various adaptor proteins to the aggregated intracellular domains of the receptors with subsequent formation of the death-inducing signaling complex (DISC) (Büttner et al., 2013). One of the adaptor molecules, Fas-associated death domain (FADD) recruits the initiator caspases 8 and/or -10 by means of homotypic death effector domain interaction (Fujikura et al., 2012). TNFR1 aggregation leads to the formation of two complexes (Fujikura et al., 2012). Complex I is formed at the plasma membrane and it consists of TNFR1, TNF-associated domain death (TRADD) TNFR-associated factor 2 (TRAF2), receptor interacting protein (RIP), cellular inhibitor of apoptosis protein (cIAP)-1 and cIAP-2 (Shalaeva et al., 2015). The formation of complex II is similar to the receptor-proximal DISC induced by FasL, TRADD, FADD and caspases 8 and/or -10. Activation of caspase-8 and caspase 10 results the activation of downstream effectors caspases including procaspase-3, -6, and -7 (Vanlangenakker et al., 2011). TRAIL also binds

the decoy receptors, DcR1 and DcR2, which not contain a cytoplasmic domain (DcR1) or contain a truncated death domain (DcR2). The functional cytoplasmic domain of DcR2 activates NFkappaB that inhibits the death signaling pathway and/or promotes inflammation (Hao et al., 2004). Transient over-expression of DcR1 or DcR2 in TRAIL-sensitive tumor cells prevents cell death triggering by TRAIL (Mérino et al., 2006).





Nature Reviews | Molecular Cell Biology

Figure 1.4: Overview of the intrinsic and extrinsic apoptotic pathways. (A). The extrinsic apoptotic pathway is activated after stimulation of death ligands like TNF, TRAIL, FasL and subsequently the death receptors (TNFR, Fas and TRAIL-R) are stimulated (B). Signaling by these receptors induce proliferation, differentiation and cell death. DNA damage and cytotoxic insults are amongst stimuli that activate the intrinsic pathways of apoptosis. The intrinsic pathway acts through the mitochondria under the influence of the Bcl-2 family. Under normal conditions, the anti-apoptotic Bcl-2 family maintains mitochondrial integrity by inhibiting the pro-apoptotic Bax and Bak leading to mitochondrial leakage of cytochrome c into the cytosol. Cyt C associates with Apaf-1 to form an apoptosome that plays a role in the activation of caspase 9. Caspase 9 in turn activates executioner caspases 3, 6 and 7 which are crucial for the execution of apoptosis.

Source (Vucic et al., 2011)

1.4.1.3 Endoplasmic reticulum-mediated (ER) pathway

ER mediated apoptosis is the third mechanism known to be involved in the caspase dependent apoptotic process. The accumulation of unfolded proteins in the ER lumen or depletion of Ca^{2+} from the ER lumen activates a signaling cascade (Fig. 1.5) known as the unfolded protein response (UPR) (Bravo-Sagua et al., 2013; Malhotra and Kaufman, 2011). The resulting extensive stress leads to apoptotic cell death. Bax and Bak can localize to the ER in response to ER stress, leading to calcium release and the activation of caspase 4.

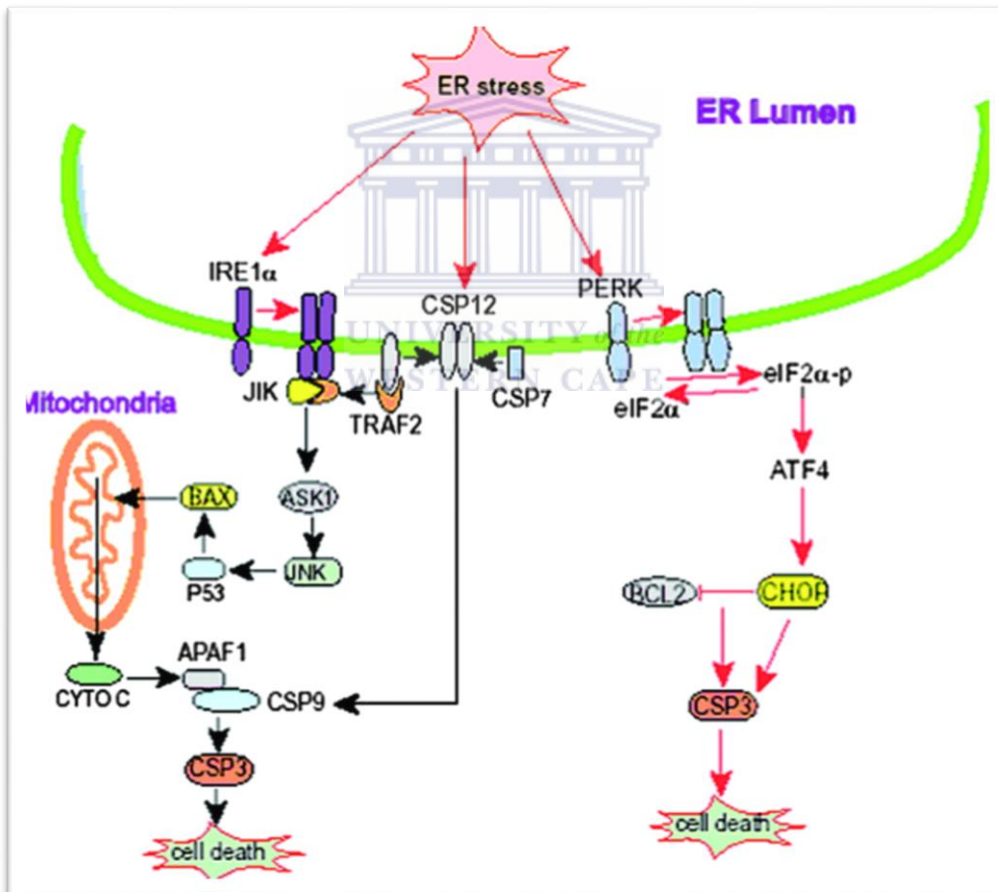


Figure 1.5: Apoptosis mediated by the unfolded protein response signaling.

Source (Cao and Kaufman, 2012)

1.4.1.4 The caspase independent pathway(s)

Caspase independent cell death (CICD) shares common features with apoptotic cell death. Upstream signaling pathways MOMP is necessary for activation of CICD. Cells undergoing CICD frequently demonstrate large-scale cytoplasmic vacuolization, autophagosome accumulation and peripheral nuclear condensation (Tait and Green, 2008). Non-caspase proteases that have been implicated in apoptotic cell death are cathepsins, calpains, granzymes, serine proteases and proteasomal proteases (Tait and Green, 2008).

Cathepsin B and L (both cysteine proteases) as well as cathepsin D (an aspartate protease) are proven to play a role in apoptosis through their translocation from lysosomes or endosomes to the cytosol (Turk and Stoka, 2007). Calpains are non-lysosomal cysteine proteases, which are activated via increased intracellular Ca²⁺ concentrations activating various signal transduction pathways, cell motility, and apoptosis and cell cycle regulation. Granzymes are serine proteases that released by cytoplasmic granules within natural killer (NK) cells and cytotoxic lymphocytes (CTLs) (Cullen et al., 2010). Granzymes cleave intracellular substrates, activating several apoptotic pathways leading cell death (Cullen et al., 2010). High temperature requirement A2 (HtrA2) or Omi, is a member of HtrA family which is an ATP-independent serine protease (Vande Walle et al., 2007). Omi/HtrA2 is a serine protease located in the mitochondrial intermembrane space that is released to the cytosol upon various apoptotic stimuli and can induce apoptosis via its protease activity (Vande Walle et al., 2007).

Apoptosis initiation factor (AIF) released from the mitochondrial inter membrane space translocates to the nucleus and initiates chromatin condensation and DNA fragmentation through enrolling or activating an endonuclease (Sevrioukova, 2011). These types of death effectors and different levels of reactive oxygen species (ROS) production are highly effective pro-apoptotic stimulators (Torres, 2010).

1.4.1.5 The role of Tumour suppressor p53 in apoptosis

The tumor suppressor p53 is a pivotal player in the negative regulation of cell cycle progression by promoting the transcription of numerous downstream regulators that either induces cell cycle arrest, apoptosis or autophagy (Kruiswijk et al., 2015). Consequently, it prevents accumulation of irreversible genetic alterations that could ultimately lead to cellular transformation.

In response to cellular stress, P53 transactivates or transrepresses many different downstream genes to trigger apoptotic responses. The p53-mediated transactivation of apoptosis-related genes include pro-apoptotic Bcl-2 family members e.g., Bax, Puma, Noxa, and Bid, which leads to the mitochondrial membrane depolarization in the intrinsic pathway; apoptotic protease activating factor-1 (APAF-1), a major component of apoptosome; and Fas/CD95, death receptor 4 (DR4), and DR5, components of the extrinsic apoptotic pathways (Kruiswijk et al., 2015). P53 can also directly bind to and inhibit the Bcl-XL and Bcl2 proteins, leading to the release of cytochrome C and the initiation of caspase cascade. There is strong evidence suggesting PUMA as a critical component of p53-mediated apoptosis, and in other cell types, NOXA seems to be equally significant (Nikoletopoulou et al., 2013).

1.4.2 Autophagy

Autophagy, a term derived from the Greek, means “self (auto)-eating (phagy)” (Mizushima et al., 2010). Autophagy is an adaptive catabolic process that serves to deliver degraded cytoplasmic materials and organelles to the lysosomes for digestion (Todde et al., 2009)

During autophagy, double- or multiple-membrane structures engulf portions of cytoplasm and/or organelles to form autophagosomes (Kroemer et al., 2010; Reggiori and Klionsky, 2005). The autophagosome merge with lysosomes to form autolysosomes, where the degradation will occur. Autophagy is mostly a cellular

survival process but could result in a cell death mechanism when different cell death pathways, including apoptosis, are deficient (Gozuacik and Kimchi, 2004).

The autophagic process (Fig. 1.6) proceeds as a result of various steps: the initiation period relating to the formation of an isolation membrane or phagophore, the elongation of the phagophore, the maturation of an autophagosome with assimilation of a cytosolic cargo, the fusion of the mature autophagosome to the lysosome, and the degradation period in which the contents are digested with lysosomal proteases (e.g., cathepsins) and other hydrolytic enzymes (Kroemer et al., 2010; Ryter et al., 2014).



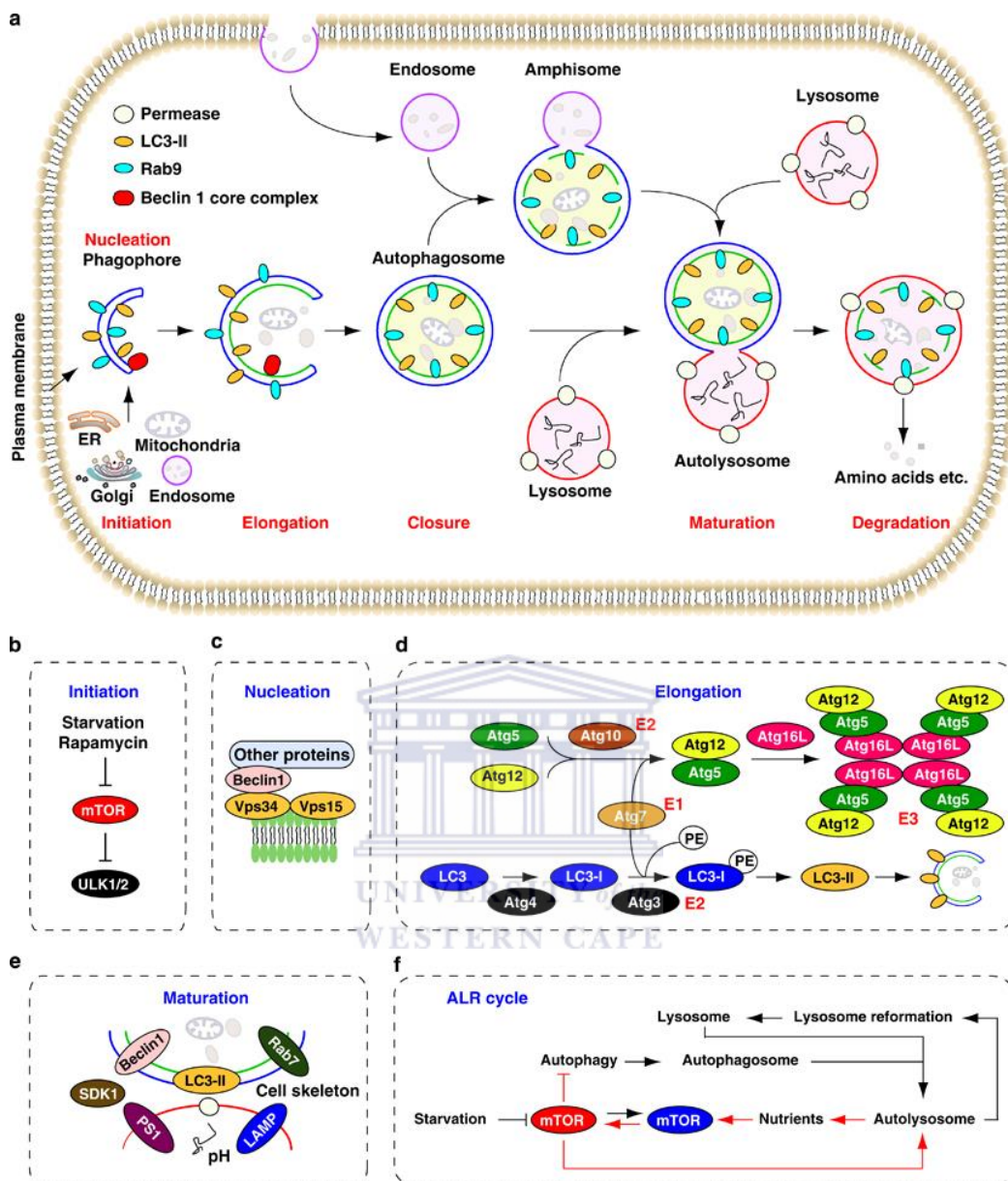


Figure 1.6: Stages of autophagy. (A) Different types of autophagy. LC3-II is a marker of Atg5/Atg7-dependent autophagy, whereas Rab-9 is a marker of Atg5/Atg7-independent autophagy. (B) The initiation is sustained by activation of ULK1 and ULK2 complexes, which are inhibited by mTOR. (C) The nucleation depends on Beclin 1-Vps34-Vps15 core complexes and other proteins. (D) The elongation of the phagophore is mediated by two ubiquitin-like conjugation systems that together promote the assembly of the ATG16L complex and the processing of LC3. PE, phosphatidylethanolamine. (E) The maturation is promoted by LC3, Beclin 1, the lysosomal membrane proteins LAMP-1 and LAMP-2, the GTP-binding protein RAB7, the ATPase SKD1, the cell skeleton, the pH of lysosomes and possibly presenilin 1 (PS1). (F) Autophagic lysosome reformation (ALR) cycle. mTOR signaling is inhibited during initiation of autophagy, but reactivated by prolonged starvation. Reactivation of mTOR is autophagy-dependent and requires the degradation of autolysosomal products. Increased mTOR activity attenuates autophagy and generates proto-lysosomal tubules and vesicles that extrude from autolysosomes and ultimately mature into functional lysosomes, thereby restoring the full complement of lysosomes in the cell.

Source:(Kang et al., 2011)

1.4.2.1 Molecular regulation of autophagy (Figs. 1.6 and 1.7)

The autophagy signaling pathways are regulated by a group of autophagy-related genes (Atgs) that were first identified and characterized in the yeast genome (Mizushima and Komatsu, 2011). Atg proteins are comprised of four functional groups that include a serine/threonine kinase complex that responds to upstream signals like Atg1/UNC-51-like kinase ULK1, Atg13, Atg17, a lipid kinase complex [Atg6/Beclin1, Atg14, Vacuolar protein sorting (Vps) 34/PI3KC3 and Vps15] and two ubiquitin-like conjugation pathways that contribute to the expansion of the vesicle (Atg8/LC3 and Atg12 systems).

The activation depends on the phosphorylation status of Atg 13 by the inhibitor of autophagy the mammalian target of rapamycin (mTOR). mTOR is mainly regulated by PI3K/Akt/mTOR signaling pathway involved in inhibition of cell apoptosis, promotion of cell proliferation, cell survival, and angiogenesis (Hassan et al., 2013; Trigka et al., 2013). There are also mTOR-independent mechanisms of inducing autophagy, mechanistic TOR complex 1 (MTORC1).

mTOR activity is regulated by the interaction with Rheb, a small GTP-binding protein that activates mTOR. The GTP hydrolysis, promoted by the TSC1/TSC2 dimer formation, inactivates Rheb, thus negatively regulating mTOR kinase activity. Phosphorylation and inactivation of TSC1/TSC2 via the class I PI3K/AKT pathway stimulates mTOR activation by Rheb thus inhibiting autophagy (Pearce et al., 2010). In contrast, AMPK, which is activated by the high AMP/ATP ratios present when nutrients are limited, induces autophagy through a phosphorylation event that stimulates TSC1/TSC2 activity (Chan et al., 2009).

Inactivation of mTOR kinase dephosphorylates Atg13 allowing association with the scaffold protein, Atg 17, complex formation with ULK1, stimulating its kinase activity. The complex then localizes to the isolation membrane where nucleation proceeds (Karanasios et al., 2013). Vesicle nucleation begins when Beclin-1 associates with the effected UV radiation resistance-associated gene (UVRAG). This stimulates

the activity of the lipid kinase class III phosphatidylinositol 3-kinase (PI3-K) (VPS 34) to promote the activation of the elongation process and autophagosome biogenesis (Zhong et al., 2009).

The Atg proteins involved in autophagosome formation consist of several functional products: Atg1 kinase and its regulators, the PI3K complex, Atg9, the Atg2-Atg18 complex, and two ubiquitin-like conjugation systems. Also, it is known as the ‘core’ molecular machinery (Xie and Klionsky, 2007). These types of core Atg proteins consist of 4 subgroups: firstly, the ULK complex secondly, two ubiquitin-like protein (Atg12 and Atg8/LC3) conjugation systems; thirdly, the class III phosphatidylinositol 3-kinase (PtdIns3K)/Vps34 complex I; and fourthly, two transmembrane proteins, Atg9/mAtg9 (and associated proteins involved in its movement such as Atg18/WIPI-1) and VMP1. The suggested site for autophagosome formation, to be able to that almost the entire core Atg proteins are recruited, is called the phagophore assembly site (PAS).

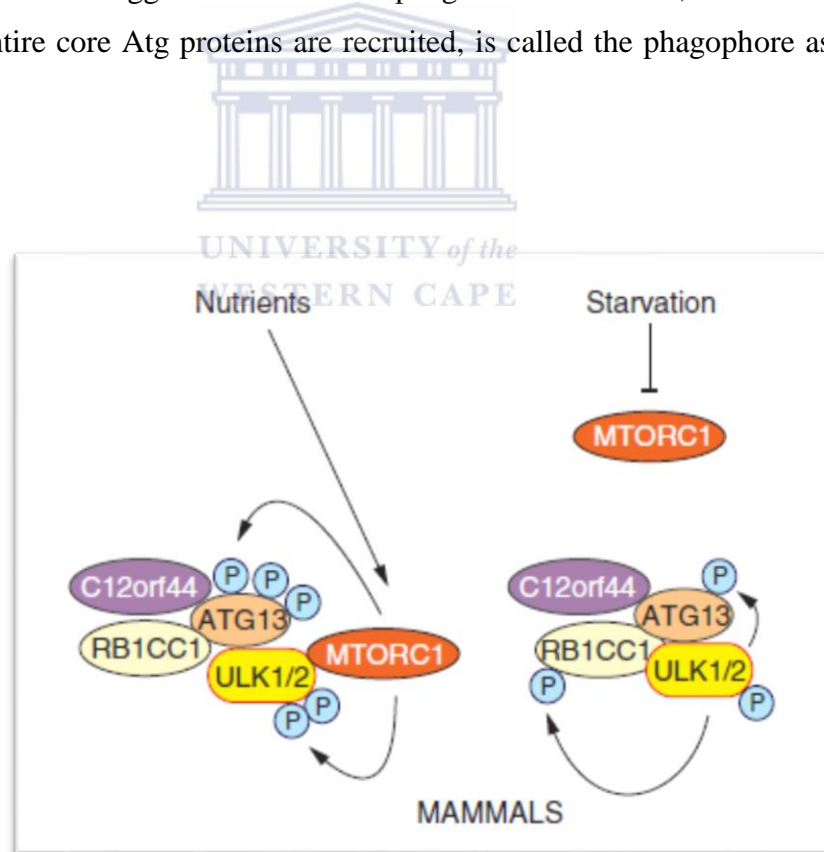


Figure 1.7: Regulation ULK1/2 complex in mammals.

Source (Mah and Ryan, 2012)

ATG13 forms a complex with ULK1/2. Under nutrient-rich conditions, mechanistic TOR complex 1 (MTORC1) also binds with the ULK1/2 complex and phosphorylates ATG13 and ULK1/2. Upon starvation MTORC1 activity is inhibited and disassociated from the ULK1/2 complex. ULK1/2 is activated and phosphorylates ATG13 and RB1CC1, the mammalian functional homolog of yeast Atg17. The mammalian ULK1/2 complex contains a component, C12orf44, which does not have a known yeast homolog, and whose function remains unclear (Feng et al., 2014).

In mammalian cells, there are two types phosphatidylinositol triphosphate kinases (PtdIns3K), class I and class III; the class III enzymes are the orthologs of yeast Vps34. PIK3C3/VPS34, BECN1 (the mammalian homolog of yeast Vps30), and PIK3R4/p150 (the homolog of Vps15) are the core components in two different complexes. One complex additionally contains the homolog of Atg14, ATG14/ATG14L/Barkor, and is required specifically for autophagy, whereas the other complex includes the homolog of Vps38, ultraviolet irradiation resistance-associated gene (UVRAG), and mediates endocytosis but also regulates autophagy in several ways (Fimia et al., 2014). Elongation entails the use of two conjugation systems, namely the Atg12-Atg5 and phosphatidylethanolamine-Atg8 systems. Both systems resemble the ubiquitin-proteasomal pathways (Nakatogawa, 2013). The two systems are illustrated in Fig. 1.6.

The first system entails the conjugation of Atg12 and Atg5 homologs through the generation of an isopeptide bond between the Atg12 C-terminal glycine and the Atg5 Lys130 residue, which is catalysed by E1-like Atg7 and E2-like Atg10 enzymes. Cys572 of Atg7 is the active site cysteine residue that is essential for its interaction with Atg12 (Mah and Ryan, 2012). This conjugate localizes onto an isolation membrane where it becomes associated with Atg1bL (mammalian homolog). The second conjugation system involves the mammalian of the yeast Atg8 homologue called microtubule-associated protein1 light chain 3 (LC3) (Mizushima et al., 2010).

Atg4 protease, Atg4b removes the amino acids located C-terminally from the last glycine residue of the nascent unprocessed form of LC3, producing soluble cytosolic

LC3-I. After activation of LC3-I by E1-like Atg7 and E2-like ATG7, it is conjugated with phosphatidylethanolamine (PE) to form membrane-associated LC3-II, which can ultimately be cleaved by Atg4B in a deconjugation step (Mah and Ryan, 2012). The site of LC3-II anchorage is dependent on Atg1bL which recruits the soluble LC3-1 polypeptide to the vicinity of PE in the membrane. Modification and localization of cytosolic LC3-1 to autophagosomal LC3-II is used as a marker for autophagosome formation (Kabeya, 2000). Upon closure of the phagophore, maturation proceeds by fusion with the endosomal or lysosomal vesicles. Sequestosome (P62/SQSTM1) is a cargo receptor protein that recognizes polyubiquitinated targets via their C terminal domains in cargo selectivity. The P62 protein is cleared along with the cargo and is used as a biomarker of the autophagic process (Jiang and Mizushima, 2014).

1.4.2.2 Signalling pathways regulating autophagy

During nutrient deprivation, autophagosome formation is dramatically induced. One of the major intracellular pathways of autophagy is the phosphatidylinositol-3-kinases–AKT (PI3K–AKT) and mammalian target of rapamycin (mTOR) kinase pathway (Yuan and Kroemer, 2010).

1.4.2.2.1 Lkb1-Ampk-Autophagy-Axis

Under bioenergetic stress conditions, the depletion of cellular ATP causes elevation in the AMP: ATP ratio (Hill et al., 2009). The parameter is sensed by the AMP-activated protein kinase (AMPK) responsible for monitoring intracellular energy status and controlling glucose (Manning et al., 2002), lipid and protein metabolism. The activity of mTOR is inversely correlated with activated AMPK (Hardie et al., 2012).

Activation of AMPK by LKB1 suppresses growth and proliferation and promotes catabolic and energy producing pathways maintaining cell polarity thereby inhibiting inappropriate expansion of tumor cells (Hardie et al., 2012). AMPK is thus a signal switch that monitors and regulates systemic and cellular energy status (Hardie et al., 2012). Furthermore, the elevated level of calcium and calmodulin-dependent protein

kinase kinase β (CAMKK β) up-regulates LKB1-AMPK-mTOR signaling pathway and induce autophagy (Xiao et al., 2011).

mTORC1 controls the translation of a number of cell growth regulators, including cyclin D1, hypoxia inducible factor 1 α (HIF-1 α), and c-myc, which in turn promote processes including cell cycle progression, cell growth and angiogenesis, all of which can become deregulated during tumorigenesis (Bell et al., 2011). Aberrant mTOR signaling is involved in many diseases states including cancer, cardiovascular disease, and metabolic disorders (Laplante and Sabatini, 2012).

1.5 Crosstalk between autophagy and apoptosis in mammalian cells (Fig. 1.8)

Death-associated protein kinase (DAPK) has been proposed to convert autophagy from a cell survival mechanism to one of the initiation of apoptosis (Xiao et al., 2011). Caspase 3 cleaves Atg4D to generate a truncated product, N63 Atg4D that, when overexpressed, induces autophagy-independent apoptosis (Fig. 1.8) (Xiao et al., 2011). Atg5, when cleaved by calpains, generate a truncated product 24KAtg5 that, when overexpressed by itself, induces apoptosis, but not autophagy (Kang et al., 2011). Cytoplasmic p53 has also been shown to suppress autophagy, through yet undetermined protein interactors. Both full-length p14ARF and a small mitochondrial isoform of this protein (smARF) have been shown to promote autophagy. In particular, smARF may promote the autophagic flow by releasing Bec-1 from Bcl-XL dependent inhibitory interactions (Mah and Ryan, 2012).

1.5.1 The role of Beclin-1 in apoptosis and autophagy

Caspases also cleave the BH3-only Beclin-1 at Asp149 during apoptosis resulting in the inhibition of autophagy (Fig. 1.8). However, unlike other known BH3-only proteins, Beclin-1 does not function as a pro-apoptotic molecule, even if it is overexpressed (Kang et al., 2011). Beclin-1 shows anti-apoptotic properties during chemotherapy, irradiation, immunotherapy, nutrient deprivation, angiogenesis inhibitors and hypoxia (Kang et al., 2011). The precise mechanism by which Beclin-1

inhibits apoptosis is not yet clear, but may be related to unregulated autophagy as an adaptive or anti-injury mechanism, clearing apoptotic cells. Caspase-3-, 7- and 8-mediated apoptosis can cleave Beclin-1 generating N- and C-terminal fragments destroying the pro-autophagic activity of Beclin-1 (Ola et al., 2011). The C-terminal fragments translocate to mitochondria and sensitize cells to apoptotic signals (Kang et al., 2011). It was shown that TRAIL, a death receptor ligand, triggered the caspase-mediated cleavage of Beclin-1 in cervical carcinoma cells *in vitro* (Trigka et al., 2013). Autophagy and apoptosis share common stimuli and signaling pathways; therefore cell life or death, depends on the cell response and which process is dominant (Trigka et al., 2013). Although apoptosis-associated cleavage of Beclin-1 and Atg5 inactivates autophagy, the cleavage of Atg4D by caspase-3 generates a fragment with increased autophagic activity (Chen and Klionsky, 2011).

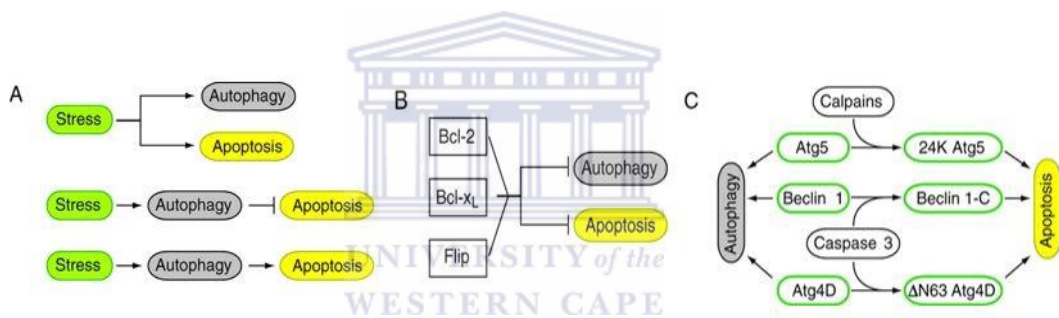


Figure 1.8: Crosstalk between autophagy and apoptosis in mammalian cells. In a cell, the same stress induces both autophagy and apoptosis as independent processes (left). A stress can also induce autophagy, which then inhibits apoptosis (middle) or, alternatively, a stress induces autophagy, which can be the trigger of apoptosis (right). (B) Both autophagy and apoptosis are negatively regulated by Bcl-2, Bcl-xL and Flip. (C) Autophagy proteins Atg5, beclin 1 and Atg4D function in autophagy in their unmodified form, but also have a role in apoptosis after cleavage by either calpains, which target Atg5 and give rise to 24 K Atg5, or caspase 3, which cleaves beclin 1, resulting in a C-terminal fragment of beclin 1 (Beclin 1-C), and Atg4D, truncating it at the canonical caspase cleavage sequence (DEVD63K) to Δ N63 Atg4D.

Source (Chen and Klionsky, 2011)

1.6 Terpenoids

Terpenoids, flavonoids and alkaloids are the three major types of plant-derived compounds used for their medicinal properties. Terpenoids which are also known as isoprenoids a form subclass of prenyllipids (terpenes, prenylquinones and sterols) of which there are almost 40 000 different types which have been isolated in plants, animals and microbial species (Brahmkshatriya and Brahmkshatriya, 2013). They serve a wide range of functions in nature including defensive resins, pheromones, antioxidants, and the pigments responsible for vision (Beukes et al., 2014). The best-known terpenoid pharmaceutical is the anticancer drug paclitaxel. Steroid hormones in animals are terpenoids and the plant hormones cytokinin, gibberellin and abscisic acid are derivatives of terpenoids (Wangersky, 1993). Terpenoids can be modified to produce thousands of different intermediates and metabolites. Oxidation of terpenes is affected by their methyl groups and by moving, removing or adding of oxygen atoms. Terpenoids are also used for communication between organisms. Triterpenoids in plants can act as repellent or attractant (Beukes et al., 2014). Some terpenoids have antibiotic characteristics. Terpenoids are electron carriers (ubiquinone) facilitate polysaccharide assembly (polyprenyl phosphates) and form part of the membrane structure (phytosterols) (Wangersky, 1993). All terpenoids are derived from one of two isomers, isopentyl diphosphate (IPP) and dimethylallyl diphosphate or geranyl pyrophosphate (GPP) via the traditional mevalonate or methylerythritol phosphate pathway or both (Fig. 1.10).

Table 1.1: The basic molecular structure of terpenes. Source (Wangersky, 1993)

Terpene	Isoprene Unit	Carbon Atoms
Monoterpenes	2	10
Sesquiterpenes	3	15
Diterpenes	4	20
Sesterpenes	5	25
Triterpenes	6	30
Carotenoids	8	40
Rubber	>100	>500

IPP and DMAPP (the isomer dimethylallyl diphosphate) are simultaneously produced from pyruvate and glyceraldehyde-3-phosphate via the non-mevalonate pathway or 2C-methyl-D-erythritol 4-phosphate (MEP) pathway whereas acetyl-CoA produces IPP via the Mevalonic acid (MVA) pathway (Pulido et al., 2012).

Despite the knowledge of the synthetic pathway involved in the synthesis of terpenes, these compounds are traditionally known as derivatives of isoprene, a five- carbon acyclic chain (C₅H₈) (Pulido et al., 2012). Based on the number of building blocks, terpenes are commonly classified as monoterpenes (C₁₀), sesquiterpenes (C₁₅), diterpenes (C₂₀), triterpenes (C₃₀) and tetraterpenes (C₄₀) (Fig. 1.9).

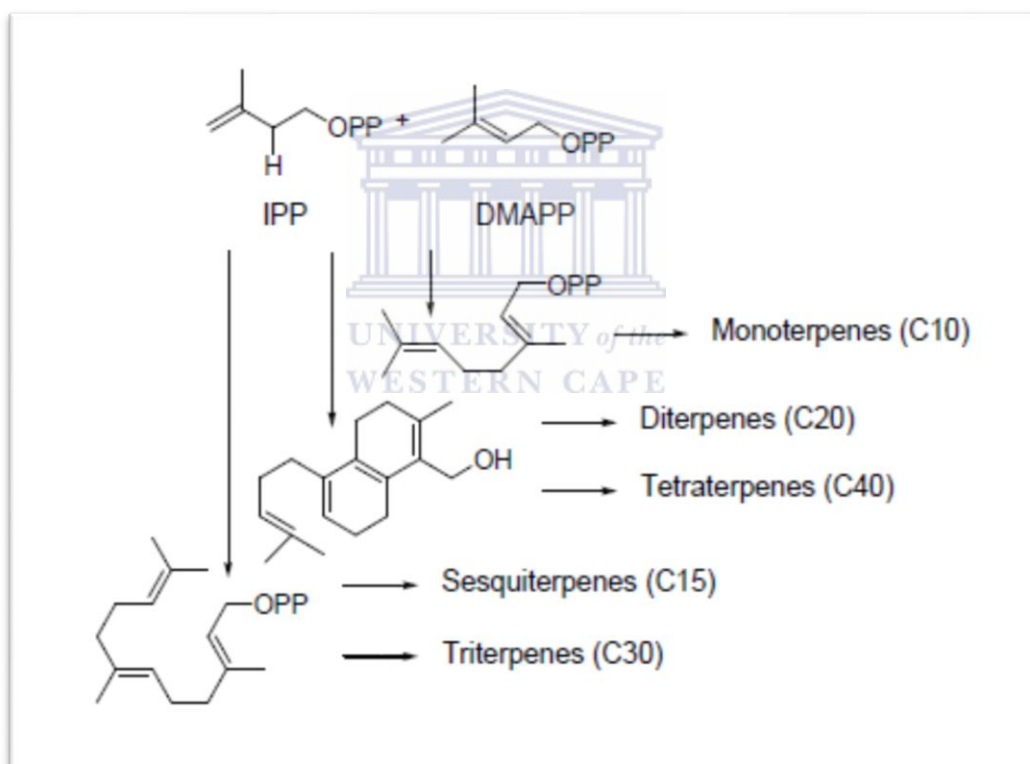


Figure 1.9: Simplified scheme of the origin of the diverse biosynthetic plant terpene classes

Source (Pulido et al., 2012)

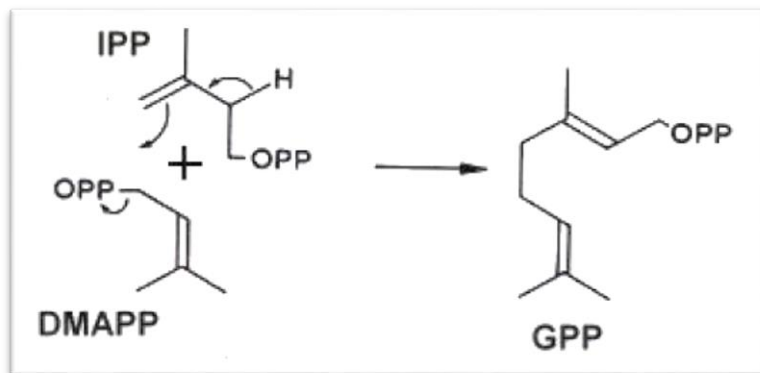


Figure 1.10: The biosynthesis of terpenes from isopentenyl diphosphate (IPP) and dimethylallyl diphosphate (DMAPP) to form geranyl pyrophosphate (GPP).

Source (Pulido et al., 2012)

Synthesis of sesquiterpenes, triterpenes, sterols and polyterpenes utilizes cytosolic IPP as precursor whereas monoterpenes, diterpenes and tetrapenes precursor IPP derives from the plastids as precursor (Pulido et al., 2012). The majority of the bioactive terpenes are found in plants (Muffler et al., 2011). With mono- and sesquiterpenes are mainly present in oils of plant raw material, and the higher terpenes, such as triterpenes, are mostly obtained in balsams and resins (Abe, 2007; Steigenberger and Herm, 2011).

1.6.1 Triterpenes

1.6.1.1 Uroslic Acid

Ursolic acid (UA) or 3 β -hydroxyurs-12-en-28-oic acid is a pentacyclic triterpenoid that occurs in numerous plants and is a constituent of several anti-inflammatory herbal medicine (Fig. 1.11) (Mitsuda et al., 2014).

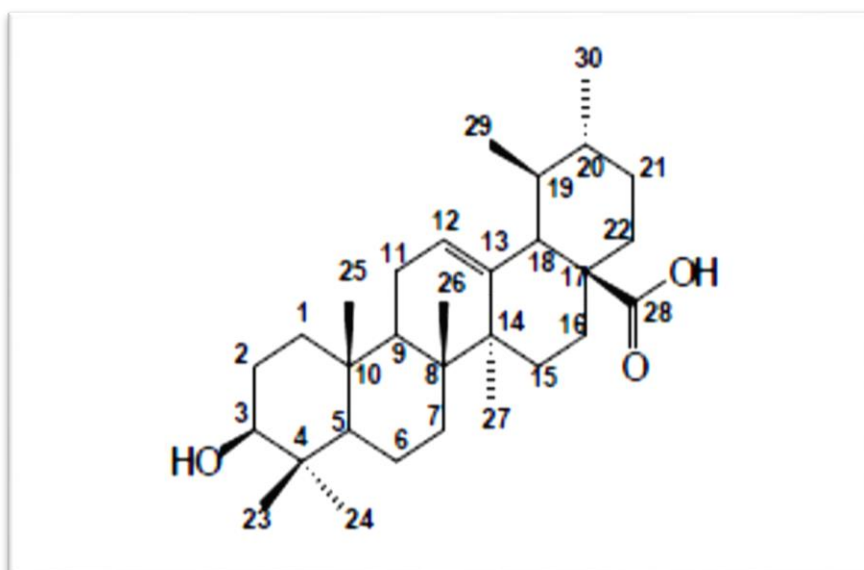


Figure 1.11: Molecular structure of UA

Source (Leipold et al., 2010)

As an effective natural anticancer drug, UA has also been reported to show significant cytotoxicity against some tumor cell lines such as, colon cancer cells, endometrial cancer cells, prostate cancer, colon- and renal cancer and melanoma (Shanmugam et al., 2012). However, the low bioavailability of UA *in vivo* restricts its clinical application (Debnath et al., 2010). Chemical modifications in UA have been widely investigated in recent years to improve its antitumor activities and bioavailability (Shanmugam et al., 2012). Following this trend, the anti-proliferative activity of UA hydroxycinnamate esters isolated from cranberry fruit was tested in tumor cell lines. The esters inhibited the growth of several lung, colon, breast and renal cancers, melanoma and leukemia cell lines.

Some studies have shown that UA exhibits growth inhibition properties against many human cancer cell lines *in vitro*, including HepG2 (Hepatoma cells), MCF-7 breast cancer cells, Caco-2 colon cancer cells and SNG-II endometrial cancer cells. The anti-cancer properties of UA seen in cultured human melanoma cells were possibly mediated through the induction of apoptosis following activation of caspases

(Mahmoudi et al., 2015). UA has also been shown to activate different apoptotic processes in the endometrial cancer SNG-II cell line and activated the mitochondrial apoptotic pathway in colon cancer cells and apoptosis in M4Beu melanoma cells (Wang et al., 2011).

UA decreased proliferation of HT-29 colon carcinoma cells by induction of apoptosis accompanied by activation of caspases-3, 8 and 9 and by intracellular Ca^{2+} release in HL 60 leukemia cells (Tsai et al., 2009). UA caused enhanced release of cytochrome C, caspase activation, and down-regulation of inhibitor of apoptosis proteins (c-IAPs) in prostate cancer (Kim et al., 2012). In B 16F-10 melanoma cells, UA resulted in apoptosis accompanied by upregulation of the tumor suppressor gene p53 and caspase-3 and down-regulation of Bel-2 (Huang et al., 2012). Caspase-3 activation by UA through the mitochondrial pathway with upregulation of pro-apoptotic Bax and a decrease in Bel-2 was reported in M4Beu human melanoma cells after UA treatment (Debnath et al., 2010). UAs have also induced apoptosis by acting as a sensitizer for TRAIL-induced apoptotic cell death in prostate cancer treatments (Shin and Park, 2013).

UA has been shown to decrease prostate tumor invasion and increased risk of metastasis (Kassi et al., 2007). An *in vitro* study on DU145 prostate cells showed that UA induced a G1-phase arrest mediated by p53/p21 (Hsu et al., 2004). The researchers furthermore found that UA up-regulated p53:NF- κ B and the expression level of apoptosis-related protein (Fas/APO-1) Fas ligand and Bax) resulting in apoptosis (Hsu et al., 2004).

According to Ovesná et al. (2006), UA and OA can act on various stages of tumor development, including the inhibition of tumorigenesis, inhibition during tumor promotion, and induction of tumor cell differentiation. Several other pharmacological effects, such as anti-tumor, hepato-protective, anti-inflammatory (oral & topical), anti-ulcer, antimicrobial, anti-hyperlipidemic, and anti-viral activities, have also been attributed to UA (Misra et al., 2014).

1.6.1.2 Biosynthesis of ursolic acid

Synthesis of the precursors of UA from squalene is shown in Fig1.12. Dammarenyl (I) undergoes ring expansion, followed by an additional cyclization to form oleanyl cation, lupenyl cation and lupeol (Leipold et al., 2010). The folding and cyclization of squalene lead to the dammarenyl ring system (I) (Fig. 13) (Leipold et al., 2010). Ursolic acid (4) contains an α -amyrin skeleton and the C30 isomer, β -amyrin is found in oleanolic acid (5).

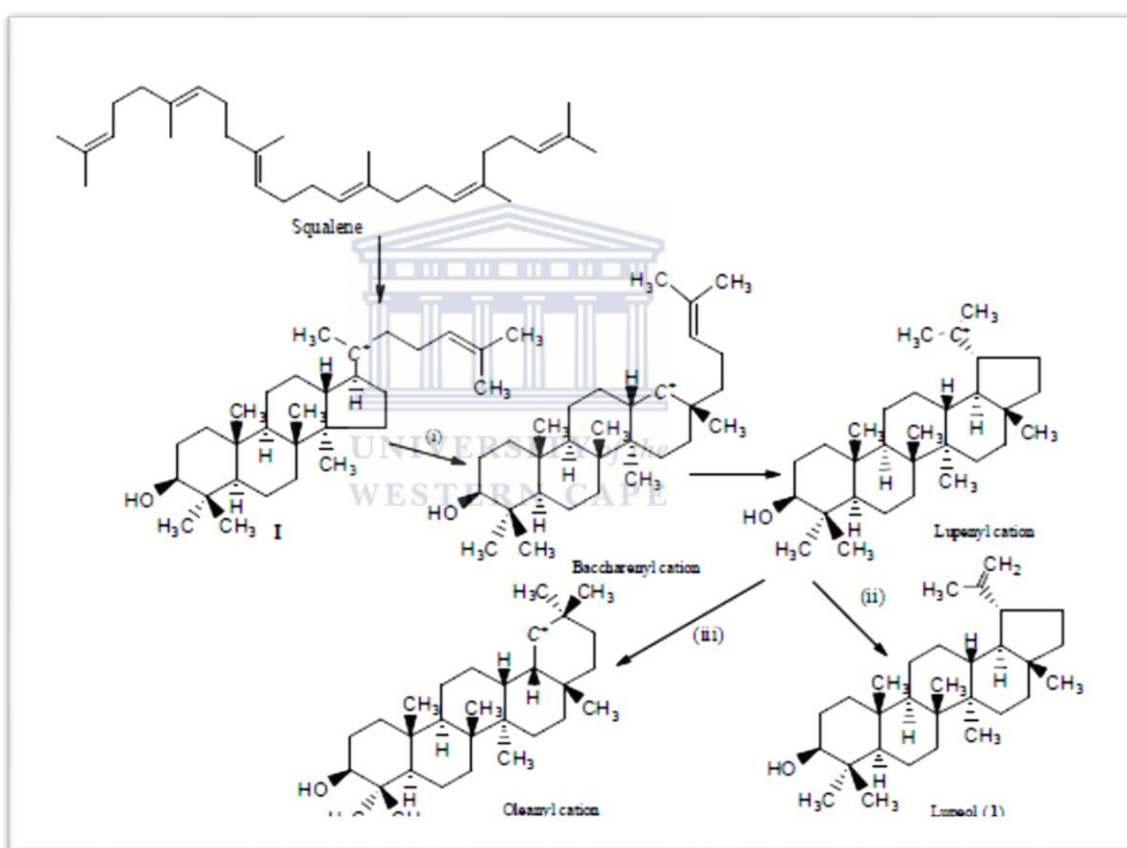


Figure 1.12: Biosynthesis of dammarenyl cation (I), oleanyl cation, lupenyl cation and lupeol (1)

Source (Babalola and Shode, 2013)

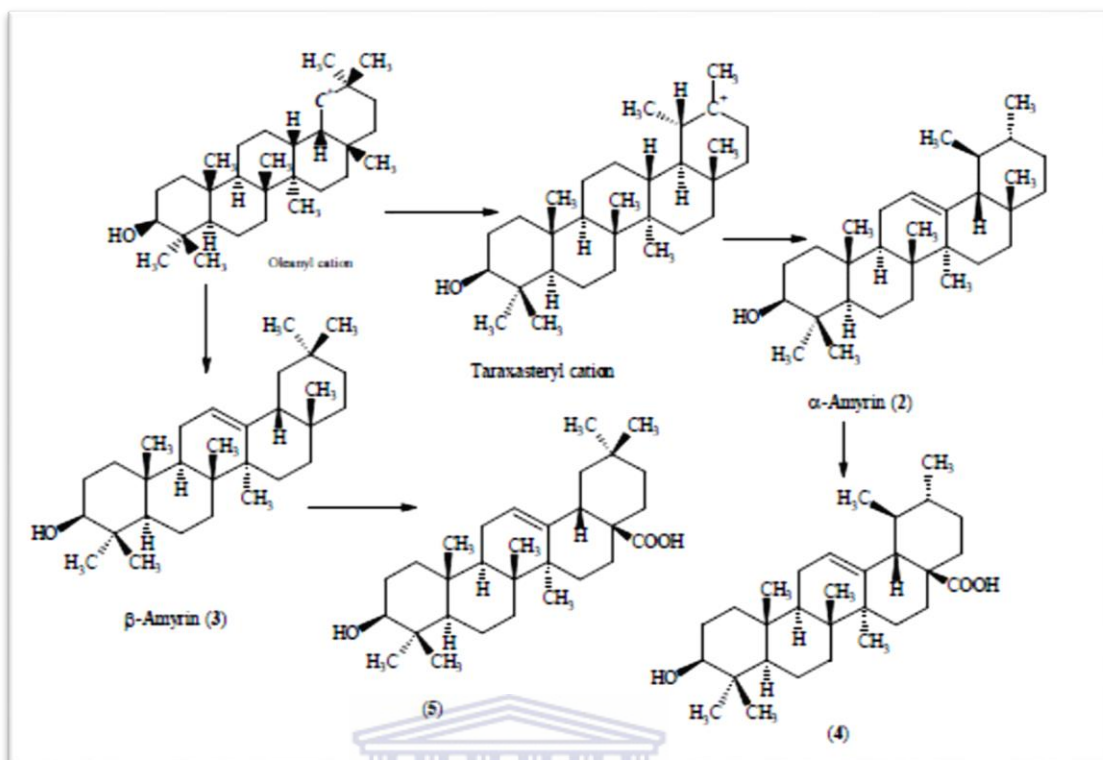


Figure 1.13: Biosynthesis of ursolic acid (4) and oleanolic acid (5) from oleanyl cation.

Source (Babalola and Shode, 2013)

UNIVERSITY of the
WESTERN CAPE

1.6.1.3 Oleanolic Acid

Oleanolic acid or oleanic acid is a pentacyclic triterpenoid found in the leaves and roots of *Olea europaea*, *Viscum album* L., *Aralia chinensis* L., *Phytolacca americana* (American pokeweed) and *Syzygium* spp and over 120 other plant species (Pollier and Goossens, 2012; Reisman et al., 2009). It is chemically known as 3 β -hydroxy-olean-12-en-28-oic acid, Fig. 1.14.

In plants OA is in the form of free or combined glycosides, it has wide range of pharmacological affects, it is mainly used for the treatment of acute jaundice hepatitis and chronic viral hepatitis currently.

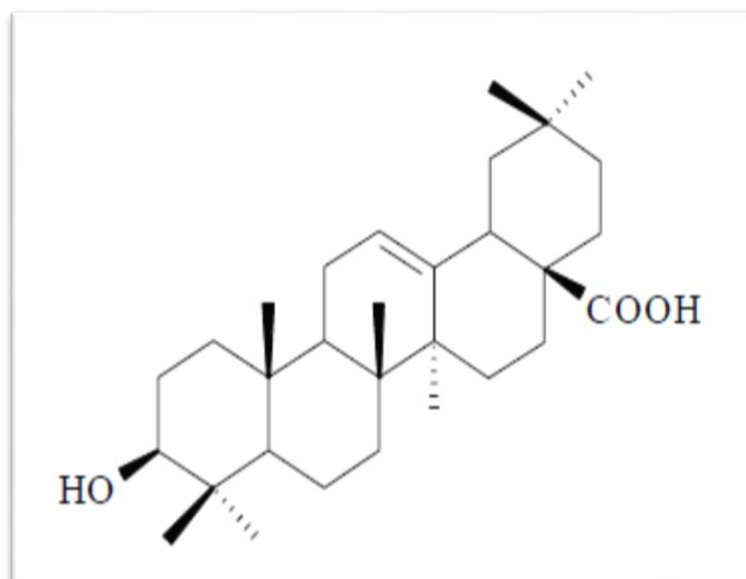


Figure 1.14: Molecular structure of OA.

Source (Leipold et al., 2010)

OA is relatively non-toxic, hepatoprotective, and exhibits antitumor and antiviral properties (Banik and Pandey, 2008). It is used in the treatment of acute chemically induced liver injury, chronic liver fibrosis and cirrhosis (Feng et al., 2009). OA exhibits many biological activities such as anti-inflammatory, antitumor, antiviral, hepatoprotective and anti-hyperlipidemic effects. OA has been used in Chinese medicine to treat liver disorders for over 20 years (Wang et al., 2010).

OA has been shown to protect mice from various hepatotoxicants that cause oxidative and electrophilic stress, including carbon tetrachloride, acetaminophen, bromobenzene and thioacetamide (Reisman et al., 2009). Despite its use as a hepatoprotective drug and various anti-proliferative studies, the mechanism of action of OA remains to be fully elucidated (Asadi-Samani et al., 2015).

Other pharmacological effects of OA include the beneficial effects on the cardiovascular systems, interaction with cytochrome P450s, protection against kainate-induced excitotoxicity in rat hippocampal neurons and immunomodulatory effects, as well as its effects on intracellular redox balance and osteoclast formation (Liu, 2005).

OA has been shown to have significant anti-tumor activity, inhibiting growth of human hepatocellular carcinoma HuH7 cells with IC₅₀ values of 100 and 75 μ M, respectively (Shyu et al., 2010). The possible mechanisms of action this of inhibitory effect is suggested to be the induction of cell-cycle arrest in HCT-15 cells and mitochondria-mediated intrinsic apoptosis in hepatocellular carcinoma cells (Shyu et al., 2010). OA induces apoptosis via up-regulation of cell cycle-related and other apoptotic genes like, p53, p21 and p27, Bax, caspase-9, and caspase-3 in lung cancer and reduces metastasis of B16F-10 melanoma cells (Lúcio et al., 2011). Inhibitory effects of OA on the growth of human bladder, prostate, pancreatic and colorectal cancer cell lines have furthermore been reported (Deretic and Levine, 2009; Kassi et al., 2007). OA was shown to induce apoptosis in human glioblastoma and neuroblastoma cells by inhibiting pro-survival p-Akt, NF- κ B (P65) and Notch1 signaling pathways (Gao et al., 2007). OA have been found to be active in various stages of tumor development, including inhibition of tumor promotion, invasion and metastasis (Shishodia et al., 2003).

Inflammation plays an important role in the development and progression of cancer (Mantovani et al., 2008) and NF- κ B, a key transcription factor involved in inflammation, is commonly overexpressed in cancer cells, thereby suppressing apoptosis of the tumor cells and maintaining a chronically inflamed microenvironment beneficial for cancer proliferation (Laszczyk, 2009). A study by Laszczyk, (2009) showed the anti-inflammatory and anticancer potential of OA. They postulated that OA acted most likely by targeting NF- κ B, however, its exact mode of action remains to be discovered. It has been shown that OA is not only a free radical-scavenger acting through direct chemical reactions with reactive oxygen species, but also that the main antioxidant activity of the molecule is due to the Nrf2-mediated increased expression of antioxidant enzymes such as catalase and thioredoxin peroxidase, and the enhanced biosynthesis of the antioxidant glutathione.

1.6.1.4 Biosynthesis of OA

The precursor molecule in the plant cell cytoplasm, 2, 3-oxidosqualene, is synthesized from isopentenyl pyrophosphate via the mevalonate pathway (Pollier and Goossens, 2012). Cyclization of 2, 3-oxidosqualene leads to the branch-point between the primary sterol and the secondary triterpenoid metabolism producing OA (Nataraju et al., 2009; Xue et al., 2012). 2, 3-oxidosqualene can also be cyclized through cycloartenol synthase (CAS) to produce this tetracyclic plant sterol precursor cycloartenol (Abe, 2007). The biosynthesis of OA (Fig. 1.15) shows that 2, 3-oxidosqualene is cyclized to the pentacyclic oleanane-type triterpenoid backbone β -amyrin by the OSC β -amyrin synthase (BAS) (Cammalleri et al., 2008). BAS was first cloned from the medicinal plant *Panax ginseng* (Kushiro et al., 1998), and later from a variety of other plant species, including the olive (Morikawa et al., 2007). Lastly, β -amyrin is further converted to OA by oleanolic acid synthase (OAS, a P450 enzyme), which catalyses a three-step, sequential oxidation at the C-28 position of β -amyrin at the C-28 position by a single cytochrome P450 enzyme to yield OA through erythrodiol (Domingo et al., 2012; Han et al., 2013). The cytochrome P450 enzyme is involved in these multi-steps of oxidation, CYP716A12 (Carelli et al., 2011; Urlacher and Girhard, 2012).

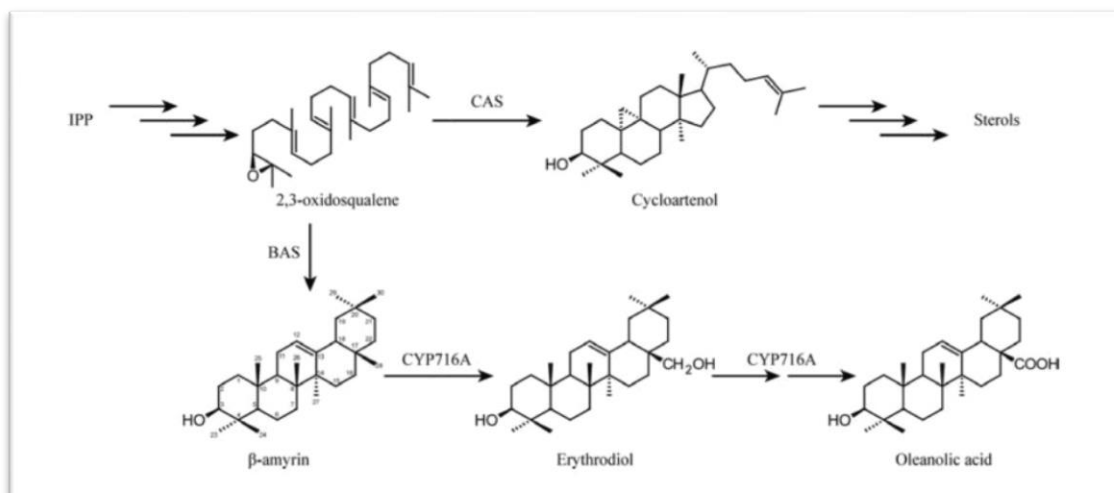


Figure 1.15: OA biosynthetic pathway. BAS = b-amyrin synthase, CAS = cycloartenol synthase, IPP = isopentenyl pyrophosphate.

Source (Pollier and Goossens, 2012)



UNIVERSITY of the
WESTERN CAPE

1.7 Objectives

This study was carried out to establish the possible anti-cancerous effects of OA and UA *in vitro* on the estrogen receptor (ER)⁺ breast epithelial adenocarcinoma cell line, MCF-7, and the non-tumorigenic human breast epithelial MCF-10 cell line.

Cellular and molecular analysis was employed to investigate the mechanisms of action of OA and UA. The aims were:

To determine OA and UA cytotoxicity in MCF-7 and MCF-10A cell lines.

To determine morphological effects of OA and UA on the two cell lines.

To establish and compare the molecular mechanisms elicited by OA and UA in cancer cells (MCF-7) and compare that to the effects in non-malignant (MCF-10A) cells.

To achieve these goals, the following steps were taken:

- I. Evaluation and quantification of influence of OA and UA on the morphology and cell growth using H & E stained cells.

- II. Quantification of a time-and-dose response of OA and UA using the crystal violet assay after exposure to 10, 20, 50 and 100ug/ml for 6-72h in both MCF-7 and MCF-10A cells.
- III. To evaluate cell death either by apoptosis or by autophagy by staining for the apoptotic/autophagic features of the cells.
- IV. Determination of ROS levels and detection apoptosis induction using Annexin-V FITC-PI.
- V. Evaluation of cell cycle progression after exposure to OA and UA.
- VI. Determination of the mechanisms of autophagy in treated MCF-7 and MCF-10A cells by evaluating Beclin-1 and LC3 using Western blot analysis.
- VII. To determine the Beclin-1 and LC3 gene-expression profile following treatment of the MCF-7 and MCF-10A cells using Quantitative PCR.



Chapter II

2 Materials and Methods

2.1 Materials

2.1.1 Biorad, UK supplied:

- Acrylamide/Bis 40%
- Polyvinyl difluoride membrane
- Prestained standard Kaleidoscope protein markers
- Temed
- Tris buffer
- Tris/glycine/SDS buffer for SDS PAGE
- Ponceau stain

2.1.2 Merck, Germany supplied:

- Ethanol (EtOH)
- Potassium chloride (KCL)
- Calcium chloride (CaCl₂)
- Sodium chloride (NaCl)
- Acetic acid (CH₃COOH)
- Methanol (MEOH)
- Sodium dodecyl sulfate (SDS)
- Xylene (XYL)
- Ribonuclease (RNase)
- Dimethylsulphoxide (DMSO)
- All chemicals were of analytical grade



2.1.3 Gibco BRL, Scotland supplied:

- Fetal bovine serum (FBS)
- Horse serum
- Gentamycin
- Penicillin/streptomycin
- Phosphate buffer saline (PBS)
- Dulbecco's Modified Eagle Medium: Nutrient Mixture F-12 (DMEM/F-12 Media)
- HyClone™ Trypsin

2.1.4 Sigma, Germany supplied:

- Epidermal growth factor (EGF)
- Hydrocortisone
- Insulin
- Trypsin 0.25%
- Bouins solution
- Haematoxylin
- Eosin B
- Trypan blue
- Ammonium persulphate (APS)
- Crystal violet stain
- Hepes
- Hoechst 33342
- Propidium iodide (PI)
- Acridine orange
- Sodium dodecyl sulphate (SDS)
- Triton X-100
- Tween® 20
- Glutaraldehyde



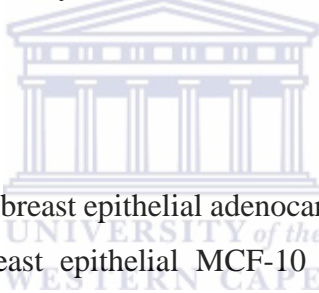
2.1.5 Life technological Sciences

- Tali® Apoptosis Kit – Annexin V Alexa Fluor® 488 and Propidium Iodide*for use with Tali® Assay: Apoptosis*
- CellROX® Orange Reagent kit.

2.1.6 Cell signaling technology

- LC3B Rabbit antibody
- Beclin-1 Rabbit antibody
- α Tublin antibody
- Anti-Rabbit Secondary Antibodies

2.2 Cell Lines



The estrogen receptor (ER)⁺ breast epithelial adenocarcinoma cell line MCF-7 and the non-tumorigenic human breast epithelial MCF-10 cell lines were acquired from American Type Culture Collection (ATCC). Low passage MCF-7 and 10A cells were used in all experiments. MCF-7 is a cell line that was first isolated in 1970 from a malignant adenocarcinoma in a pleural effusion of a Caucasian woman. MCF-7 cells have retained several characteristics of the mammary epithelium as well as intracellular estrogen receptors.

Genetic discrepancies exist between the MCF-7 cell line from the Michigan Cancer Foundation and the MCF-7 cell lines obtained from ATCC which has a karyotype containing 69 chromosomes. Although the ER status of MCF-10A and MCF-7 has been previously documented it has become widely accepted that receptor expression profiles may vary between different lots or batches of the same cell line (Marchese and Silva, 2012).

The MCF-10A human breast epithelial cells (Spink et al., 2006; Yusuf and Frenkel, 2010) stem from a 36 year old Caucasian female with fibrocystic breast disease (Soule et al., 1990). It is characterized as a non-tumorigenic cell line with estrogen and progesterone negative receptors (Tait et al., 1990). This cell line was chosen for this study as it can mimic the *in vivo* environment of normal breast epithelia (Soule et al., 1990; Tait et al., 1990).

2.3 Culture medium

The MCF-7 cells were maintained in Dulbecco's modified Eagle's medium (DMEM/F12) and Ham's F12 medium (1:1) mixture. This was supplemented with 5% fetal bovine serum and 0.2% penicillin/streptomycin (100 U/ml penicillin and 100µg/ml streptomycin).

The MFC-10A cells were maintained in DMEM F12. This was supplemented with 5% horse serum, 20ng/ml epidermal growth factor EGF, 1mg/ml hydrocortisone, and 1mg/ml cholera toxin, 10µg/ml, insulin and 5.0 ml penicillin/streptomycin. The cells were maintained in 75cm² culture flasks in a humidified atmosphere at 37°C. The media was changed every 3-4 days depending on the cell's growth and allowed to grow to 70-80% confluence before sub-culturing.

2.4 Supplements

2.4.1 Oleanolic acid and ursolic acid

The Oleanolic acid (purity $\geq 97\%$) and uroslic acid (purity $\geq 90\%$) were obtained from Sigma. The oleanolic acid (OA) and uroslic acid (UA) were made up as stock solutions in dimethyl sulfoxide (DMSO) and stored at 4°C until needed. Because the experiments required uniform levels of OA or UA throughout, the required amount of OA and UA was added to medium prior to dispensing it into the flasks or wells of the 96 or 6 well plates containing the attached cells. This method rules out effects of actual

contact of the OA or UA on cell viability when added directly. The final highest concentration of DMSO in the treated samples did not exceed 0.1%.

2.5 Cell treatments for experimental techniques

For all experimental procedure unless stated otherwise, the required amount of cells for each experiment were seeded and allowed to attach for 24 hours. Cells were then exposed to OA and UA separately at the following doses: 10µg/ml, 20µg/ml, 50µg/ml, and 100µg/ml for 6, 12, 24, 48 and 72h incubation periods. The effects of OA and UA on the two cell line were studied looking at following: cell viability (crystal violet staining), morphological changes and cell proliferation using light microscopy and haematoxylin and eosin stained cells, using fluorescence possible cell death including apoptosis and autophagy microscopy (Hoechst stain and triple stain (Hoechst, Propidium iodide and Acridine orange), apoptosis detection and quantification (Tali® Apoptosis Kit - Annexin V Alexa Fluor® 488 & Propidium Iodide), reactive oxygen stress (ROS) detection (Tali® Image-Based Cytometer and CellROX®Orange Reagent), cell cycle progression analysis (flow cytometry) and for further autophagy detection, western blotting and RT-PCR.

2.5.1 Estradiol proliferative assay

As described in section 2.5.3. 5000 cells were seeded per well in 96 well plates and allowed to attach for 24 hours, after which the culture medium was removed from the wells and the cells were exposed to 10, 20, 50, 80 and 100pg/l 17β-estradiol for 48 and 72 hours. Proliferative effects of 17β-estradiol on MCF-7 and MCF-10A cells were determined using a crystal violet assay (section 2.5.3).

2.5.2 ER status of MCF-10A cells

MCF-10A cells are mammary epithelial cells which are one of the targets of sex hormones to stimulate development (Musgrove et al., 1998). As mentioned in Section 2.3, receptor expression profiles may vary between different lots or batches of the same

cell line. To establish the ER status in this specific MCF-10A line as the status could have an influence on cell signalling, MCF-10A cells were exposed to combinations of 17 β -estradiol, estriol and progesterone (10, 20 and 40pg/l estriol-progesterone respectively) for 48 and 72 hour periods. The “priming” of MCF-10A cells was carried out in an attempt to elicit expression of ERs in the cells. This was done to assist with the interpretation of signalling effects induced by OA and UA. The method is described in Section 2.11. Modifications include the use of 1/5000 v/v diluted horse-radish peroxidase conjugated anti-mouse immunoglobulin (Stressgen bioreagents). The primary anti-ER α mouse monoclonal antibody was a gift from Prof EJ Pool, Department of Medical Biosciences, University of the Western Cape.

2.5.3 Cell Viability

The crystal violet staining (CVS) assay is used to detect cytotoxicity as it stains only viable cells (Itagaki et al., 1991; Saotome et al., 1989). This assay is based on the growth reduction rate reflected by the colorimetric determination of the stained cells. Cells were seeded at approximately 5000 cells per well in 200 μ l of culture medium in 96-well plates, and allowed to attached for 24 hours. The cells were exposed to the different concentrations 10-100 μ g/ml of OA and UA for periods of 6, 12, 24, 48 and 72 hours.

After cells were treated, the medium was removed from each well and 100 μ l of 1% gluteraldehyde in phosphate buffered saline (PBS) was added for 15 minutes. The cells were stained with 0.1% crystal violet (CV) in PBS for 30 min. The culture plates were then immersed in running tap water for 15 minutes and left to dry. 200 μ l of 0.2% Triton X-100 in PBS were added to each well and incubated at room temperature for 30 min. 100 μ l of staining solution was transferred to new 96 well plates. The absorbances of the samples were measured at 570 nm using an ELISA reader (GloMax Multi Detection System). The viability was calculated independent colour using the formula (Equation 1) below.

Equation 1:

$$\text{Rate of cell proliferation/inhibition (\%)} = \frac{\text{Control samples} - \text{Treatments samples (absorbation)}}{\text{Control samples} \times 100}$$

2.5.4 Morphological effects

2.5.4.1 Light microscopy: Haematoxylin and Eosin staining

Hematoxylin and eosin cell staining (H and E) was conducted as a standard microscopic technique for qualitative evaluation of cellular morphology and in order to calculate the mitotic indices for quantitation of the cell cycle phase shift and abnormal morphology. Equal numbers of cells were seeded on sterilized coverslips placed in 6 well plates and allowed to attach for 24 hours. Thereafter, the cells were exposed to OA and UA at concentrations and times periods as explained in section 2.6.

The cover slips with the attached treated cells were fixed in Bouin's solution and stained with haematoxylin and eosin using standard procedures. The cover slips were cleared in xylene and mounted on glass slides. The slides were then examined for morphological changes using a light microscope Nikon. Quantification of cell proliferation was carried out by counting 1000 cells on every coverslip of the H and E stained cells.

2.5.5 Fluorescent microscopy

2.5.5.1 Apoptosis, autophagy and necrosis detection

Hoechst 33342 (2'-[4-ethoxyphenyl]-5-[4-methyl-1-piperazinyl]-2,5'-bi-1H-benzimidazole trihydrochloride trihydrate) is a fluorescent dye that can penetrate intact cell membranes of viable cells and cells undergoing apoptosis and binds to adenine-thymine (A-T) base pair sections of DNA thus staining the nucleus (Latt et al., 1975).

MCF-7 and MCF-10A cells were plated at a density of 3×10^5 cells per well onto cover slips in 6-well plates. After incubation for 24h to allow attachment, the cells were treated with OA and UA at dosages 10-100 μ g/ml and incubated for 6-72h. The cells attached to the cover slips were stained with 1 μ g/ml Hoechst in medium for 30 min at 37°C. Following this, the cells were washed three times with PBS and mounted using a solution of 0.5% p-phenylenediamine in 20mM Tris (pH 8.8) and 90% glycerol. The cells were analysed by a Nikon fluorescent microscope using a 450nm emission filter.

2.5.5.2 Triple Fluorescence staining: Hoechst, Propidium iodide and Acridine Orange stain.

A triple Fluorescence dye staining method using acridine orange (green), Hoechst 33342 (blue) and propidium iodide (red) was used to identify the presence of apoptosis, autophagy or necrosis. Hoechst nucleic acid stain, as mentioned in section 2.4.3.1, is often used to distinguish condensed pycnotic nuclei in apoptotic cells while propidium iodide (PI) is a red-fluorescent dye that is unable to penetrate an intact membrane and therefore stains the nucleus of cells that have lost their membrane's integrity due to necrotic processes. Acridine orange (AO) is a lysosomotropic fluorescent compound that serves as a tracer for acidic vesicular organelles including autophagic vacuoles and lysosomes (Klionsky et al., 2007). Cells undergoing autophagy will have an increased tendency for acridine staining when compared to viable cells, however acridine orange is not a specific marker for autophagy and therefore other techniques are needed to verify increased autophagic activity.

The cells were seeded and treated with OA and UA as explained in section 2.4.3.1. 0.5ml Hoechst was added to the cells to provide a final concentration of 0.9 μ M. After 25 minutes into incubation, 0.5 ml of AO solution (4 μ g/ml in PBS) was added to the medium to give a final concentration of 1 μ g/ml and incubated for 5min at 37°C. Finally 0.5 ml of PI solution (40 μ g/ml in PBS) was also added to the medium to provide a final concentration of 12 μ M and incubated for the next 5 minutes at 37°C. The cells were washed thrice with PBS and mounted in an antifade solution of 0.5% p-phenylenediamine in 20mM Tris (pH 8.8) and 90% glycerol on glass slides. Samples

were examined with a Zeiss inverted Axiovert CFL40 microscope and Zeiss Axiovert MRm monochrome camera using Zeiss Filter 2 for Hoechst 33342-stained cells (blue emission), Zeiss Filter 9 for acridine orange-stained cells (green emission) and Zeiss filter 15 for propidium iodide stained cells (red emission). In order to prevent fluorescent dye quenching all procedures were performed in dark room by using plates and reagents covered with foil.

2.5.6 Apoptosis and necrosis detection using the Tali® Apoptosis Kit - Annexin V Alexa Fluor® 488 and Propidium Iodide

The Tali® Apoptosis Kit allows for the identification of apoptotic cells and necrotic and live cells in a population of live cells. Apoptotic cells stained with this mixture will produce a green emission with Annexin V–Alexa Fluor® 488 while necrotic cells are stained with both red propidium iodide and green Annexin V–Alexa Fluor® 488. This kit allows the discrimination between apoptotic and necrotic cells with two-color staining. It recognizes phosphatidyl serine (PS) that is translocated from the inner to the outer membrane during apoptosis. The Tali® Apoptosis Kit contains:

- Annexin V – Alexa Fluor® 488 conjugate
- Annexin Binding solution
- Propidium Iodide (PI) solution

MCF-7 and MCF-10A cells were exposed to OA and UA at the following concentrations: 10, 20, 50 and 100µg/ml for 6h, 12h, 24h, 48h, and 72h periods as mentioned in (section 2.6). Cells were harvested from the flasks, centrifuged and the supernatant discarded. The cells were re-suspended in Annexin binding buffer (ABB) to a concentration of approximately 5×10^5 - 5×10^6 cells/ml. To each 100µl of sample 5µl of Annexin V Alexa Fluor® 488 was added and thoroughly mixed. The samples were then incubated at room temperature in the dark for 20min. After incubation, samples were centrifuged and the cells re-suspended in 100µl of ABB. Next, 1µl of Tali™ Propidium Iodide was added to each 100µl sample, thoroughly mixed and incubated at RT in the dark for 1-5 minutes. Subsequently, 25µl of the stained cells were loaded into a Tali™ Cellular Analysis Slide by pipetting the sample at an angle

of approximately 80 degrees into the half-moon-shaped sample loading area. The slides were analysed by the Tali™ Image-Based Cytometer. The experiment was repeated three times.

2.5.7 Determination of Reactive oxygen species (ROS) using the Cell ROX

In this study, the Tali® Image-Based Cytometer was used to assess oxidative stress in cells. CellROX® Orange Reagent, used in this application, is a probe for the detection of ROS in live cells. This cell permeant dye remains non-fluorescent until it is oxidized by ROS. Cells stained with CellROX® Orange Reagent are analyzed using the Tali® Image-Based Cytometer to assess increases in ROS levels.

For the detection of ROS in the current experiment, OA and UA were used to induce oxidative stress in MCF-7 and MCF-10A. Cells cultures were left treated with 10, 20, 50 and 100µg/ml for 6, 12, 24, 48, and 72h and control were untreated. After treatment, CellROX® Orange Reagent was directly added to 1mL of cells (at 1 x 10⁶ cells/mL) in complete medium at a 1:500 dilution (2µL dye to 1mL cell solution) and incubated for 30 minutes at 37°C. The medium and excess dye was removed by centrifugation and samples re-suspended in Hank's balanced salt solution.

After labeling with CellROX® Orange Reagent, cells were analyzed with the Tali® Image-Based Cytometer using the RFP channel, collecting 9 fields per sample. In this assay, “RFP fluorescence” represented the fluorescence signal from CellROX® Orange Reagent. The controls, which were also labelled with CellROX® Orange Reagent, were used to determine baseline levels of oxidative activity and to set the fluorescence threshold for the Tali® instrument.

This threshold was set manually and confirmed visually, and all cells with signal greater than the threshold were counted by the Tali® instrument as positive for ROS. Orange Reagent excites/emits fluorescence at maximum 545/565nm, which makes it compatible to the RFP channel of the Tali® instrument, which is excited at 530nm and

uses a 580nm long pass emission filter. The activity was recorded and statistical analyses conducted.

2.5.8 Flow cytometry

2.5.8.1 Cell cycle progression

Cell cycles G1, S, G2 were analysed in MCF-7 and MCF-10A cells using propidium iodide to stain the nucleus in order to determine the amount of DNA. Laser beam of a single frequency is directed onto a hydrodynamically focused stream of fluid. A number of detectors are aimed at the point where the stream passes through the light beam: one in line with the light beam Forward Scatter (FSC) and several perpendicular to it Side Scatter (SSC) and one or more fluorescence detectors. Each suspended particle passing through the beam scatters the light. Fluorescent chemicals in the particle may be excited into emitting light at a lower frequency than the light source. This combination of scattered and fluorescent light is detected by the detectors. By analyzing fluctuations in brightness at each detector (one for each fluorescent emission peak) it is possible to deduce the size, quantity and fluorescent intensity (DNA content when stained with propidium iodide) of cells. FSC correlates with the cell volume and SSC depends on the inner complexity of the particle e.g. amount of DNA, shape of nucleus, etc.

The cells were seeded at 5×10^5 in 25cm^2 flasks and allowed to attach for 24h. The cells were treated as described previously in section 2.6. After treatment the cells were trypsinized and centrifuged for 5 min at 300g. The supernatant was discarded. The cells were fixed in 4ml ice cold 70% ethanol that was added drop wise to the cell pellet while vortexing and were stored at -20°C for 24 hours. After 24 hours, the cells were centrifuged at 300g for 5 min and the supernatant removed. The cells were washed twice in PBS and re suspended in 400 μl PI in an RNase solution and incubated for 45min. Samples were analysed by flow cytometry in the PI/RNaseA solution and each analysis was based on at least 10000 events. Data from cell debris and clumps of 2 or more cells were removed from further analysis. Cell cycle distributions were

calculated by assigning relative DNA content per cell to sub-G1, G1, S and G2/M fractions.

2.5.9 Western Blotting

2.5.9.1 Protein Extraction

For the electrophoresis and western blot experiments the protein content of each sample had to be determined as all quantified data were expressed per mg proteins. All the procedures involved in the extraction of total protein from cells were performed on ice (4°C). The cells were seeded in 25cm² flasks and treated as described in section 2.6. The cells were harvested by scraping the cells from the tissue culture flask and creating a suspension using 1ml of ice cold PBS. The suspension was then aspirated, transferred to conical tubes and centrifuged at 3000 rpm for 4 minutes. The supernatant was aspirated and the resulting pellet was re-suspended in 200 µl of lysis buffer (M-PER™ Mammalian Protein Extraction Reagent). Lysates were clarified by centrifugation 800rpm for 10 minutes which removed the insoluble cellular debris

2.5.9.2 Determination of protein concentration

All the procedures involved in the determination of protein content in lysates, as well as sample preparation were performed on ice (4°C). Protein quantification was performed by taking an aliquot from the prepared cell lysates and protein content determined using the Nano-Drop® ND-1000 UV/V spectrophotometer. The remaining samples were stored at -20°C.

2.5.9.3 SDS-PAGE and electrophoresis

Equalized samples were mixed with sample buffer and incubated at 100°C for 2 minutes. A 12% polyacrylamide gel was used. Equivalent amounts of protein (50 µg) were loaded per lane with a molecular marker being loaded in the first lane to assist with orientation and sizing of separated proteins. Proteins were fractionated by sodium

dodecyl sulphate polyacrylamide gel electrophoresis (SDS-PAGE; Mini-PROTEAN® Tetra Cell - Bio-Rad) at a constant voltage of 100 V and current of 200 mA (Bio-Rad Power Pac 1000) until the migration front reached the bottom of the gel.

Resolved proteins were then electro-transferred onto polyvinylidene fluoride membrane (PVDF; Immobilon, Millipore, USA) using a horizontal semi-dry electrotransfer system (Bio-Rad Trans-Blot® SD, USA) at voltage of 15 V and constant current of 0.5 A (Bio-Rad Power Pac 1000).

2.5.9.4 Immuno-detection

Non-specific hydrophobic binding site were blocked with incubation in 5% non-fat milk and incubated for 1 hour at room temperature. The blots were washed in TBS-T then incubated overnight at 4°C in the primary antibody. The primary antibodies: LC3 and Beclin-1 were diluted 1:500 in TBS-T solution. The blots were washed as before and the blots were incubated in 1:10000 anti-rabbit horseradish peroxidase-conjugated secondary antibody for 2h at RT. Membranes were then exposed to ECL Western Blotting Substrate (Bio-Rad, South Africa). Chemiluminescent signals were captured with the UVP Bioimaging system. To provide a positive control for protein loading, all blots were probed for the representative protein β -actin.

2.5.10 Quantitative PCR

2.5.10.1 RNA extractions

RNA was extracted using the QIAzol lysis reagent (Qiagen) according to manufacturer's protocol.

2.5.10.2 Quality control of RNA samples

To determine the concentration and purity of the RNA samples, 1.2µl of each RNA sample was analyzed on a Nanodrop (ND-1000, ThermoScientific). Nuclease free water was used as the blank control.

2.5.10.3 cDNA synthesis

cDNA synthesis of 500ng RNA was performed in duplicate for each sample. RNA was diluted to 50ng/µl and 10µl of the diluted RNA sample was added to 10µl of a cDNA synthesis master mix consisting of reverse transcriptase buffer, random primers, dNTP mix, MultiScribe™ reverse transcriptase (High Capacity cDNA synthesis Kit, Life Technologies, Part # 4368814) and nuclease free water. The components were thoroughly mixed and spun down using a bench top centrifuge to collect all the liquid. Cycling was performed on the GeneAmp® PCR System 9700 (Life Technologies) using the cycling parameters tabulated below:

Table 2.1: cDNA synthesis cycling parameters

Step	1	2	3	4
Temperature (°C)	25	37	85	4
Time (minutes)	10	120	5	Infinity

The experimental cDNA samples were made by combining 10µl of each duplicate. Before expression analysis, each experimental cDNA sample was diluted 1:16 with nuclease-free water. However, samples that were going to be run with GAPDH primer set were diluted to 1:64. The original cDNA synthesis plate, which still had 10µl of each sample in duplicate, was kept at -80 °C.

2.5.10.4 qPCR analysis

To test the efficiency of the primers, a serial dilution of a cDNA pool was used as template for standard curve analysis. To test for DNA contamination, an RNA

pool was made and diluted in accordance with the protocol for cDNA synthesis and the subsequent dilution. Water was included as a NTC to detect contamination.

For gene expression analysis, each reaction (for standard curves and samples) consisted of 1µl cDNA template; 0.2µl of each of the primers (final concentration 200nM); 5µl KAPA SYBR® FAST qPCR KIT MasterMix (2X) ABI Prism (Lasec, KK4604) and nuclease-free water up to 10µl. Expression analysis was performed on the ABI 7900HT Fast Real Time PCR system using the following cycling parameters and followed by a dissociation (melt) curve analysis:

Table 2.2: qPCR cycling parameters

Stage	1		2		3		
Cycles	1		40		1		
Temperature (°C)	95	95	60 or 62*	95	60	95	
Time	3 mins	3 secs	1 min	15 sec	15 sec	15 sec	

Post cycling, the data was analysed using the SDS v2.4 software (Life Technologies) and relative expression analysis performed using qBase+ (BioGazelle).

2.6 Statistical analysis

Statistical analysis of the quantitative data was done by GraphPad Prism (GraphPad Prism version 6.04 for Windows, GraphPad Software, San Diego California USA, www.graphpad.com). Cell viability studies were repeated thrice, with sample size (n) — 12 in each experiment and analyzed by means of two-way ANOVA followed by Tukey's multiple comparisons test. Annexin V and mitotic index were repeated thrice each analyzed by means of two-way ANOVA followed by Tukey's multiple comparisons test. A P-value of less than 0.05 was accepted as significant. Means of quantitative experiments are presented in bar charts, with T-bars referring to the standard error of the mean (SEM). All experiments included a set of appropriate controls.

CHAPTER III

3 Results

3.1 Determining the influence of 17 β -Estradiol on cellular proliferation as a parameter of ER α antagonistic properties

Estrogen related carcinogenesis with regard to breast cancer typically results from the activation of distinct signalling pathways (Iwasaki and Tsugane, 2011). These pathways are not mutually exclusive and are often constituted by receptor mediated stimulation of cell proliferation. Activation of these pathways is purportedly a consequence of prolonged exposure to high levels of estrogen, specifically in the form of 17 β -estradiol. In order to evaluate the behaviour of the cells that was imported from ATCC for this study, a time and dose study with 17 β -estradiol on both cell lines, was done. The results could then be related to other similar studies and could assist in clarification of the effects of OA and UA on cell signalling. Consistent with previous *in vitro* studies (Mohammed et al., 2015), 17 β -estradiol caused cellular proliferation in MCF-7 cells. On the other hand, except for 10pg/l for 72h, 17 β -estradiol failed to stimulate significant proliferation in MCF-10A cells.

Table 3.1: The quantification of the effects of 17 β -Estradiol on the proliferation of MCF-7 and MCF-10A cells after 48- and 72 hours. Significant differences between treated and control samples are indicated by *P \leq 0.05 compared to respective controls (Two-way ANOVA followed by Tukey's multiple comparisons test).

Time	17 β -Estradiol	MCF-7: Proliferation %	MCF-10A: Proliferation %
48 Hours	Control	100	100
	10pg/L	109*	99.5
	20pg/L	105	91
	50pg/L	103	80*
	80pg/L	103	76*
	100pg/L	105	82*
72 Hours	Control	100	100
	10pg/L	111	105
	20pg/L	116*	97
	50pg/L	115*	90*
	80pg/L	102	90*
	100pg/L	103	91*

3.1.1 ER status of MCF-10A cells

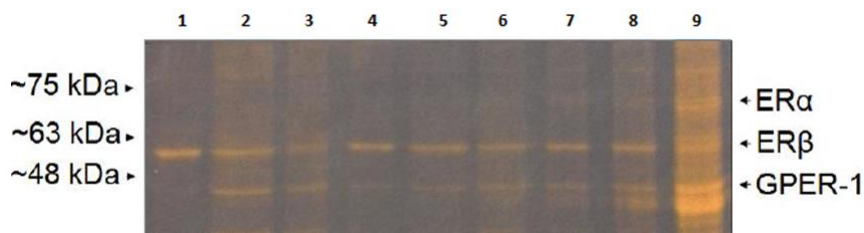


Figure 3.1: SDS-PAGE gel of MCF-10A whole cell lysates after combination treatment.

Lane 1, MCF-10A 48 hour control cell lysates; lanes 2, 3 and 4 denotes MCF-10A cell lysates after 48 hour exposure to 10, 20 and 40 pg/l estriol-progesterone combination treatments respectively; lane 5, MCF-10A 72 hour control cell lysates; lanes 6, 7 and 8 denotes MCF-10A cell lysates after 72 hour exposure to 10, 20 and 40pg/l estriol-progesterone combination treatments respectively; lane 9, MCF-7 cell lysates after culture in maintenance medium.



3.2 Cell viability studies

Gillies et al. (1986) used crystal violet to quantify cell numbers in monolayer cultures as a function of the absorbance of dye taken up by the cells. Cell numbers were expressed as a percentage of the cells propagated in growth medium in order to determine the anti-proliferation effects of OA and UA on tumorigenic MCF-7 and non-tumorigenic MCF-10A cells.

3.2.1 The effect of OA on the viability of MCF-7 and MCF-10A cells

OA, at four different concentrations 10, 25, 50 and 100µg/ml on MCF-7 breast cancer cells and MCF-10A mammary epithelial cells and incubated for 6, 12, 24, 48 and 72 hours were used. The dose-dependent responses for the MCF-7- and MCF-10A cells are shown in Figs 3.2-A and B respectively.

Cell numbers were affected by OA and UA in both all cell lines in a time and dose – dependent manner. It has been found that 10µg/ml OA increased cell proliferation of MCF-7 ($P \leq 0.001$) after 12h (116%). 20µg/ml had no effect on the

viability of MCF-7 cells when compared to the control. 50µg/ml significantly ($P \leq 0.001$) decreased MCF-7 cell viability after 6h (45.06%), 12h (52.93%), 24h (61.37%), 48h (59.57%), and 72h (66.73%). The highest concentration 100µg/ml caused an outspoken decrease in cell viability of MCF-7 cells ($P \leq 0.001$) after 6h (35.82%), 12h (41.82%), 24h (58.42%), 48h (47.66%), and 72h (50.05%) as shown in Fig. 3.2-A.

Similar to the effect on MCF-7 cells, OA also affected the MCF-10A cells. At a concentration of 10µg/ml OA increased cell viability of MCF-10A after 6h (110.75%) compared to control Fig. 3.2-B. Cell viability after 20µg/ml was also significantly ($P \leq 0.05$) increased after 72h (110.35%) but significantly ($P \leq 0.05$) decreased after 24h (90.31%) and 48h (81.47%) compared to control as shown in Fig. 3.2-B.

The results showed that 50µg/ml significantly ($P \leq 0.001$) decreased cell viability after 6h (54.07%), 12h (48.22%), 24h (60.02%), 48h (60.90%) and 72h (63.49%) Fig. 3.1-B. 100µg/ml also decreased cell viability significantly ($P \leq 0.001$) in MCF-10A cells after 6h (44.74%), 12h (40.56%), 24h (57.85%), 48h (39.66%) and 72h (48.90%) Fig. 3.2-B.

The results presented in (Fig. 3.2-A and B) show that the two higher concentrations of 50µg/ml and 100µg/ml OA respectively decreased cell proliferation in both cell lines. 20µg/ml decreased proliferation in both cell lines after 24h. However, 72h the cells seemed to recover with the MCF-10A cells showing a significant increase in proliferation (110.35%).

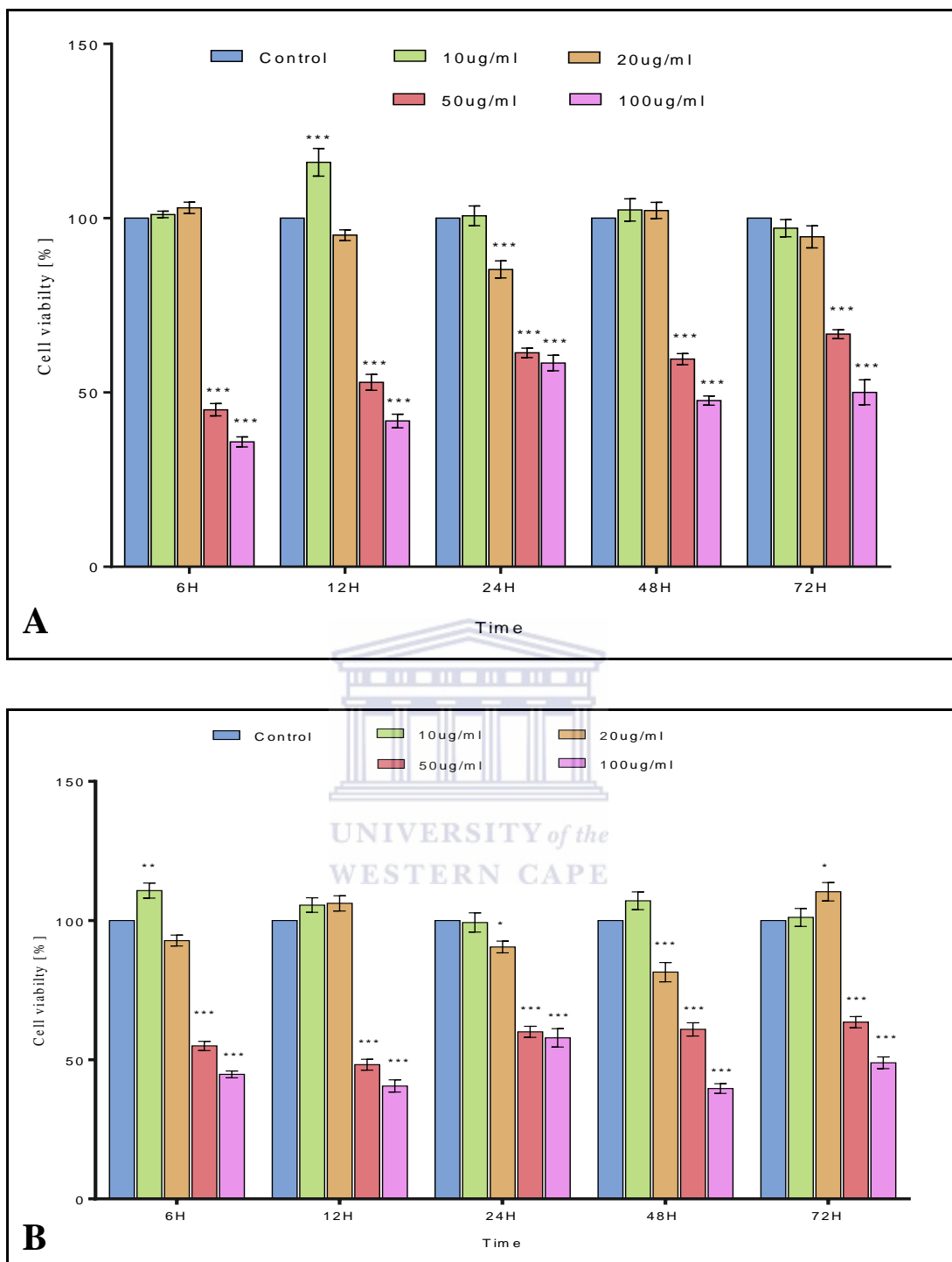


Figure 3.2: Cell viability percentage of A: MCF-7 and B: MCF-10A cells as determined by crystal violet assay in 96-well plates following 6, 12, 24, 48 and 72-hour exposure to OA. Data is shown as mean \pm SEM of three separate experiments. Significant differences between treated and control samples are indicated by * $P \leq 0.05$, ** $P \leq 0.01$, *** $P \leq 0.001$ compared to respective controls (Two-way ANOVA followed by Tukey's multiple comparisons test)

3.2.2 The effect of UA on the viability of MCF-7 and MCF-10A cells

UA was tested at four different concentrations 10, 25, 50 and 100µg/ml on MCF-7 and MCF-10A cells and incubated for 6, 12, 24, 48 and 72 hours. The time and dose-dependent responses for the MCF-7 cells are shown in Fig. 3.3-A and for the MCF-10A cells in Fig. 3.3-B. It is evident that 10µg/ml UA significantly ($P \leq 0.001$) increased the MCF-7 cell viability after 6h (121.96%), 24h (114.24%) and 72h (115.13%). 20µg/ml had a biphasic effect. It decreased the MCF-7 cell viability after 12h (89.3%) but after 24h it significantly increased (111.56%) the MCF-7 cell viability. Fig. 3.3-A shows that 50 and 100µg/ml UA both significantly decreased cell viability in of the MCF-7 after 6h (46.35%; 42,66%), 12h (56.94%; 53,29%), 24h (53,84%; 49.61%), 48h (63.04%; 45.64%) and 72h (50.78%; 49.44%).

In the MCF-10A cells (Fig. 3.3-B) 10µg/ml UA significantly increased cell numbers in all the time periods. After 6h the increase was (109.38%), after 12h (108.36%), 24h (120.75%), (118.66%), and 72h (113.21%). The MCF-10A cell viability was significantly ($P \leq 0.05$) decreased by 20µg/ml UA after 12h (91.19%) and 48h (91.70%), and after 72h it was decreased to 87.84% ($P \leq 0.001$) (Fig. 3.2-B). 50µg/ml UA significantly ($P \leq 0.001$) decreased the MCF-10A cell viability after 6h (57.45%), 12h (51.21%), 24h (65.83%), 48h (43%), and 72h (53.61%) compared to the control. 100µg/ml UA significantly ($P \leq 0.001$) decreased the MCF-10A cell viability after 6h (29.77%), 12h (27.4%), 24h (45.99%), 48h (32.09%), and 72h (37.44%) compared to the control as shown in (Fig. 3.3-B).

10µg/ml UA significantly increased the proliferation in both cell lines for all the time periods. 20µg/ml generally decreased cell proliferation both cell lines, but to a greater extent in MCF-10A cells. The two higher concentrations (50 and 100µg/ml) decreased cell proliferation throughout in both cell lines. However, 100µg/ml UA inhibited cell proliferation to a greater extent in the MCF-10A cells with the most outspoken effect after 6 and 12h periods.

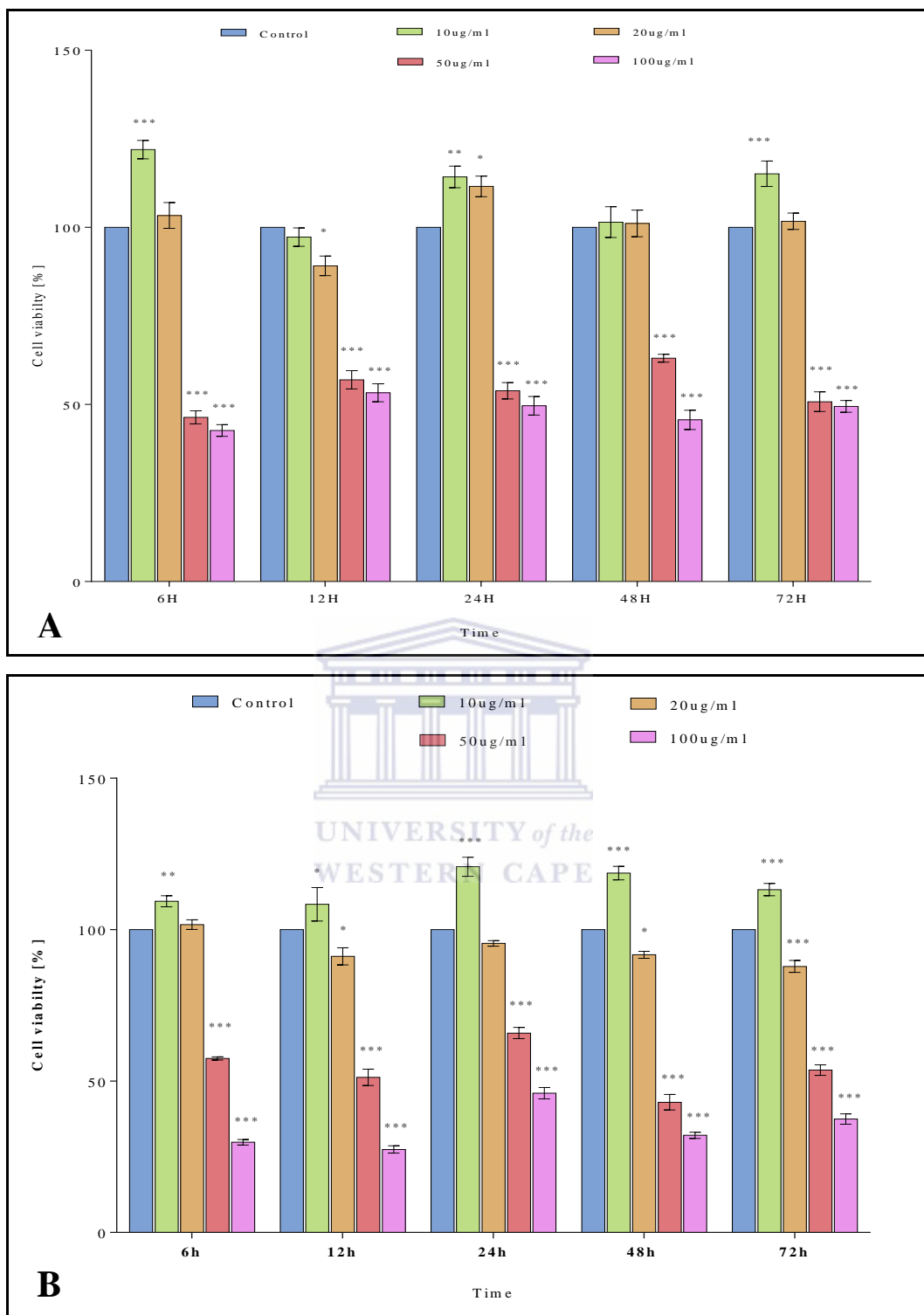


Figure 3.3: Cell viability percentage of (A); MCF-7 and (B); MCF-10A cells as determined by crystal violet assay in 96-well plates following 6, 12, 24, 48 and 72-hour exposure to UA. Data is shown as mean \pm SEM of three separate experiments. Significant differences between treated and control samples are indicated by $p < 0.05$ are presented as * $P \leq 0.05$, ** $P \leq 0.01$, *** $P \leq 0.001$ compared to respective controls (Two-way ANOVA followed by Tukey's multiple comparisons test)

3.3 Morphological studies: Haematoxylin and Eosin (H&E) staining

3.3.1 The effect of OA on MCF-7 and MCF-10A cells after 6h.

Morphological changes were investigated in H&E stained cells. Figure 3.4-A and F show control MCF-7 and MCF-10A cells respectively. Figs B and G, C and H and D and I show cells treated with 10, 20, and 50µg/ml OA. No morphological changes can be observed with the 10, 20 and 50µg/ml exposure to OA in either of the cell lines. MCF-7 cells exposed to 100µg/ml OA (Fig. 3.4-E) display smaller cells with less cellular attachments. The effects on the MCF-10A cells were more outspoken. The cells were round with condensed chromatin indicative of pycnosis (Fig. 3.4-J).

3.3.2 Mitotic index the effect of OA on MCF-7 and MCF-10A cells after 6h.

Quantification of cell proliferation is indicated by the mitotic index obtained by counting 1000 cells on every coverslip of the H and E stained cells. The effect of the various concentrations of OA on the two cell lines is shown in Figures 3.5 and 3.6. Both cell lines showed reduced metaphases when compared to control. Total mitosis was significantly decreased in the MCF-7 cells exposed to OA for 6h. 2% of cells were mitotic in the 50µg/ml and 1.6% in the 100µg/ml treated cultures (Fig. 3.5) in comparison to MCF-10A cells which had a mitosis index of 0.7% at 50µg/ml and 0.9% at 100µg/m (Fig. 3.6). The study showed that OA inhibited the number of mitotic MCF-7 cells. Some apoptotic, but mostly pycnotic cells (20% and 35%) for 50 and 100µg/ml OA respectively were observed in these cultures exposed for 6h (Fig. 3.5). Quantification of the effects of OA in MCF-10A cells are shown in (Fig 3.6). The decrease in normal dividing and the increase in dying cells (50µg/ml; 27%; 100µg/ml; 48.2%) were dose dependent.

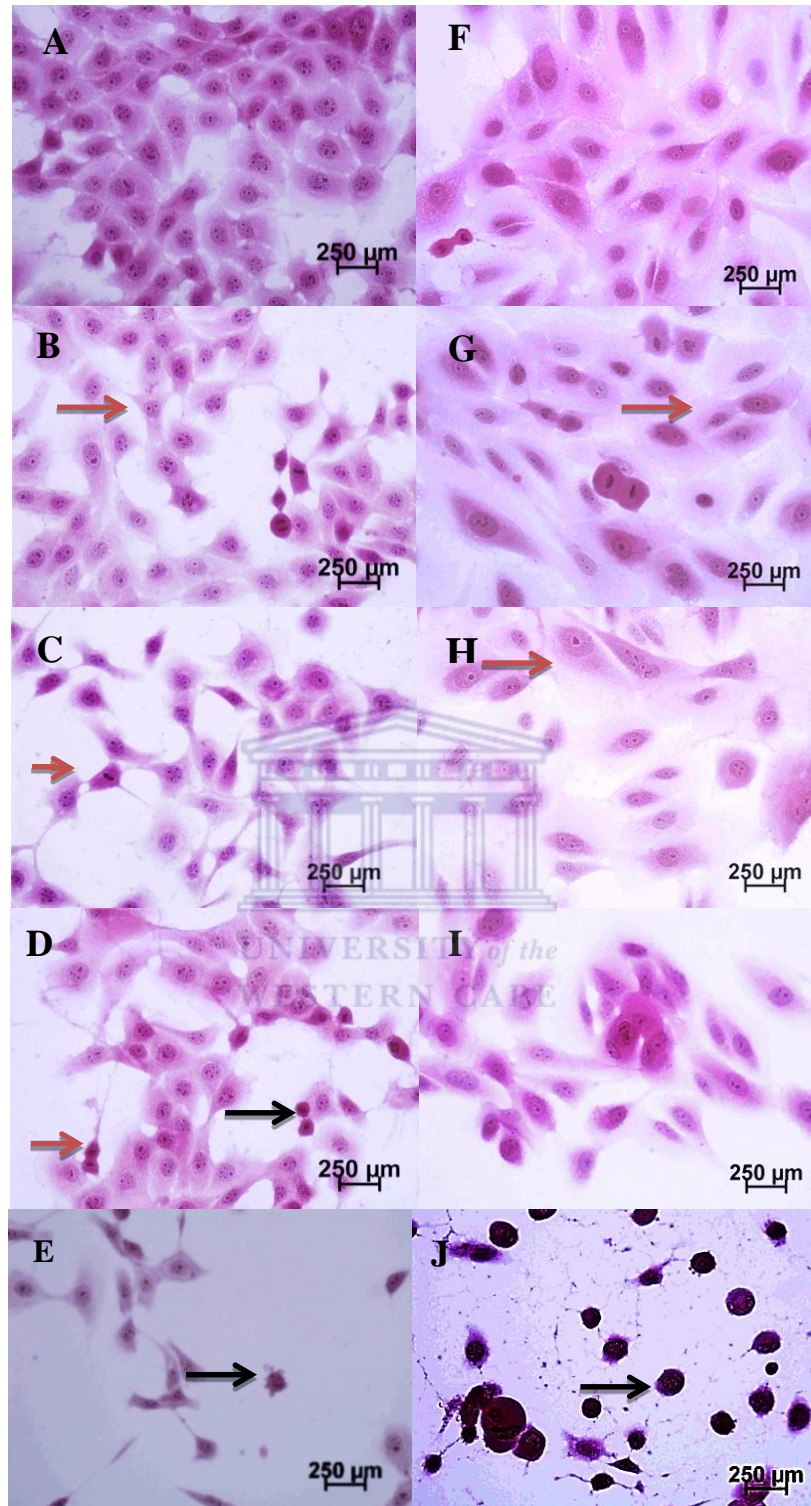


Figure 3.4: MCF-7 and MCF-10A cell morphology. MCF-7 (A, B, C, D, E) and MCF-10A (F, G, H, I, J) cells were treated with OA for 6h and stained with haematoxylin-eosin. Control MCF-7 cells (A); 10 μ g/ml (B); 20 μ g/ml (C); 50 μ g/ml (D); 100 μ g/ml (E); Control MCF-10A cells (F); 10 μ g/ml (G); 20 μ g/ml (H); 50 μ g/ml (I) and 100 μ g/ml (J). Red arrows indicate normal cells dividing, and black arrows indicate complete apoptosis with cells presenting with condensed chromatin and cytoplasmic shrinkage. All pictures are typical of three independent experiments each performed under identical conditions

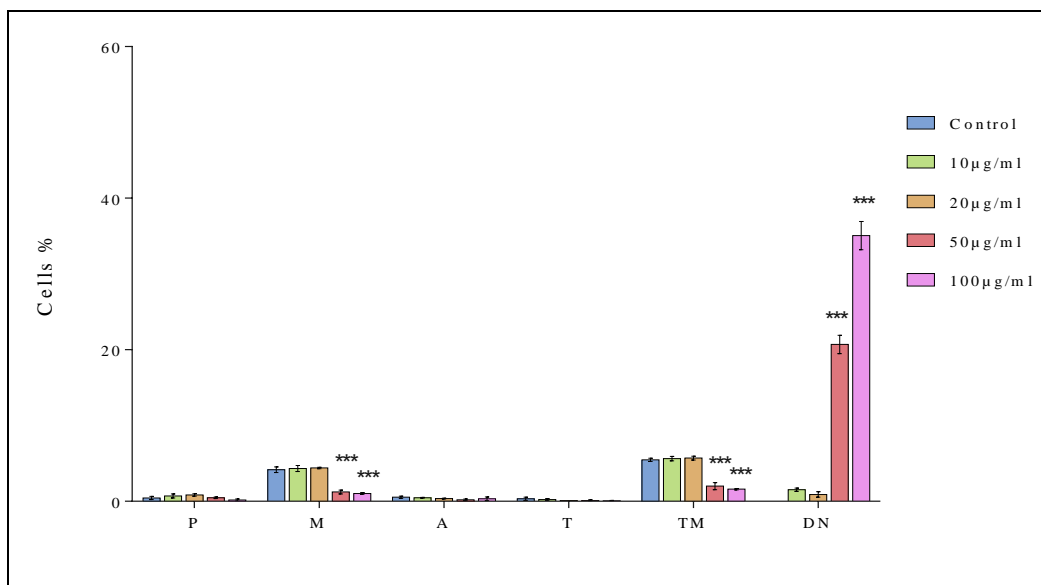


Figure 3.5: MCF-7: quantification of the effects of OA on dividing and pycnotic and apoptotic cells after 6h exposure. Prophase (P), metaphase (M), anaphase (A), telophase (T) and total mitosis (TM) after 6h exposure to 10, 20, 50 and 100µg/ml OA are shown. TM was significantly decreased. An increase in pycnotic and apoptotic cells (DN) were in the cultures exposed to 50 and 100µg/ml OA. Significant differences between treated and control samples are indicated by $p < 0.05$ are presented as * $P \leq 0.05$, ** $P \leq 0.01$, *** $P \leq 0.001$ compared to respective controls (Two-way ANOVA followed by Tukey's multiple comparisons test)

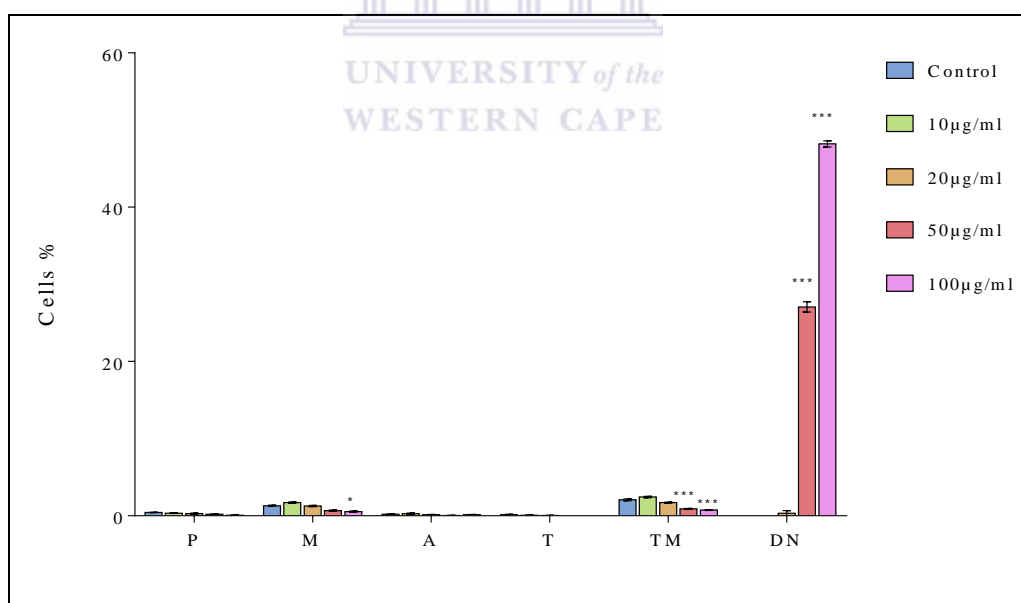


Figure 3.6: MCF-10A: quantification of the effects of OA on dividing pycnotic and apoptotic cells after 6h exposure. Prophase (P), metaphases (M), anaphases (A), telophases (T), total mitosis (TM) and death necrosis (DN) after exposure to 10, 20, 50 and 100µg/ml OA are shown. TM was significantly decreased. An outspoken increase in pycnotic and apoptotic cells (DN) were seen in the cultures exposed to the high concentrations of OA. Significant differences between treated and control samples are indicated by $p < 0.05$ are presented as * $P \leq 0.05$, ** $P \leq 0.01$, *** $P \leq 0.001$ compared to respective controls (Two-way ANOVA followed by Tukey's multiple comparisons test)

3.3.3 The effect of OA on MCF-7 and MCF-10A cells after 12h.

Morphological changes were investigated in H&E stained cells. Figure 3.7 A and F show control MCF-7 and MCF-10A cells, respectively. Figs 3.7 B and G and C and H show cells treated with 10 and 20µg/ml OA. No morphological changes can be observed with these OA concentrations. Figs 3.7 D and I show cells treated with 50µg/ml OA. Changes in the cell shape and decreased cells numbers can be observed. The effects on the MCF-7 and MCF-10A cells were more outspoken after 100µg/ml OA (Figs. E and J). The cells were small, round, and detached with condensed chromatin indicative of either apoptosis or pycnosis (Fig. 3.7-J).

3.3.4 Mitotic index: effect of OA on MCF-7 and MCF-10A cells after 12h

Quantification of the effect of the various concentrations of OA on cell proliferation of the two cell lines is shown in Figs 3.8 and 3.9. The study showed that OA inhibited the number of mitotic MCF-7 cells after 12h treatment. Cells undergoing apoptosis and pycnosis (14.76% and 19.86%) for 50 and 100µg/ml OA respectively were observed ($P \leq 0.001$) in these cultures (Fig. 3.8). Quantification of the effects of OA in MCF-10A cells are shown in Fig. 3.9. The decrease in normal dividing and the increase in dying cells (50µg/ml; 13.56%; 100µg/ml; 26.6%) were dose dependent. OA after 12h exposure, significantly decreased the TM in MCF-7 cells to 2.33% at 50µg/ml and 1% at 100µg/ml compared to MCF-10A cells where the TM was decreased from 2.1% in the control cells to 0.83% after 50µg/ml and 0.53% after 100µg/ml.

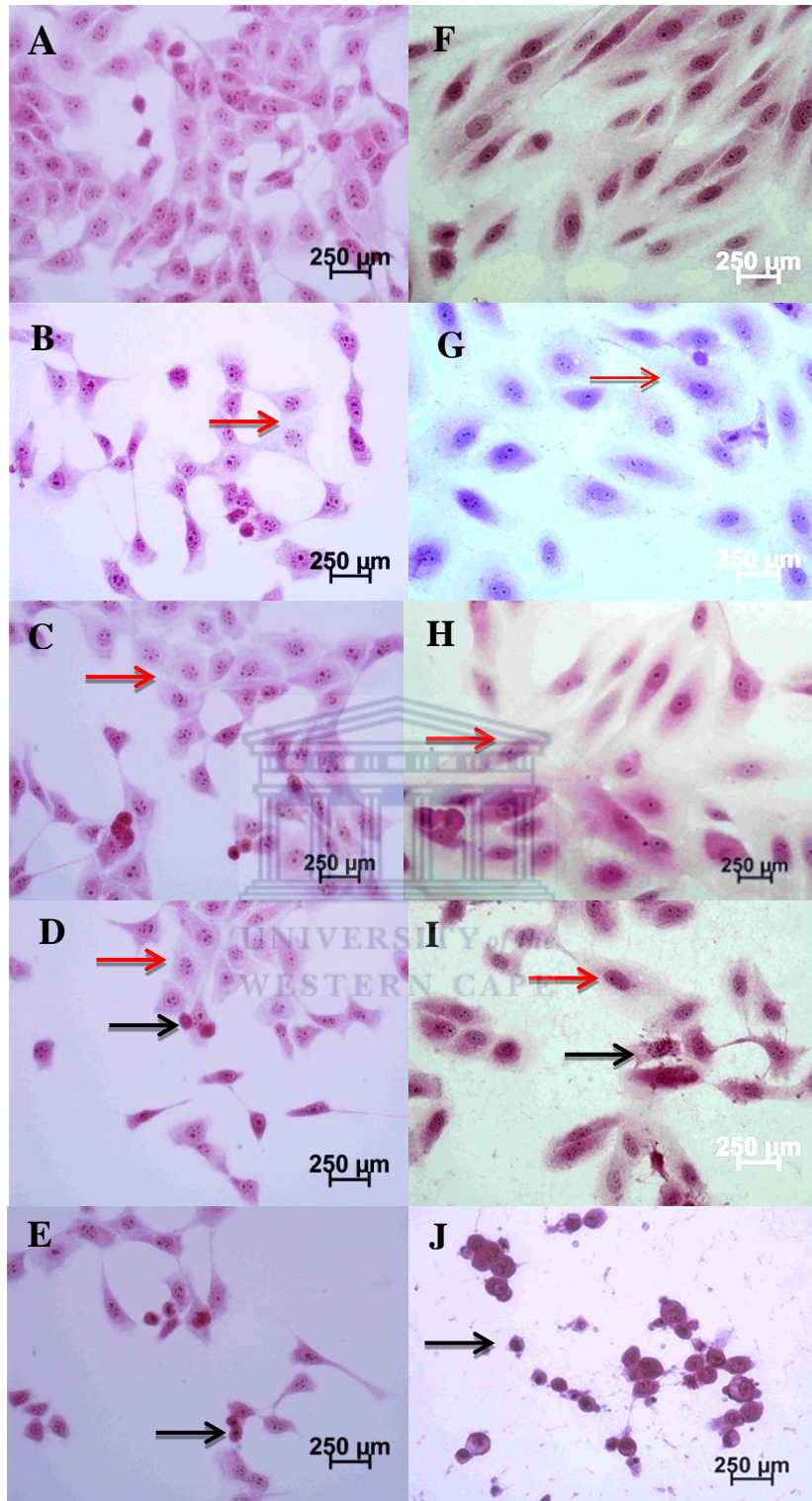


Figure 3.7: Haematoxylin and eosin stained. MCF-7 (A, B, C, D, E) and MCF-10A (F, G, H, I, J) cells were treated with OA after 12h is shown. control MCF-7 cells (A); 10µg/ml (B); 20µg/ml (C); 50µg/ml (D); 100µg/ml (E); control MCF-10A cells (F); 10µg/ml (G); 20µg/ml (H); 50µg/ml (I) and 100µg/ml (J). Red arrows indicate normal cells, and black arrows indicate apoptosis with cells presenting with condensed chromatin and cytoplasmic shrinkage. All pictures are typical of three independent experiments each performed under identical conditions

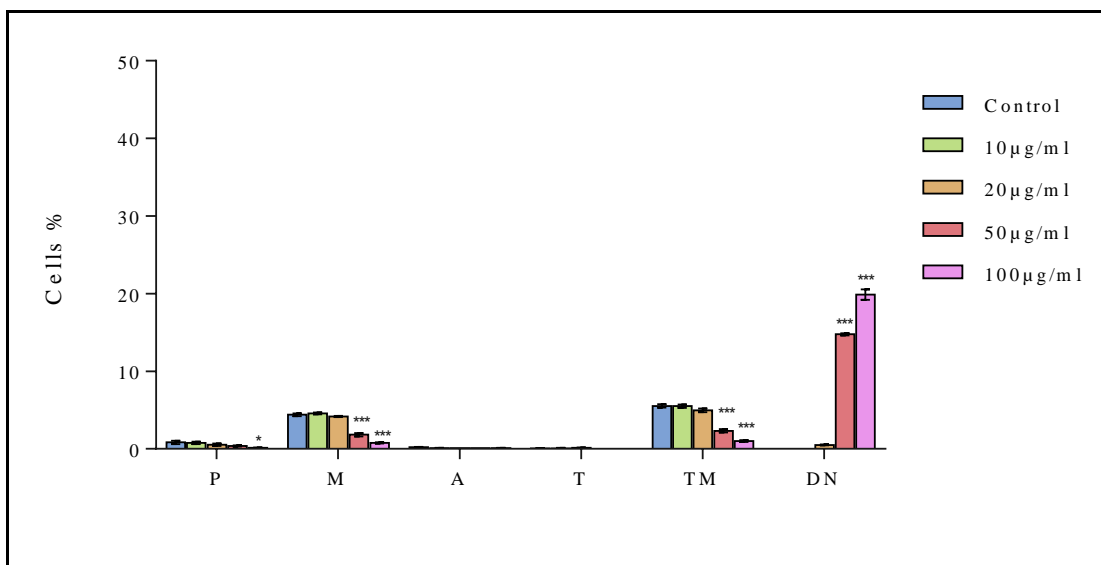


Figure 3.8: MCF-7: quantification of the effects of OA on dividing pycnotic and apoptotic cells after 12h exposure. Prophase (P), metaphase (M), anaphase (A), telophase (T), total mitosis (TM) and death necrosis (DN) after exposure to 10, 20, 50 and 100µg/ml OA are shown. TM was significantly decreased. An outspoken increase in pycnotic and apoptotic cells (DN) were seen in the cultures exposed to the high concentrations of OA. Significant differences between treated and control samples are indicated by $p < 0.05$ are presented as * $P \leq 0.05$, ** $P \leq 0.01$, *** $P \leq 0.001$ compared to respective controls (Two-way ANOVA followed by Tukey's multiple comparisons test)

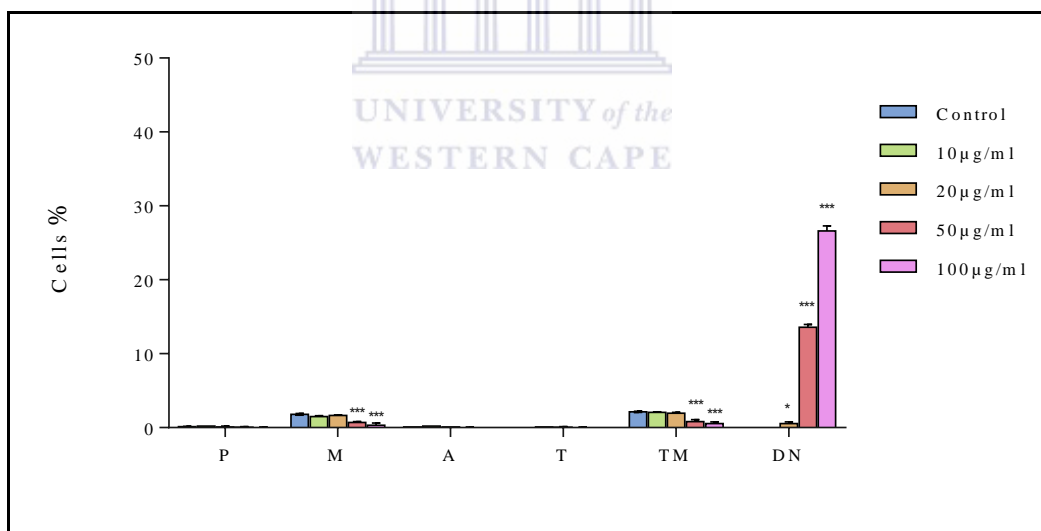


Figure 3.9: MCF-10A quantification of the effects of OA on dividing pycnotic and apoptotic cells after 12h exposure. Prophase (P), metaphase (M), anaphase (A), telophase (T), total mitosis (TM) and cell death (CD) after exposure to 10, 20, 50 and 100µg/ml OA are shown. TM was significantly decreased. An outspoken increase in pycnotic and apoptotic cells (CD) were seen in the cultures exposed to the high concentrations of OA. Significant differences between treated and control samples are indicated by $p < 0.05$ are presented as * $P \leq 0.05$, ** $P \leq 0.01$, *** $P \leq 0.001$ compared to respective controls (Two-way ANOVA followed by Tukey's multiple comparisons test)

3.3.5 The effect of OA on MCF-7 and MCF-10A cells after 24h

Morphological changes were investigated in H&E stained cells. Figs 3.10-A and F show control MCF-7 and MCF-10A cells, respectively. Figs 3.10 B & G and C & H demonstrate cells treated with 10 and 20 μ g/ml OA. No morphological effects were observed with the low concentrations on MCF-7 and MCF-10A cells. Figs D & J and I & E illustrate the effects of 50 and 100 μ g/ml OA after 24h in the MCF-7 and MCF-10A cell line. A decrease in cell numbers with an increase in small, darkly stained cells shown condensed chromatin, density and some apoptotic bodies can be observed. The MCF-10A cells seem to be affected to a greater degree than the MCF-7 cells.

3.3.6 Mitotic index: MCF-7 and MCF-10A cells after 24h OA exposure

The mitotic effects induced on MCF-7 and MCF-10A cells following 24h exposure to various concentrations of OA is shown in Figs 3.11 and 3.12, respectively. A similar response as in the 6 and 12h treatment was observed at 24h. OA exposure inhibited the amount of TM in MCF-7 and MCF-10A cells. OA exposure (24h) significantly ($P \leq 0.001$) decreased dividing MCF-7 cells to 2.36% at 50 μ g/ml and 1.23% at 100 μ g/ml. MCF-7 cells showing features of apoptotic and pycnotic cells (36.5% and 46.46%) were observed in these cultures exposed to 50 and 100 μ g/ml OA for 24h (Fig. 3.11). Cell death caused by OA was significantly enhanced at only 50 and 100 μ g/ml, $P \leq 0.001$. Quantification of the effects of OA in MCF-10A cells are also shown in Fig 3.12. The decrease in normal dividing and the increase in dying cells (50 μ g/ml: 11.63%; 100 μ g/ml: 24.16%) was significant with ($P \leq 0.001$). The cell's response to OA was concentration dependent.

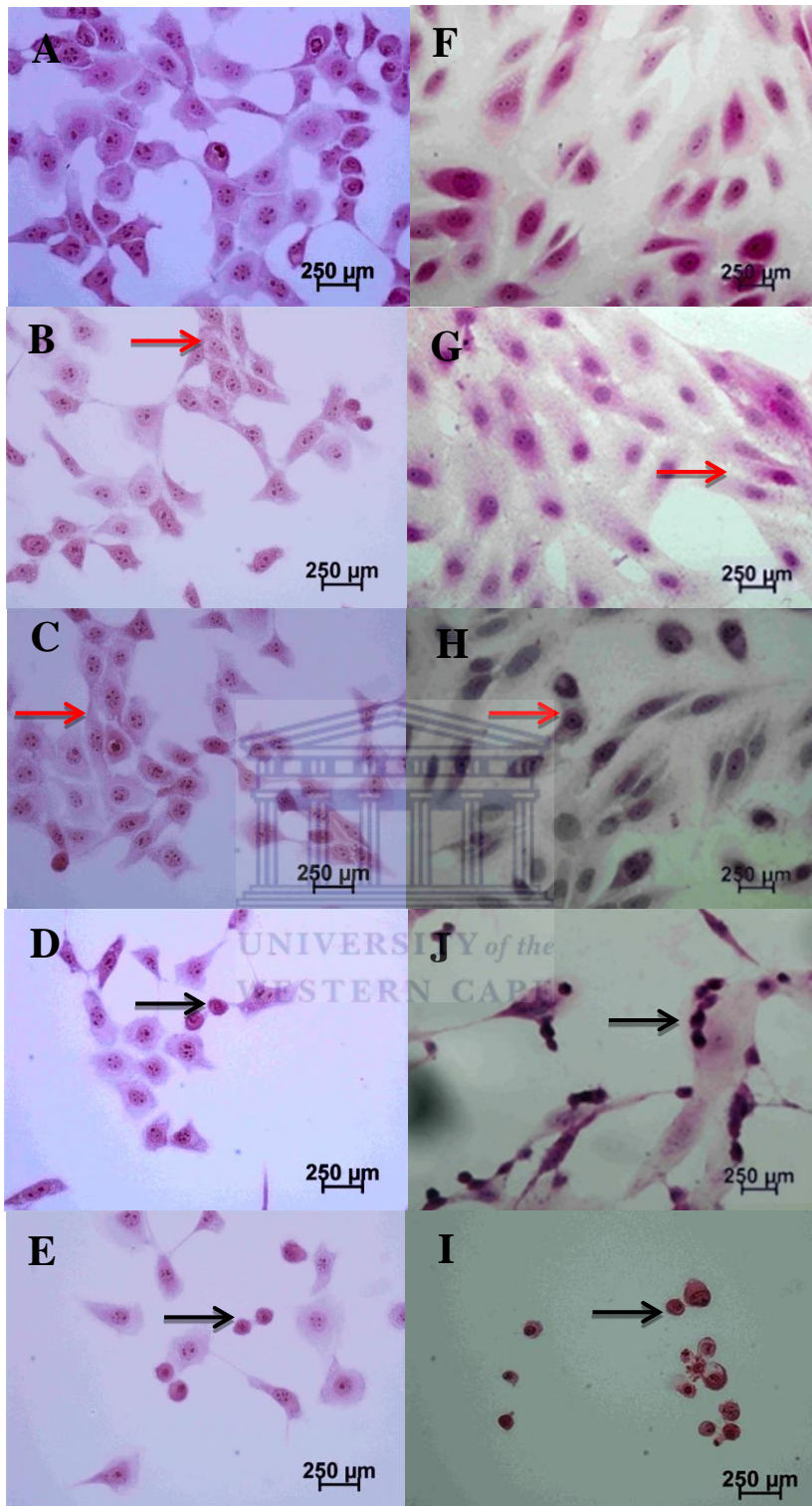


Figure 3.10: MCF-7 and MCF-10A cell morphology. MCF-7 (A, B, C, D, E) and MC-F10A (F, G, H, I, J) cells were treated with OA after 24h and stained with haematoxylin and eosin. control MCF-7 cells (A); 10 μ g/ml (B); 20 μ g/ml (C); 50 μ g/ml (D); 100 μ g/ml (E); control MCF-10A cells (F); 10 μ g/ml (G); 20 μ g/ml (H); 50 μ g/ml (I) and 100 μ g/ml (J). Red arrows indicate irregular-shaped dividing cells, and black arrows indicate complete apoptosis with cells shown condensed chromatin and cytoplasmic shrinkage. All pictures are typical of three independent experiments each performed under identical conditions

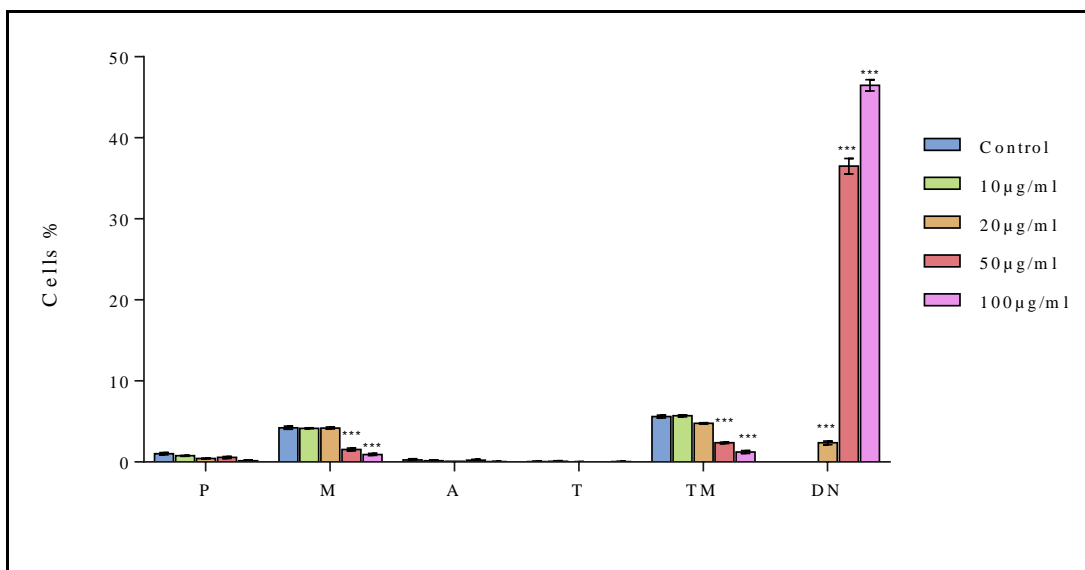


Figure 3.11: The quantification of the effects of OA on dividing pycnotic and apoptotic MCF-7 cells after 24h exposure. Prophase (P), metaphase (M), anaphase (A), telophase (T) and total mitosis (TM) after 24h exposure to 10, 20, 50 and 100µg/ml OA are shown. TM was significantly decreased. An outspoken increase in pycnotic and apoptotic cells (DN) were observed in the cells exposed to 50 and 100µg/ml. Significant differences between treated and control samples are indicated by $p < 0.05$ are presented as * $P \leq 0.05$, ** $P \leq 0.01$, *** $P \leq 0.001$ compared to respective controls (Two-way ANOVA followed by Tukey's multiple comparisons test)

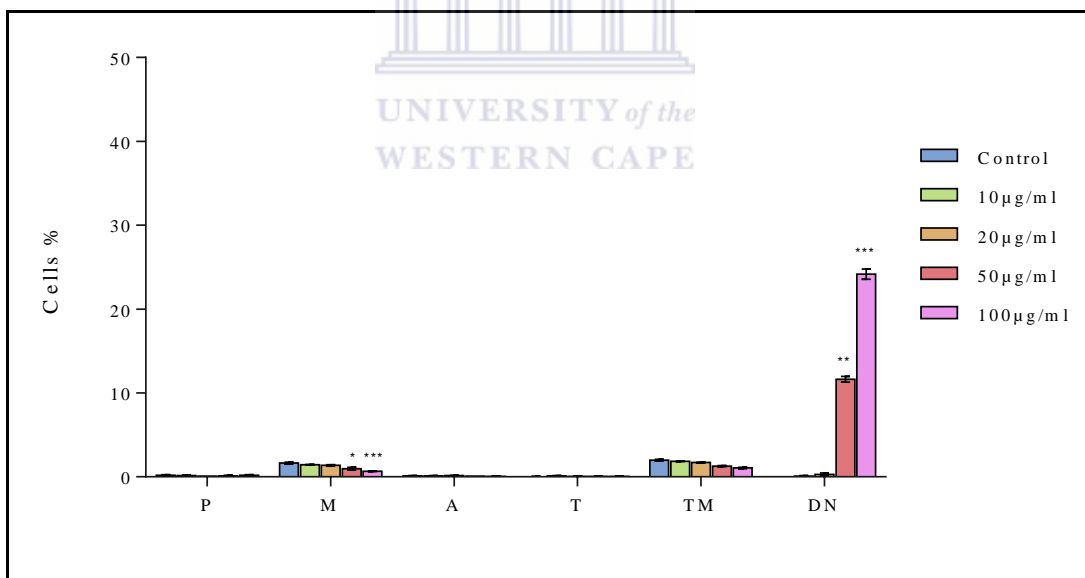


Figure 3.12: Quantification of the effects of OA on dividing pycnotic and apoptotic MCF-10A cells after 24h exposure. Prophase (P), metaphase (M), anaphase (A), telophase (T) and total mitosis (TM) after 24h exposure to 10, 20, 50 and 100µg/ml OA are shown. TM was decreased while an outspoken increase in pycnotic and apoptotic cells (DN) were seen in the cells exposed to 50 and 100µg/ml. Significant differences between treated and control samples are indicated by $p < 0.05$ are presented as * $P \leq 0.05$, ** $P \leq 0.01$, *** $P \leq 0.001$ compared to respective controls (Two-way ANOVA followed by Tukey's multiple comparisons test)

3.3.7 The effect of OA on MCF-7 and MCF-10A cells after 48h

Figure 3.13-A and F show control MCF-7 and MCF-10A cells respectively. Figs B & G, C & H and D & I show cells treated with 10 and 20µg/ml OA. Morphological changes were not observed with the lower concentrations after 48h exposure on two cell lines. Figs D & J and I & E illustrate the effects of 50 and 100µg/ml OA after 48h in the MCF-7 and MCF-10A cell lines. Morphological changes can be seen associated with apoptosis such as apoptotic bodies, chromatin condensation and shrunken cells. Round, darkly stained pycnotic cells can also be seen in the MCF-10A cells (J).

3.3.8 Mitotic index: MCF-7 and MCF-10A cells after 48h exposure to OA

The influence of various concentrations OA on the mitosis of the two cell lines is shown in Figures 3.14 and 3.15. The study displayed that OA inhibited the percentage of mitotic MCF-7 cells. An increase apoptotic and pycnotic cells (12.46% and 19.5%) for 50 and 100µg/ml OA respectively were observed in these cultures exposed for 48h (Fig. 3.14). Quantification of the effects of OA in MCF-10A cells are shown in Fig 3.14. The decrease in normal dividing and the increase in dying cells (20µg/ml: 0.7%; 50µg/ml: 13.26%; 100µg/ml: 13.26%) were dose dependent. After 48h exposure to 50 and 100µg/ml OA significantly decreased TM in MCF-7 cell ($P \leq 0.001$) to 3.3% and 1.56% and in MCF-10A cells TM was also significantly decreased ($P \leq 0.001$) to 1.7% and 1.13% when compared to normal cells growth.

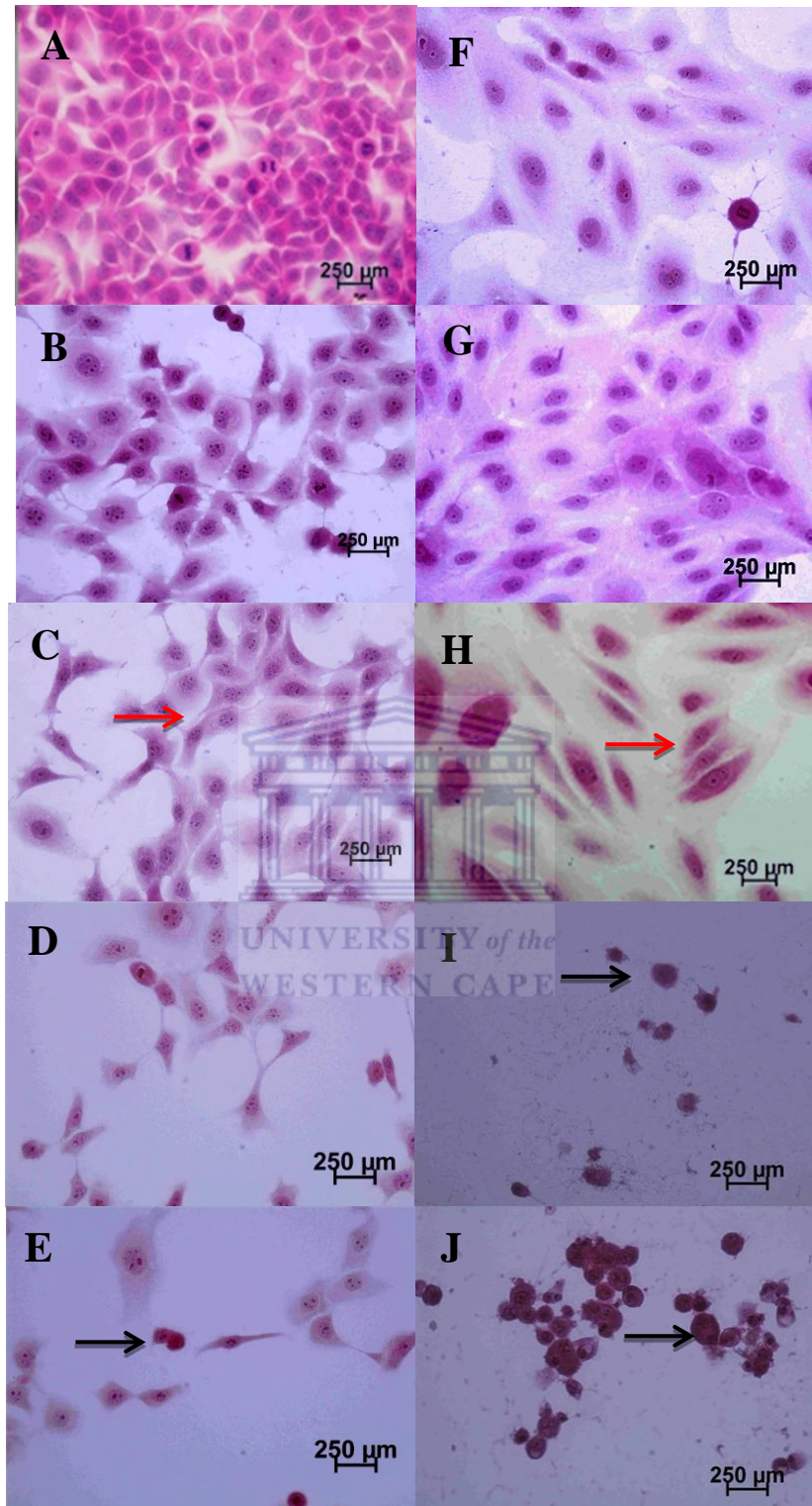


Figure 3.13: Shows H and E stained. MCF-7 (A, B, C, D, E) and MCF-10A (F, G, H, I, J) cells were treated with OA after 48h using haematoxylin-eosin staining. Control MCF-7 cells (A); 10 μ g/ml (B); 20 μ g/ml (C); 50 μ g/ml (D); 100 μ g/ml (E); control MCF-10A cells (F); 10 μ g/ml (G); 20 μ g/ml (H); 50 μ g/ml (I) and 100 μ g/ml (J). Red arrows indicate normal dividing cells and black arrows indicate cytotoxic and possibly presenting with condensed chromatin and cytoplasmic shrinkage. All pictures are typical of three independent experiments each performed under identical conditions.

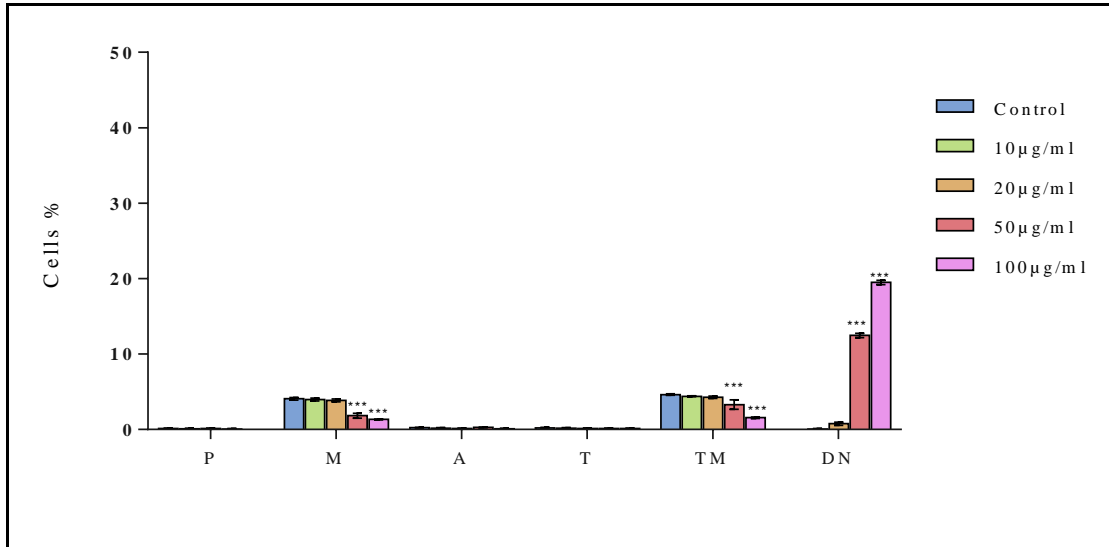


Figure 3.14: The quantification of the effects of OA on dividing pycnotic and apoptotic MCF-7 cells after 48h exposure. Prophase (P), metaphase (M), anaphase (A), telophase (T) and total mitosis (TM) after exposure to 10, 20, 50 and 100µg/ml OA are shown. TM was significantly decreased. An increase in pycnotic and apoptotic cells (DN) after 50 and 100 was observed. Significant differences between treated and control samples are indicated by $p < 0.05$ are presented as * $P \leq 0.05$, ** $P \leq 0.01$, *** $P \leq 0.001$ compared to respective controls (Two-way ANOVA followed by Tukey's multiple comparisons test)

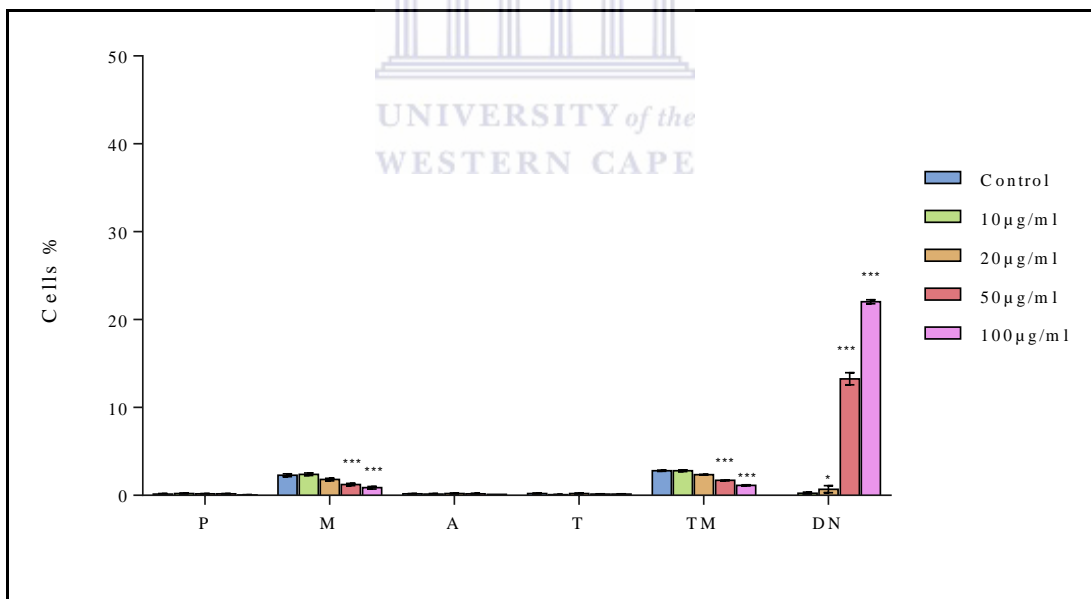


Figure 3.15: The quantification of the effects of OA on dividing pycnotic and apoptotic MCF-10A cells after 48h exposure. Prophase (P), metaphase (M), anaphase (A), telophase (T) and total mitosis (TM) after exposure to 10, 20, 50 and 100µg/ml OA are shown. TM was significantly decreased. 50 and 100µg/ml caused an increased in dead cells. Significant differences between treated and control samples are indicated by $p < 0.05$ are presented as * $P \leq 0.05$, ** $P \leq 0.01$, *** $P \leq 0.001$ compared to respective controls (Two-way ANOVA followed by Tukey's multiple comparisons test)

3.3.9 The effect of OA on MCF-7 and MCF-10A cells after 72h

Figure 3.16-A and F show H and E stained control MCF-7 and MCF-10A cells respectively. Figs B & G and C & H show cells treated with 10 and 20µg/ml OA. Morphological changes were not evident after exposure to these two concentrations in either of the cell lines. Figs D & J and I & E show the effects of 50 and 100µg/ml OA after 72h in the MCF-7 and MCF-10A cell line. The cells appear to be smaller with a loss of the growth pattern observed in the control cultures. Decreases in the number of darkly stained pycnotic and apoptotic cells can be seen. The MCF-10A cells appeared rounded after 100µg/ml OA while the MCF-7 cells seem elongated (E and J).

3.3.10 Mitotic index effect of OA on MCF-7 and MCF-10A cells after 72h

The effect of the various concentrations of OA on the two cell lines is shown in Figures 3.17 and 3.18. The study displayed that OA inhibited the percentage of mitotic MCF-7 cells. In both cell lines there was a significant decrease in mitosis after 72h. OA exposure significantly decreased TM in MCF-7 cells to 1.93% at 50µg/ml and 1.4% at 100µg/ml as shown in Fig 3.17 when compared the reduction in MCF-10A cells as shown in Fig 3.18. The reduction in TM in both the MCF-7 cells and the MCF-10A cells can be ascribed to a decrease in the number metaphase. Some apoptotic, but mostly pycnotic cells (10.03% and 18.9%) for 50 and 100µg/ml OA respectively were observed in these cultures exposed for 72h (Fig. 3.17). OA exposure of MCF-10A cells are shown in Fig 3.18. Normal dividing cells decreased significantly and concentration was an increase in dying cells (50µg/ml: 11.93%; 100µg/ml: 19.96%) were dose dependent ($P < 0.001$).

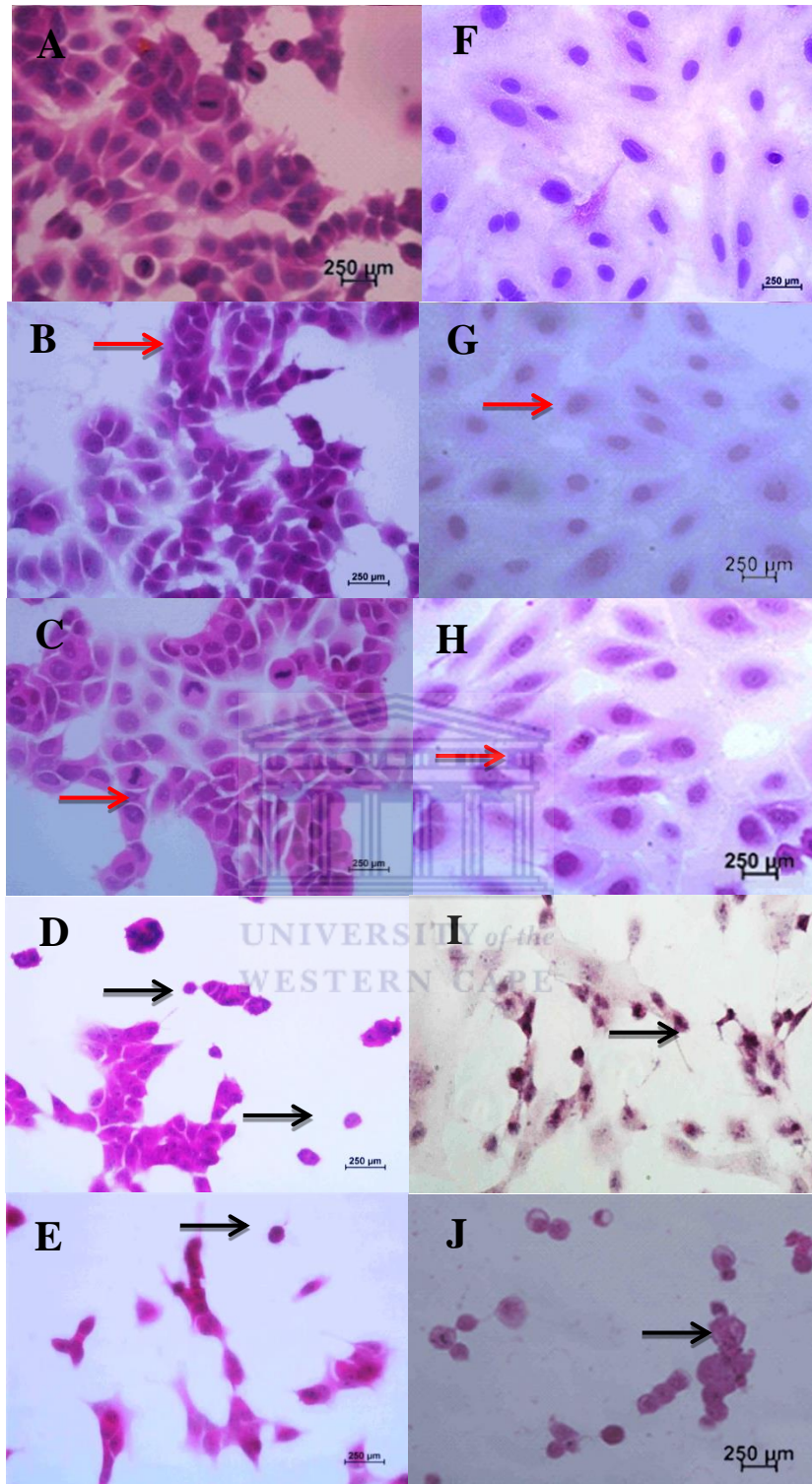


Figure 3.16: MCF-7 (A, B, C, D, E) and MCF-10A (F, G, H, I, J) cells were treated with OA after 72h and stained with haematoxylin eosin are shown. control cells (A); 10 μ g/ml (B); 20 μ g/ml (C); 50 μ g/ml (D); 100 μ g/ml (E); control cells (F); 10 μ g/ml (G); 20 μ g/ml (H); 50 μ g/ml (I) and 100 μ g/ml (J). Red arrows indicate normal cells dividing, and black arrows indicate complete apoptosis with all cells presenting with condensed chromatin and cytoplasmic shrinkage. All pictures are typical of three independent experiments each performed under identical conditions.

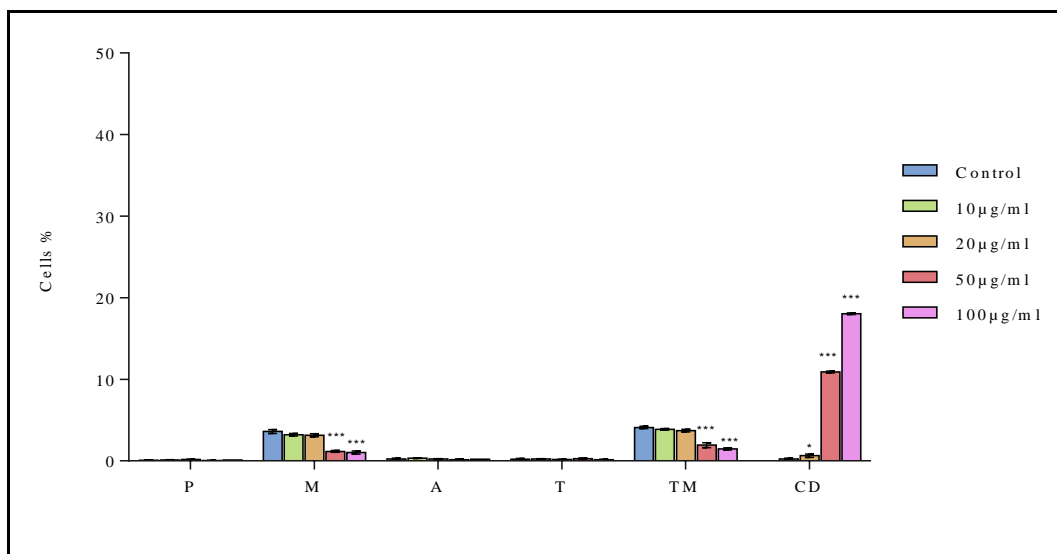


Figure 3.17: The quantification of the effects of OA on dividing, pycnotic and apoptotic MCF-7 cells after 72h exposure. Prophase (P), metaphase (M), anaphase (A), telophase (T) and total mitosis (TM) after exposure to 10, 20, 50 and 100µg/ml OA are shown. TM was significantly decreased. An increase in pycnotic and apoptotic cells (CD) after 50 and 100 was observed. Significant differences between treated and control samples are indicated by $p < 0.05$ are presented as * $P \leq 0.05$, ** $P \leq 0.01$, *** $P \leq 0.001$ compared to respective controls (Two-way ANOVA followed by Tukey's multiple comparisons test)

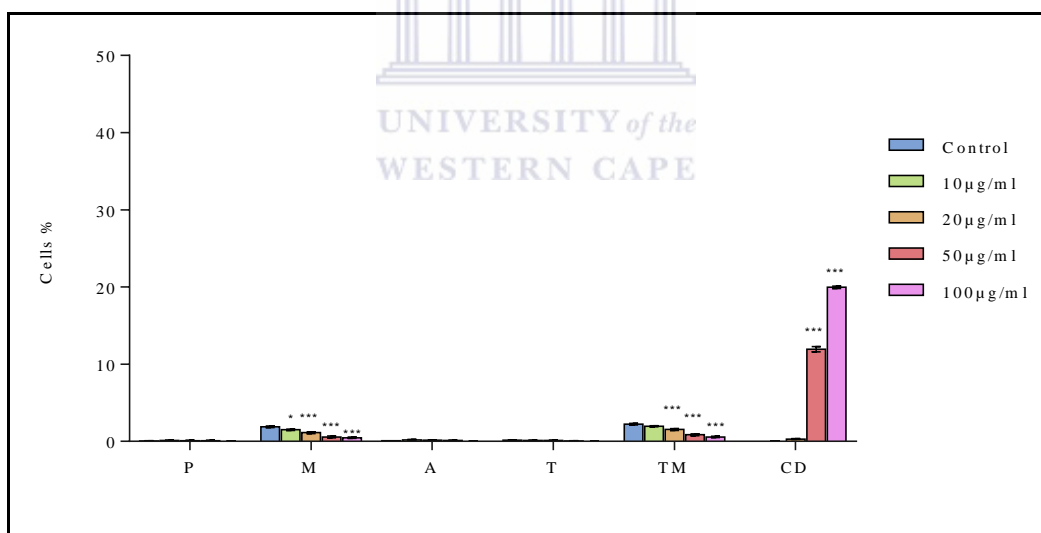
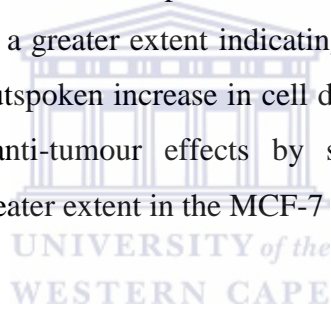


Figure 3.18: The quantification of the effects of OA on dividing, pycnotic and apoptotic MCF-10A cells after 72h exposure. Prophase (P), metaphase (M), anaphase (A), telophase (T) and total mitosis (TM) after exposure to 10, 20, 50 and 100µg/ml OA are shown. TM was decreased while an outspoken increase in pycnotic and apoptotic cells (CD) were seen in the cells exposed to 50 and 100µg/ml. Significant differences between treated and control samples are indicated by $p < 0.05$ are presented as * $P \leq 0.05$, ** $P \leq 0.01$, *** $P \leq 0.001$ compared to respective controls (Two-way ANOVA followed by Tukey's multiple comparisons test)

3.3.11 Effect OA: Comparison between MCF-7 and MCF-10A cell lines

The effect of various concentrations of OA on cancerous (MCF-7) and non-cancerous (MCF-10A) cell lines showed no visible morphological changes in the cells treated with 10 and 20 µg/ml OA when compared to untreated (control) cells. Pronounced effects were observed for the two cell lines treated with 50 and 100 µg/ml. Significant cell death was observed in cells treated with 50 and 100 µg/ml OA, starting from 6h and all the other time periods. The cellular response showed a similar trend in both MCF-7 and non-cancerous MCF-10A cell lines.

The cellular proliferative response was quantified by means of the mitotic index. TM was reduced in both cell lines at all-time points. The results showed that OA inhibited MCF-7 cell proliferation to a greater extent indicating a dose-dependent decrease in cell proliferation with an outspoken increase in cell death. These results suggest that OA exhibits significant anti-tumour effects by suppressing cell proliferation, promoting apoptosis to a greater extent in the MCF-7 cells than the MCF-10A cells.



3.3.12 The effect of UA on MCF-7 and MCF-10A cells after 6h

Morphological changes were studied in H&E stained cells. Figure 3.19-A and F illustrate control MCF-7 and MCF-10A cells respectively. Figs B & G and C & H appearance cells treated with 10 and 20µg/ml UA. No changes in either cell's morphology were observed after treatment 10 and 20µg/ml. 50µg/ml UA in MCF-10A cells did not effect, any outspoken morphological changes. In contrast, outspoken changes can be observed in the MCF-7 cells exposed to 50µg/ml UA. The cells display cytotoxic effects including shrinkage and condensation of chromatin (Fig. D). After 100µg/ml the MCF-10A cells appeared rounded and also display condensation chromatin while only a few dark, shrunken cells can be observed in the MCF-7 cells (Figs. J and E).

3.3.13 Mitotic index: the effect of UA on MCF-7 and MCF-10A cells after 6h

Quantification of UA treatment on cell proliferation is shown in Figures 3.20 and 3.21. The TM in MCF-7 cells was increased significantly ($P \leq 0.001$) after treatment with 10 and 20µg/ml UA to 5.3%. The cells exposed to 50 and 100µg/ml UA, however showed a decrease in TM (2.23% and 1.63%). Quantitative analyses revealed that MCF-7 cells exposed to UA showed an increase in the number of dead cells being either apoptotic or pycnotic (18.03% and 31.4%) for 50 and 100µg/ml UA respectively after the 6h exposure (Fig. 3.20). In MCF-10A cells the decrease in normal dividing and the increase in dying cells (20µg/ml; 7.5%; 50µg/ml; 27.3%; 100µg/ml; 36.6%) were time-and-dose dependent. The TM was reduced by 50 and 100µg/ml UA to 1% and 0.53%.

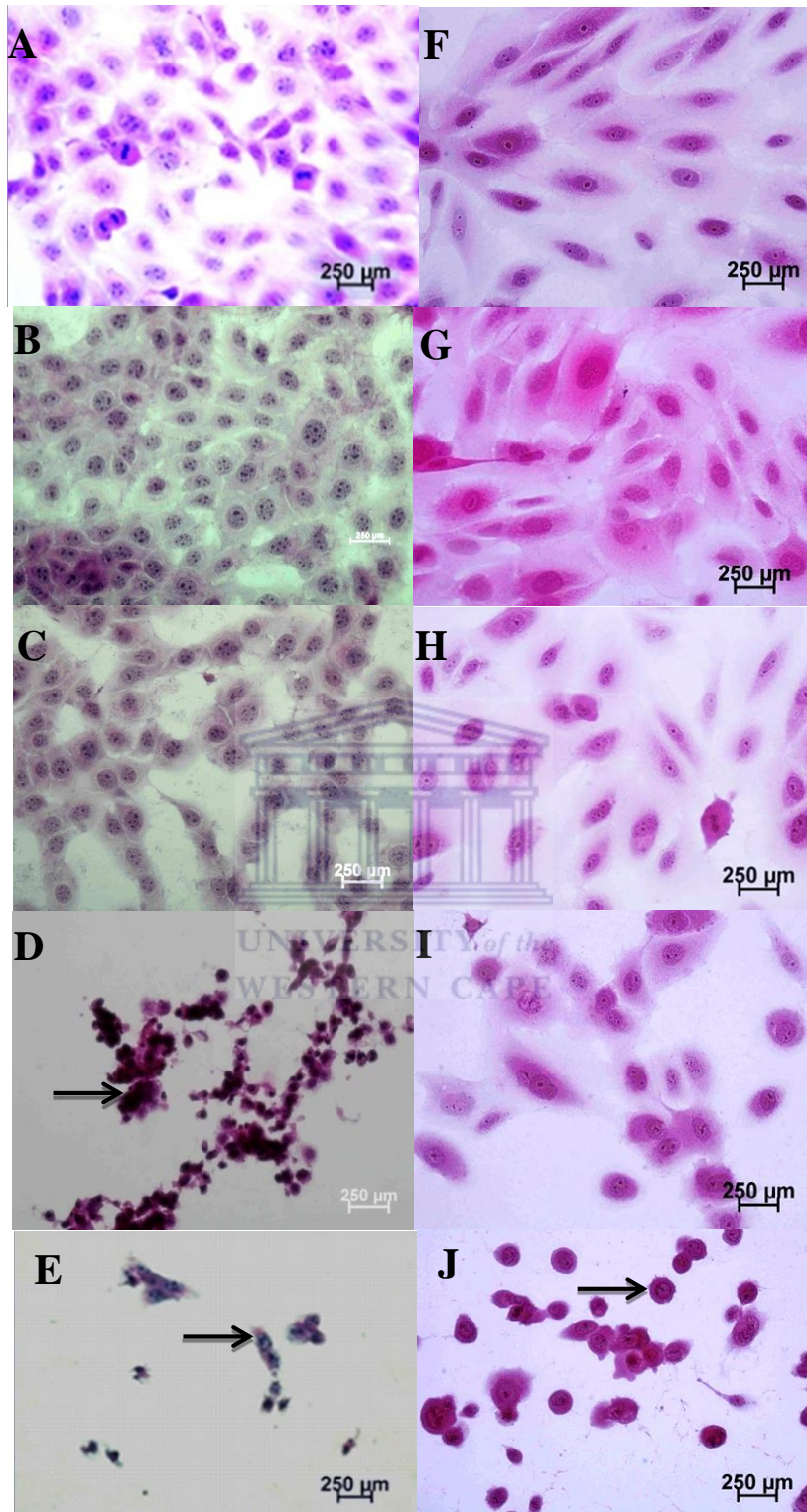


Figure 3.19: MCF-7 and MCF-10A cell morphology. MCF-7 (A, B, C, D, E) and MCF-10A (F, G, H, I, J) cells were treated with UA after 6h using haematoxylin-eosin staining. Control cells (A); 10 μ g/ml (B); 20 μ g/ml (C); 50 μ g/ml (D); 100 μ g/ml (E); Control cells (F); 10 μ g/ml (G); 20 μ g/ml (H); 50 μ g/ml (I) and 100 μ g/ml (J). Red arrows indicate normal cells dividing, and black arrows indicate complete apoptosis with all cells presenting with condensed chromatin and cytoplasmic shrinkage. All pictures are typical of three independent experiments each performed under identical conditions.

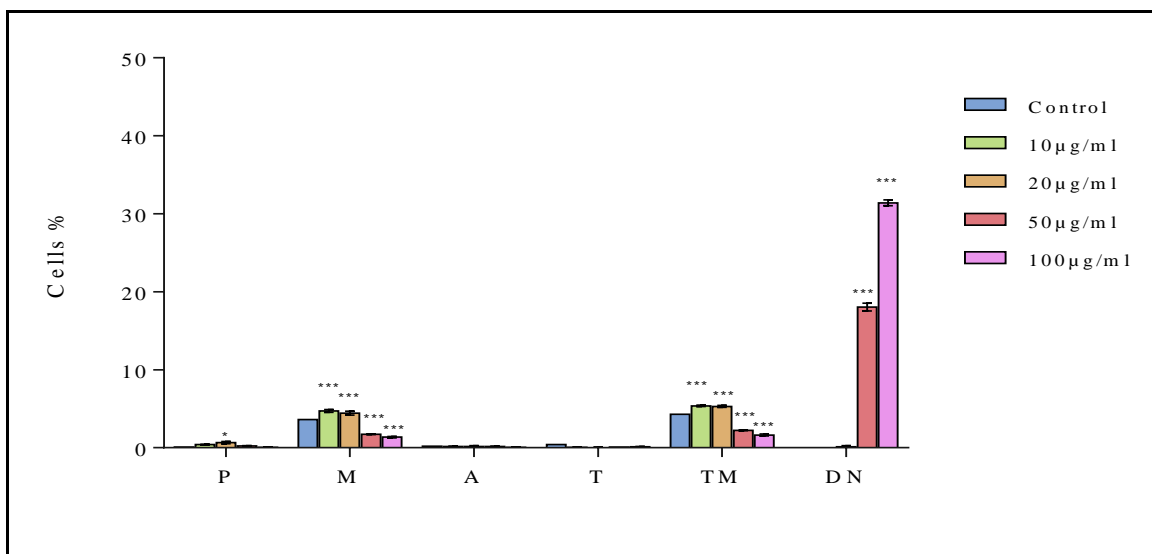


Figure 3.20: The quantification of the effects of UA on dividing pycnotic and apoptotic MCF-7 cells after 6h exposure. Prophase (P), metaphase (M), anaphase (A), telophase (T) and total mitosis (TM) after exposure to 10, 20, 50 and 100µg/ml UA are shown. TM was significantly decreased while an increase in pycnotic and apoptotic cells (DN) were observed. Significant differences between treated and control samples are indicated by $P < 0.05$ are presented as * $P \leq 0.05$, ** $P \leq 0.01$, *** $P \leq 0.001$ compared to respective controls (Two-way ANOVA followed by Tukey's multiple comparisons test)

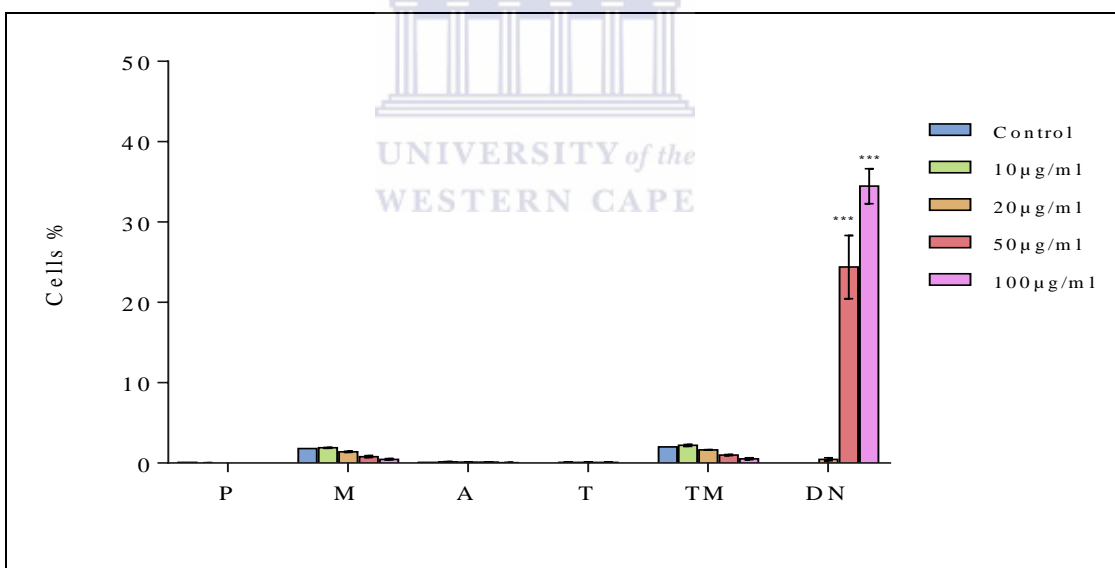


Figure 3.21: The quantification of the effects of UA on dividing pycnotic and apoptotic MCF-10A cells after 6h exposure. Prophase (P), metaphase (M), anaphase (A), telophase (T) and total mitosis (TM) after exposure to 10, 20, 50 and 100µg/ml UA are shown. TM was decreased while an outspoken increase in pycnotic and apoptotic cells (DN) were seen in the cells exposed to 50 and 100µg/ml. Significant differences between treated and control samples are indicated by $P < 0.05$ are presented as * $P \leq 0.05$, ** $P \leq 0.01$, *** $P \leq 0.001$ compared to respective controls (Two-way ANOVA followed by Tukey's multiple comparisons test)

3.3.14 The effect of UA on MCF-7 and MCF-10A cells after 12h

Figure 3.22-A and F illustrates control MCF-7 and MCF-10A interphase cells respectively. Figs B & G and C & H display cells treated with 10 and 20µg/ml UA. No morphological changes were observed. Figs D & J and I & E showed effects after 50 and 100µg/ml UA on the MCF-7 and MCF-10A cell lines after 12h. Morphological changes indicative of apoptosis, such as overall cell shrinkage, blebbing of the plasma membrane, changes in nuclear morphology including chromatin condensation, were observed. The number of cells was also reduced in these cultures.

3.3.15 Mitotic index: effect of UA on MCF-7 and MCF-10A cells after 12h

The mitotic indices in MCF-7 and MCF-10A cells incubated with UA after 12h is shown in Figs 3.23 and 3.24. The study displayed that UA inhibited the percentage of mitotic MCF-7 cells. Exposure to UA for 12h caused the total mitosis to be reduced in the MCF-7 cells after 50 and 100µg/ml to 2.06% and 0.8% and in MCF-10A cells after 50 and 100 µg/ml to 0.86% and 0.23% when compared to control. Some apoptotic, but mostly pycnotic cells (13.8% and 28.16%) for 50 and 100µg/ml UA treated cells respectively were observed (Fig. 3.23). A decrease in normal MCF-10A dividing cells compared to an increase in dying cells (50µg/ml; 12.8%; 100µg/ml; 29.8%) were seen.

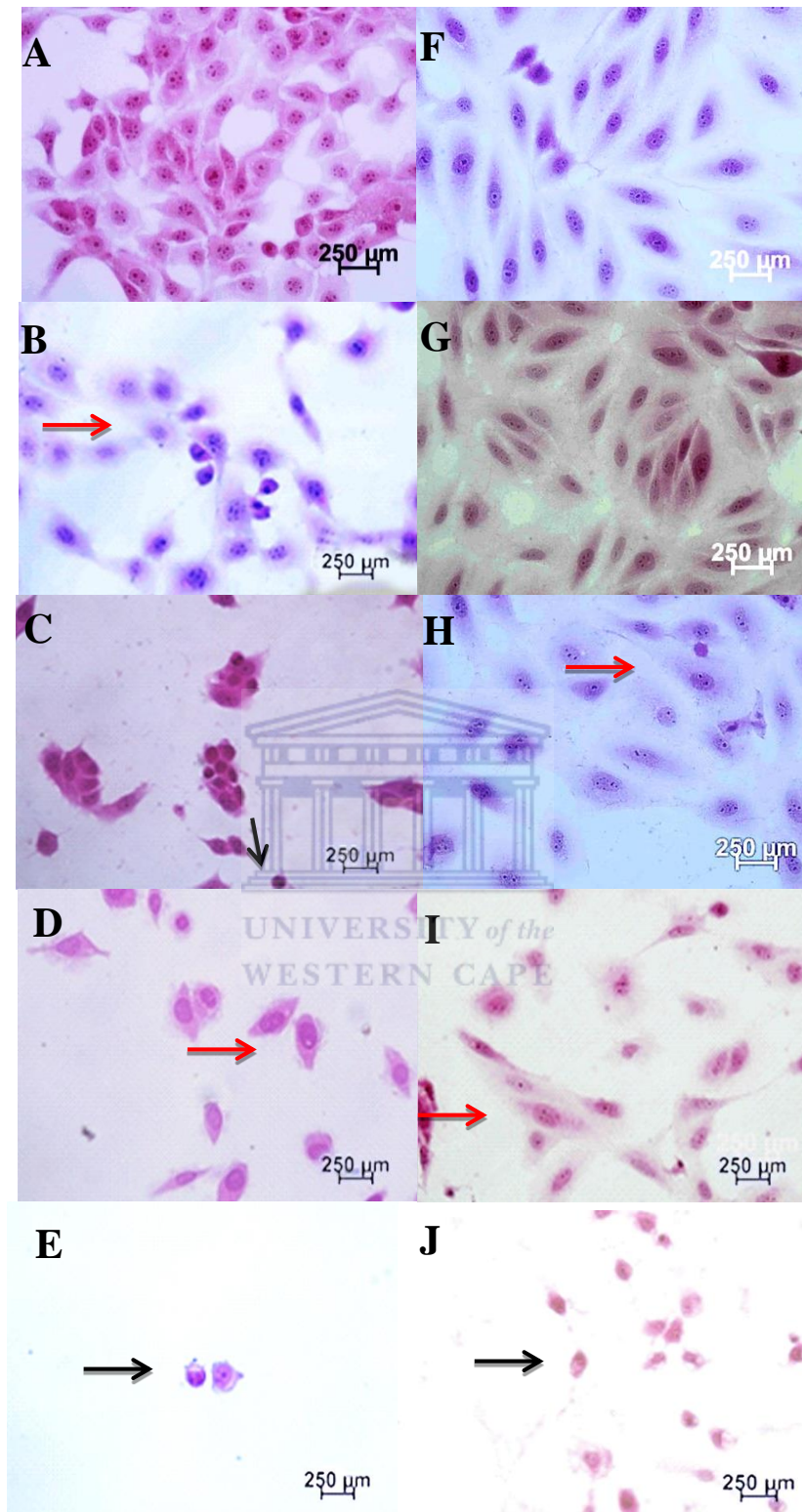


Figure 3.22: MCF-7 and MCF-10A cell morphology. MCF-7 (A, B, C, D, E) and MCF-10A (F, G, H, I, J) cells were treated with UA after 12h using haematoxylin-eosin staining. Control cells (A); 10 μ g/ml (B); 20 μ g/ml (C); 50 μ g/ml (D); 100 μ g/ml (E); Control cells (F); 10 μ g/ml (G); 20 μ g/ml (H); 50 μ g/ml (I) and 100 μ g/ml (J). Red arrows indicate normal cells dividing, and black arrows indicate complete apoptosis with all cells presenting with condensed chromatin and cytoplasmic shrinkage. All pictures are typical of three independent experiments each performed under identical conditions.

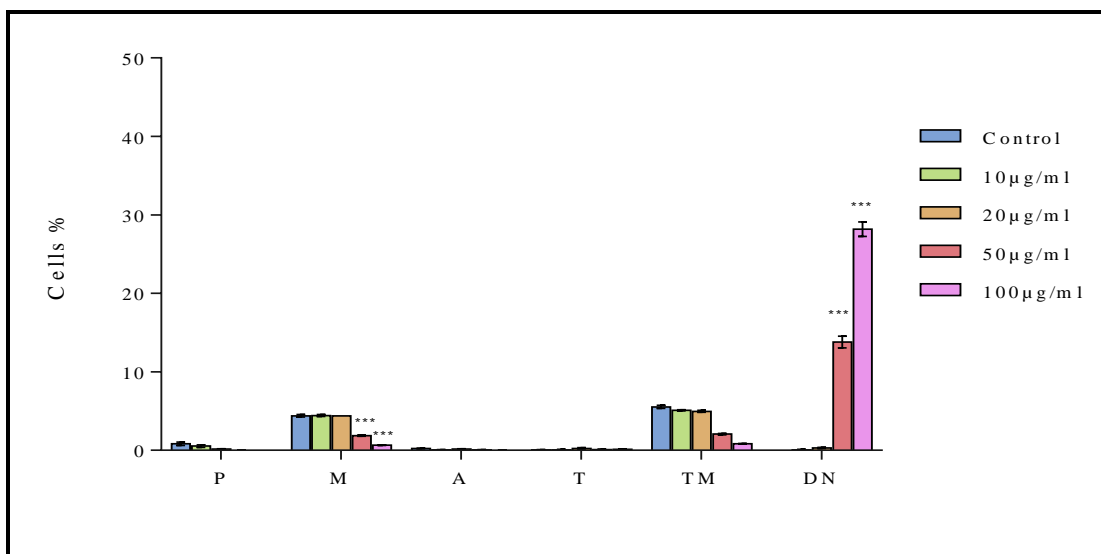


Figure 3.23: The MCF-7 quantification of the effects of UA on dividing and pycnotic and apoptotic cells after 12h exposure. Prophase (P), metaphase (M), anaphase (A), telophase (T) and total mitosis (TM) after 12h exposure to 10, 20, 50 and 100µg/ml UA are shown. TM was significantly decreased while an increase in pycnotic and apoptotic cells (DN) were present. Significant differences between treated and control samples are indicated by $p < 0.05$ are presented as * $P \leq 0.05$, ** $P \leq 0.01$, *** $P \leq 0.001$ compared to respective controls (Two-way ANOVA followed by Tukey's multiple comparisons test)

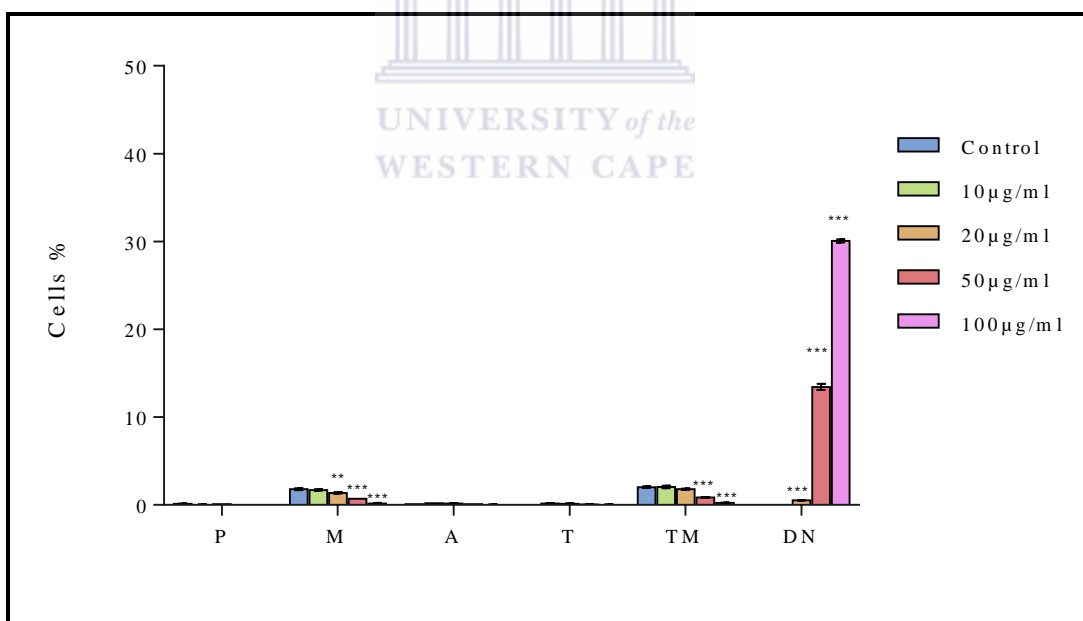


Figure 3.24: The MCF-10A quantification of the effects of UA on dividing and pycnotic and apoptotic cells after 12h exposure. Prophase (P), metaphase (M), anaphase (A), telophase (T) and total mitosis (TM) after exposure to 10, 20, 50 and 100µg/ml UA are shown. TM was decreased while an outspoken increase in pycnotic and apoptotic cells (DN) were seen in the cells exposed to 50 and 100µg/ml. Significant differences between treated and control samples are indicated by $P < 0.05$ are presented as * $P \leq 0.05$, ** $P \leq 0.01$, *** $P \leq 0.001$ compared to respective controls (Two-way ANOVA followed by Tukey's multiple comparisons test)

3.3.16 The effect of UA on MCF-7 and MCF-10A cells after 24h

Figure 3.25-A and F shows control MCF-7 and MCF-10A cells respectively. Figs B & G and C & H display cells exposed to 10 and 20µg/ml UA. Morphological changes were not observed with the low concentrations on the two cell lines. Figs D & I showed changes after 50µg/ml UA on the MCF-7 and MCF-10A cells. The cells appeared rounded with condensed chromatin and cell shrinkage that can be either pycnotic or apoptotic. Figs E & J showed MCF-7 and MCF-10A cells exposed to 100µg/ml UA. Morphological changes, including apoptotic cells revealing characteristic changes in nuclear morphology, including chromatin condensation and fragmentation can be observed.

3.3.17 Mitotic index: effect of UA on MCF-7 and MCF-10A cells after 24h

Quantification of the effects of UA treatment on MCF-7 and MCF-10A cells after 24h is shown in Figures 3.26 and 3.27. The study revealed that UA inhibited the number of mitotic MCF-7 cells. An increase in the number of apoptotic cells (13.46% and 18.86%) for 50 and 100µg/ml UA respectively in the cultures exposed for 24h, was observed (Fig. 3.26). In MCF-10A cells, the percentage of cells affected by UA is shown in Fig 3.27. A decrease in normal MCF-10A dividing cells compared to an increase in dying cells (50µg/ml; 12.53%; 100µg/ml; 27.66%) was discerned. Total mitosis in MCF-7 was significantly increased by 50 and 100µg/ml UA to 3.06% and 1.63%, while in the MCF-10A cells TM was decreased by 50 and 100 µg/ml UA to 1.26% and 0.66% ($P \leq 0.001$).

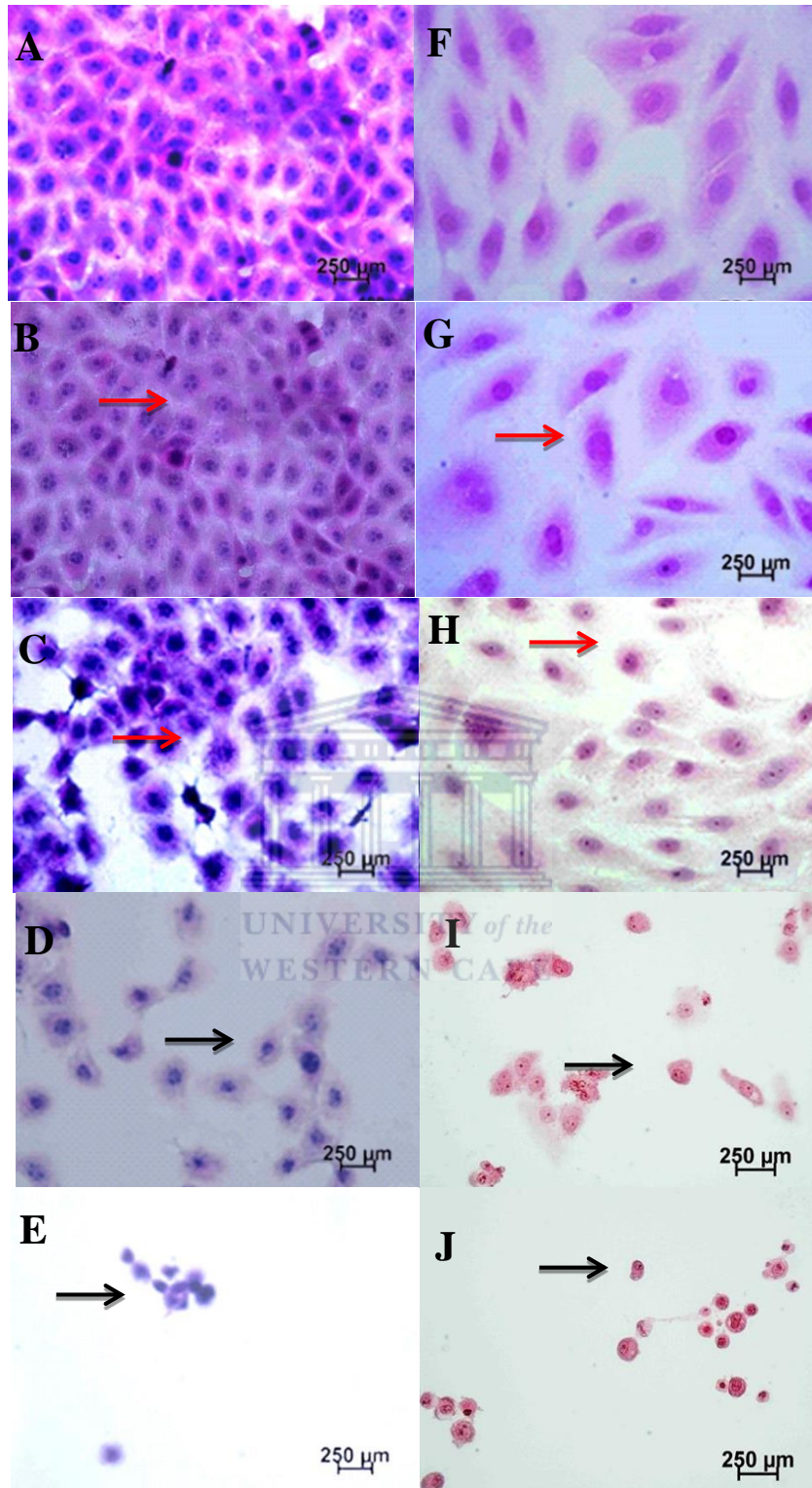


Figure 3.25: MCF-7 and MCF-10A cell morphology. MCF-7 (A, B, C, D, E) and MCF-10A (F, G, H, I, J) cells were treated with UA after 24h using haematoxylin-eosin staining. Control cells (A); 10µg/ml (B); 20µg/ml (C); 50µg/ml (D); 100µg/ml (E); Control cells (F); 10µg/ml (G); 20µg/ml (H); 50µg/ml (I) and 100µg/ml (J). Red arrows indicate normal cells dividing, and black arrows indicate complete apoptosis with all cells presenting with condensed chromatin and cytoplasmic shrinkage. All pictures are typical of three independent experiments each performed under identical conditions.

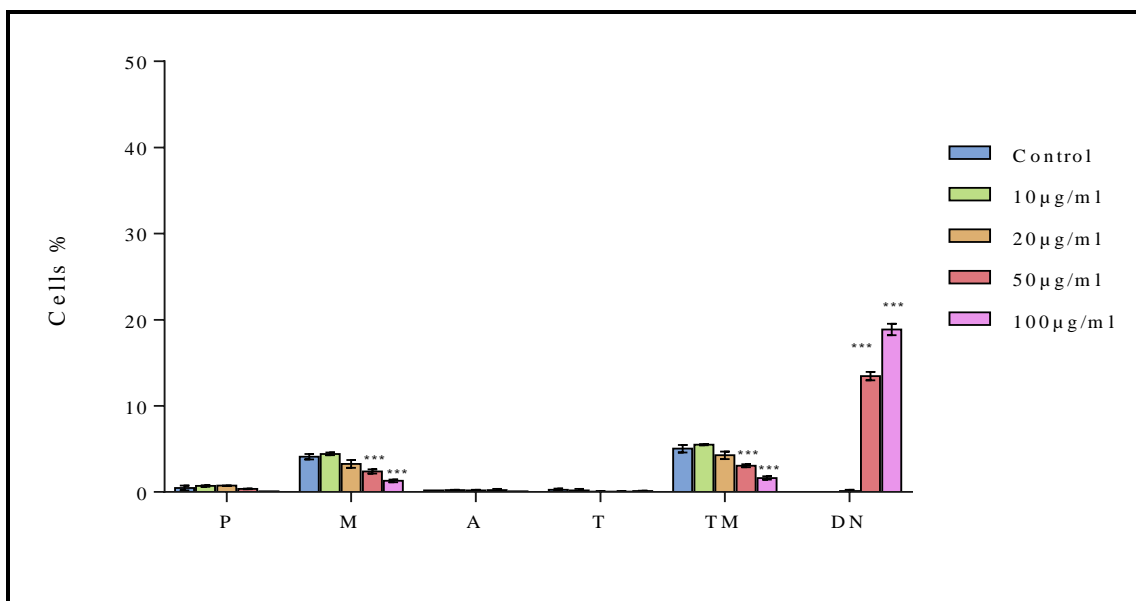


Figure 3.26: The quantification of the effects of UA on dividing pycnotic and apoptotic MCF-7 cells after 24h exposure. Prophases (P), metaphase (M), anaphase (A), telophase (T) and total mitosis (TM) after exposure to 10, 20, 50 and 100µg/ml UA are shown. TM was significantly decreased while an increase in pycnotic and apoptotic cells (DN) were present. Significant differences between treated and control samples are indicated by $P < 0.05$ are presented as * $P \leq 0.05$, ** $P \leq 0.01$, *** $P \leq 0.001$ compared to respective controls (Two-way ANOVA followed by Tukey's multiple comparisons test)

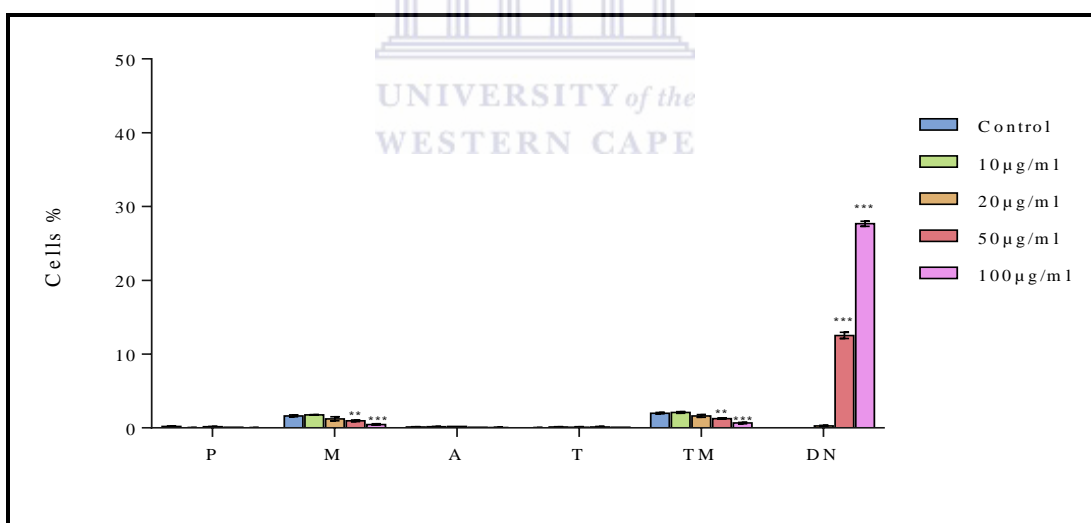


Figure 3.27: The quantification of the effects of UA on dividing pycnotic and apoptotic MCF-7 cells after 24h exposure. Prophase (P), metaphase (M), anaphase (A), telophase (T) and total mitosis (TM) after exposure to 10, 20, 50 and 100µg/ml UA are shown. TM was decreased while an outspoken increase in pycnotic and apoptotic cells (DN) were seen in the cells exposed to 50 and 100µg/ml. Significant differences between treated and control samples are indicated by $P < 0.05$ are presented as * $P \leq 0.05$, ** $P \leq 0.01$, *** $P \leq 0.001$ compared to respective controls (Two-way ANOVA followed by Tukey's multiple comparisons test)

3.3.18 The effect of UA on MCF-7 and MCF-10A cells after 48h

Morphological changes were studied in H&E stained cells. Figure 3.28-A and F display control MCF-7 and MCF-10A cells respectively. Figs B & G, C & H and D & I show cells after treatment with 10 and 20 μ g/ml UA. No outspoken morphological changes were observed in either of the two cell lines.

Figs I and E showed cells exposed to 50 μ g/ml UA for 48h. UA affected many of the MCF-10A dividing cells. Morphological changes include decreased cell size and darkly stained rounded cells. The MCF-7 cells showed only a few cells affected by 50 μ g/ml UA. 100 μ g/ml UA (Figs. I and E) showed enlarged ghost-like MCF-7 cells and small darkly stained rounded MCF-10A cells.

3.3.19 Mitotic index: effect of UA on MCF-7 and MCF-10A cells after 48h

The effect of the various concentrations of UA on dividing cells in the two cell lines is shown in Figures 3.29 and 3.30. Quantitative analyses by means of mitotic indices showed a distinct increase in the number of apoptotic and abnormal cells in MCF-7 (9.13% and 17.16%) for samples exposed to 50 and 100 μ g/ml UA respectively (Fig. 3.29). In MCF-10A cells, the percentage of cells affected by UA is shown in Fig 3.30. A decrease in normal dividing MCF-10A cells is observed parallel to an increase in dying cells (50 μ g/ml; 8.96%; 100 μ g/ml; 14.5%). After 72h cells exposure with UA, total mitosis decreased MCF-7 cell proliferation to 1.56% at 50 μ g/ml and 0.7% at 100 μ g/ml. Similarity, total mitosis was reduced in MCF-10A cells to 1.33% at 20 μ g/ml, 1.06% at 50 μ g/ml and 0.76% at 100 μ g/ml when compared to control.

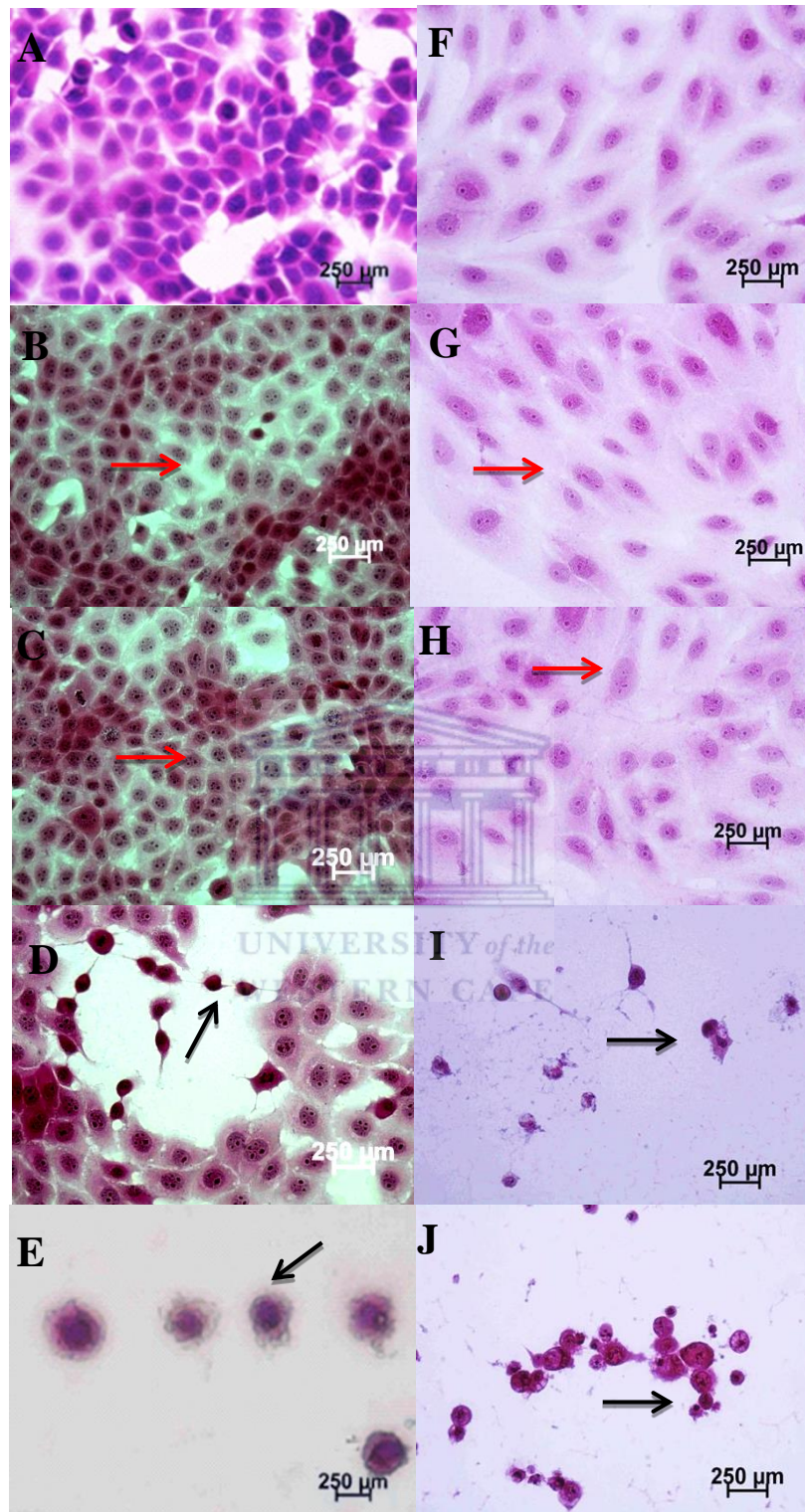


Figure 3.28: MCF-7 and MCF-10A cell morphology. MCF-7 (A, B, C, D, E) and MCF-10A (F, G, H, I, J) cells were treated with UA after 48h using haematoxylin-eosin staining. Control cells (A); 10 μ g/ml (B); 20 μ g/ml (C); 50 μ g/ml (D); 100 μ g/ml (E); Control cells (F); 10 μ g/ml (G); 20 μ g/ml (H); 50 μ g/ml (I) and 100 μ g/ml (J). Red arrows indicate normal cells dividing, and black arrows indicate complete apoptosis with all cells presenting with condensed chromatin and cytoplasmic shrinkage. All pictures are typical of three independent experiments each performed under identical conditions.

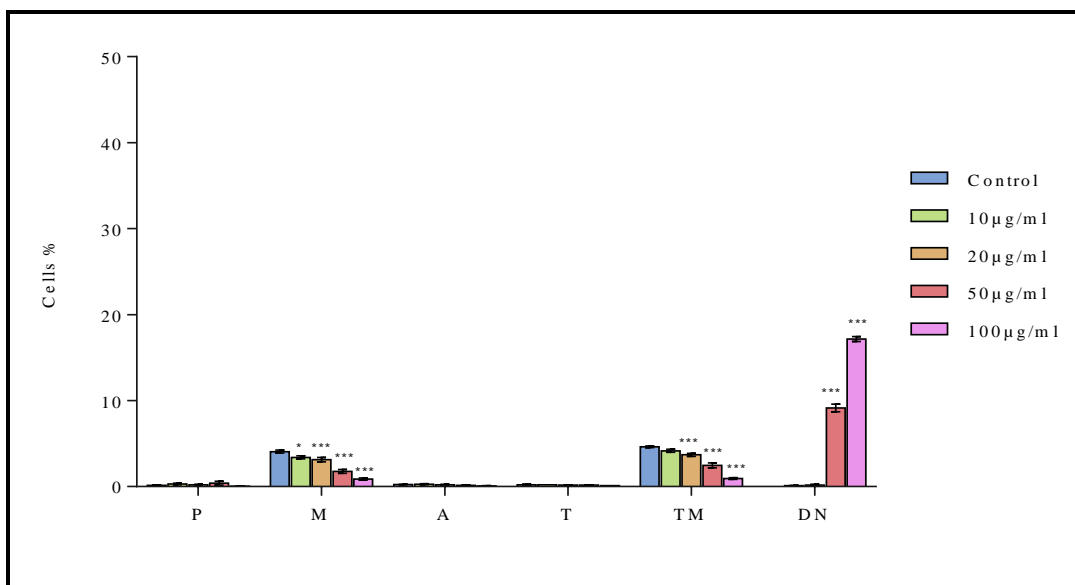


Figure 3.29: The MCF-7 quantification of the effects of UA on dividing and pycnotic and apoptotic cells after 48h exposure. Prophase (P), metaphase (M), anaphase (A), telophase (T) and total mitosis (TM) after 48h exposure to 10, 20, 50 and 100µg/ml UA are shown. TM was significantly decreased while an increase in pycnotic and apoptotic cells (DN) were present. Significant differences between treated and control samples are indicated by $P < 0.05$ are presented as * $P \leq 0.05$, ** $P \leq 0.01$, *** $P \leq 0.001$ compared to respective controls (Two-way ANOVA followed by Tukey's multiple comparisons test)

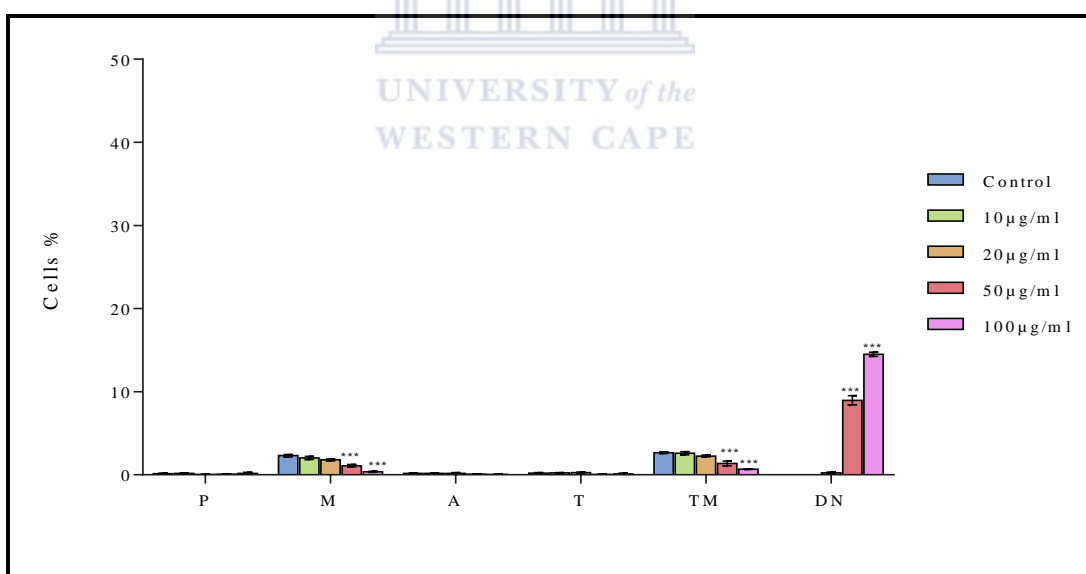


Figure 3.30: The MCF-10A quantification of the effects of UA on dividing and pycnotic and apoptotic cells after 48h exposure. Prophase (P), metaphase (M), anaphase (A), telophase (T) and total mitosis (TM) after 48h exposure to 10, 20, 50 and 100µg/ml UA are shown. TM was significantly decreased while an increase in pycnotic and apoptotic cells (DN) were present. Significant differences between treated and control samples are indicated by $P < 0.05$ are presented as * $P \leq 0.05$, ** $P \leq 0.01$, *** $P \leq 0.001$ compared to respective controls (Two-way ANOVA followed by Tukey's multiple comparisons test)

3.3.20 The effect of UA on MCF-7 and MCF-10A cells after 72h

Morphological changes were studied in H&E stained cells. Figure 3.31-A and F displayed control MCF-7 and MCF-10A cells respectively. As observed for all the other time periods, 10 and 20µg/ml had no effect on the morphology of either of the cell lines. 50µg/ml UA had an outspoken effect on the MCF-10A cell line causing a decrease in cells and smaller fragmented cells. The MCF-7 cells were not affected by 50µg/ml UA. 100µg/ml UA observed the MCF-7 cells can be observed (Figs. E and J).

3.3.21 Mitotic index: effect of UA on MCF-7 and MCF-10A cells after 72h

Quantification of cell proliferation is indicated by mitotic indices obtained by counting 1000 cells on every coverslip. Total mitosis (expressed as a percentage) included all the normal phases of dividing cells as well as pycnotic and apoptotic cells. The effect of the various concentrations of UA on the two cell lines is shown in Figures 3.32 and 3.33. UA inhibited the percentage of mitotic MCF-7 cells. Mitotic indices revealed an increase in the number of apoptotic cells (7.73% and 16.1%) for 50 and 100µg/ml UA respectively (Fig. 3.32). In MCF-10A cells UA decreased normal dividing MCF-10A cells while inducing an outspoken increase in dying cells (50µg/ml; 6.3 %; 100µg/ml; 15.9%). TM significantly decreased by 20, 50 and 100µg/ml UA to 3.7, 2.46% and 0.9% in the MCF-7, ($P \leq 0.001$) and by 50 and 100µg/ml UA to 1.36% and 0.66% in MCF-10A cells ($P \leq 0.001$) can be observed.

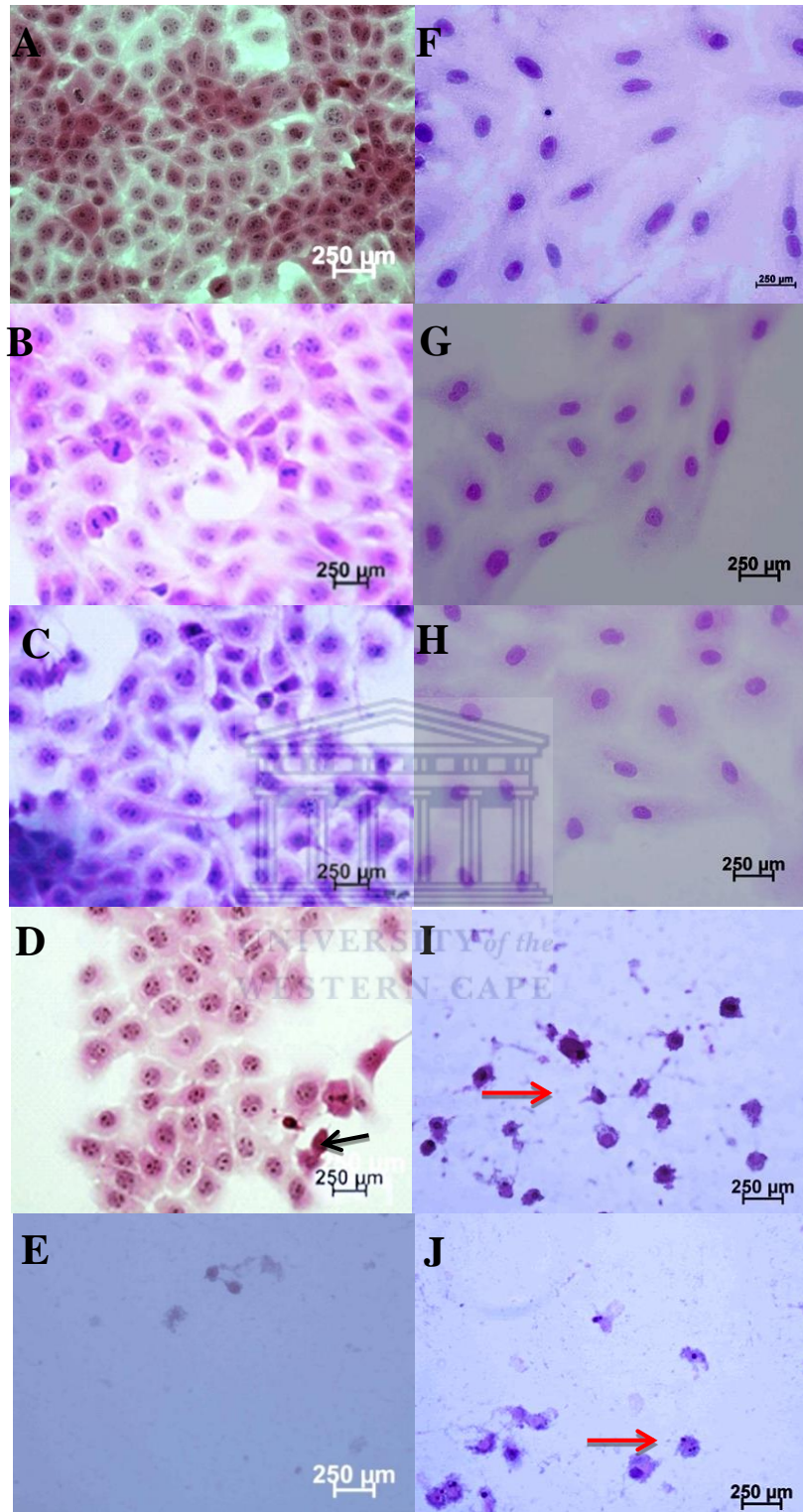


Figure 3.31: MCF-7 and MCF-10A cell morphology. MCF-7 (A, B, C, D, and E) and MCF-10A (F, G, H, P, and Q) cells were treated with UA after 72 h stained with haematoxylin-eosin. Control cells (A); 10µg/ml (B); 20µg/ml (C) 50µg/ml and (D) 100µg/ml (E); Control cells (F); 10µg/ml (G); 20µg/ml (H) 50µg/ml and (I) 100µg/ml (J). Red arrows indicate irregular-shaped dividing cells, and black arrows indicate complete apoptosis with all cells presenting with condensed chromatin and cytoplasmic shrinkage. All pictures are typical of three independent experiments each performed under identical conditions.

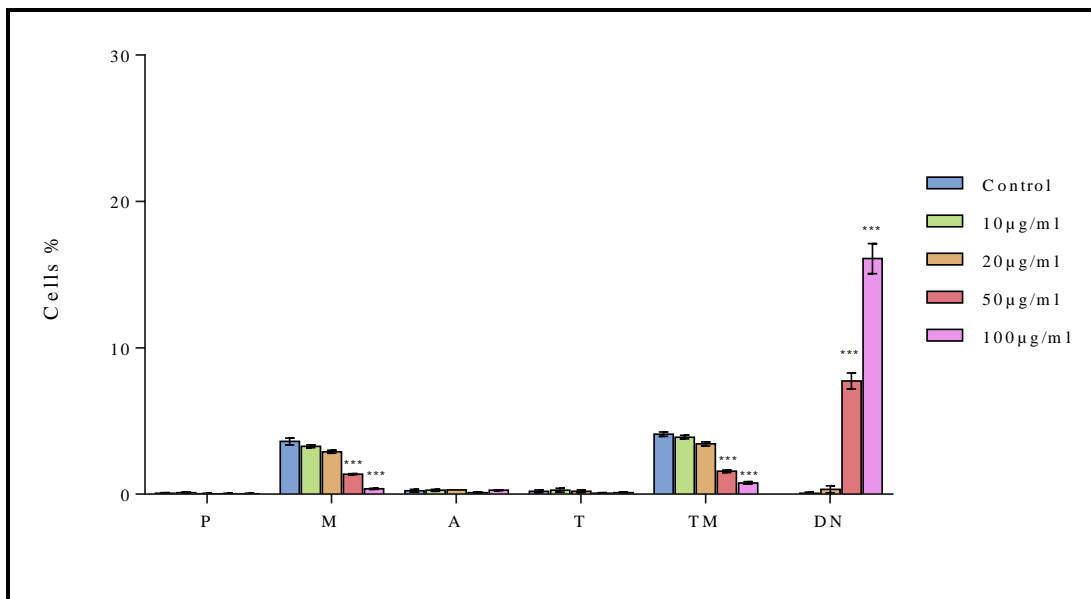


Figure 3.32: The MCF-7 quantification of the effects of UA on dividing and pycnotic and apoptotic cells after 72h exposure. Prophase (P), metaphase (M), anaphase (A), telophase (T) and total mitosis (TM) after 48h exposure to 10, 20, 50 and 100µg/ml UA are shown. TM was significantly decreased while an increase in pycnotic and apoptotic cells (DN) were present. Significant differences between treated and control samples are indicated by $P < 0.05$ are presented as * $P \leq 0.05$, ** $P \leq 0.01$, *** $P \leq 0.001$ compared to respective controls (Two-way ANOVA followed by Tukey's multiple comparisons test)

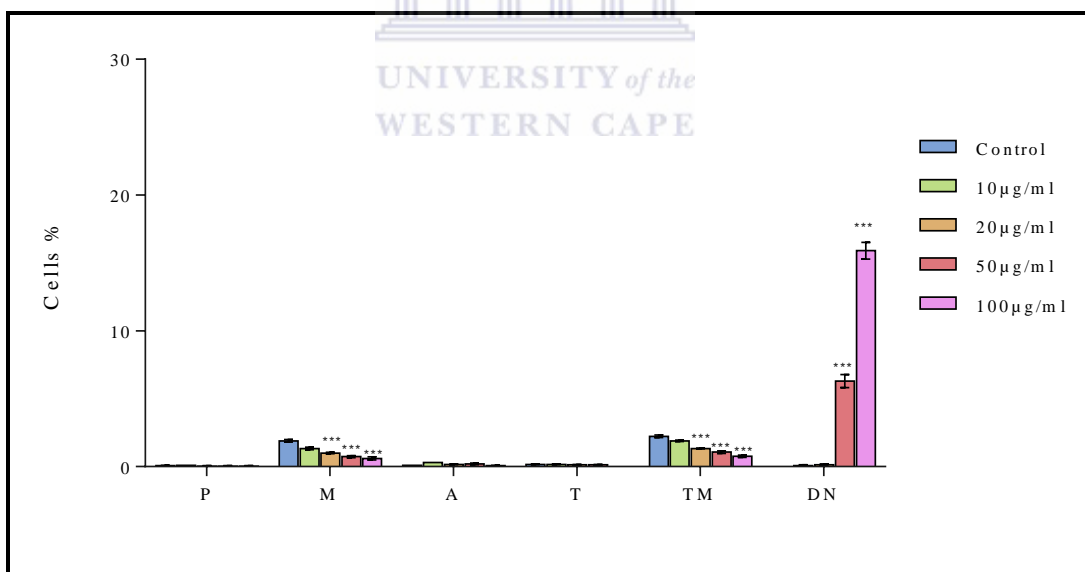


Figure 3.33: The MCF-10A quantification of the effects of UA on dividing and pycnotic and apoptotic cells after 72h exposure. Prophase (P), metaphase (M), anaphase (A), telophase (T) and total mitosis (TM) after 72h exposure to 10, 20, 50 and 100µg/ml UA are shown. DN was significantly decreased while an increase in pycnotic and apoptotic cells (DN) were present. Significant differences between treated and control samples are indicated by $P < 0.05$ are presented as * $P \leq 0.05$, ** $P \leq 0.01$, *** $P \leq 0.001$ compared to respective controls (Two-way ANOVA followed by Tukey's multiple comparisons test)

3.3.22 Mitotic index: effect of UA on MCF-7 and MCF-10A cells

As was the case with OA, UA caused no outspoken morphological changes in either of the cell types treated with 10 and 20 µg/ml OA. TM was reduced in both cell lines at all-time points. Pronounced effects were observed for the two cell lines treated with 50 and 100 µg/ml UA. Significant cell death was observed in cells treated with 50 and 100 µg/ml UA. The cellular response showed a similar trend in both MCF-7 and non-cancerous MCF-10A cell lines but more outspoken cytotoxic morphological changes were observed in MCF-10A cells. A dose response effect was also observed for UA exposure in MCF-7 and MCF-10A cells. However, UA had a greater effect on MCF-10A cells, seemingly being more cytotoxic to the non-transformed breast cells.

According to Nikolettou et al., (2013), apoptotic cell death shows a distinct and characteristic morphology that includes the rounding up of the cell so that it appears pyknotic, the condensation of chromatin, the fragmentation of the nucleus and the shedding of apoptotic bodies, vacuoles containing cytoplasm and intact organelles. It is because of this observation that no distinction is made morphologically between apoptosis and pycnosis observed in both cell lines after exposure to either triterpene.

3.3.23 Contrasting proliferative effects between MCF-7 and MCF-10A

Comparison of dissimilarity between the two cell lines following treatment with a specific concentration of OA and UA is shown in Figs. 3.34 – 3.37. It is clear from the comparative histograms that although the same amount of cells were seeded at the start of the experiment, after 24h attachment and the various treatment times, the mitotic index in MCF-10A cells is lower. This is due to the fact that the two cell lines have different doubling times with MCF-10A having a longer cell cycle than MCF-7 cells.

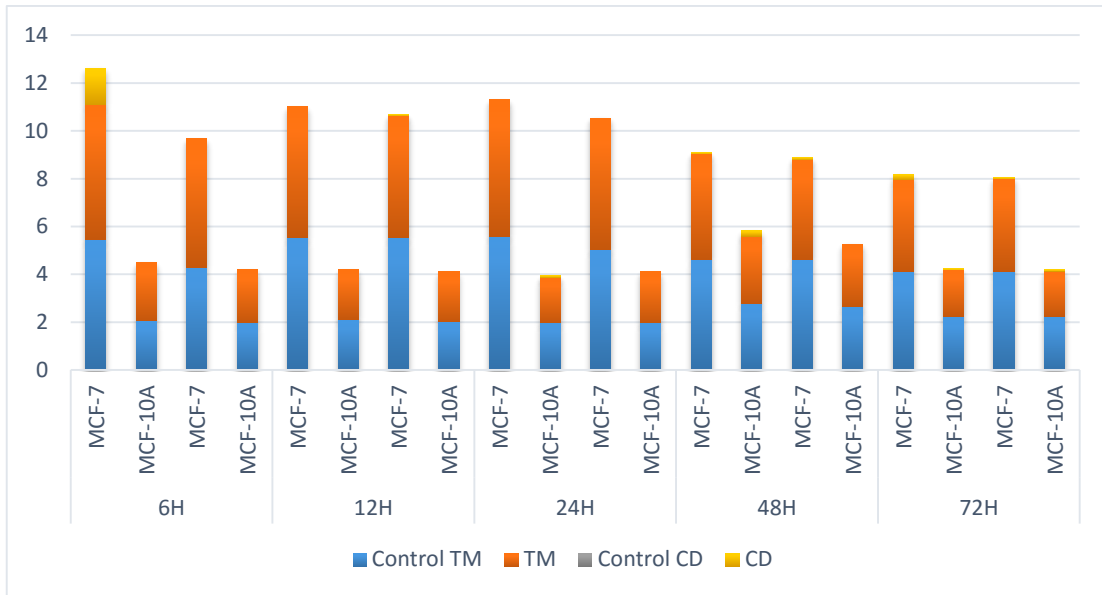


Figure 3.34: The percentage mitotic – and dead cells in MCF-7 and MCF-10A cells exposed to 10µg/ml for the different time periods. The first two bars in each time slot show OA and the last two show the effect of UA. No outspoken differences between the different cell lines before and after treatment were observed. MCF-7 cells exposed to OA for 6h had the highest percentage dead cells. (Excel 2013)

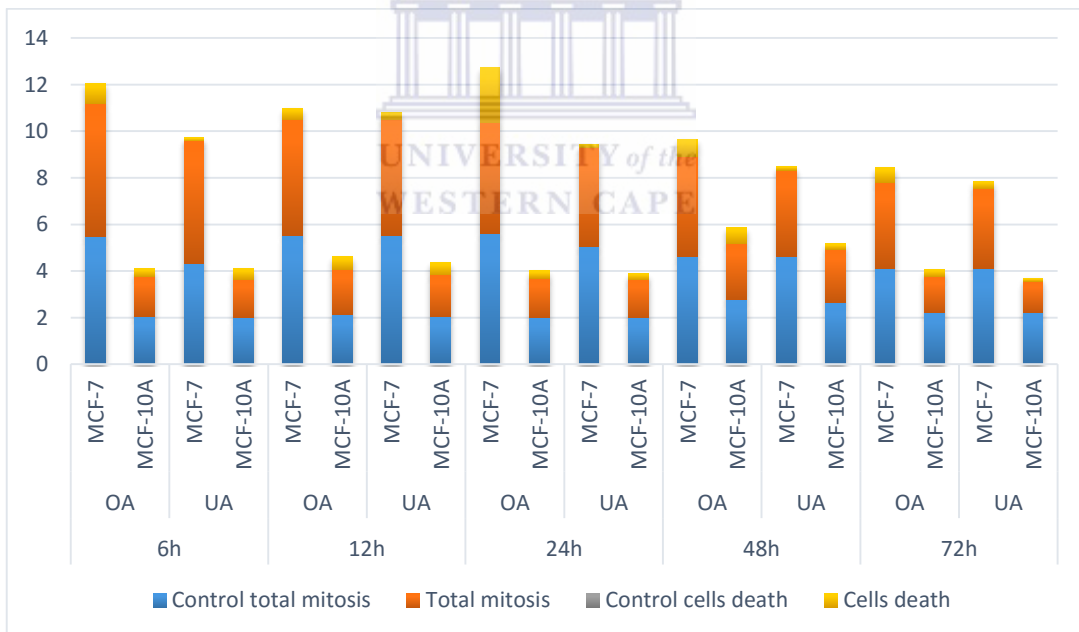


Figure 3.35: The percentage mitotic – and dead cells in MCF-7 and MCF-10A cells exposed to 20µg/ml for the different time periods. MCF-7 cells exposed for 24h had the highest percentage dead cells. (Excel 2013)

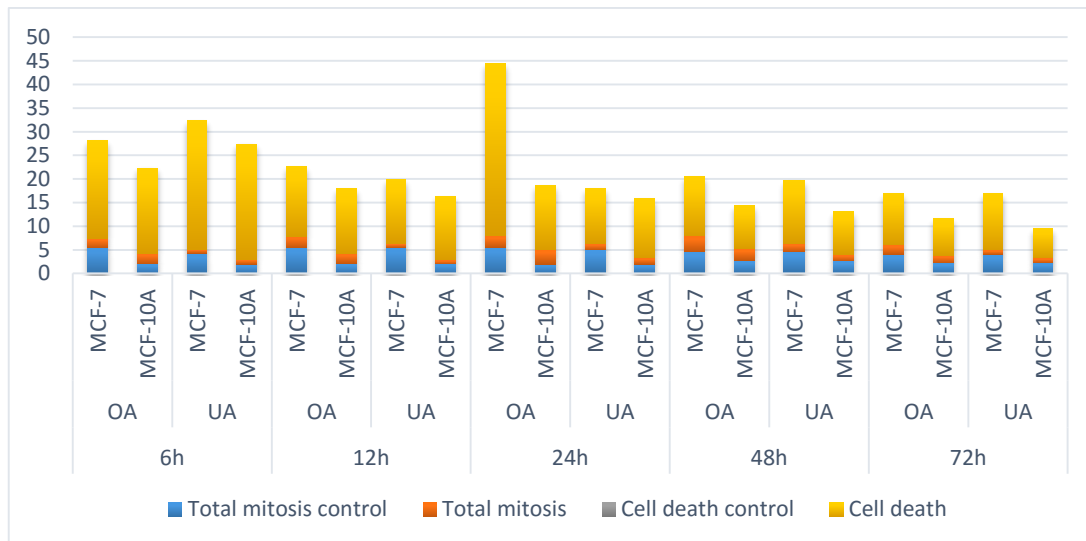


Figure 3.36: The percentage mitotic – and dead cells in MCF-7 and MCF-10A cells exposed to 50µg/ml for the different time periods. The highest percentage dead cells were seen in MCF-7 cells after 6- and 24h exposure to 50µg/ml OA. (Excel 2013)

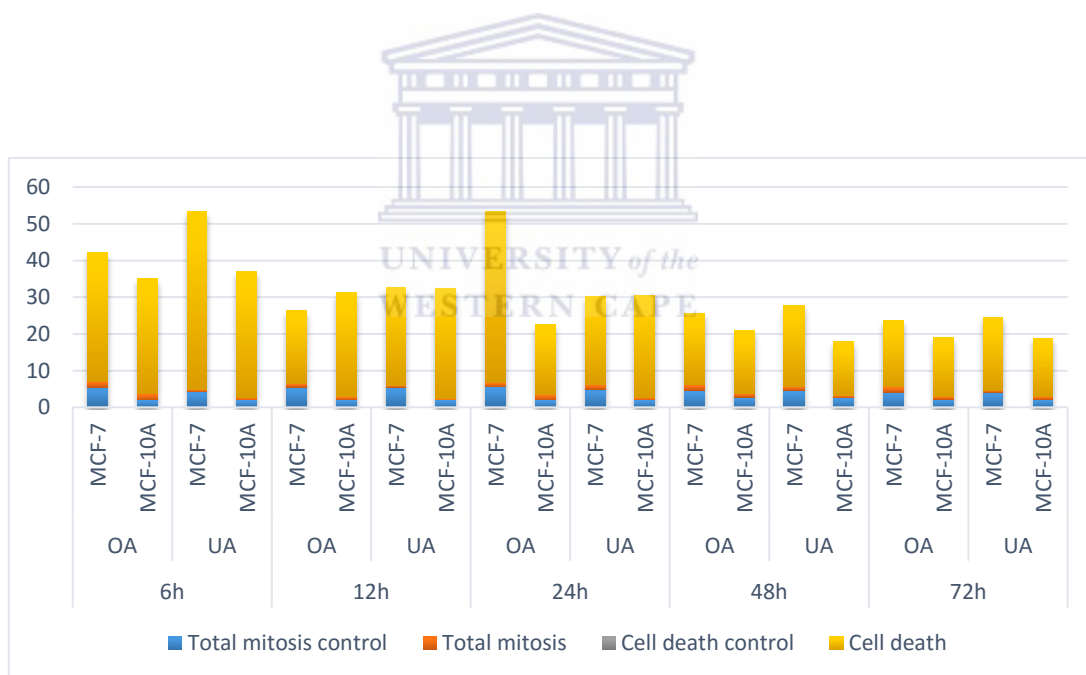


Figure 3.37: The percentage mitotic – and dead cells in MCF-7 and MCF-10A cells exposed to 100µg/ml for the different time periods. MCF-7 cells showed the greatest amount of dead cells after treatment with UA after 6h and OA after 24h. (Excel 2013)

3.4 Hoechst 33342 staining (HOC)

3.4.1 Effect of OA and UA on MCF-7 and MCF-10A cells after 6h

Hoechst 33342 staining was carried out to establish the possible induction of apoptosis after the treatment of OA (Fig. 3.38 A-J) and UA (Fig. 3.38 K-T) on the MCF-7 and MCF-10A cell lines after 6h.

As shown in Fig. 3.38-A, MCF-7 control cells display normal nuclei. Fig. 3.38-B (10 μ g/ml) and Fig. 3.38-C (20 μ g/ml) show cells with smaller nuclei and a few cells undergoing apoptosis. No outspoken induction of apoptosis can be observed after 50 μ g/ml (Fig. 3.38-D) and 100 μ g/ml (Fig. 3.38-E).

Fig. 3.38 F and J show MCF-10A cells stained with Hoechst. No difference is seen between the control and cells treated with 10 and 20 μ g/ml OA for 6h (Figs. 3.38 G and H). 50 and 100 μ g/ml OA (Figs. 3.38 I and J) treatments had an outspoken effect on the cells and only a few shrunken nuclei are evident. Figs. 3.38 K-O and P-T show MCF-7 cells and MCF-10A cells exposed to UA respectively. No change between the control and cells treated with 10 and 20 μ g/ml is seen in the MCF-7 cells. The MCF-10A cells after 10 and 20 μ g/ml UA show thin elongated nuclei (Q and R). In both cell lines 50 μ g/ml UA Figs. 3.38 N (MCF-7 cells) and Figs. 3.38 S (MCF-10A) cells show shrunken nuclei indicative of apoptosis however, only a few cells can be observed as most of the cells lost cellular attachments and was lost in the staining process.

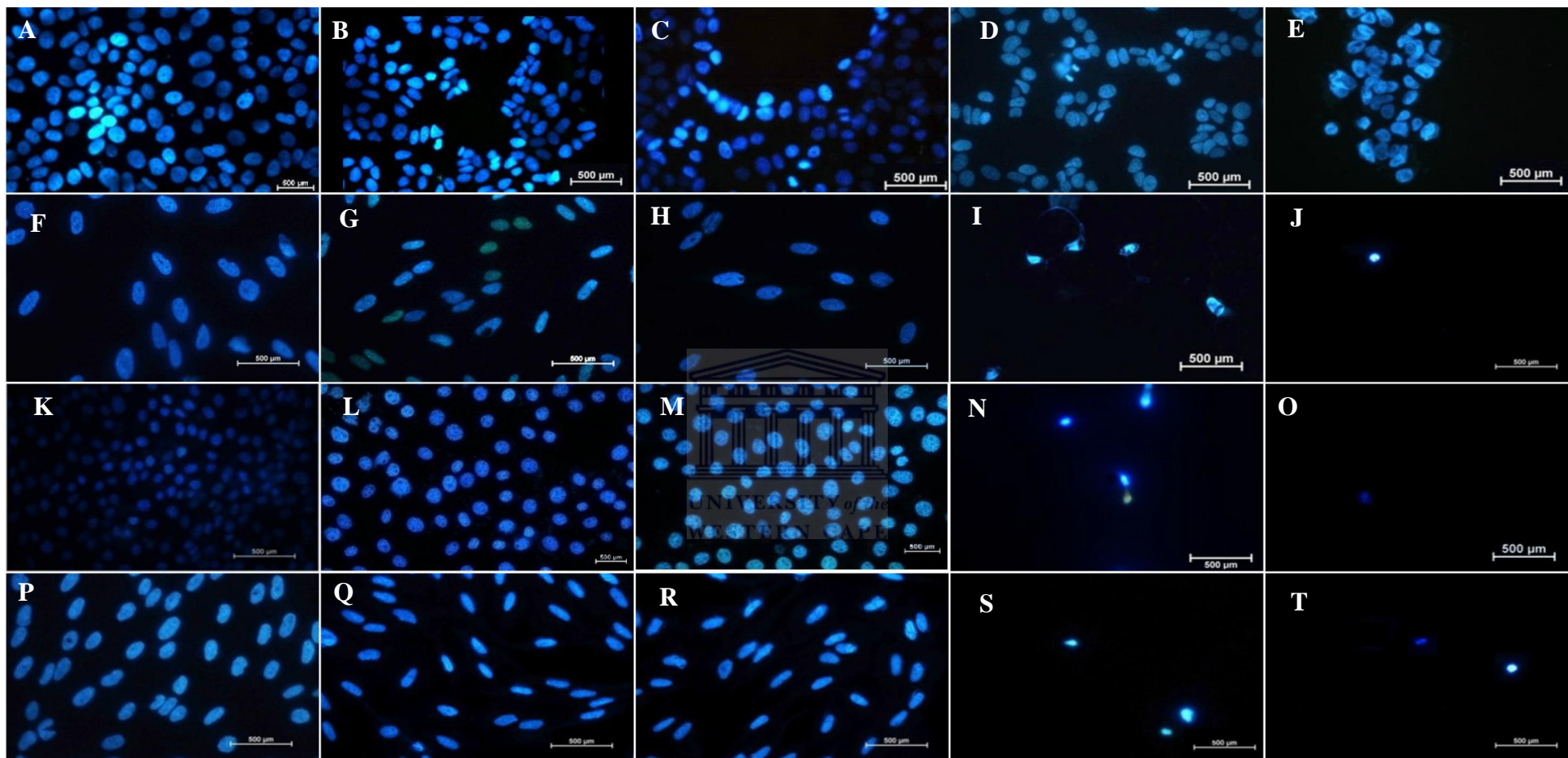


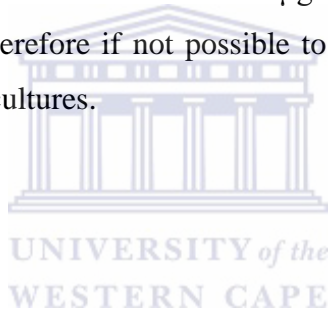
Figure 3.38: MCF-7 (A, B, C, D, and E) and MCF-10A (F, G, H, I, and J) cells treated with OA and MCF-7 (K, L, M, N, and O) and MCF-10A (P, Q, R, S, and T) cells treated with UA for 6h and stained with Hoechst. Control cells (A); 10µg/ml (B); 20µg/ml (C) 50µg/ml and (D) 100µg/ml (E). Control cells (F); 10µg/ml (G); 20µg/ml (H) 50µg/ml and (I) 100µg/ml (J). Control cells (K); 10µg/ml (L); 20µg/ml (M) 50µg/ml and (N) 100µg/ml (O). Control cells (P); 10µg/ml (Q); 20µg/ml (R) 50µg/ml and (S) 100µg/ml (T). All pictures are typical of three independent experiments each performed under identical conditions

3.4.2 Effect of OA and UA on MCF-7 and MCF-10A cells after 12h

Hoechst 33342 staining was used to investigate the possible induction of apoptosis by OA and UA treatment of MCF-7 and MCF-10A cells after 12h.

Fig. 3.39 A-E shows MCF-7 cells. No outspoken differences can be observed between the control (A) and treated cell nuclei (B-D). The nuclei of the cells exposed to 100 μ g/ml OA look deformed and a few apoptotic cells can be observed. Figs. 3.39 K-O and P-T show MCF-7 cells and MCF-10A cells exposed to UA. As for the OA treated cells, 10 and 20 μ g/ml UA had no observable effect on the nuclei of both cell lines.

For both MCF-7 and MCF-10A the 50 and 100 μ g/ml treated cells possibly washed off the coverslips and therefore if not possible to ascertain if any apoptosis was induced in these treated cultures.



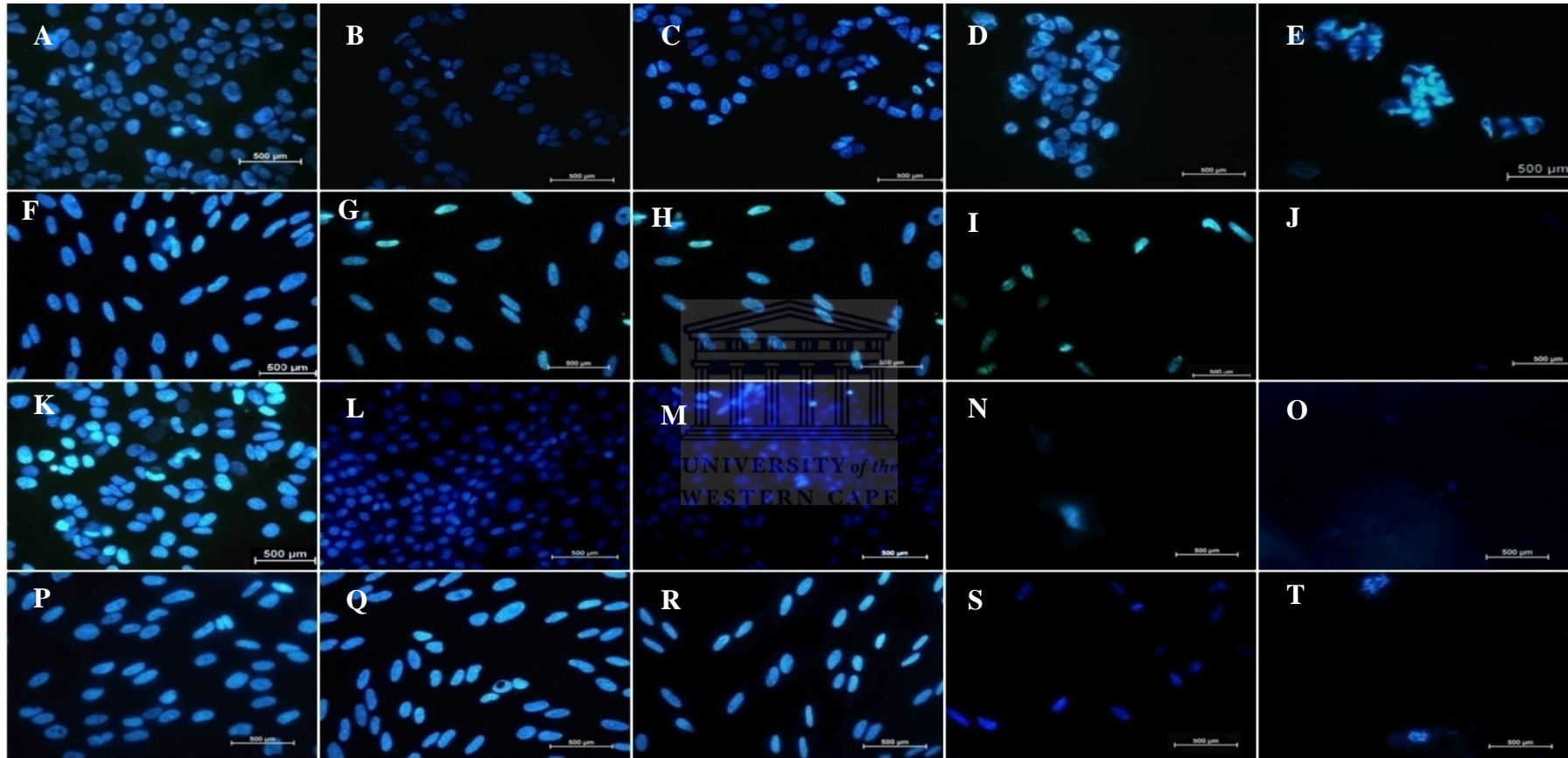
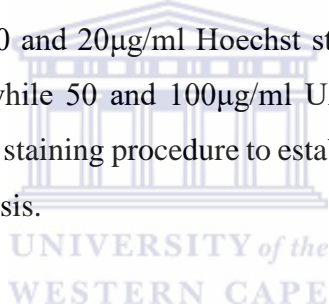


Figure 3.39: MCF-7 (A, B, C, D, and E) and MCF-10A (F, G, H, I, and J) cells treated with OA and MCF-7 (K, L, M, N, and O) and MCF-10A (P, Q, R, S, and T) cells treated with UA for 12h and stained with Hoechst. Control cells (A); 10µg/ml (B); 20µg/ml (C) 50µg/ml and (D) 100µg/ml (E). Control cells (F); 10µg/ml (G); 20µg/ml (H) 50µg/ml and (I) 100µg/ml (J). Control cells (K); 10µg/ml (L); 20µg/ml (M) 50µg/ml and (N) 100µg/ml (O). Control cells (P); 10µg/ml (Q); 20µg/ml (R) 50µg/ml and (S) 100µg/ml (T). All pictures are typical of three independent experiments each performed under identical cond

3.4.3 Effect of OA and UA on MCF-7 and MCF-10A cells after 24h

Hoechst 33342 staining of control MCF-7 cells (A) show normal nuclei. Fig. 3.40-B the (10 μ g/ml) and Fig. 3.40-C (20 μ g/ml) treated samples show cells with smaller nuclei and a few cells undergoing apoptosis. No outspoken induction of apoptosis can be observed after 50 μ g/ml (3.40-D) and unfortunately too few cells are left after 100 μ g/ml OA to ascertain if apoptosis was induced. Fig. 3.40 F to J shows MCF-10A cells. No difference can be observed between the control and the cells expose to 10 and 20 μ g/ml OA.

Not enough cells were left on the coverslip after 50 μ g/ml and 100 μ g/ml of OA (Figs. 3.40 I and J) to establish the effect or apoptosis induction of OA. Figs. 3. 40 K-O and P-T show MCF-7 cell and MCF-10A cells exposed to UA respectively. As with OA treatment 10 and 20 μ g/ml Hoechst stained cells show no noticeable induction of apoptosis while 50 and 100 μ g/ml UA treated cultures do not have enough cells left after the staining procedure to establish the effect of the treatments or the presence of apoptosis.



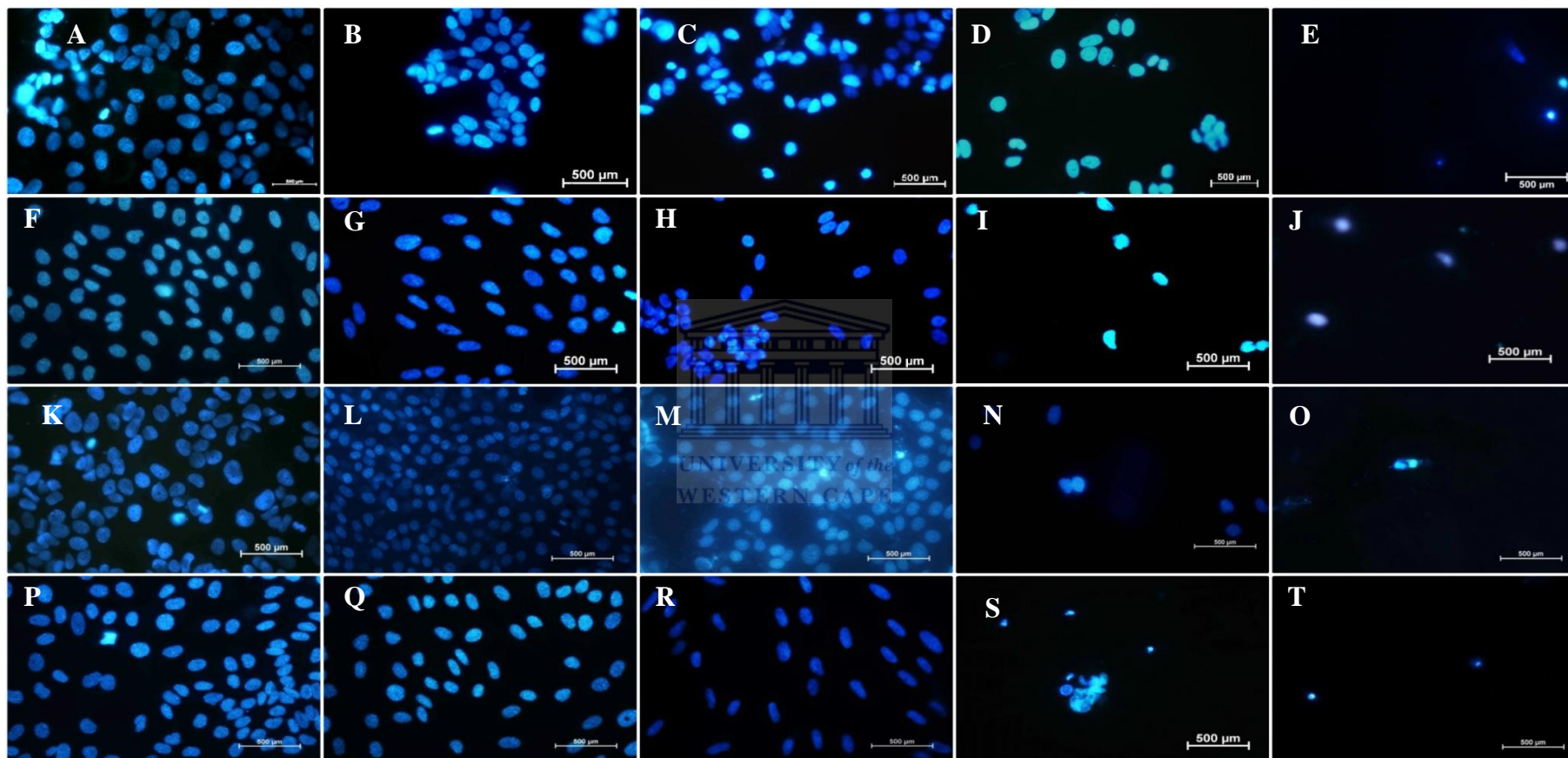


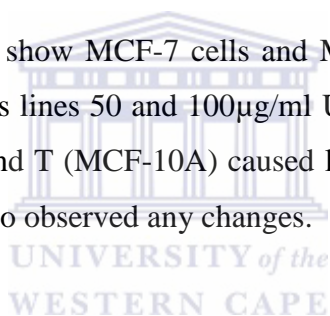
Figure 3.40: MCF-7 (A, B, C, D, and E) and MCF-10A (F, G, H, I, and P) cells treated with OA and MCF-7 (K, L, M, N, and O) and MCF-10A (P, Q, R, S, and T) cells treated with UA for 12h and stained with Hoechst. Control cells (A); 10µg/ml (B); 20µg/ml (C) 50µg/ml and (D) 100µg/ml (E). Control cells (F); 10µg/ml (G); 20µg/ml (H) 50µg/ml and (I) 100µg/ml (J). Control cells (F); 10µg/ml (L); 20µg/ml (M) 50µg/ml and (N) 100µg/ml (O). Control cells (P); 10µg/ml (Q); 20µg/ml (R) 50µg/ml and (S) 100µg/ml (T). All pictures are typical of three independent experiments each performed under identical conditions.

3.4.4 Effect of OA and UA on MCF-7 and MCF-10A cells after 48h

Hoechst 33342 staining was carried out to establish the possible induction of apoptosis after the treatment of OA and UA on the MCF-7 and MCF-10A cells after 48h.

Fig. 3.41-A MCF-7 show control cells displaying normal nuclei. Fig. 3.41-B (10 μ g/ml) and Fig. 3.41-C (20 μ g/ml) show cells with smaller nuclei and a few cells undergoing apoptosis. No outspoken induction apoptosis of apoptosis can be observed after 50 μ g/ml (Fig.3.41-D) and 100 μ g/ml (Fig. 3.41-E). A similar effect is seen in the MCF-10A cells (F-J) again the 50 and 100 μ g/ml OA (Figs. 3.41 I and J) treated cultures show only a few cells.

Figs. 3.41 K-O and P-T show MCF-7 cells and MCF-10A cells exposed to UA respectively. In both cells lines 50 and 100 μ g/ml UA Figs 3.41 N and O (MCF-7 cells) and Figs. 3.41 S and T (MCF-10A) caused loss of cellular attachments and thus to few cells are left to observed any changes.



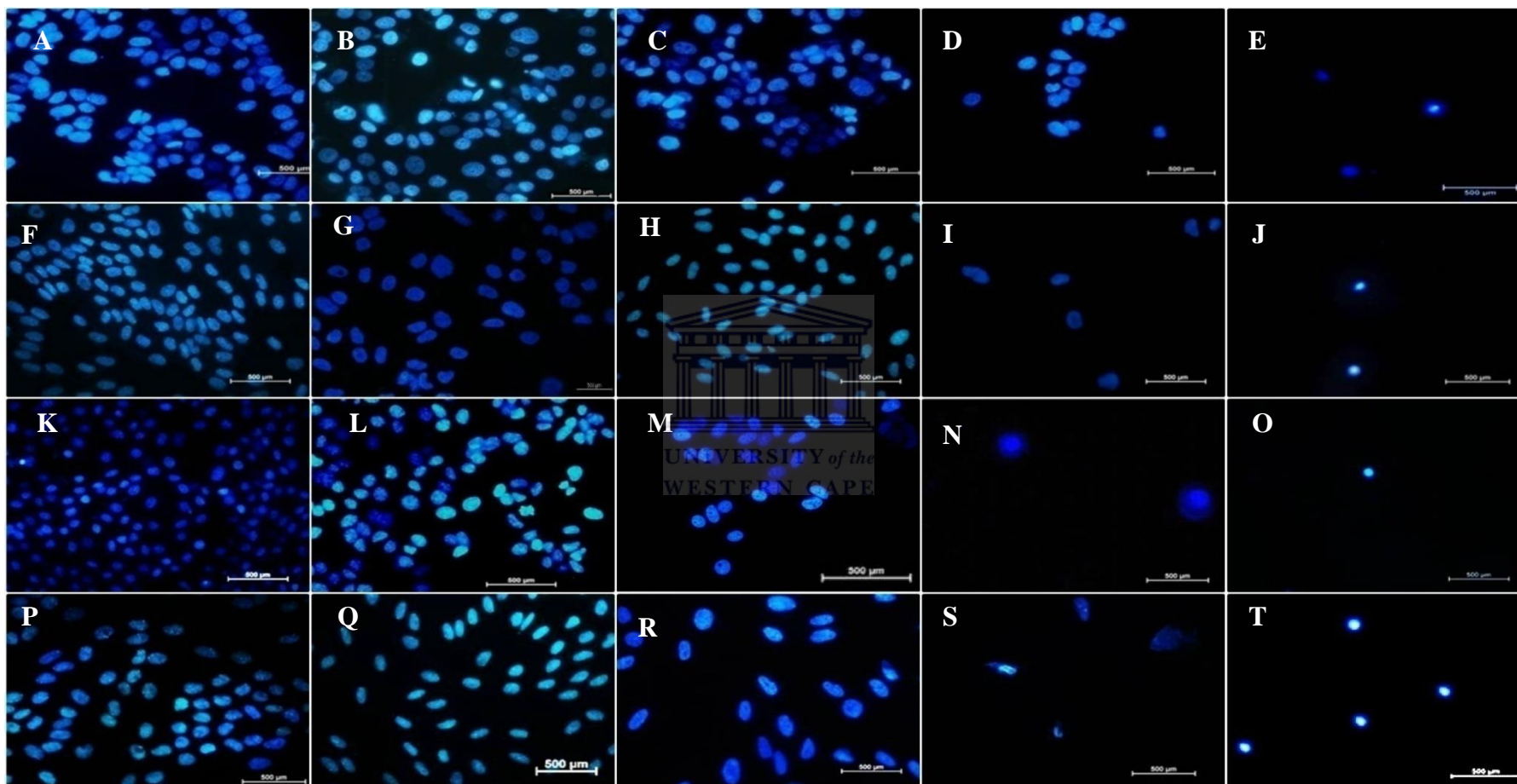


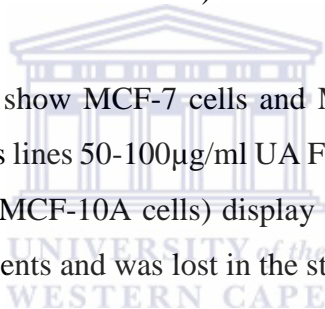
Figure 3.41: MCF-7 (A, B, C, D, and E) and MCF-10A (F, G, H, I, and J) cells treated with OA and MCF-7 (K, L, M, N, and O) and MCF-10A (P, Q, R, S, and T) cells treated with UA for 48h and stained with Hoechst. Control cells (A); 10µg/ml (B); 20µg/ml (C) 50µg/ml and (D) 100µg/ml (E). Control cells (F); 10µg/ml (G); 20µg/ml (H) 50µg/ml and (I) 100µg/ml (J). Control cells (K); 10µg/ml (L); 20µg/ml (M) 50µg/ml and (N) 100µg/ml (O). Control cells (P); 10µg/ml (Q); 20µg/ml (R) 50µg/ml and (S) 100µg/ml (T). All pictures are typical of three independent experiments each performed under identical conditions.

3.4.5 Effect of OA and UA on MCF-7 and MCF-10A cells after 72h

Hoechst 33342 staining was carried out to investigate the possible induction of apoptosis after the treatment of OA and UA in the MCF-7 and MCF-10A cell lines after 72h.

As shown in Fig. 3.42-A MCF-7 control cells display normal nuclei. Fig. 3.42-B (10 μ g/ml) and Fig. 3.42-C (20 μ g/ml) show cells with smaller nuclei and a few cells undergoing apoptosis. No outspoken induction apoptosis of apoptosis can be observed after 50 μ g/ml (Fig. 3.42-D) and after 100 μ g/ml (Fig. 3.42-E), no cells could be observed. Fig 3.42 F-J shows MCF-10A cells stained with Hoechst. No difference can be observed between the control and the cells expose to 10 and 20 μ g/ml OA for 72h (Figs. 3.42 G and H).

Figs. 3.42 K-O and P-T show MCF-7 cells and MCF-10A cells exposed to UA respectively. In both cells lines 50-100 μ g/ml UA Figs. 3.42 N and O (MCF-7 cells) and Figs. 3.42 S and T (MCF-10A cells) display only a few cells as most of the cells lost cellular attachments and was lost in the staining process.



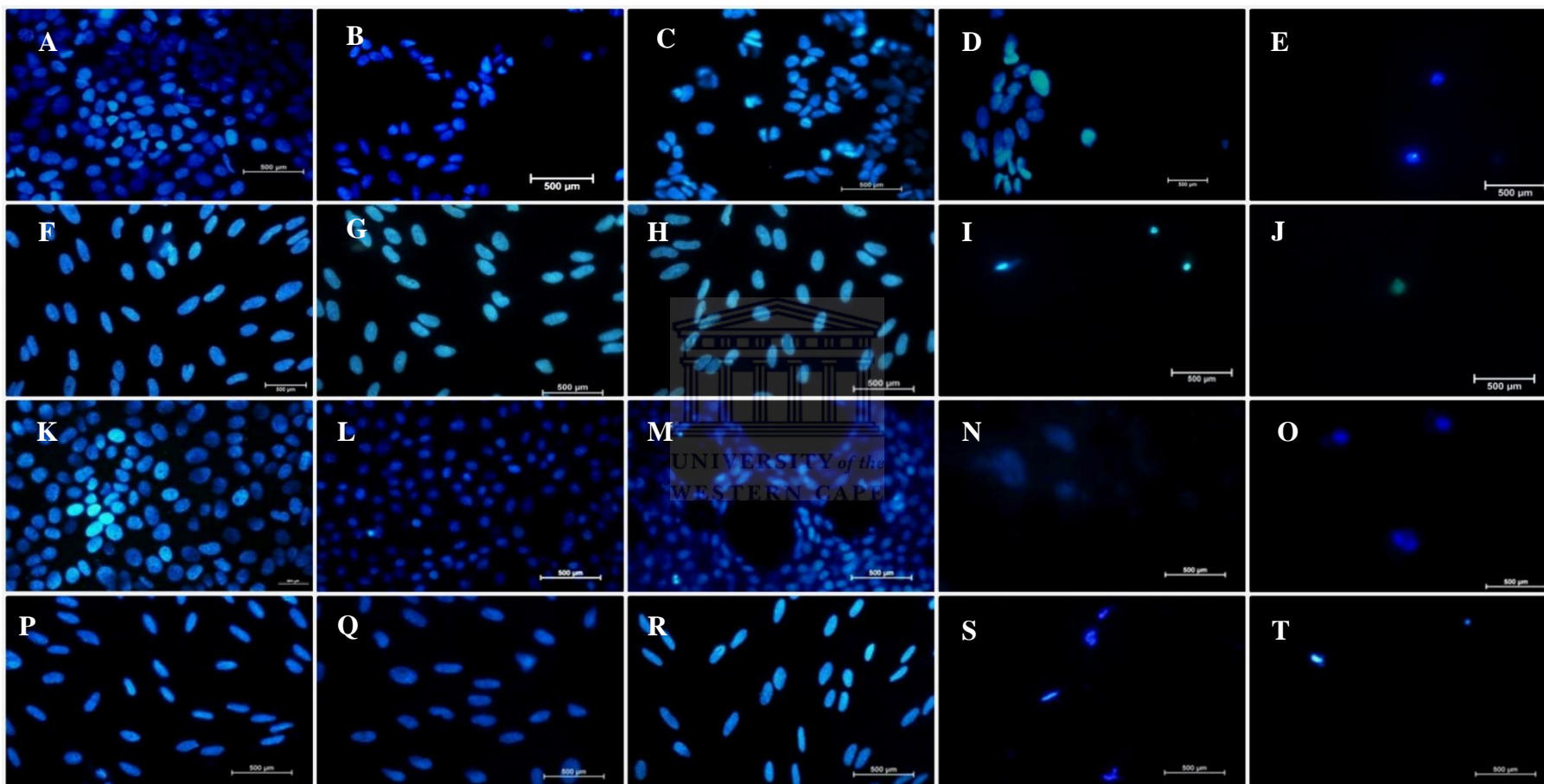


Figure 3.42: MCF-7 (A, B, C, D, and E) and MCF-10A (F, G, H, I, and J) cells treated with OA and MCF-7 (K, L, M, N, and O) and MCF-10A (P, Q, R, S, and T) cells treated with UA for 72h and stained with Hoechst. Control cells (A); 10µg/ml (B); 20µg/ml (C) 50µg/ml and (D) 100µg/ml (E). Control cells (F); 10µg/ml (G); 20µg/ml (H) 50µg/ml and (I) 100µg/ml (J). Control cells (K); 10µg/ml (L); 20µg/ml (M) 50µg/ml and (N) 100µg/ml (O). Control cells (P); 10µg/ml (Q); 20µg/ml (R) 50µg/ml and (S) 100µg/ml (T). All pictures are typical of three independent experiments each performed under identical conditions

3.5 Apoptosis, autophagy and necrosis detection using triple staining: Hoechst (HOC), acridine orange (AO) and propidium iodide (PI) staining

Since so few apoptotic cells were observed after the Hoechst staining method, it was decided to see if a different type of cell death was induced by OA and UA. Therefore, a triple staining fluorescent microscopy method was employed to visualize autophagy and the influence of OA and UA on morphology and cell viability. A triple fluorescent dye staining method was developed utilizing acridine orange (green), Hoechst 33342 (blue) and propidium iodide (red) fluorescent dyes. Acridine orange is a lysosomotropic fluorescent compound that serves as a tracer for acidic vesicular organelles including autophagic vacuoles and lysosomes (Kusuzaki et al., 2000). Cells undergoing autophagy has an increased tendency for acridine orange staining when compared to viable cells, however acridine orange is not a specific marker for autophagy and therefore other techniques are needed to verify the appearance of increased autophagic activity. Hoechst 33342 is capable of penetrate intact cell membranes of viable cells and cells undergoing apoptosis and stains the DNA. Propidium iodide is a fluorescent dye and unable to penetrate an intact membrane and therefore stains the nucleus of cells where the membrane is compromised due to oncotic or necrotic processes.

3.5.1 The effect of OA and UA on apoptosis, autophagy and necrosis induction in MCF-7 and MCF-10A cells after 6h.

Figs. 3.43-A show control MCF-7 cells with normal nuclei and cytoplasm. Fig. 3.43-C (20 μ g/ml) show cells with increased green acridine orange fluorescence. Necrotic cells can be observed in MCF-7 cells (50 μ g/ml) while virtually no cells were left on coverslips after (100 μ g/ml) as shown in Figs. 3.43-E.

Figs. 3.43-F show control MCF-10A cells displaying normal nuclei and cytoplasm morphology. No change in morphology is observed in the low concentration OA treated cells Fig. 3.43-G (10 μ g/ml) and Fig. 3.43-H (20 μ g/ml). Fewer cells are

observed following exposure of the MCF-10A cells to 50µg/ml and after 100µg/ml possibly autophagic cells are observed Figs. 3.43 I and J.

Figs. 3.43 K-O and P-T respectively show micrographs of MCF-7 and MCF-10A cells exposed to UA. No indication of dead cells can be seen after 10 and 20µg/ml and not enough cells are left after treatment with the two high concentrations in MCF-7 cells and only a few necrotic cells are observed in the MCF-10A treated cultures Figs. 3.43 S and T.



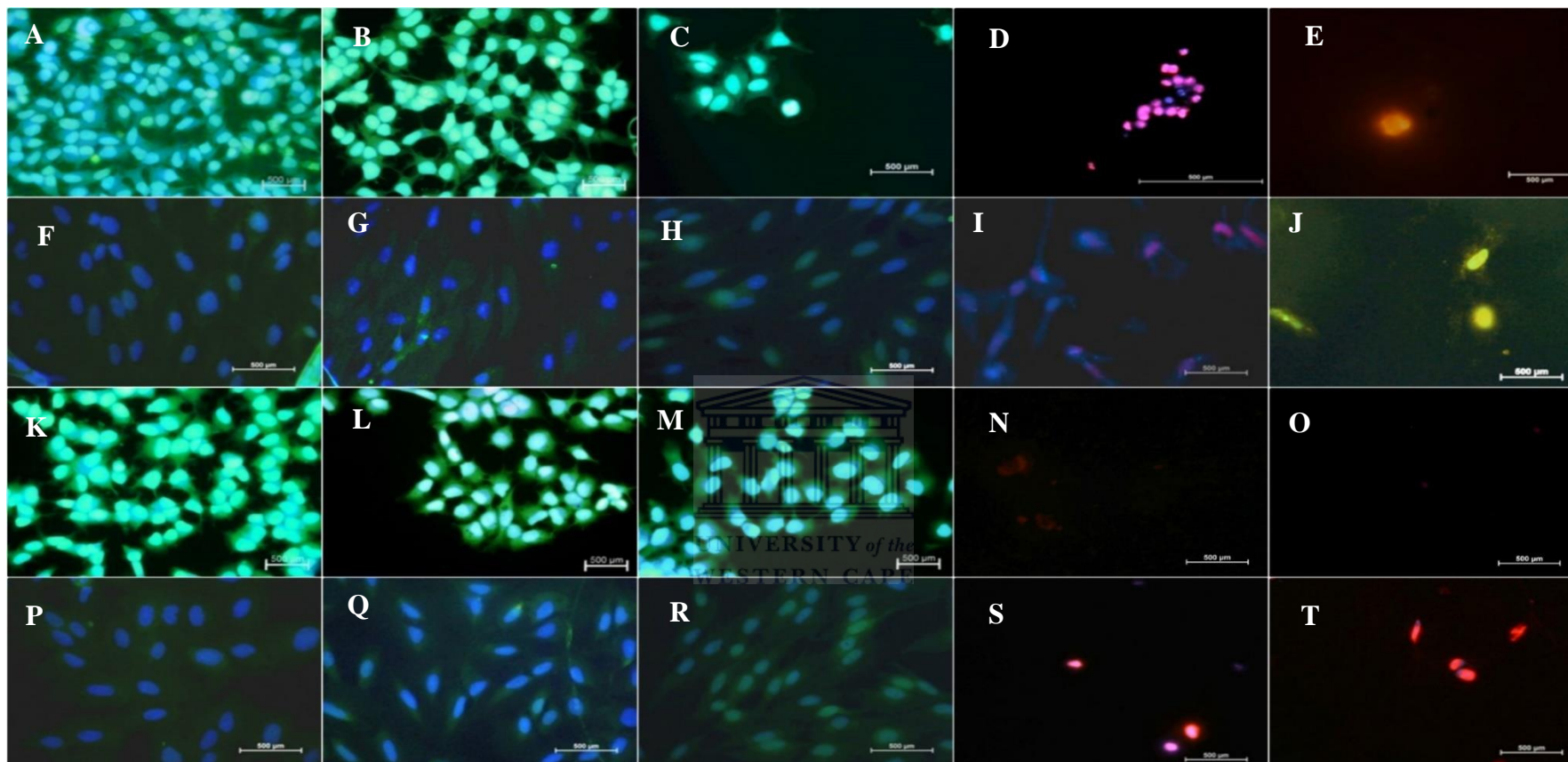


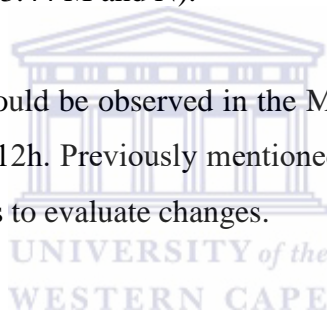
Figure 3.43: MCF-7 and MCF-10A cell morphology. MCF-7 (A, B, C, D and E) and MCF-10A (F, G, H, I and J) cells were treated with OA and MCF-7 (K, L, M, N and O) and MCF-10A (P, Q, R, S and T), cells treated with UA for 6h. The cells were stained with a triple stain made up of Hoechst, acridine orange and propidium iodide. Control cells (A); 10µg/ml (B); 20µg/ml (C) 50µg/ml and (D) 100µg/ml (E). Control cells (F); 10µg/ml (G); 20µg/ml (H) 50µg/ml and (I) 100µg/ml (J). Control cells (K); 10µg/ml (L); 20µg/ml (M) 50µg/ml and (N) 100µg/ml (O). Control cells (P); 10µg/ml (Q); 20µg/ml (R) 50µg/ml and (S) 100µg/ml (T). All pictures are typical of three independent experiments each performed under identical conditions

3.5.2 The effect of OA and UA on apoptosis, autophagy and induction in MCF-7 and MCF-10A cells after 12h.

HOC, AO and PI staining was applied to study possible induction of apoptosis and autophagy after the treatment of OA and UA in the MCF-7 and MCF-10A for 12h. No change can be observed in the cultures exposed to 10 and 20µg/ml OA Figs. 3.44 B-C and G-H. After 50µg/ml OA, MCF-10A cells show rounded green nuclei possibly indicative of autophagy. Only a few dead (red fluorescence) cells were observed in the cultures exposed to 100µg/ml OA 3.44 -J.

No difference can be observed in MCF-7 cells treated with 10µg/ml UA (Fig. 3.44 -L) when compared to control (Fig. 3.44 -K). 20 and 50µg/ml show a decrease in the number of cells (Fig. 3.44 M and N).

No outspoken changes could be observed in the MCF-10A cells after exposure to 10 and 20µg/ml UA for 12h. Previously mentioned the 50 and 100µg/ml samples did not have enough cells to evaluate changes.



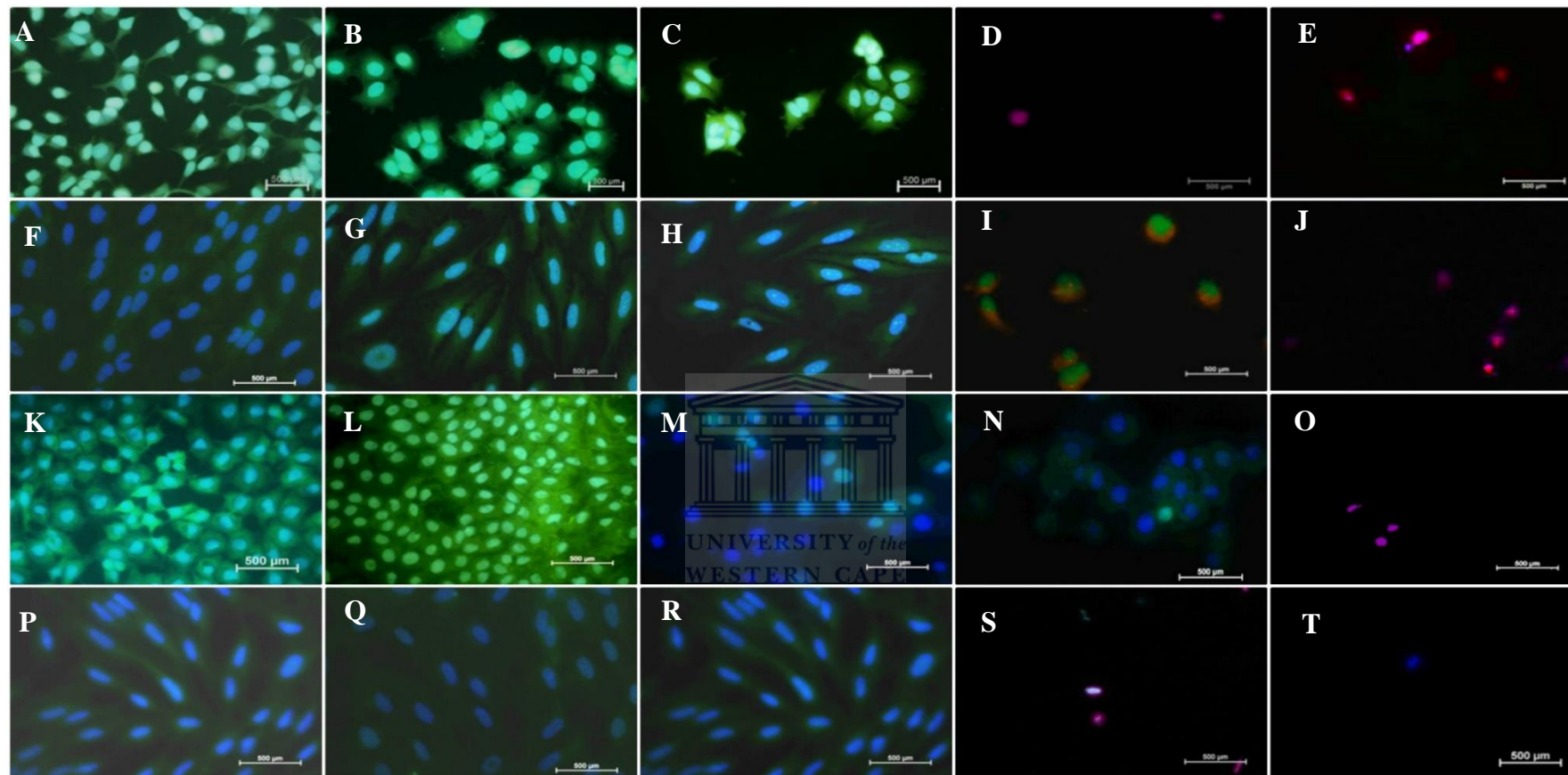


Figure 3.44: MCF-7 and MCF-10A cell morphology. MCF-7 (A, B, C, D and E) and MCF-10A (F, G, H, I, J) cells were treated with OA and MCF-7 (K, L, M, N and O) and MCF-10A (P, Q, R, S and T), cells treated with UA for 12h. The cells were stained with a triple stain made up of Hoechst, acridine orange and propidium iodide. Control cells (A); 10µg/ml (B); 20µg/ml (C) 50µg/ml and (D) 100µg/ml (E). Control cells (F); 10µg/ml (G); 20µg/ml (H) 50µg/ml and (I) 100µg/ml (J). Control cells (K); 10µg/ml (L); 20µg/ml (M) 50µg/ml and (N) 100µg/ml (O). Control cells (P); 10µg/ml (Q); 20µg/ml (R) 50µg/ml and (S) 100µg/ml (T). All pictures are typical of three independent experiments each performed under identical conditions.

3.5.3 The effect of OA and UA on apoptosis, autophagy and induction in MCF-7 and MCF-10A cells after 24h.

Investigating the possible induction of apoptosis, autophagy and necrosis after the treatment of OA (Figs. 3.45 A-J) and UA (Figs. 3.45 K-T) in the MCF-7 and MCF-10A for 24h, HOC, AO and PI staining was applied.

Figs. 3.45 K-M and P-R show MCF-7 and MCF-10A cells exposed to OA or UA respectively. No changes were observed in either cell line after 10 and 20 μ g/ml UA. Unfortunately the higher concentrations of both OA and UA caused the cells to lose attachment to the cover slips and could not be evaluated.



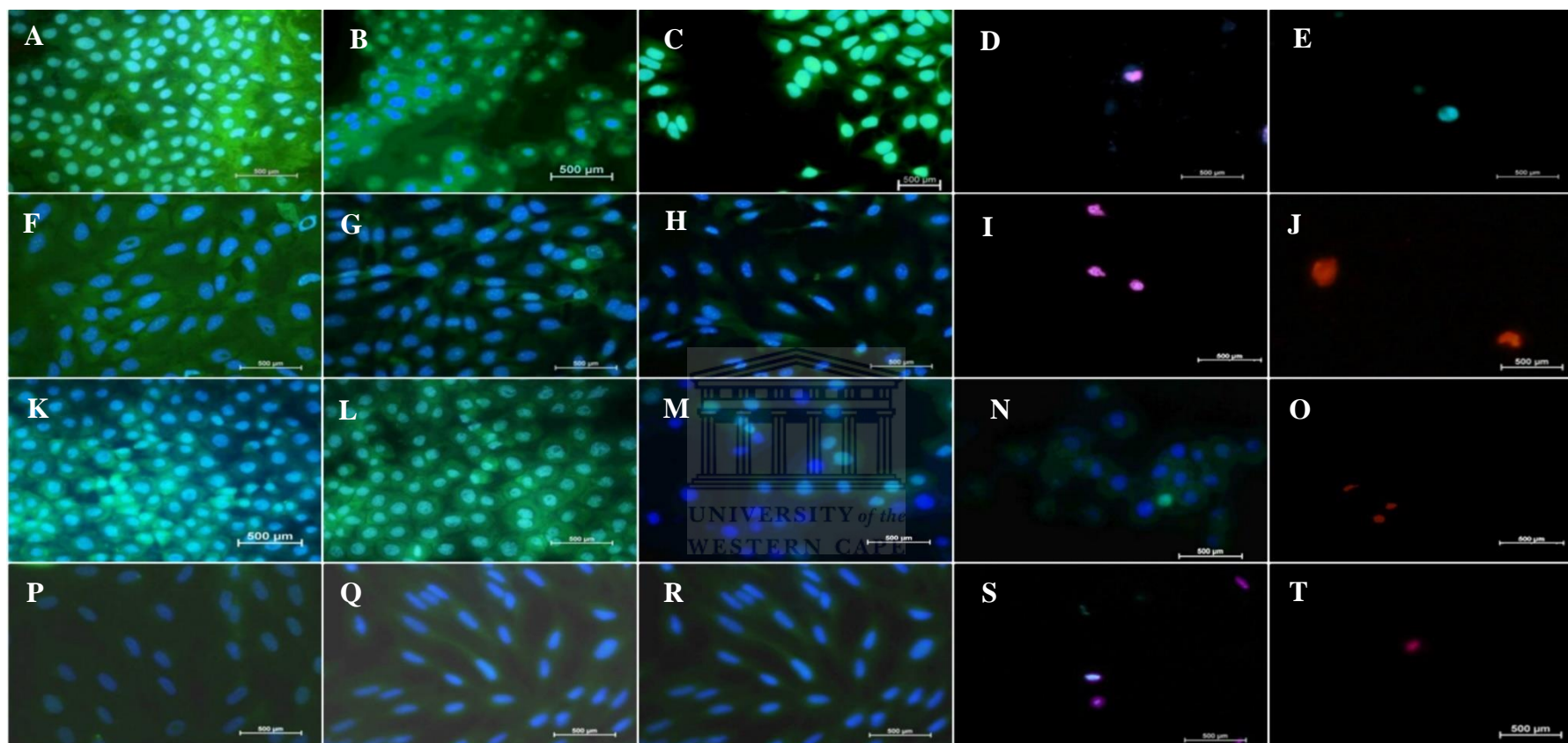


Figure 3.45: MCF-7 and MCF-10A cell morphology. MCF-7 (A, B, C, D and E) and MCF-10A (F, G, H, I and J) cells were treated with OA and MCF-7 (K, L, M, N and O) and MCF-10A (P, Q, R, S and T), cells treated with UA for 24h. The cells were stained with a triple stain made up of Hoechst, acridine orange and propidium iodide. Control cells (A); 10µg/ml (B); 20µg/ml (C) 50µg/ml and (D) 100µg/ml (E). Control cells (F); 10µg/ml (G); 20µg/ml (H) 50µg/ml and (I) 100µg/ml (J). Control cells (K); 10µg/ml (L); 20µg/ml (M) 50µg/ml and (N) 100µg/ml (O). Control cells (P); 10µg/ml (Q); 20µg/ml (R) 50µg/ml and (S) 100µg/ml (T). All pictures are typical of three independent experiments each performed under identical conditions.

3.5.4 The effect of OA and UA on apoptosis, autophagy and induction in MCF-7 and MCF-10A cells after 48h

HOC, AO and PI staining was applied to study possible induction of apoptosis and autophagy after the treatment of OA and UA in the MCF-7 and MCF-10A for 48h.

No outspoken increase in either apoptosis or autophagy is observed in either cell line after OA (Figs. 3.46 A-J) or UA (Figs. 3.46 K-T). Figs. 3.46 D and I (50µg/ml OA) show some intact cells left after treatment. However the rest of the samples exposed to 50 and 100µg/ml OA and UA show only a few shrunken (red fluorescence) dead cells. Again the dramatic decrease in cell numbers after the high concentration OA and UA is caused by loss of cellular attachments due to the treatment.



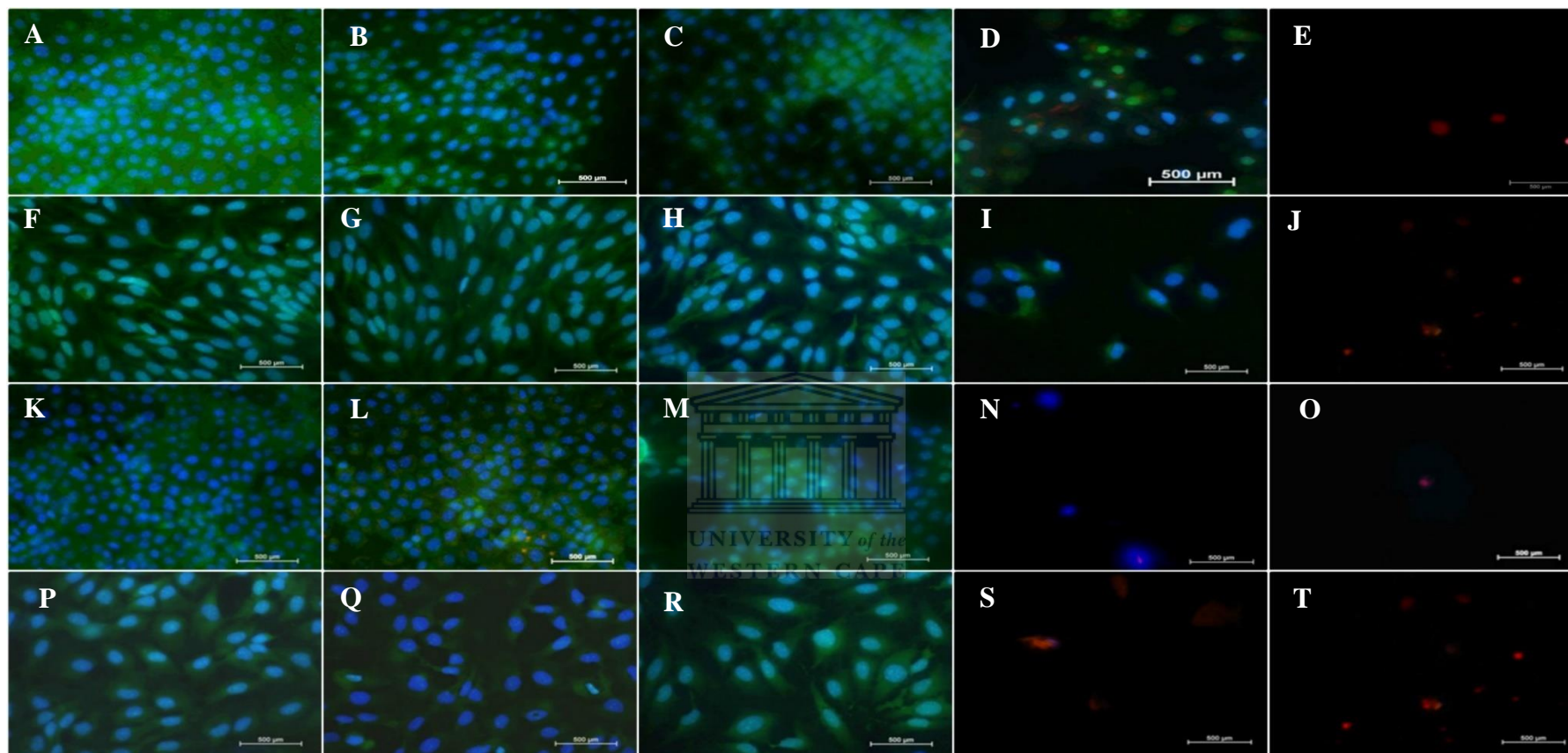


Figure 3.46: MCF-7 and MCF-10A cell morphology. MCF-7 (A, B, C, D and E) and MCF-10A (F, G, H, I and J) cells were treated with OA and MCF-7 (K, L, M, N and O) and MCF-10A (P, Q, R, S and T), cells treated with UA for 48h. The cells were stained with a triple stain made up of Hoechst, acridine orange and propidium iodide. Control cells (A); 10µg/ml (B); 20µg/ml (C) 50µg/ml and (D) 100µg/ml (E). Control cells (F); 10µg/ml (G); 20µg/ml (H) 50µg/ml and (I) 100µg/ml (J). Control cells (K); 10µg/ml (L); 20µg/ml (M) 50µg/ml and (N) 100µg/ml (O). Control cells (P); 10µg/ml (Q); 20µg/ml (R) 50µg/ml and (S) 100µg/ml (T). All pictures are typical of three independent experiments each performed under identical conditions.

3.5.5 The effect of OA and UA on apoptosis, autophagy and induction in MCF-7 and MCF-10A cells after 72h.

Studying possible induction of apoptosis and autophagy after the treatment of OA and UA in the MCF-7 and MCF-10A in HOC, AO and PI stained cells showed no difference between controls and cells treated with 10 and 20µg/ml OA and UA after 72h.

As with all the previous treatments for the others time periods, no conclusive undergoing a specific cell death possibly induced by OA or UA could be established. Some deformed cells are observed after 50 µg/ml OA and UA (Figs. 3.47 D, I, N and S), but no cells were observed in the samples exposed to 100 µg/ml OA and UA due to loss of culture attachments and loss of cells in the staining procedure.

Neither the studies with Hoechst stain nor studies using the combination of three stains could give a definite answer as to a type of cell death possibly induced by OA and UA. The biggest challenge was in the samples exposed to 50 and 100µg/ml OA and UA where the cells seemed to wash off from the coverslips possibly due to weaker cellular attachments thus causing the cells to be lost in the staining solution. To overcome this hurdle a method employing annexin V was employed to study the possible presence of apoptosis after exposure to OA and UA.

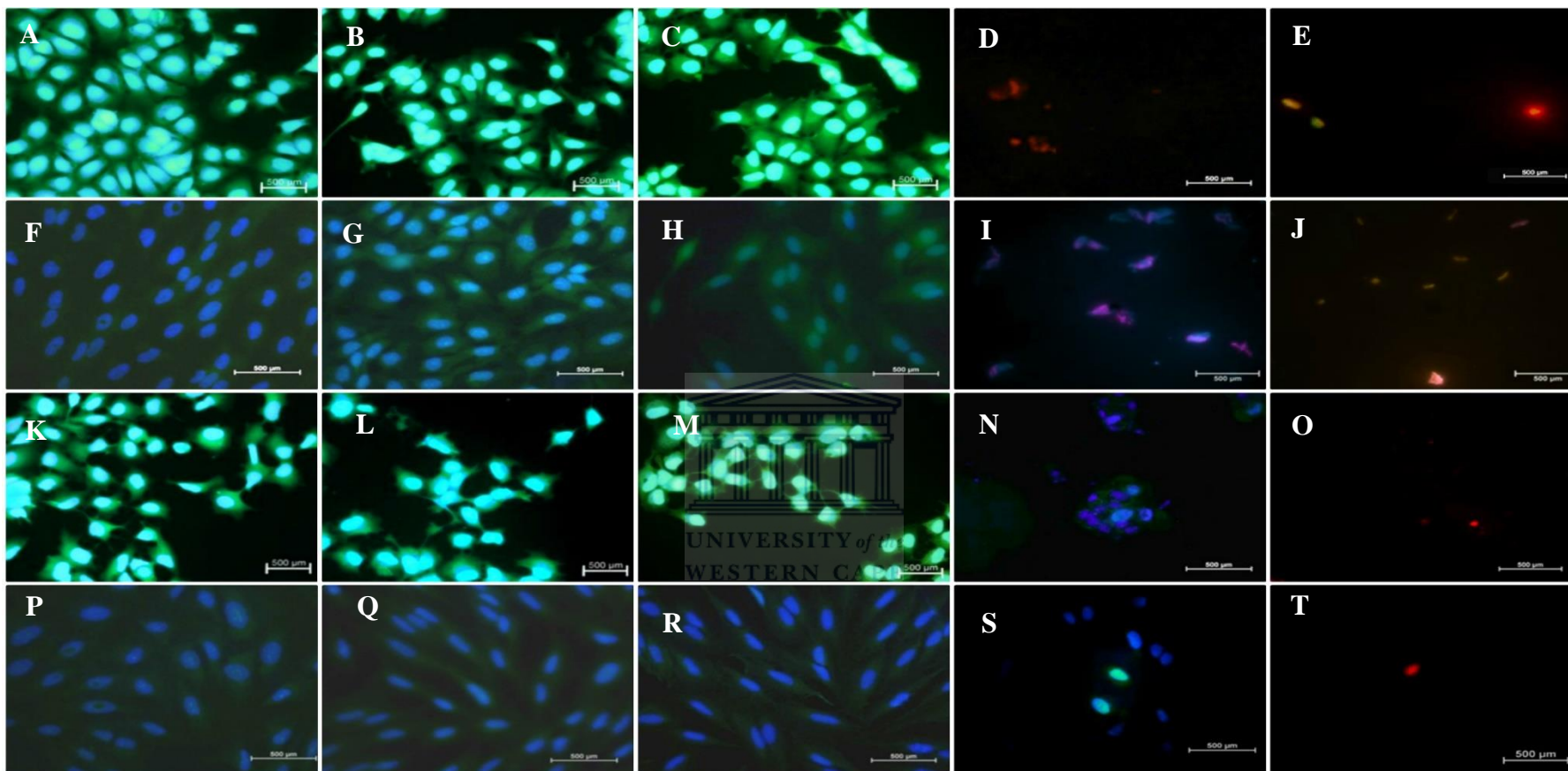


Figure 3.47: MCF-7 and MCF-10A cell morphology. MCF-7 (A, B, C, D and E) and MCF-10A (F, G, H, I and J) cells were treated with OA and MCF-7 (K, L, M, N and O) and MCF-10A (P, Q, R, S and T), cells treated with UA for 72h. The cells were stained with a triple stain made up of Hoechst, acridine orange and propidium iodide. Control cells (A); 10 μ g/ml (B); 20 μ g/ml (C) 50 μ g/ml and (D) 100 μ g/ml (E). Control cells (F); 10 μ g/ml (G); 20 μ g/ml (H) 50 μ g/ml and (I) 100 μ g/ml (J). Control cells (K); 10 μ g/ml (L); 20 μ g/ml (M) 50 μ g/ml and (N) 100 μ g/ml (O). Control cells (P); 10 μ g/ml (Q); 20 μ g/ml (R) 50 μ g/ml and (S) 100 μ g/ml (T). All pictures are typical of three independent experiments each performed under identical condition

3.6 Quantification of apoptosis using the Tali® Image Cytometer

As the triple staining method also failed to provide answers regarding the specific type of cell death induced by OA and UA, a different method using annexin V was employed.

Apoptotic induction was analysed in the two cell lines after treatment with OA and UA. To determine apoptosis, cells were stained with the annexin V-Alexa Fluor® 488 conjugate. PI was used to differentiate the cells that were dead (annexin V positive/PI positive or annexin V negative/ PI positive). The cells size gate on the Tali® Image Cytometer is adjusted to exclude debris from the samples (www.lifetecologies.com).

3.6.1 The effect of OA and UA after 6h on apoptosis induction in MCF-7 and MCF-10A cells as quantified by the Tali® Image Cytometer

The possible induction of apoptosis after OA and UA using four different (10, 25, 50 and 100µg/ml) concentrations were measured using the Tali® Image-based Cytometer (Fig. 3.48).

Fig. 3.48-A show that 20µg/ml OA significantly ($P \leq 0.05$) increased MCF-7 apoptotic cells 34% compared to control 8.5%. 50 and 100µg/ml OA increased the dead cells by 45.33% and 43.66% ($P \leq 0.01$) respectively. Concomitantly the live MCF-7 cells decreased significantly ($P \leq 0.001$) after 50µg/ml to 44.33% and to 45.33% after 100µg/ml OA ($P \leq 0.01$). 20µg/ml decreased the number of live cells to 53% compared to control as shown in Fig. 3.48-A.

The MCF-10A cells (Fig. 3.48-B) did not show the same level of apoptosis as seen in the MCF-7 cells. 100µg/ml OA caused 16% increase in apoptotic cells compared to control (2.66%). However, the number of dead cells was increased significantly ($P \leq 0.001$) after 50µg/ml (48.66%) and 100µg/ml (42.66%). The live MCF-10A cells decreased significantly ($P \leq 0.001$) after 50µg/ml (42%) and 100µg/ml (29%).

UA caused a dose dependent decrease in live accompanied by a dose dependent increase in dead cells in both MCF-7 (Fig. 3.48-C) and MCF-10A (Fig. 3.48-D). Apoptosis was induced mainly by 100µg/ml UA in MCF-7 (16%) and (35%) in MCF-10A cells.

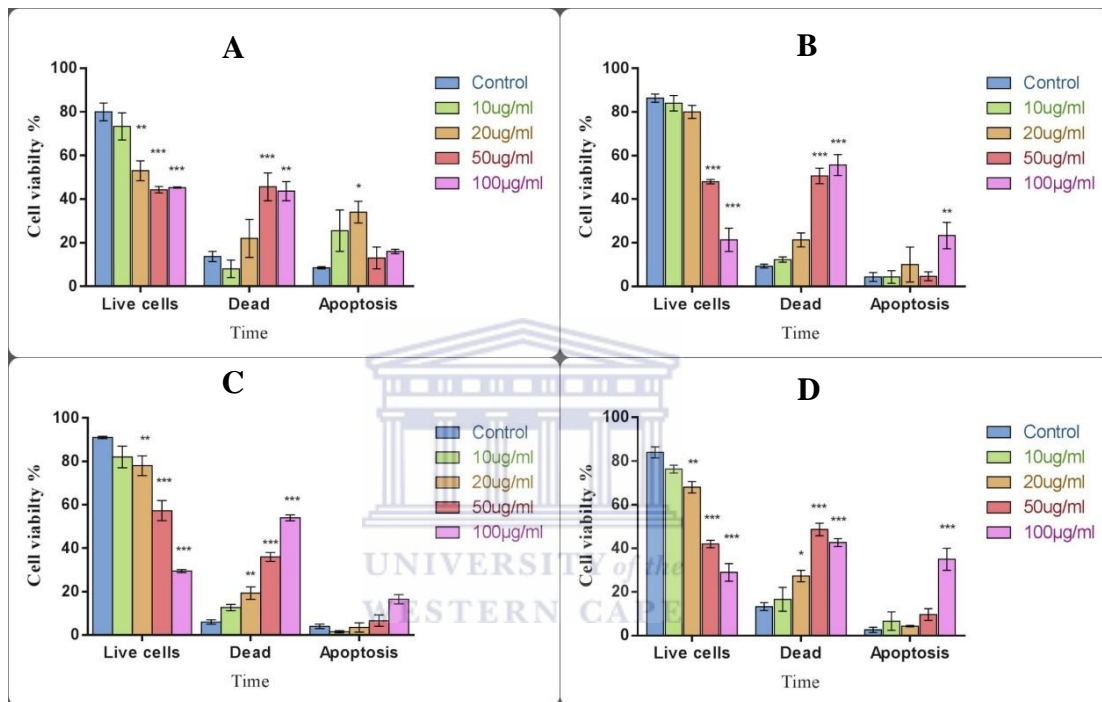


Figure 3.48: Comparison of live, dead and apoptotic cells as analyzed by the Tali® Image Cytometer after exposure to OA and UA for 6h. A and B show MCF-7 and MCF-10A cells exposed to OA; C and D show MCF-7 and MCF-10A cells after exposure to UA. Data is shown as mean \pm SEM of three separate experiments. Treatments significantly different from the untreated control at $p < 0.05$ are presented as * $P \leq 0.05$, ** $P \leq 0.01$, *** $P \leq 0.001$ compared to respective controls (Two-way ANOVA followed by Tukey's multiple comparisons test).

3.6.2 The effect of OA and UA after 12h on apoptosis induction in MCF-7 and MCF-10A cells as quantified using the Tali® Image Cytometer

Figure 3.49-A show a significant ($P \leq 0.01$) increase in dead MCF-7 cells after 50 and 100µg/ml OA at 35.33% and 38.33% respectively. Concurrently the MCF-7 live cells was decreased significantly ($P \leq 0.001$) by 50µg/ml (51%) and 100µg/ml (41%) compared to the control (90.66%), Fig. 3.49-A.

OA induced a similar decrease in the live cells in the MCF-10A cell line (Fig. 3.49-B). A far more outspoken increase in dead cells was induced by 100µg/ml in the MCF-10A cells when comparing the results to that obtained in the MCF-7 cells. Less apoptotic cells were seen in the MCF-10A cells following OA treatment for 12h.

Figures 3.49 C and D show the MCF-7 and MCF-10A cells exposed to UA. Similar effects to that obtained with OA in the two cell lines was seen. However, a significant increase in apoptotic cells in both cell lines were seen in the samples treated with 100µg/ml UA (29.33%) in MCF-7 cells and 41.5% in MCF-10A cells (Fig. 3.49 C and D).

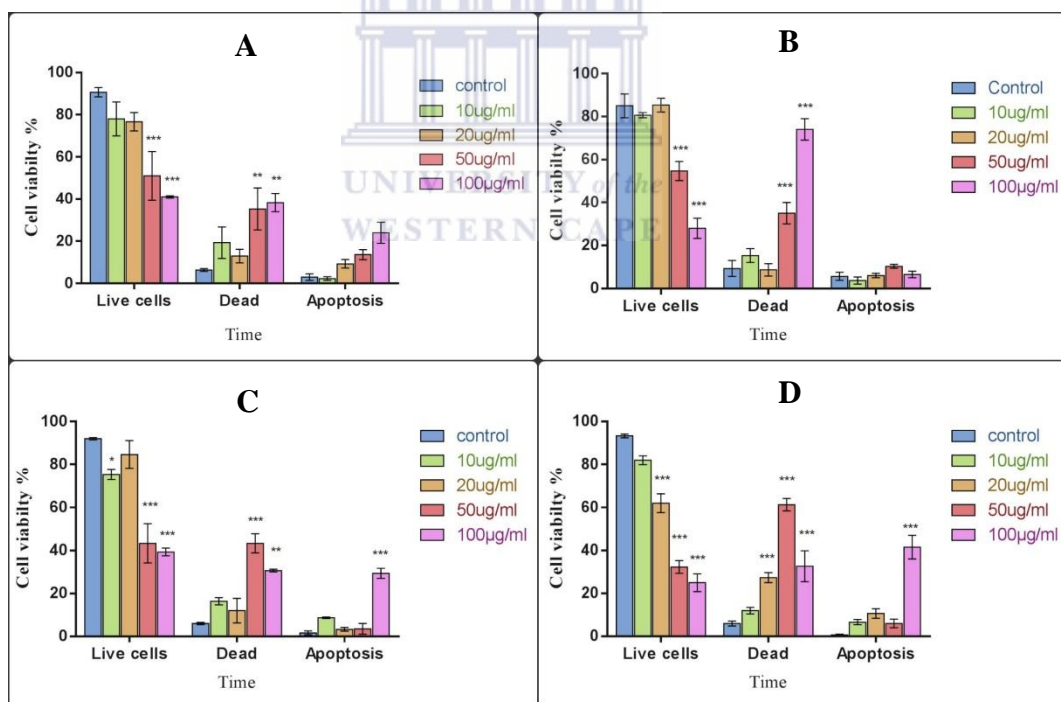


Figure 3.49: Comparison of live, dead and apoptotic cells as analyzed by the Tali® Image Cytometer after exposure to OA and UA for 12h. The effect of OA on MCF-7 cells (A) and MCF-10A (B) and the effect of UA on MCF-7 (C) and MCF-10A (D) are shown above. Data is shown as mean ± SEM of three separate experiments. Treatments significantly different from the untreated control at $p < 0.05$ are presented as * $P \leq 0.05$, ** $P \leq 0.01$, *** $P \leq 0.001$ compared to respective controls (Two-way ANOVA followed by Tukey's multiple comparisons test).

3.6.3 The effect of OA and UA after 24h on apoptosis induction in MCF-7 and MCF-10A cells as quantified by the Tali® Image Cytometer

In the MCF-7 cell line apoptotic cells were increased significantly ($P \leq 0.01$) after 20 and 50 $\mu\text{g/ml}$ OA at 21% and 25.66% respectively. The number dead cells were also significantly increased after 50 and 100 $\mu\text{g/ml}$ OA at 32% and 43.33% when compared to the control (Fig. 3.50-A). Live MCF-7 cells were decreased to 63% by 10 $\mu\text{g/ml}$, to 56.66% by 20 $\mu\text{g/ml}$ and finally to 42.33% and 43.33% by 50 $\mu\text{g/ml}$ and 100 $\mu\text{g/ml}$ respectively.

OA induced a similar decrease in the live cells in the MCF-10A (Fig. 3.50-B). A far more outspoken increase in dead cells seen after 50 and 100 $\mu\text{g/ml}$ in the MCF-10A cells when comparing the results to that obtained in the MCF-7 cells. Less apoptotic cells were seen in the MCF-10A cells following OA treatment for 24h.

Figures 3.50 C and D show the MCF-7 and MCF-10A cells exposed to UA. Similar effects to that obtained with OA in the two cell lines was seen. However, a significant increase in apoptotic cells in both cell lines were seen in the samples treated with UA. 20% after 20 $\mu\text{g/ml}$ and 30.33% after 100 $\mu\text{g/ml}$ in MCF-7 cells and 27.33% in MCF-10A cells (Fig. 3.50 C and D).

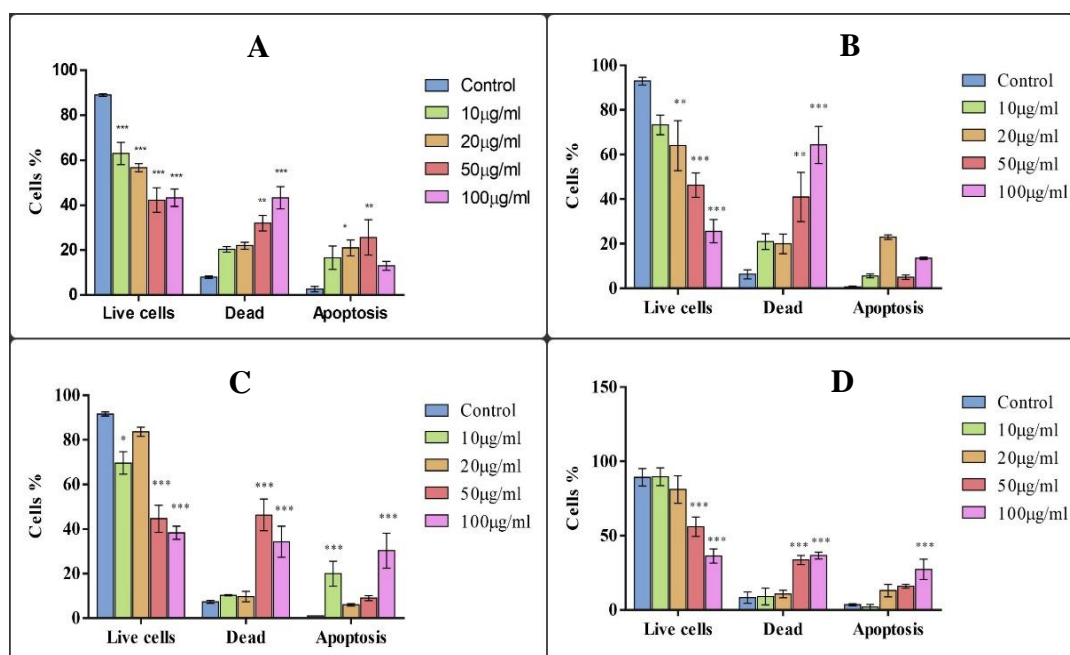


Figure 3.50: Comparison of live, dead and apoptotic cells as analysed by the Tali® Image Cytometer after exposure to OA and UA for 24h. The effect of OA on MCF-7 cells (A) and MCF-10A (B) and the effect of UA on MCF-7 (C) and MCF-10A (D) are shown above. Data is shown as mean \pm SEM of three separate experiments. Treatments significantly different from the untreated control at $p < 0.05$ are presented as * $P \leq 0.05$, ** $P \leq 0.01$, *** $P \leq 0.001$ compared to respective controls (Two-way ANOVA followed by Tukey's multiple comparisons test).

UNIVERSITY of the
WESTERN CAPE

3.6.4 The effect of OA and UA after 48h on apoptosis induction in MCF-7 and MCF-10A cells as quantified by the Tali® Image Cytometer

Figs. 3.51 A and B show MCF-7 and MCF-10A cells respectively. The number of dead cells increased after exposure from 5.66% to 50µg/ml OA to 50.33% and 100µg/ml OA 55.66% in MCF-7 cells and from 10.66% to 62.66% and 59.66% in MCF-10A cells, showing the MCF-10A cells to be more sensitive to OA treatment.

OA caused a corresponding to reduction in the living cells in MCF-10A (Figs. 3.51- A and B). Apoptosis was induced by OA in both cell lines after 48h. However, the high number of dead cells not ascribed to apoptosis is probably necrosis or autophagy.

Figs. 3.51C and D show the MCF-7 and MCF-10A cells exposed to UA and similar effects that of OA is observed. However, 50µg/ml UA did not have the outspoken death inducing effect on MCF-7 cells that UA that had.

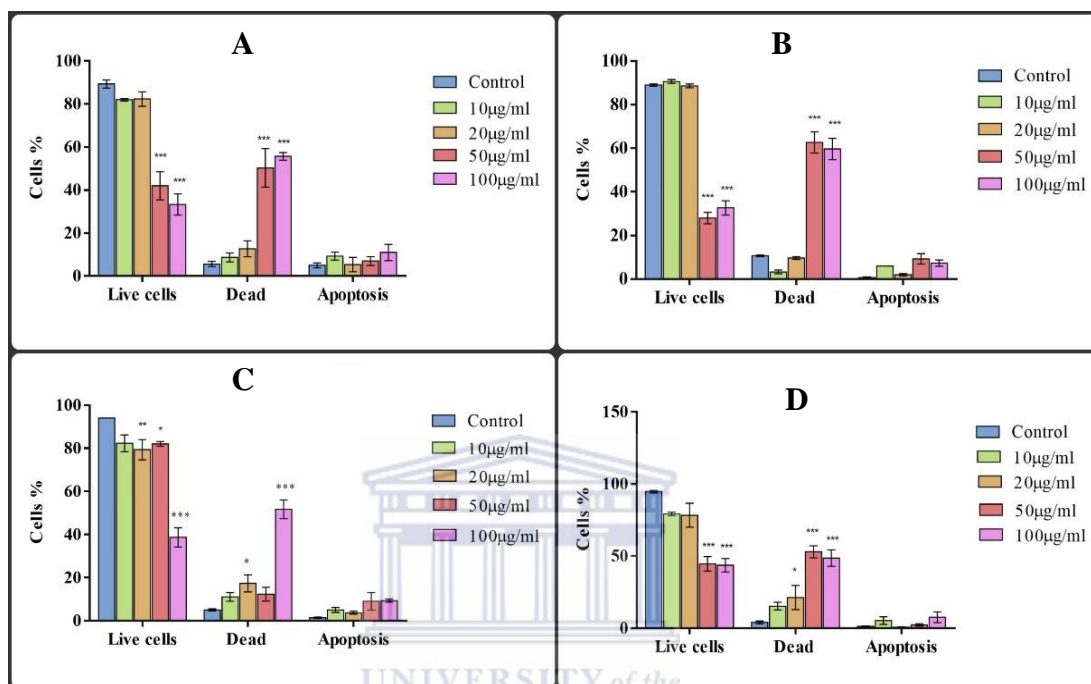


Figure 3.51: Comparison of live, dead and apoptotic cells as analysed by the Tali® Image Cytometer after exposure to OA and UA for 48h. The effect of OA on MCF-7 cells (A) and MCF-10A (B) and the effect of UA on MCF-7 (C) and MCF-10A (D) are shown above. Data is shown as mean \pm SEM of three separate experiments. Treatments significantly different from the untreated control at $p < 0.05$ are presented as * $P \leq 0.05$, ** $P \leq 0.01$, *** $P \leq 0.001$ compared to respective controls (Two-way ANOVA followed by Tukey's multiple comparisons test).

3.6.5 The effect of OA and UA after 72h on apoptosis induction in MCF-7 and MCF-10A cells as quantified by the Tali® Image Cytometer

Fig. 3.52-A show that (50 and 100µg/ml) OA significantly ($P \leq 0.05$) increased MCF-7 apoptotic cells (18.5% and 14.66%) when compared to control. 50 and 100µg/ml OA increased the dead MCF-7 cells by 32% and 61% ($P \leq 0.01$) respectively. Concomitantly the live MCF-7 cells decreased significantly ($P \leq 0.001$) after 50µg/ml to 52% and to 24.33% after 100µg/ml OA ($P \leq 0.01$) when compared to control as shown in Fig. 3.52-A.

The MCF-10A cells (Fig. 3.52-B) did not show the same level of apoptosis as seen in the MCF-7 cells. However the dead cells number was increased significantly ($P \leq 0.001$) after 50 $\mu\text{g/ml}$ (42%) and 100 $\mu\text{g/ml}$ (35.33%). Live MCF-10A cells decreased significantly ($P \leq 0.001$) only after 50 $\mu\text{g/ml}$ (38 %) and 100 $\mu\text{g/ml}$ (49%).

Figs. 3.52 C and D show the MCF-7 and MCF-10A cells exposed to UA. UA caused a dose dependent decrease the live cells and a dose dependent increase both the MCF-7 (Fig. 3.52-C) and MCF-10A (Fig. 3.52-D) dead cells. Apoptosis was induced after 100 $\mu\text{g/ml}$ UA (21%) in MCF-7 and in MCF-10A cells after 10, 20, 50 and 100 $\mu\text{g/ml}$ UA to 25.33%, 16.33% 34.33% and 12.33% respectively.

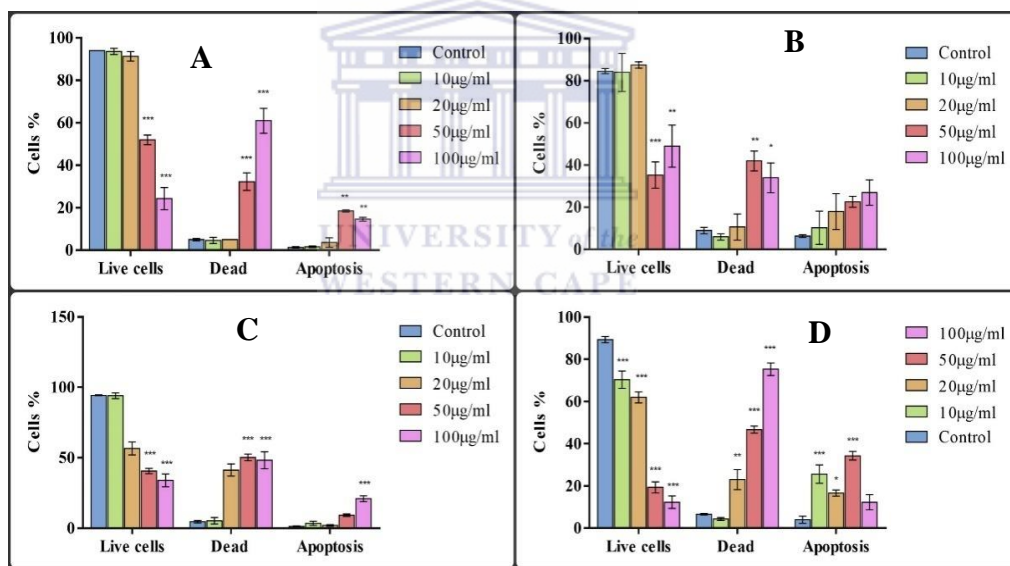


Figure 3.52: Comparison of live, dead and apoptotic cells as analysed by the Tali® Image Cytometer after exposure to OA and UA for 72h. The effect of OA on MCF-7 cells (A) and MCF-10A (B) and the effect of UA on MCF-7 (C) and MCF-10A (D) are shown above. Data is shown as mean \pm SEM of three separate experiments. Treatments significantly different from the untreated control at $p < 0.05$ are presented as * $P \leq 0.05$, ** $P \leq 0.01$, *** $P \leq 0.001$ compared to respective controls (Two-way ANOVA followed by Tukey's multiple comparisons test).

3.7 Cell cycle progression

Propidium iodide (PI) staining detected by flow cytometry was utilized to investigate the effects of OA and UA on cell cycle distribution, an S-phase block and a G2M block.

3.7.1 Effect of OA on MCF-7 and MCF-10A cell cycle progression

The dose-dependent responses for the MCF-7 cells are shown in Table 3.2 and for MCF-10A in Table 3.3.

After 6h, the S-phase of MCF-7 cells was increased by 10, 20, 50 and 100µg/ml OA to 18.43%, 31.61%, 30.96% and 27.6% respectively. After 12h that it was found that all OA concentrations increased the S-phase fractions compared to control with an accompanying decrease in the G1 and G2 phases. After 24, 48 and 72h, OA showed a similar increase in the S-phase peak as observed for the 6h and 12h treated cells. In comparison to control sample after 24h which had 3.78% of cells in the S-phase, OA at all concentrations, pushed the levels of cells in S-phase up to 30%. After 48h, in comparison to the control sample (2.78%) the increase varied from 16.68% for 10µg/ml to 44.33% (100 µg/ml OA). After 72h the percentage of cells in the S-phase ranged from 19.44% (10 µg/ml) to 27.25% (100µg/ml OA). Furthermore the MCF-7 cells treated with 10, 50 and 100µg/ml OA showed an increase in the G2 peak (44.24%; 19.93% and 29.53%) after 48h, when compared to control cells. This increase was not observed after 72h.

A similar increase in the S-phase peaks was observed in the MCF-10A cells after the different times of exposure. It can however be seen that cells moved to the G2 phase after 6h 10, 50 and 100µg/ml, at 12h, (50 and 100µg/ml) at 24h (10 and 20µg/ml OA), 48h (10µg/ml) and after 72h it was the MCF-10A cells exposed to 50- and 100µg/ml (21.26% and 10.13%) that showed an accumulation of cells the G2 phase. Thus when comparing the effects of OA on MCF-7 and MCF-10A cells, it was seen that in both cells lines an intra-S-phase block was activated.

The accumulation of cells in the S-phase started at 6h and continued throughout the different time and doses indicating that OA affects the cell cycle progression possibly by activating the intra-S-phase checkpoint. Activation of the intra-S-phase block slows down the processes of DNA synthesis allowing time for DNA repair thus preventing genomic instability.

The MCF-7 cells showed increase of cells in the G2 phase after 48h could indicate that these cells had managed to repair the initial DNA damage induced by OA. However, the MCF-10A cells show this increase in the G2 peaks for most of the time period which could indicate that the DNA damage in these cells were not as severe as that induced by OA in the MCF-7 cells.



Table 3.2: The percentage distribution for control and OA treated MCF-7 cells. As the OA concentration increased, the percentage of cells that arrested in the phase of the cell cycle also increases.

MCF-7 OA	Time	Cell cycle phases	Control	10µg/ml	20µg/ml	50µg/ml	100µg/ml
	6h	G1	89	71.59	59.06	61.62	69.52
		S	3.75	18.43	31.61	30.96	27.6
		G2	7.25	9.98	9.34	7.42	2.88
	12h	G1	88	59.6	54.51	78.86	82.01
		S	2.78	38.89	45.49	17.78	13.47
		G2	9.22	1.51	0	3.36	4.52
	24h	G1	86	67.19	64.35	67.12	66.22
		S	3.78	31.66	30.66	30.73	33.78
		G2	10.86	1.15	4.35	2.15	0
48h	G1	92	39.07	56.44	54.96	26.14	
	S	2.78	16.68	37.17	25.11	44.33	
	G2	5.22	44.25	6.39	19.93	29.53	
72h	G1	91	75.35	68.3	70.55	67.58	
	S	3.74	19.44	25.68	24.59	27.25	
	G2	5.26	5.21	6.02	4.86	5.17	

Table 3.3: The percentage distribution for control and OA treated on MCF-10A cells. As the OA concentration increased, the percent of cells that arrested in the S phase of the cell cycle also increases.

MCF-10A OA	Time	Cell cycle phases	Control	10µg/ml	20µg/ml	50µg/ml	100µg/ml
	6h	G1	90.56	60.03	64.18	62.42	62.3
		S	2.71	19.07	13.61	18.57	15.42
		G2	6.73	20.9	22.2	19.01	22.28
	12h	G1	93.56	56.94	56.55	65.9	68.83
		S	2.71	34.87	38.83	10.6	0
		G2	5.73	8.19	4.62	23.5	31.17
	24h	G1	91.56	70	85.62	88.86	93.31
		S	2.71	11.63	4.33	1.93	2.45
		G2	6.73	17.64	10.05	9.22	4.45
48h	G1	90.56	69.98	45.85	56.1	51.52	
	S	3.72	1.97	46.47	43.9	42.6	
	G2	4.72	28.05	7.68	0	5.88	
72h	G1	90.88	53.9	61.93	62.14	64.26	
	S	4.33	46.1	38.07	16.59	25.61	
	G2	4.79	0	0	21.26	10.13	

3.7.2 Effect of UA on MCF-7 and MCF-10A cell cycle progression

The dose-dependent UA exposed effects on MCF-7 cells are shown in Table 3.4 and for MCF-10A in Table 3.5.

After 6h the S-phases of MCF-7 cells increased following treatment with 10, 20, 50 and 100µg/ml UA. The G1-phase was decreased after exposure to UA and the G2-phase remained the same except after 20 µg/ml UA when it was 0%. After 12h that it was found that 20µg/ml UA increased the S-phase fraction (51.04%) compared to control (2.78%) with an accompanying decrease in the G1 (20 and 100µg/ml) while the G2 phase increased marginally after 100µg/ml UA.

After 24h the S-phase of MCF-7 cells were increased by 10, 20, 50 and 100µg/ml UA to 57.56%, 58.73%, and 54.2% and 45.96% respectively. G1-phase decreased when exposed to 10, 20, 50 and 100µg/ml UA and the G2-phase increased after to exposed 10 and 20µg/ml UA (18.86% and 16.06%) respectively.

After 48h the S-phases of MCF-7 cell line increased when exposed to 10µg/ml (44.19%), 50µg/ml (78.53%) and 100µg/ml (63.18%). And except for the 50µg/ml, the G2 phases were also increased after UA exposure with an outspoken decline in the G1 phases. After 72h S-phases increased after 10µg/ml (83.7%) and 100µg/ml (69.39%) when compared to control (3.74%).

A similar increase in the S-phase peaks was observed in the MCF-10A cells after the different times of exposure. However, it can be seen that cells moved to the G2 phase after 6h (10, 50 and 100 µg/ml UA concentrations). At 12h and 24h UA increased S and G2 phases, except for 20 µg/ml after 12h and 50 µg/ml after 24h. After 48h, S-phase peaks were seen after 20 and 100µg/ml UA and after 72h the MCF-10A cells exposed to all the UA concentrations showed elevated S-phase peaks. Increased cells in the G2 phase were seen after 10µg/ml UA. Thus, when comparing the effects of UA on MCF-7 and MCF-10A cells, it was seen that in both cell lines an intra-S-phase block was activated.

The accumulation of cells in the S-phase after treated with UA started after 6h and continued during the different times and doses demonstrating that UA affects the cell cycle progression as did OA, probably by activating the intra-S-phase checkpoint, resulting in a S-phase block. Activation of the intra-S-phase block slows down the processes of DNA synthesis allowing time for DNA repair thus preventing genomic in stability.

The non-tumorigenic cell line, MCF-10A showed an overall increase of cells in the G2 phase after UA treatment when compared to the MCF-7 cells. This accumulation could be indicative of a G2/M block, but it also indicates that the intra S-phase block caused by UA exposure was overcome by in the non-tumorigenic cells.



Table 3.4: The percentage distribution for control and UA treated MCF-7 cells. As the UA concentration increased, the percentage of cells that arrested in the S phase of the cell cycle also increased.

MCF-7 UA	Time	Cell cycle phases	Control	10µg/ml	20µg/ml	50µg/ml	100µg/ml
	6h	G1	89	84	63.32	71.39	67.85
S		3.75	10	36.68	21.74	24.31	
G2		7.25	6	0	6.87	7.84	
12h	G1	88	76.8	48.96	62.89	54.98	
	S	2.78	19.85	51.04	37.11	37.36	
	G2	9.22	3.35	0	0	7.66	
24h	G1	86	23.58	25.21	42.27	54.69	
	S	3.78	57.56	58.73	54.2	45.96	
	G2	10.86	18.86	16.06	3.53	0	
48h	G1	92	32.62	23.98	21.47	21.98	
	S	2.78	44.19	34.37	78.53	63.18	
	G2	5.22	23.19	41.65	0	14.84	
72h	G1	91	12.8	67.67	71.75	26.06	
	S	3.74	83.7	28.69	28.25	69.39	
	G2	5.26	3.5	3.64	0	4.55	

Table 3.5: The percentage distribution for control and UA treated on MCF-10A cells. As the UA concentration increased, the percentage of cells that arrested in the S phase of the cell cycle also increased.

MCF-10A UA	Time	Cell cycle phases	Control	10µg/ml	20µg/ml	50µg/ml	100µg/ml
	6h	G1	90.56	37.36	37.42	57.58	67.76
S		2.71	41.74	56.18	1.6	9.41	
G2		6.73	20.9	6.41	40.82	22.82	
12h	G1	93.56	65.14	45.29	55.27	56.89	
	S	2.71	19	0	37.11	32.54	
	G2	5.73	15.86	54.71	7.62	10.86	
24h	G1	91.56	38.18	38.9	37.83	24.53	
	S	2.71	47.4	29.13	0	22.4	
	G2	6.73	14.42	31.96	62.17	53.07	
48h	G1	90.56	43.27	52.15	71.28	47.07	
	S	3.72	5.48	26.02	0	51.54	
	G2	4.72	51.25	21.83	28.72	1.54	
72h	G1	90.88	50.83	64.03	41.31	40	
	S	4.33	30.56	29.08	49.43	60	
	G2	4.79	18.61	6.89	9.26	0	

3.8 Reactive oxygen species (ROS)

3.8.1 Effects of OA on ROS in MCF-7 cells after 6, 12, 24, 48 and 72h

CellROX[®] Oxidative Stress Reagents specifically detect oxidative stress in cells. While a low level of ROS can serve as signalling molecules, ROS at higher concentrations could be indicative of pre-lethal toxicity induced by various drugs. After labeling with CellROX[®] Orange Reagent, cells were analyzed with the Tali[®] Image-Based cytometer using the RFP channel (representative of the fluorescence signal), collecting 8 fields per sample.

The results, as seen in Table 3.6 indicate that treatment with OA produced a dose responsive increase in ROS levels of the MCF-7 cells after 6h. The treatment with 10µg/ml and 20µg/ml OA produced an increase in ROS (14% and 21%). 55% and 99% of the MCF-7 cells treated with 50µg/ml and 100µg/ml OA showed an increase in ROS compare to 2% in the control.

Treatment with OA produced an increase in ROS levels of the MCF-7 cells after 12 and 24h. The treatment with 10µg/ml and 20µg/ml OA produced an increase in ROS (17% and 25%). 36% and 80% of the MCF-7 cells treated with 50µg/ml and 100µg/ml OA showed an increase in ROS compared to 5% in the control.

After 24h, 10µg/ml caused a 20% ROS level, with 50 and 100µg/ml OA inducing 22% and 89% increase in ROS compared to 2% in the control. After 48h and 72h ROS was increased only in the cells exposed to 50µg/ml and 100µg/ml.

Table 3.6: The percentage oxidative stress in MCF-7 cells treated with OA concentrations (10, 20, 50, and 100µg/ml) respectively, and at different times of exposure. A consecutive increase in the percentage of cells that stained positive with CellRox orange after exposure to OA, is seen.

Time	Control	OA			
		10µg/ml	20µg/ml	50µg/ml	100µg/ml
6h	2	14	21	55	99
12h	5	17	25	36	80
24h	2	20	8	22	98
48h	1	1	5	25	67
72h	2	9	4	39	84

3.8.2 Effects of OA on ROS in MCF-10A cells after 6, 12, 24, 48 and 72h

Treatment with OA produced a dose dependent increase in ROS levels of the MCF-10A cells. After 6h, 10µg/ml and 20µg/ml OA produced an increase in ROS (14% and 73%) while 57% and 96% of the cells treated with 50µg/ml and 100µg/ml OA respectively showed an increase in ROS MCF-10A compared to 4% control as shown in Table 3.7.

A similar dose dependent increase in ROS was observed after 12, 24, 48 and 72h however, the greatest increase in ROS was after 6h. No difference in oxidative stress was observed between the two cell lines after OA exposure of and both cell lines showed dose dependent increases in ROS.

Table 3.7: MCF-10A cells ROS levels induced by OA (10, 20, 50, and 100µg/ml) for the different times of exposure. A dosed dependent increase in ROS is observed for all the different tome periods.

Time	Control	OA			
		10µg/ml	20µg/ml	50µg/ml	100µg/ml
6h	4	14	73	57	96
12h	3	14	52	65	70
24h	7	20	40	39	76
48h	1	18	43	57	84
72h	5	12	38	47	69

UNIVERSITY of the
WESTERN CAPE

3.8.3 Effects of UA on ROS in MCF-7 cells after 6, 12, 24, 48 and 72h

It was mainly treatment with 20, 50 and 100µg/ml UA that increased ROS in the MCF-7 cells. After 6h treatment with 20µg/ml UA, an increase in ROS from 4% in control cells to 20% was observed, and an increase to 59% and 67% in cells treated with 50µg/ml and 100µg/ml UA (Table 3.8).

After 12h a 38%, 53% and 68% increase in ROS was seen after 20, 50µg/ml and 100µg/ml UA. Similar increases were observed after 24, 48 and 72h with the 100µg/ml UA inducing the highest level of ROS MCF-7 cells.

Table 3.8: Oxidative stress in MCF-7 cells treated with UA concentrations, 10, 20, 50, and 100µg/ml respectively, and at different time of exposure. A consecutive increase in the % of cells that stained positive with CellRox orange was observed after exposure to increasing concentrations of UA, excluding 10µg/ml. ROS is shown as percentage.

Time	Control	UA			
		10µg/ml	20µg/ml	50µg/ml	100µg/ml
6h	4	6	20	59	67
12h	3	11	38	53	68
24h	3	4	34	75	89
48h	1	11	13	44	78
72h	4	4	14	61	93

3.8.4 Effects of UA on ROS in MCF-10A cells after 6, 12, 24, 48 and 72h

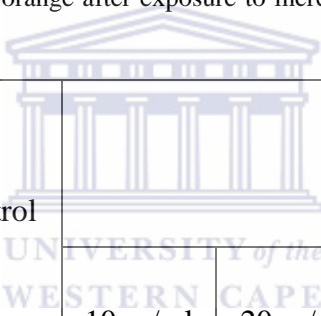
The results demonstrate that treatment with UA produced an increase in ROS levels of the MCF-10A cells in all the times of exposure. The treatment with 10µg/ml and 20µg/ml UA produced an increase in ROS MCF-10A levels (18% and 51%) after 6h and 86% and 98% of the cells treated with 50µg/ml and 100µg/ml UA showed an increase in ROS MCF-10A compared to the 4% observed in control cells (Table 3.9).

The treatment with 10µg/ml and 20µg/ml UA for 12h produced an increase in ROS (22% and 49%) and extremely high levels, 90% and 97% were seen after 50µg/ml

and 100µg/ml UA showed compared to 1% in the control. This trend continued in the 24, 48 and 72h exposure times with 50 and 100µg/ml UA inducing extremely high levels of ROS in MCF-10A cells.

It seems that the higher concentrations UA not only caused a more outspoken increase in ROS in the MCF-10A cells than the MCF-7 cells but that UA also affected the MCF-10A cells to a great extent than OA had affected the MCF-10A cells. With 50µg/ml and 100µg/ml UA increasing ROS between (86%) to (98%) in the MCF-10A cells.

Table 3.9: Oxidative stress in MCF-10A cells treated with UA after 10, 20, 50, and 100µg/ml respectively for 6-, 12-, 24-, 48-, and 72 hours. A dose dependent increase in the % of cells that stained positive with CellRox orange after exposure to increasing concentration of UA was seen. ROS is shown as percentage.



Time	Control	UA			
		10µg/ml	20µg/ml	50µg/ml	100µg/ml
6h	4	18	51	86	98
12h	1	22	49	90	97
24h	3	14	43	87	95
48h	7	26	44	88	98
72h	3	16	56	89	96

3.9 Western blot

3.9.1 LC3 and Beclin-1 expression in MCF-7 and MCF-10A after OA and UA exposure for 6h

Since no conclusive results regarding the possible induction of autophagy by OA and UA could be obtained for 50 and 100 μ g/ml OA or UA using the triple staining method, it was decided to investigate markers (LC3 and Beclin1) for autophagy in cells exposed to 50 and 100 μ g/ml OA and UA. Fig. 3.53 shows 100 μ g/ml OA increased Beclin-1 expression in MCF-7 cells and to a lesser extent in MCF-10A cells. 50 μ g/ml OA increased the LC3 expression in MCF-10A.

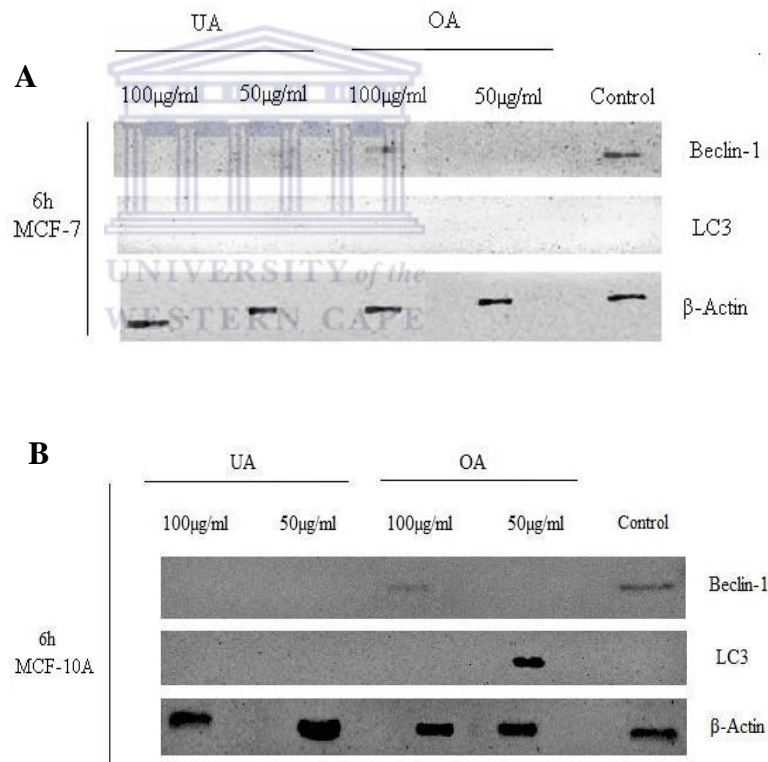


Figure 3.53: Beclin-1 and LC3 Expression in MCF-7 and (B): MCF-10A in cells exposed OA and UA for 6h

3.9.2 LC3 and Beclin-1 expression in MCF-7 and MCF-10A after OA and UA exposure for 12h

50 and 100 $\mu\text{g/ml}$ OA and 50 $\mu\text{g/ml}$ UA increased Beclin-1 in MCF-7 cells after 12h. Also, 100 $\mu\text{g/ml}$ UA increased Beclin-1 in MCF-10A cells. Fig. 3.54A shows 50 $\mu\text{g/ml}$ OA increased the LC3 expression in the MCF-7.

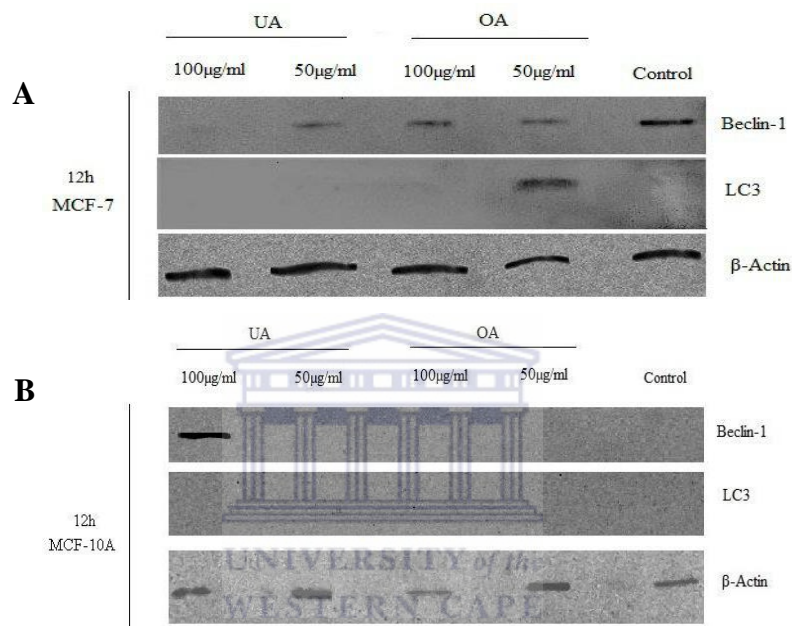


Figure 3.54: Beclin-1 and LC3 expression in MCF-7 and MCF-10A cells following OA and UA exposure for 12h

3.9.3 LC3 and Beclin-1 expression in MCF-7 and MCF-10A affected by OA and UA for 24h

Fig. 3.55 shows that 100 $\mu\text{g/ml}$ OA and UA increase Beclin-1 in MCF-7 cells. After 24h, 50 and 100 $\mu\text{g/ml}$ OA increased Beclin-1 expression in MCF-10A cells when compared to control. 50 $\mu\text{g/ml}$ OA and UA increased LC3 expression in MCF-7 cells and 50 and 100 $\mu\text{g/ml}$ OA and 50 $\mu\text{g/ml}$ UA increased LC3 expression in MCF-10A after 24h.

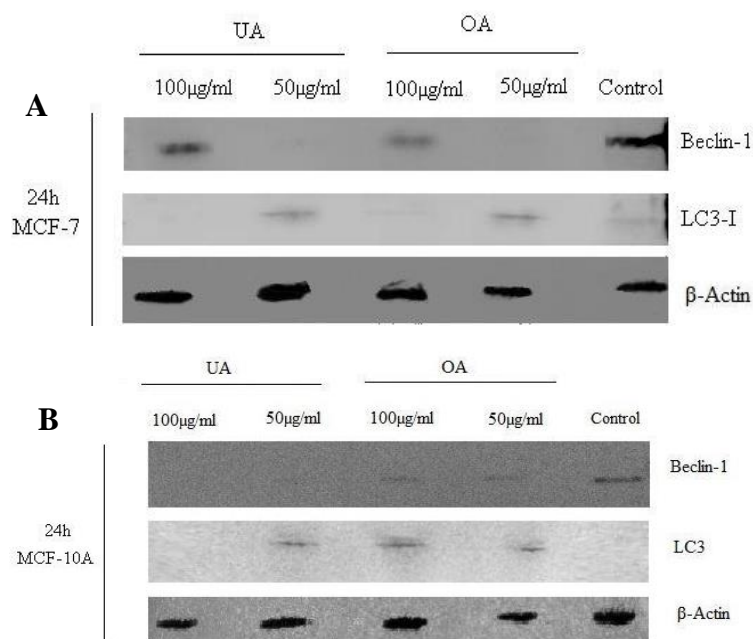
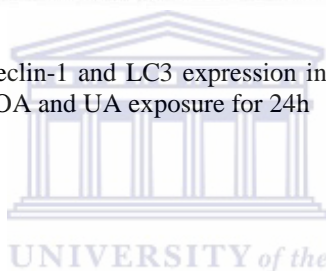


Figure 3.55: Beclin-1 and LC3 expression in MCF-7 and MCF-10A cells following OA and UA exposure for 24h



3.9.4 LC3 and Beclin-1 expression in MCF-7 and MCF-10A affected by OA and UA for 28h

50 and 100 µg/ml OA and 50 and 100µg/ml UA increased Beclin-1 expression in MCF-7 cells and 50µg/ml OA and 100µg/ml UA increased Beclin-1 expression in MCF-10A cells when compared to control as shown in Fig. 3.56.

50µg/ml UA and 100µg/ml OA increased LC3 expression in the MCF-7 and 100µg/ml OA and 50µg/ml UA increased LC3 expression in MCF-10A cells when compared to control as shown in Fig. 3.56.

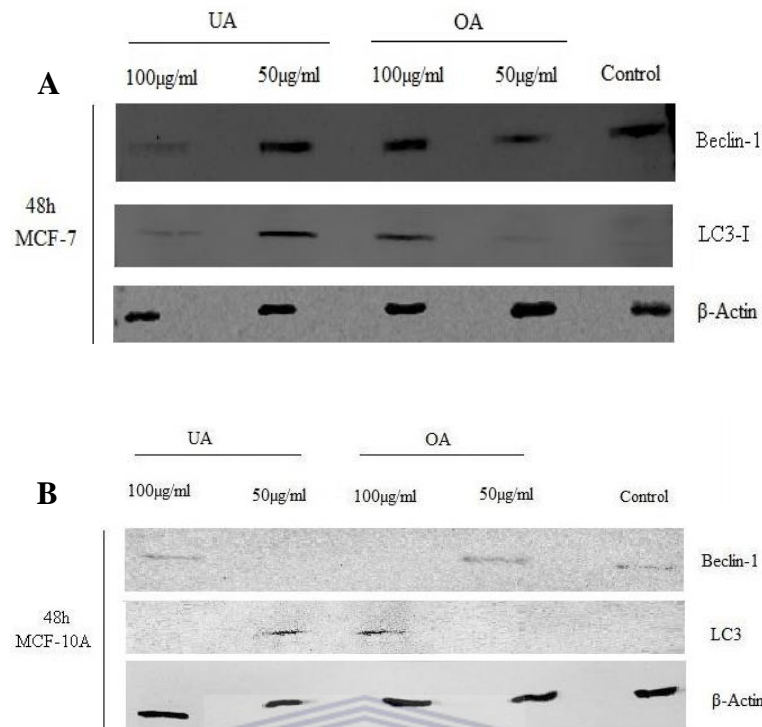
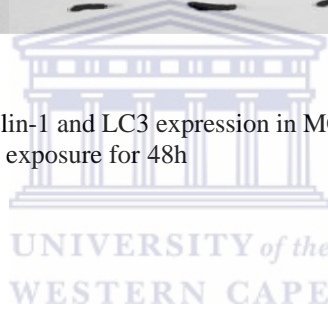


Figure 3.56: Beclin-1 and LC3 expression in MCF-7 and MCF-10A cells after OA and UA exposure for 48h



3.9.5 LC3 and Beclin-1 expression in MCF-7 and MCF-10A after OA and UA for 72h

50 and 100 µg/ml OA and 50 UA increased Beclin-1 expression in MCF-7 and 50µg/ml OA and UA increase Beclin-1 expression in MCF-10A cells when compared to control as shown in Fig. 3.57.

50 and 100 µg/ml OA and 50µg/ml UA increased LC3 expression in the MCF-7 cells and 50µg/ml OA and UA increased LC3 expression in the MCF-10A cells compared to control as shown in Fig. 3.57.

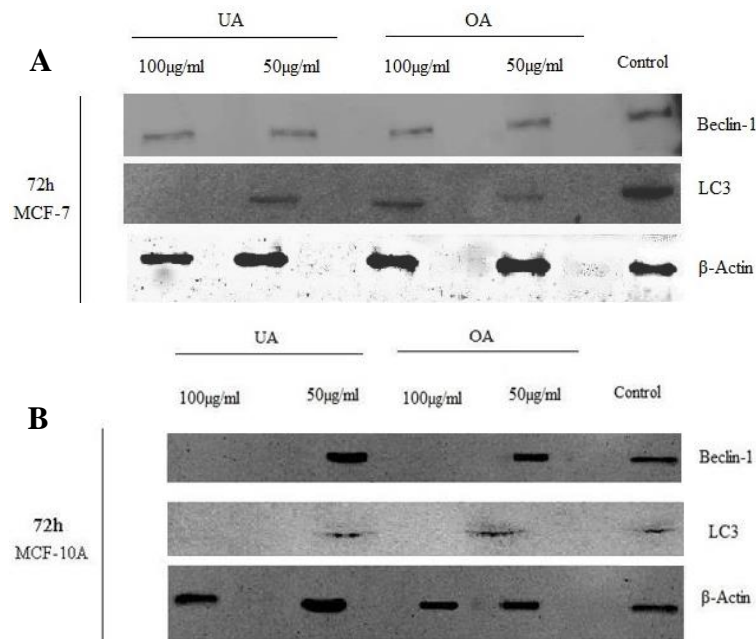


Figure 3.57: Beclin-1 and LC3 expression in MCF-7 and MCF-10A cells following OA and UA exposure for 72h

3.10 Analysis of gene expression

Primer efficiency QC was performed on the primer pairs using a serial dilution of pooled cDNA samples. The slope of the standard curve should be between -3.1 to -3.6 and display an R^2 value of >0.98 as shown in Table 3.10. The disassociation curve should display one peak indicative of the target product and no peaks in the water (no template control, NTC) to indicate no contamination. In some instances, primer dimers are formed in the NTC or in samples where no target is present. Standard curve and disassociation curves analysed using the SDS software (Life Technologies) for each primer pair can be found in the Appendices. Primer pairs which passed QC, ATG6; RAB7A and GAPDH, were used for qPCR sample analysis and results can be found below. The ATG6 data was analysed with qbase software (www.biogazelle.com). The maximum allowed variability on technical replicates was set at 0.65 cycles. ATG6 is also known as Beclin-1.

Table 3.10: Primer efficiency (E), slope and R² value for each primer pair as calculated using qbase software. An E value of 2 indicates 100% primer efficiency and an R² value of 0.99 indicates a good correlation between Ct and sample concentration.

Cell Line	Gene	Efficiency	R ²	Slope
MCF-7	ATG6	2.072	0.968	-3.16
	GAPDH	1.87	0.994	-3.68
	RAB7A	1.807	0.992	-3.892
MCF-10A	ATG6	2.131	0.97	-3.042
	GAPDH	2.869	0.967	-2.184
	RAB7A	1.923	0.957	-3.52

The relative quantities of the samples were normalized to the geometric mean of the two reference genes and scaled to the control group (Figs 3.58, 3.59, 3.60 and 3.61). The graphs below show the individual relative quantities of the biological samples. I indicate a better representation of the variability of the biological replicates. The results of a relative quantification analysis do not have a particular scale. Because of this they can be multiplied (or divided) by a common factor, i.e. in this case an average of 3-6 biological replicates in the control group. This process will alter the actual values, but not the sample to sample relationships (i.e. the fold changes).

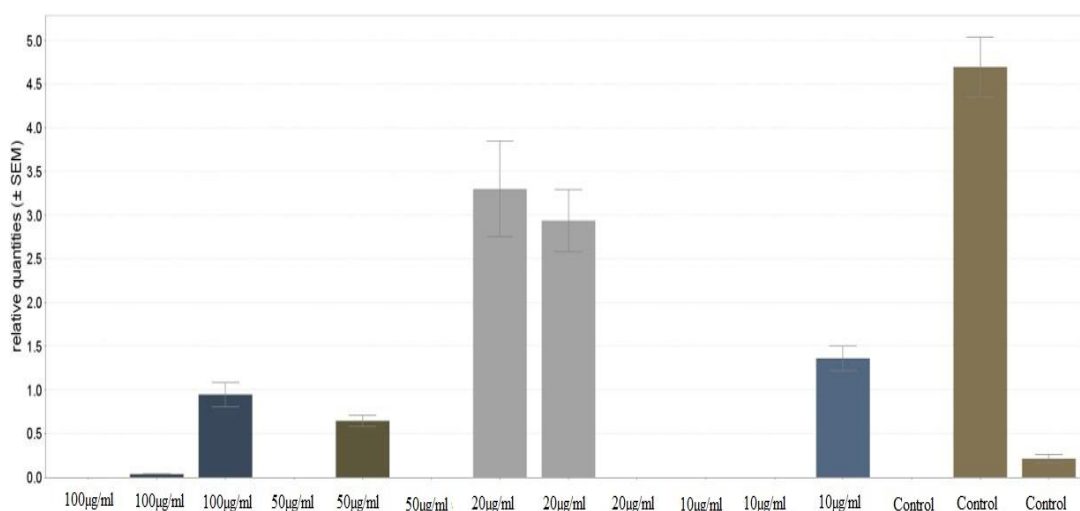


Figure 3.58: The relative quantity of ATG6 in MCF-7 cell lines treated with various concentrations of OA. The graph shows the relative quantity of ATG6 normalized to the reference genes, GAPDH and RAB7A, and scaled to the control group (COA17-37) for each biological sample submitted.

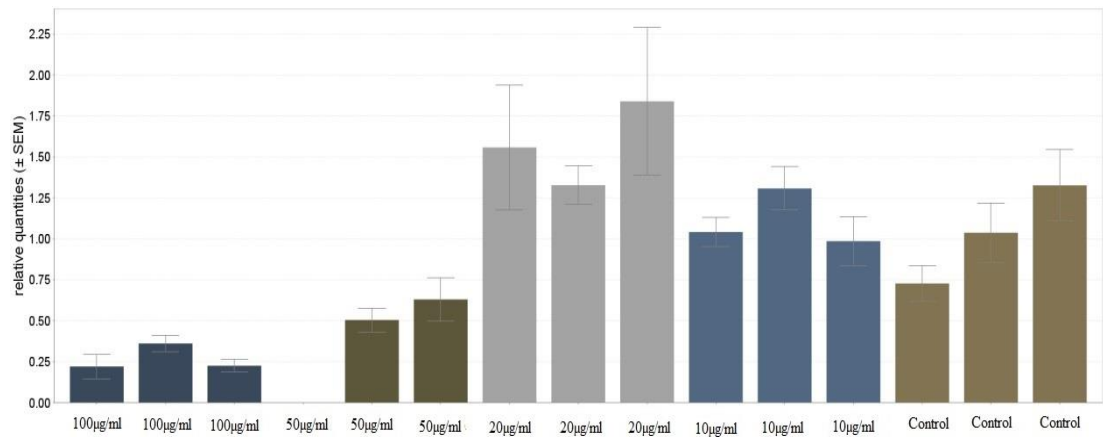


Figure 3.59: The relative quantity of ATG6 in MCF-7 cell lines treated with various concentrations of UA. The graph shows the relative quantity of ATG6 normalized to the reference genes, GAPDH and RAB7A, and scaled to the control group (CUA17-37) for each biological sample submitted.

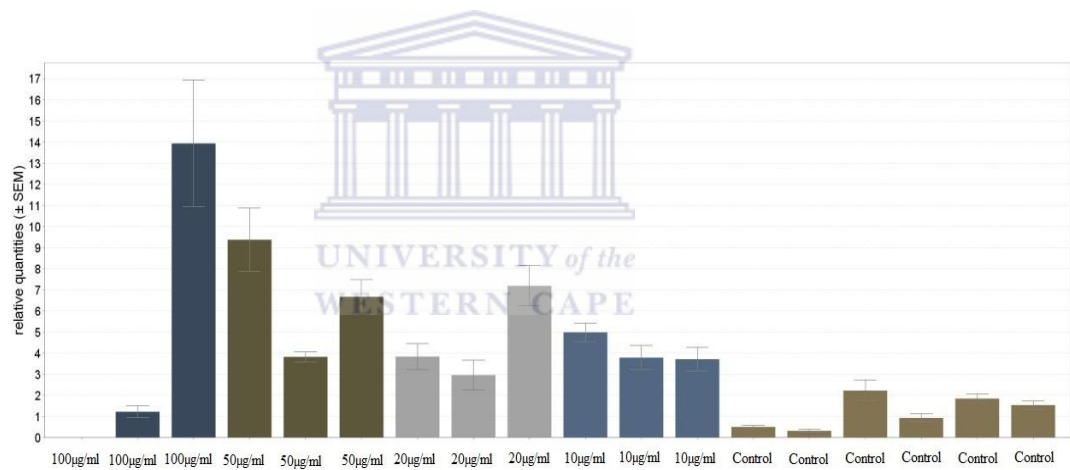


Figure 3.60: The relative quantity of ATG6 in MCF-10A cell lines treated with various concentrations of OA. The graph shows the relative quantity of ATG6 normalized to the reference genes, GAPDH and RAB7A, and scaled to the control group (C1-C6) for each biological sample submitted.

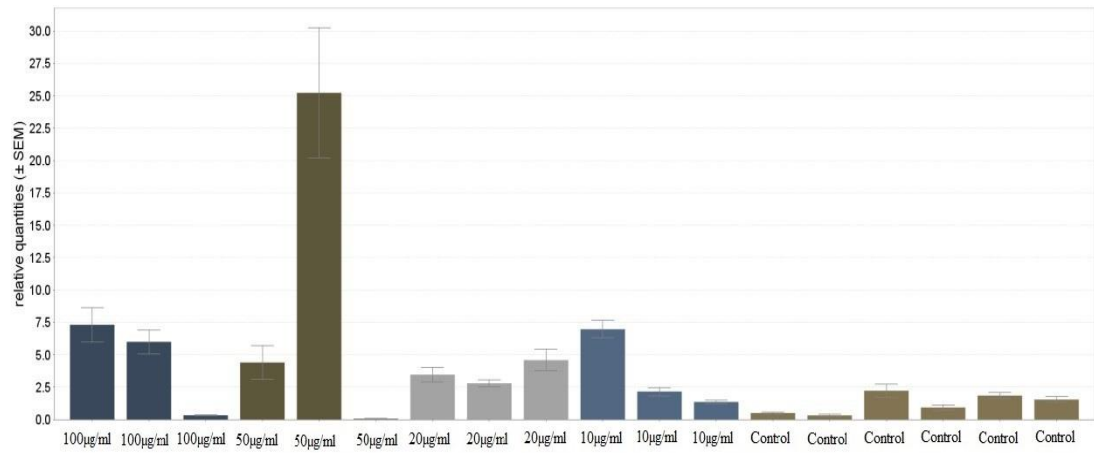


Figure 3.61: The relative quantity of ATG6 in MCF-10A cell lines treated with various concentrations of UA. The graph shows the relative quantity of ATG6 normalized to the reference genes, GAPDH and RAB7A, and scaled to the control group (C1-C6) for each biological sample submitted.



Chapter IV

4 Discussion

Breast cancer is the second leading cause of cancer death after lung cancer (American Cancer Society, 2015) In South Africa 1 in 34 women can develop breast cancer and this high rate is indicative of a significant public health problem. The lifetime risk of breast cancer differs according to ethnicity with 1/52 in black women, 1/18 in white women, 1/22 in coloured women and 1/19 in Indian women. Despite the progress made in breast cancer research, traditional treatment for breast cancer has not changed much over the past decades (Matsen & Neumayer 2013; Simic & Weiland 2003).

Breast cancer treatment entails surgical removal of the tumor that is followed by chemotherapy with or without radiation (Ananthakrishnan et al., 2012; Coley, 2008; Ragaz et al., 2005; Yagata et al., 2011). However, the notorious effect of such treatments has in many cases exacerbated the overall diminishing health and quality of life of the recipients. Although early detection has improved survival, the chemotherapeutic agents used in the treatment of breast cancer have not proven to be efficient in all patients, as 50-60% of patients with metastatic disease fail to respond when treated with therapeutic agents (Chia et al., 2007; Conley et al., 2012). This warrants further investigation into safer and more effective treatment strategies. Focus has been turned to natural compounds which have been shown to have anti-tumor effects. This study focused on two phytochemicals, namely UA and its isomer OA as an alternative treatment for breast cancer.

Both UA and OA have a range of biological effects such as hepatoprotective, antitumor, cardiovascular and inflammatory actions (Raphael and Kuttan, 2003; Shanmugam et al., 2013; Sultana and Ata, 2008). Their activities have been reported in breast, endometrial, pancreatic and prostate cancer, leukemia a melanoma cells. Several studies have been undertaken in vivo and in vitro and have suggested that

OA and UA inhibit the growth of cancer cells, including breast cancer cells (Hwang et al., 2014; Wang et al., 2013; Weng et al., 2014).

The aim of the present study was to examine the influence of OA and UA on breast cancer cell proliferation to determine whether these compounds induce autophagy or apoptosis and to investigate the effect on the molecular mechanisms influencing cell growth in the ER α positive (ER α / β +/+) MCF-7 and ER α negative (ER α / β -/+) MCF-10A cells.

The ER status of MCF-10A and MCF-7 has been previously documented (Marchese and Silva, 2012) however, receptor expression profiles may vary between different lots or batches of the same cell line (Marchese and Silva, 2012). Additionally, MCF-10A is considered an ER α negative cell line but, some studies have reported the presence of ER α among in MCF-10A cells. Breast cancers are typically assessed for ER α , progesterone receptor and HER2 expression to define histological subtype and guide treatment options.

It is known that the ER status of cells can influence cell signaling possibly influencing the effects of OA and UA on cell proliferation. The ER status of the cells used in this study was therefore determined and a time and dose study with 17 β -estradiol carried out. 17 β -estradiol serves as a ligand for nuclear estrogen receptors, estrogen receptor alpha (ER α) and beta (ER β) that function by binding to DNA directly altering gene transcription, usually by up or down regulating adjacent gene expression. ER α regulate the transcription of several hundred genes (Santiago and Bashaw, 2014) including enhanced cellular proliferation in response to estrogen binding. ER β has not been well documented in this regard (Santiago and Bashaw, 2014).

Consistent with previous in vitro studies Spink et al., (2006), 17 β -estradiol caused cellular proliferation in MCF-7 cells. On the other hand, except for 10pg/l, 17 β -estradiol failed to stimulate significant proliferation in MCF-10A cells (Table 3.1). In fact a significant reduction in proliferation was observed after 48 hours exposure

to 50, 80 and 100pg/l 17 β -estradiol. The inability of 17 β -estradiol to significantly stimulate MCF-10A proliferation corroborates earlier studies by Spink et al., (2006) Spink et al., 2006. The reduced proliferation may possibly be attributed to ER β that is frequently co-expressed with ER α at a measurably higher concentration in normal breast tissue (Marchese and Silva, 2012). ER β have been reported to inhibit in vitro cellular proliferation in response to 17 β -estradiol. It has been suggested that this is achieved through the suppression of cyclin D1, c-myc and cyclin a gene transcription in concurrence with an increased expression of p27 and p21 which ultimately results in G2 cell cycle arrest (Musgrove et al., 1998).

Analysis of MCF-10A cells showed bands corresponding to the approximate region where ER β is reported to be situated (~ 59kDa) (UniprotKB), thus supporting the ER α negative status of MCF-10A cells. Furthermore, the absence of any other band corresponding to the relative position of ER α (~ 66kDa) (UniprotKB) further supports this notion. Another faint band, consistently present corresponded to the approximate region (~ 42kDa) (UniprotKB) where GPER-1 would be located. In the MCF-7 protein preparation, another band corresponding to the approximate position of ER α ~ 66kDa (UniprotKB) was present.

The activation of the epidermal growth factor receptor is a fundamental integration point in the biological action triggered by GPER-1, a receptor for estrogen that is a member of the 7-transmembrane G protein-coupled receptor family. A wide number of natural and synthetic compounds, including estrogens and anti-estrogens, elicit stimulatory effects in breast cancer through GPER up-regulation and activation, suggesting that GPER function is associated with breast tumor progression and tamoxifen resistance (Lappano et al., 2014).

Tamoxifen, a powerful estrogen antagonist exerts its effects on breast cancer cells by binding to the ER receptors thereby displacing estrogen (Katzenellenbogen et al., 2000) but no beneficial effects was observed regarding the progression of ER-negative tumors. Unfortunately tamoxifen is associated with uterotrophic effects such as, hyperplasia, polyps and the development of uterine cancer (Cohen, 2004).

Therefore, alternatives to the use of Tamoxifen, such as the pentacyclic triterpenoids, OA and UA, require exploration.

4.1 Proliferation studies

OA and UA at concentrations of 50 μ g/ml and 100 μ g/ml suppressed cell growth in both MCF-7 and MCF-10A cell lines as shown with both the mitotic index and the crystal violet cell assay as early as six hours. The 10 μ g/ml OA and UA increased the proliferation slightly in both cell lines with the MCF-10A cells exposed to 20 μ g/ml showing recovery and increased proliferation at 72h (110.35%) when treated with OA but not with UA (Fig. 3.2-A and B). UA had a more outspoken suppressive proliferative effect at 50- and 100 μ g/ml when looking at both the mitotic index and crystal violet studies compared to OA. In previous studies, anti-cancer effects of OA and UA was reported by independent researchers in vitro on MCF-7, MDA-MB-231, HepG2, Hep3B, Huh7 and HA22T cancer cell lines (Chen et al., 2015; Krukiewicz et al., 2015; Man et al., 2015; Pertino et al., 2013). The OA and UA used in the study by Chen et al were extracted from plants and the compounds were not pure while in this study the OA and UA were produced commercially and 97% pure. Although both were extracted and commercially obtained (Sigma), OA and UA have similar chemical structures while the impure plant extracted compounds have one methyl group on their E ring (Wang et al. 2010; Yin & Chan 2007; Ovesná et al. 2006; Scarbath-Evers et al. 2015). The pentacyclic triterpenoids are a class of C30 isoprenoid compounds, they are relatively non-polar occurring widely in plants. Folding and cyclization of squalene leads to the dammarenyl ring system, which has a slightly different stereochemistry and ring structure from that of the major sterols (Dewick, 2009). Ring expansion and additional cyclization forms the characteristic fifth ring found in the lupeol, α -amyirin and β -amyirin skeletons (Brendolise et al., 2011; Holanda Pinto et al., 2008; Santos et al., 2012). UA contains the β -amyirin skeleton; its C30 isomer α -amyirin is found in OA (Misra et al., 2014; Siewert et al., 2014). The 3-OH may be esterified with a phenolic acid.

The aggressive suppression by higher doses in contrast to the stimulatory effects of the lower concentrations OA and UA can possibly be related to the biphasic nature of the respective triterpenes. In this context, estriol has been reported to display dual agonist/antagonist behaviour by inhibiting and/or distorting dimerization of estrogen-ER complex formation (Lappano et al., 2014). Regardless of the poor estrogenicity of estriol, it retains the ability to interact with ER depending on ER status and estrogen availability exerting agonistic activity if used alone and anti-estrogenic effects in the presence of estrogen. A similar mechanism could be underlying the different outcomes on proliferation seen in both cell lines after OA and UA treatment.

In this study, it was hypothesized that the cell viability analysis of the toxic effects of OA and UA in cancer cells will reveal biochemical changes in breast cancer cell lines. OA have shown anti-proliferation effect in both MCF-7 and MCF-10A cell lines *in vitro* as shown with crystal violet cell viability assay as early as six hours at concentrations of 50 μ g/ml and 100 μ g/ml. OA and UA decreased cell proliferation in MCF-7 and MCF-10A cell lines. However, the MCF-10A cells recovered and increased proliferation at 72h (110.35%) when treated with OA but not with UA (Fig. 3.1-A and B). Thus, UA is a stronger anti-proliferator compared to OA and should be used at lower concentrations for treatment. OA and UA have similar chemical structures while the impure plant extracted compounds have one methyl group on their E ring (Ovesná et al., 2006; Scarbath-Evers et al., 2015; Yin and Chan, 2007). The pentacyclic triterpenoids are a class of C30 isoprenoid compounds occurring widely in plants. Folding and cyclization of squalene leads to the dammarenyl ring system, which has a slightly different stereochemistry and ring structure from that of the major sterols (Dewick, 2009). Ring expansion and additional cyclization forms the characteristic fifth ring found in the lupeol, α -amyirin and β -amyirin skeletons (Brendolise et al., 2011; Holanda Pinto et al., 2008; Santos et al., 2012). UA contains the β -amyirin skeleton; its C30 isomer α -amyirin is found in OA (Misra et al., 2014; Siewert et al., 2014). The 3-OH may be esterified with a phenolic acid. As these compounds are relatively nonpolar, they can be found

in the waxy outer coating of fruits and other plant parts. UA induce apoptosis in a variety of tumor cells, including HL-60, human leukemia cancer cells (Baek et al., 1997; Kim et al., 2000), K562 (Liu and Jiang, 2007), HEC108 and SCG-II, human endometrial cancer cells (Achiwa et al., 2005a, 2005b), M4Beu human melanoma cells (Harmand et al., 2005), A549, human non-small cell lung cancer cells PC-3 and LNCaP, human prostate cancer cells (Kassi et al., 2007), Ha-CaT, human keratinocyte cells (Harmand et al., 2003), human Burkitt's lymphoma Daudi cells (Lauthier et al., 2000) in a dose- and time-dependent manner. Both OA and UA also had anti-proliferative effect on MCF-7 and MCF-10A in a dose and time dependent manner (Fig. 3.2-A and B).

Alternatively, antagonism by high concentrations of OA or UA of GPER-1, a receptor for estrogen that is a member of the 7-transmembrane G protein-coupled receptor family could result in decreased cell proliferation (Lappano et al., 2014).

GPER-1 mediates its activities through the stimulation of adenylyl cyclase and epidermal growth factor receptor (EGFR) pathway activation (Lappano et al., 2014) and GPER-1 action has been associated with the proliferation of breast cancer cell lines (Lappano et al., 2014). GPER and EGFR physically and functionally interact in both ER-negative and ER-positive cancer cells. Antagonism by OA or UA of GPER-1 would inhibit transactivation of epidermal growth factor receptor (EGFR) and inactivate ERK/AP-1 signalling resulting in decreased cell proliferation (Lappano et al., 2014). Studies showed that concentration differences of estriol caused the switch between ER α agonism and antagonism of GPER-1 (Lappano et al., 2014). It can thus be speculated that differences in concentration of either OA or UA could potentially also cause the switch between ER α agonism by OA/ UA or antagonism by OA/UA of GPER-1 thus stimulating proliferation at the lower concentrations and inhibiting proliferation of the cells at the higher concentrations (Fig s. 3.2-3.3).

Conversely, GPER-1 stimulation has also been reported to inhibit cellular proliferation. Furthermore, comparative studies on the actions of ER and GPER-1

have indicated that ER antagonists, serves as agonists to GPER-1 (Li et al., 2010). It is conceivable that the effects of these triterpenes may have converged on the inhibition of transcriptional gene activation and as a result, reduced proliferation. Alternatively, the presence of ER β in MCF-10A cells may account for the reduced proliferation in these cells.

4.2 Morphological studies

We further investigated the morphological changes in MCF-7 and MCF-10A cells to determine the pycnotic or apoptotic outcome after exposure to OA and UA treatment. Several studies have shown that treatment with UA, and OA, on cancer cells can cause apoptosis and cell cycle arrest (Domingues et al., 2014; Fontanay et al., 2008; Madhok et al., 2010; Pietenpol and Stewart, 2002; Shan et al., 2011; Steigerová et al., 2010; Tsai and Yin, 2008; Wójciak-Kosior et al., 2011). Apoptotic cells display typical common features such as cell shrinkage, nuclear condensation, membrane blebbing, chromatin cleavage, and formation of pycnotic bodies of condensed chromatin (Moongkarndi et al., 2004). Determination of the morphological changes and quantification of changes indicative of cell death including pycnosis or apoptosis was done in H and E stained cells. Morphological changes, indicative of mainly pycnosis in both MCF-7 and MCF-10A cells were observed in the cells exposed to the higher concentrations of both OA and UA. Characteristics, such as rounding, shrinkage, membrane blebbing, and loss of contact to adjacent cells were also observed. Evidence shows that apoptosis and autophagic cell death are crucial mechanisms that manipulate the development, homeostasis and elimination of cancer cells.

Independent studies have reported that mitotic catastrophe often leads to cell death (Bröker et al., 2005; Castedo et al., 2004a; Mansilla et al., 2006; Portugal et al., 2010; Vakifahmetoglu et al., 2008). During or after mitosis, the cellular morphology, discernible by multi-nucleation or micro-nucleation and/or mitotic arrest can be observed before the cells adopt the morphology of an apoptotic or necrotic cell (Green et al., 2009; Zhou et al., 2011). This may possibly explain the

increase in abnormal cells and cell death of MCF-7 cells treated with OA for 6h. In contrast, the effect by OA on the MCF-10A cell line was not as outspoken.

It was observed that as the dose of the OA and UA was increased, MCF-7 and MCF-10A cells undergoing pycnosis or apoptosis increased with an accompanying decrease in viable cells. Loss of cellular attachments by the affected cells resulted in loss of these cells during the staining procedure. This hampered the study of and interpretation regarding the type of cell death induced by the 50- and 100 µg/ml concentrations of OA and UA in the Hoechst and triple staining procedures. It was observed that OA and UA increased MCF-7 and MCF-10A cell death while level of total mitosis in both cells decreased.

Mitotic catastrophe is a mechanism that senses mitotic failure resulting in an irreversible fate, such as apoptosis, necrosis or senescence. Mitotic catastrophe can either kill the cell during or close to the metaphase, in a p53-independent manner. This occurs in a checkpoint kinase (Chk2) inhibited syncytia or in Polo-like kinase 2 (PLK2) Plk2-depleted cells (Burns et al., 2003; Castedo et al., 2004b; Gonçalves et al., 2011; Kimura et al., 2013), or mitotic catastrophe can occur after failed mitosis, during the activation of the polyploidy checkpoint, in a partially p53-dependent manner (Aylon et al., 2006; Castedo et al., 2004a; Eckerdt et al., 2005; Tominaga et al., 2006).

Since no abnormal metaphases or lagging chromosomes were observed during the determination of the mitotic index, mitotic catastrophe has to be ruled out as a cause of cell death by OA and UA. Wang et al. (2011) reported that UA decreased proliferation of tumour cells both in vitro and in vivo. A study by Ya Ling Hsu et al. (2004) also reported that UA up-regulated P21 expression through a P53-dependent manner and decreased expression of cyclins and their activating partner CDKs. Kassi et al. (2009) also demonstrated that the ability of UA to induce apoptosis and to modulate glucocorticoid receptor (GR) and activator Protein-1 (AP-1) in MCF-7 cells and UA is a GR modulator and may be considered as a potential anticancer agent in breast cancer (Kassi et al., 2009).

We further analyzed the possibility that the cells underwent autophagy. Generally autophagy blocks the induction of apoptosis, and apoptosis-associated caspase activation shuts off the autophagic process. But, in special cases, autophagy or autophagy-relevant proteins may help to induce apoptosis or necrosis, and autophagy has been shown to degrade the cytoplasm excessively, leading to 'autophagic cell death (Mariño et al., 2014). We selected triple staining to try to determine the presence of autophagy or apoptosis after a study done by Visagie et al., (2011) where OA and UA have been shown to induce an autophagic response in PC3-protate cancer cells. They found that autophagy inhibition enhanced UA-induced apoptosis in PC3 cells. No outspoken increases in cells undergoing autophagy or apoptosis after treatment, was observed in the Hoechst and triple stained cells. As mentioned before, the cells exposed to the higher concentrations were mostly lost in the staining procedure and therefore other experiments were employed to establish the presence of apoptosis and autophagy.

4.3 Apoptosis and cell death detection

Several forms of cell death may typically be induced within the same tissue although apoptosis is the fastest, while other forms, like necrosis or autophagy, only become visible when apoptosis is inhibited (Ciechomska et al., 2008; Ouyang et al., 2012). Several studies suggest that OA and UA has potent cancer-preventive activity and great therapeutic potential (Ikeda et al., 2008; Kassi et al., 2007; Neto, 2011; Sultana, 2011). The H and E and Hoechst stained treated samples did display some cells displaying typical morphology associated with apoptosis. A study by Kassi et al. (2009) and Zhang et al. (2006) showed that MCF-7 cells exhibited typical apoptotic features, including chromatin clumps and aggregation and DNA fragmentation after UA treatment. These changes were correlated with the down-regulation of Bcl-2 and up-regulation of caspase-3 (Kassi et al., 2009; Zhang et al., 2006). This was confirmed in another human hormone-refractory prostate cancer cell line, DU145 exposed to UA. Apoptotic cell death ensues by the activation of either the extrinsic pathway, which is initiated by activation of death receptors

leading to cleavage of caspase-8, or the intrinsic pathway, which is marked by mitochondrial depolarization, release of cytochrome c, and subsequent activation of caspase-9 (Anichini et al., 2006; Johnstone et al., 2002). In this study, quantification of the live, dead and apoptotic cells, showed an outspoken increase in dead cells of which the smaller fraction resulted from apoptosis.

Changing of intracellular ATP levels can affect the form of cell death. High ATP levels lead to apoptosis, while a low ATP level leads to necrosis confirming that an intracellular ATP depletion switches the energy-dependent apoptotic cell death to necrosis (Golstein and Kroemer, 2007; Ha and Snyder, 1999; Latta et al., 2007; Leist et al., 1999, 1997; Nicotera et al., 1998; Tsujimoto, 1997). However, a complete ATP depletion leads to a yet another type of cell death, differing from apoptosis and necrosis (Ashkenazi and Salvesen, 2014; Dixon and Stockwell, 2014). It is possible that levels ATP decreased in MCF-7 and MCF-10A cells influencing the type of cell death observed after OA and UA treatment. Our study is similar to another which showed an intracellular ATP reduction switches the energy-dependent apoptotic cell death to necrosis (Ashkenazi and Salvesen, 2014; Golstein and Kroemer, 2007; Latta et al., 2007; Leist et al., 1999, 1997; Martins et al., 2013; Nicotera et al., 1998). The result showing some apoptotic, but mostly the presence of unspecified dead cells in both cell lines after OA and UA respectively warrants investigation into the specific type of cell death induced. It is also known that a relationship exists between apoptotic or autophagic induction. Autophagy allows a cell to respond to changing environmental conditions, such as nutrient deprivation. On starvation, autophagy is greatly increased, allowing the cell to degrade proteins and organelles and thus obtain a source of macromolecular precursors, such as amino acids, fatty acids, and nucleotides, which would not be available otherwise. Thus, autophagy serves as protective role allowing cells to survive during nutrient deprivation. However, when autophagy is prevented under these conditions, cells undergo apoptosis (Boya et al., 2005; Lum et al., 2005).

In times of nutritional stress, the inhibitory effect of mTORC1 is lost. In addition, autophagy pathway activation is assisted by AMP-activated protein kinase

(AMPK). AMPK is acutely sensitive to the energy state of the cell, and is activated by low ATP to AMP ratios. However, low ATP levels, while stimulating autophagy, can also switch to necrosis, including pycnosis (Ashkenazi and Salvesen, 2014) as was observed in both the MCF-7 and MCF-10A cells. An increase in the number of dead cells was observed in both MCF-7 and MCF-10A. Overall OA caused a higher reduction in the live MCF-10A cells along with an increase in the % dead cells. In contrast to the MCF-10A cells, a similar effect was observed in MCF-7 cells after UA exposure and to a lesser extent with OA exposure (Figs. 3.47 – 4.51). Taking the different receptor profiles of the two cell lines into consideration, it does appear that the two cell lines are affected in a different way by the two triterpenes.

The less aggressive suppression by UA in MCF-10A and OA in MCF-7 cells could possibly be due to the different receptor profiles of the two cell lines leading to activation of dissimilar signalling pathways affecting cell growth.

4.4 OA and UA effect on cell cycle progression in MCF-7 and MCF-10A cells

Regulation of the cell cycle is important in the growth and development of cancer (Alberghina et al., 2012; Inzé and De Veylder, 2006; Johnson and Walker, 1999; Malumbres and Barbacid, 2007; Orford and Scadden, 2008; Ruzinova and Benezra, 2003; van den Heuvel, 2005; Weinberg, 1995; Williams and Stoeber, 2012). Cell cycle progression revealed a significant S-phase peak in MCF-7 and MCF-10A cells treated with OA and UA. The intra-S phase checkpoint activated by genotoxic insults causes only temporary, reversible delay in cell cycle progression, mainly by inhibition of new replicons initiation and thereby slowing down DNA replication (Bartek & Lukas 2001), but not permanently arresting DNA replication.

In this study the S-phases of MCF-7 and MCF-10A cells increased with the treatment of OA and UA. There was a decrease in the G1 and G2 phases in MCF-7 cells exposed to both triterpenes, except for the 48h exposure time where an increase in the G2 phase was observed after 10-, 50- and 100µg/ml OA and 10-, 20

and 100µg/ml UA. The non-tumorigenic cell line, MCF-10A showed an overall increase of cells in the G2 phase after OA treatment when compared to the MCF-7 cells that showed only movement to G2 during the 48h treatments as mentioned above. This accumulation could be indicative of a G2/M block, but it also indicates that the intra S-phase block caused by OA exposure was overcome by the non-tumorigenic cells.

Our data suggest that OA and UA inhibits cell proliferation by invoking a transition delay or block in S-phase to G2 phase of the cell cycle. This delay may possibly involve more than one total passage of a number of cells during the cell cycle, while cell number more than doubled before level growth was observed, and since 6, 12, 24, 48 and 72 h were necessary for maximal accumulation of cells in S-phase. A small percentage of MCF-10A but most of the MCF-7 cells were refractory to OA and UA and remained in the proliferative in S phase.

In this study the increase of cells in the S-phase after treated with OA and UA started at 6h and continued throughout the different time and doses indicating that the treatment affects the cell cycle progression maybe via activating the intra-S-phase checkpoint. Activation of the intra-S-phase block slows down the processes of DNA synthesis allowing time for DNA repair thus preventing genomic instability. During S phase, both DNA damage and inhibition of DNA synthesis can be sensed by S-phase-specific mechanisms (Biondi et al., 2006; Nelson et al., 2002; Sjögren and Ström, 2010).

S-phase progression requires a checkpoint signal to induce recombination repair and to allow completion of DNA synthesis (Bartek et al., 2004; Lopes et al., 2001; Sancar et al., 2004). S-phase-regulation relies on interaction of Cdc25A with the CDK1/cyclinA/B complex generating a rate-limiting stimulus for the G2/M transition. The lack of activity of the complex can delay completion of the cell division cycle (Lee et al., 2013; Mailand et al., 2002; Park and Koff, 2001). The role of Cdc25A in initiation of DNA replication is also consistent with the ubiquitin-proteasome-mediated destruction of Cdc25A in G1- and intra-S-phase checkpoint

responses to DNA damage and replication stress (Demidova et al., 2009; Lukas et al., 2001). Cdc25A is required for progression from G1 to the S phase of the cell cycle. It activates CDK2 by removing two phosphate groups. Cdc25A is specifically degraded in response to DNA damage, which prevents cells with chromosomal abnormalities from progressing through cell division. There is 3 types of S phase checkpoints namely I) DSB-induced replication dependent intra-S phase checkpoint, II) replication dependent intra-S phase checkpoint / or replication , III) S-M checkpoint (J. Bartek and Lukas, 2001; Bartek et al., 2004; Ben-Yehoyada et al., 2007; Ye et al., 2003).

A long term intra-S-phase block is probably activated by OA and UA in MCF-7 cells as only the 48h exposure samples showed cells in the G2 phase. This could limit the amount of sister chromatids and therefore reduce available templates for efficient repair by homologous recombination (J Bartek and Lukas, 2001; Sjögren and Nasmyth, 2001; Watanabe et al., 2009). Complete inhibition of CDKs and prolonged intra-S phase arrest may cause regaining of replication competence of already fired origins, making the recovery process prone to over-replication of at least parts of the genome (Bartek & Lukas 2001a). It is therefore possible that the insult caused by OA and UA treatments could act by inducing this block that could later progress to cell death. Inhibition of the CDK/cyclin complexes would also lead to a reduction of substrates including pRB and p107 (Musgrove et al., 1998).. They showed that treatments that bind to the ER and progesterone receptors in breast cancer cells lead to a reduction in total and the underphosphorylated form pRB and p107. Since the mammary gland differs from most other tissues in that differentiation is followed by involution, some differences in control of differentiation is present and it was found that pRB deficiency is associated with increased apoptosis (Musgrove et al., 1998).

Willis and Rhind 2009 suggest that this checkpoint may be more concerned with tolerating and accommodating damage during replication rather than repairing it, thus the MCF-7 cells most probably proceed to apoptosis or necrosis in the presence of outspoken DNA damage by specially the high concentrations OA and UA.

MCF-7 cells exposed to OA and UA yielded a seemingly opposite effect to that observed in MCF-10A cells. These results may be indicative of OA and UA successfully blocking or down regulating ER α causing cell cycle arrest. In contrast with the MCF-7 cells, most treated MCF-10A cells did proceed to the G2 phase. This is indicative of a recovery from the S-phase block possibly due to less DNA damage by OA and UA followed by DNA repair and movement to G2.

Reactive oxygen species (ROS) can act as signalling molecules and, in cancer, are involved in cell cycle progression and proliferation, cell survival and apoptosis, energy metabolism and cell morphology (Diaz-Moralli et al., 2013; Evan and Vousden, 2001; Kroemer and Pouyssegur, 2008; Maddika et al., 2007). A study by Kong et al. (2013) showed that cancer cells increased levels of ROS, and sub-lethal levels of ROS within these cells can promote proliferation and genomic instability. However, the increased levels of ROS can also make cancer cells more sensitive to ROS-inducing agents such as chemotherapeutic drugs (Lau et al., 2008).

The prime site of ROS generation is the mitochondrial electron transport chain (complex I and III). Hypoxic conditions have been shown to amplify the amount of ROS produced, specifically at complex III (Diaz-Moralli et al., 2013). The relationship between mitochondrial ROS and the two triterpenes has not yet been confirmed. Similarly, effects of OA and UA on the concentration of tricarboxylic acid cycle intermediates leading to increased ROS levels have not been established and are suggested for future studies in order to clarify whether they influence the stability of the master regulator. Some chemotherapeutic methods increase cellular ROS levels, inducing damage leading to apoptosis induction in cancer cells (Circu and Aw, 2010; Macip et al., 2003; Martin and Barrett, 2002; Trachootham et al., 2009). Apart from apoptosis induction, ROS also induce other types of cell death, including pycnosis (Chung et al., 2003; Li et al., 2009; Loo et al., 2010; Marchi et al., 2012; Spinner et al., 2010).

This prompted the investigation of ROS as a cause of cell death in the MCF-7 and MCF-10A cells treated by OA and UA. This study shows that ROS was increased in the MCF-7 and MCF-10A cells treated by OA and UA and at higher concentrations, coinciding with the proliferation quantification and morphology study where an increased number of dead cells were observed in the samples exposed to the higher doses of OA and UA (Figs. 4.47-51). A study by Carew et al. (2003) reported that in human cancer, mutations in mitochondrial genes, such as the gene encoding cytochrome C oxidase II, are associated with increased ROS generation. Chemotherapeutic treatment of cancer patients with DNA damaging agents that induce mutations in the mitochondrial DNA can increase cellular ROS to a toxic level and kill tumour cells (Brawek et al., 2010; El-Khoury et al., 2013; Indran et al., 2011; Leadsham et al., 2013; Lee and Wei, 2007; Shen, 2010). The resulting release of mitochondrial inter-membrane proteins, including cytochrome C, trigger apoptosis, or in case of the permeability transition pore dependent failure of ATP generation, to necrosis (Bonora et al., 2013; Brookes et al., 2004; Kokoszka et al., 2004; Orrenius et al., 2007; Scarlett and Murphy, 1997; Tsujimoto and Shimizu, 2007). Furthermore, TNF α , the best characterized necrosis-inducing ligand, has a direct involvement on mitochondrial ATP production, as well as the generation of ROS (Nikoletopoulou et al., 2013). TNF α also induces the activation of PARP1 (presumably via mitochondrial ROS, causing DNA-damage) leading to ATP depletion and subsequent necrosis (Arslan and Scheidereit, 2011; Eguchi et al., 1997; Jelezcova et al., 2010). PARP1 is a nuclear enzyme involved in DNA repair, DNA stability and transcriptional regulation, and becomes activated by DNA damage (Das et al., 2014; Mannuss et al., 2012; Mao et al., 2011; Paull et al., 2000). Its inhibition in cells exposed to genotoxic factors leads decreased rates of DNA repair and increased ROS (Cieřlar-Pobuda et al., 2012; Ryabokon et al., 2008). PARP1 over-activation consumes large amounts of NAD⁺, Therefore, PARP1 functions as a molecular switch between apoptosis and necroptosis by regulating ATP levels in the cell.

ROS-sensitive signalling pathways are persistently elevated in many types of cancers where they participate in cell growth/proliferation, differentiation, protein

synthesis, glucose metabolism, cell survival and inflammation (Wu, 2006). ROS can act as second messengers in cellular signalling (Feissner et al., 2009; Mazars et al., 2010; Paravicini and Touyz, 2006) and regulate protein activity through reversible oxidation of its targets including protein tyrosine phosphatases, protein tyrosine kinases, receptor tyrosine kinases and transcription factors (Liou and Storz, 2010).

The increase in the levels of ROS after treatment of both MCF7 and MCF 10 cells with UA and OA may lead to apoptosis, however, as seen in the aforementioned study, more cells died from a non-apoptotic death pointing to a switch from apoptosis to possibly autophagy, pycnosis or necrosis As mentioned previously, autophagy pathway activation is assisted by AMP-activated protein kinase (AMPK). AMPK is acutely sensitive to the energy state of the cell, and is activated by low ATP to AMP ratios. A study by Amoa Onguéné et al., (2013) revealed that augmented ROS produced by mitochondria under 1.5% O₂ caused increased activation of AMPK, independent of the AMP/ATP ration thus possibly inducing autophagy. However, low ATP levels, while stimulating autophagy, can also switch to pycnosis or necrosis (Ashkenazi and Salvesen, 2014). This would explain the induction of the high levels of dead cells in both the malignant MCF-7 cells and the non-transformed MCF-10A cells after OA and UA treatment.

4.5 Autophagy detection

Protein expression of Beclin-1 and LC-3 was investigated in MCF-7 and MCF-10A treated with either OA or UA for 6- 72 hours. Autophagy is generally monitored by western blotting to assess the conversion of the microtubule associated light chain 3 (LC3) from LC3-I to LC3-II, and establish the presence of a second autophagy-related marker, Beclin-1 that is associated with nucleation (Kang et al., 2010; Mizushima et al., 2011). During the initiation stage of the autophagic process, the formation of autophagosomes requires the lipidation of the cytosolic form LC3-I, followed by the incorporation of the product LC-II into the outer and inner membranes of the early autophagic vesicles. It is known that the maturation of the

autophagosomes entails their fusion with acidic lysosomes to degrade the encapsulated cargo. Since LC3-II molecules are present on both the outer and inner membranes of the autophagosomes, the degradation of the cargo along with the inner membrane will also digest the LC3-II.

The accumulation of LC-II generally indicates one of two situations (Mizushima et al., 2011). The detection of LC3-II by western blotting may indicate the beginning stages of the autophagic process. Less LC3-II is detected in the later stages of autophagy upon fusion with, and digestion by, the lysosomes. Both signify that autophagy is occurring. However, many inhibitors of the autophagic process block the fusion of autophagosomes with lysosomes. This prevents the turn-over of LC3-II, allowing it to be visualised by immune-detection.

Differential expressions of the two proteins were observed in cells treated with OA and UA when compared to untreated the cells. The OA and UA reduced Beclin-1 expression in the cells treated for 6, 12, and 24h but 50- and 100 μ g/ml increased Beclin-1 after 48 and 72h. LC-3 expression was mostly increased in both cell lines. These data suggests the possibility that OA and UA induced MCF-7 and the MCF-10A cell death by apoptosis and/ or autophagy pathway. During autophagy the cells certain processes are activated to remove unwanted of foreign substances that are detrimental to the cells (Abounit et al., 2012; Gomes et al., 2011; Huang and Klionsky, 2007; Liu et al., 2009; Mizushima and Komatsu, 2011). Deletion of autophagy-specific genes in cells of various organisms increases cell death through development and susceptibility to starvation and other apoptotic stimuli. However, high levels of autophagy can induce cell death (Berry and Baehrecke, 2008; Fulda, 2012; Platini et al., 2010). These scenarios cannot be significant to normal development or to physiological adaptations of cells to stress; they may be relevant to the development of cancer and to cancer therapy. Cancer cells frequently include mutations with the purpose of give resistance to apoptosis; as such several chemotherapeutic agents that are toxic to the cell usually induce high levels of autophagy. Autophagy and apoptosis are interlinked which regulators of apoptosis, such as Beclin-1 (Maiuri et al., 2010, 2007; Shimizu et al., 2004). The BH3 domain

of Beclin-1 is bound to, and inhibited by Bcl-2 or Bcl-XL and Beclin-1 dysfunction has been implicated in many disorders, including cancer and neurodegeneration (Kang et al., 2011). Compounds that stabilize the complex may be useful in scenarios in which it may be desirable to inhibit autophagy, such as in established tumours in which autophagy is considered a pro-survival mechanism.

The current study showed that OA and UA are capable of reducing the protein levels of Beclin-1 and increasing levels of LC-3. Reduced Beclin-1 expression after 6h and 12h of OA and UA treatment was observed in the MCF-7 cells but not in the MCF-10A cells. The other time periods (24-, 48- and 72h) showed a slight increase in Beclin-1 expression in the MCF-7 cells.

The increased levels of LC-3 and Beclin-1 expression in the MCF-10A cells points to the presence of autophagy in the cells after OA and UA treatments after 6-, 12-, and 24h periods it was reduced after treatment with OA and UA for 48 and 72h. The longer exposure periods could possibly lead to a change in the autophagy process leading to cell death by activation of a different signalling pathway.

LC-3 levels were also enhanced by OA and UA in the MCF-7 cell line. The detection of LC3-II by western blotting indicates the beginning stages of the autophagic process. Less LC3-II is detected in the later stages of autophagy. Thus the presence of LC-3 in the MCF-7 cells could indicate the start of autophagy after stimulation by OA and UA, while the lack and low levels of Beclin-1 in these cells could point to a switch from autophagy to apoptosis. Suppression of Beclin-1 expression can impair autophagy and sensitize the cells to starvation-induced apoptosis (Boya et al., 2005; Gordy and He, 2012; Luo and Rubinsztein, 2007). These results indicate that Beclin-1 may be an immediate-early response gene in tumorigenesis. Evidence suggests that at least one 'autophagy-specific' protein (Atg5) when cleaved can activate an apoptotic program. Inactivation of autophagy-specific genes, such as Beclin-1 and ATG5, leads to increased tumorigenesis in mice (Pua et al., 2007; Takahashi et al., 2007; Tang et al., 2013). Therefore,

autophagy could be a tumour-suppressor pathway, and its decreased activity may contribute to the development of human cancer.

4.6 QPCR

Beclin-1, the mammalian orthologue of yeast Atg6, has a central role in autophagy, a process of programmed cell survival, which is increased during periods of cell stress and extinguished during the cell cycle. In autophagy, vesicle nucleation begins when Beclin-1 associates with the cofactor UV irradiation resistance-associated gene (UVRAG) (Kang et al., 2011). This stimulates the activity of the lipid class III phosphatidylinositol-3-kinase (PI3-K) named Vps34 to promote the activation of the elongation process and autophagosome biogenesis. This study focuses on the Beclin-1 network of associating proteins and its regulation of MCF-7 and MCF-10A cells.

Autophagy allows a cell to respond to changing environmental conditions, such as nutrient deprivation. On starvation, autophagy is greatly increased, allowing the cell to degrade proteins and organelles and thus obtain a source of macromolecular precursors, such as amino acids, fatty acids, and nucleotides, which would not be available otherwise. Thus, autophagy serves as protective role allowing cells to survive during nutrient deprivation. Moreover, when autophagy is prevented under these conditions, cells undergo apoptosis (Boya et al., 2005; Lum et al., 2005). Caspases can cleave Beclin-1 in apoptosis, thereby destroying its pro-autophagic activity. Caspase-3-, 7- and 8-mediated cleavage of Beclin-1 generates N- and C-terminal fragments that lose their ability to induce autophagy. The C-terminal fragments translocate to mitochondria and sensitize cells to apoptotic signals (Kang et al., 2011). This process represents an amplifying loop for inducing massive apoptotic cell death.

The molecular analysis of AGT6 in both cancer and non-cancer cell lines that was treated with ascending concentration of OA and UA seem to be indicate that UA is a more valuable agent in treating breast cancer as high expression of AGT6 was

noted after UA treatment. On the hand, high concentration of UA was required for the immortalized mammary cell line, MCF-10A to undergo autophagy. The inconsistency of the expression may be attributed to the heterogeneous cells expression of breast cancer cell lines and the fact that the gene might be mutated. The assembly of the Beclin-1 complexes appears in a cell- or tissue-dependent fashion. One possible explanation is that their interaction with Beclin-1 may be relatively unstable, transient or occur only under specific conditions. However, more extensive gene expression analyses of other markers of autophagy are needed to confirm this data.

4.7 Conclusion

The OA and UA used in previous studies were extracted from plants and the compounds were not pure while in this study the OA and UA were produced commercially and 97% pure (Sigma). This OA and UA have similar chemical structures while the impure plant extracted compounds have one methyl group on their E ring (Wang et al. 2010; Yin & Chan 2007; Ovesná et al. 2006; Scarbath-Evers et al. 2015).

In conclusion, this study was able to show that OA and UA inhibited the proliferation of a breast cancer cell line in a dose- and time-dependent manner and that the two compounds OA and UA can be introduced as new treatment for breast cancer. GPER-1, a receptor for estrogen that is a member of the 7-transmembrane G protein-coupled receptor family and EGFR physically and functionally interact in both ER-negative and ER-positive cancer cells. Antagonism by OA or UA of GPER-1 would inhibit transactivation of epidermal growth factor receptor (EGFR) and inactivate ERK/AP-1 signalling resulting in decreased cell proliferation (Lappano et al., 2014). It is possible that differences in concentration of either OA or UA could potentially also cause the switch between ER α agonism by OA/ UA or antagonism by OA/UA of GPER-1 thus stimulating proliferation at the lower concentrations and inhibiting proliferation of the cells at the higher concentrations. It is conceivable that the effects of these triterpenes may have converged on the inhibition of transcriptional gene activation and as a result, reduced proliferation.

Alternatively, the presence of ER β in MCF-10A cells may account for the reduced proliferation in these cells.

Both OA and UA inhibited cell growth at the S-phase and G1/G2 phase of the cell cycle, indicating DNA damage in both cell lines after OA and UA. However, most treated non-tumorigenic MCF-10A cells did progress to the G2 phase indicating a recovery from the S-phase block possibly due to less DNA damage by OA and UA followed by DNA repair and movement to G2. This study shows that ROS was increased in the MCF-7 and MCF-10A cells treated by OA and UA and at higher concentrations, coinciding with the proliferation quantification and morphology study where an increased number of dead cells were observed in the samples exposed to the higher doses of OA and UA. However, low ATP levels, while stimulating autophagy, can also switch to pycnosis or necrosis explaining the induction of the high levels of dead cells in both the malignant MCF-7 cells and the non-transformed MCF-10A cells after OA and UA treatment.

Furthermore OA and UA induced cell death by pycnosis or apoptosis. Autophagy is a process that is important in the treatment of cancer cells to self-destruct. OA and UA were able to induce autophagy and suppressed Beclin-1 in MCF-7 cells but not in MCF-10A cells LC3, an early autophagic stage protein was present in both cell lines after treatment, but disappeared after prolonged exposure to OA and UA. Thus the presence of LC-3 in the MCF-7 cells could indicate the start of autophagy after stimulation by OA and UA, while the lack and low levels of Beclin-1 in these cells could point to a switch from autophagy to apoptosis.

However, further studies must be conducted to understand the mechanism of OA and UA on the breast cancer cells. Taken together, this study may enhance our understanding on cancer chemotherapy by OA and UA.

Future studies: The detection of LC3-II by western blotting may indicate the beginning stages of the autophagic process. Less LC3-II is detected in the later stages of autophagy upon fusion with, and digestion by, the lysosomes. Both signify that autophagy is occurring. However, many inhibitors of the autophagic process

block the fusion of autophagosomes with lysosomes. This prevents the turn-over of LC3-II, allowing it to be visualised by immune-detection. Therefore, in order to elucidate whether LC3-II detection represents early autophagosome genesis of an uninterrupted autophagic flow or the amassing of these vesicles due to dysfunction in their degradation requiring the coupling to p62, an alternative marker of autophagy, a study evaluating the levels of p62 in addition to the LC3-II conversion is encouraged.



5 Reference

- Abe, I., 2007. Enzymatic synthesis of cyclic triterpenes. *Nat. Prod. Rep.* 24, 1311–1331.
- Abounit, K., Scarabelli, T.M., McCauley, R.B., 2012. Autophagy in mammalian cells. *World J. Biol. Chem.* 3, 1–6.
- Achiwa, Y., Hasegawa, K., Komiya, T., Udagawa, Y., 2005a. Ursolic acid induces Bax-dependent apoptosis through the caspase-3 pathway in endometrial cancer SNG-II cells. *Oncol. Rep.* 13, 51–7.
- Achiwa, Y., Hasegawa, K., Udagawa, Y., 2005b. Molecular mechanism of ursolic acid induced apoptosis in poorly differentiated endometrial cancer HEC108 cells. *Oncol. Rep.* 14, 507–512.
- Alberghina, L., Mavelli, G., Drovandi, G., Palumbo, P., Pessina, S., Tripodi, F., Coccetti, P., Vanoni, M., 2012. Cell growth and cell cycle in *Saccharomyces cerevisiae*: Basic regulatory design and protein–protein interaction network. *Biotechnol. Adv.* 30, 52–72.
- American Cancer Society, 2015. What are the key statistics about breast cancer? | American Cancer Society [WWW Document].
- Amoa Onguéné, P., Ntie-Kang, F., Lifongo, L.L., Ndom, J.C., Sippl, W., Mbaze, L.M., 2013. The potential of anti-malarial compounds derived from African medicinal plants, part I: a pharmacological evaluation of alkaloids and terpenoids. *Malar. J.* 12, 449.
- Ananthakrishnan, P., Balci, F.L., Crowe, J.P., 2012. Optimizing Surgical Margins in Breast Conservation. *Int. J. Surg. Oncol.* 2012, 1–9.
- Anichini, A., Mortarini, R., Sensi, M., Zanon, M., 2006. APAF-1 signaling in human melanoma. *Cancer Lett.* 238, 168–79.
- Arslan, S.Ç., Scheidereit, C., 2011. The prevalence of TNF α -induced necrosis over apoptosis is determined by TAK1-RIP1 interplay. *PLoS One* 6.
- Asadi-Samani, M., Kafash-Farkhad, N., Azimi, N., Fasihi, A., Alinia-Ahandani, E., Rafieian-Kopaei, M., 2015. Medicinal plants with hepatoprotective activity in Iranian folk medicine. *Asian Pac. J. Trop. Biomed.* 5, 146–157.
- Ashkenazi, A., Salvesen, G., 2014. Regulated Cell Death: Signaling and Mechanisms. *Annu. Rev. Cell Dev. Biol.* 30, 337–356.
- Aylon, Y., Michael, D., Shmueli, A., Yabuta, N., Nojima, H., Oren, M., 2006. A positive feedback loop between the p53 and Lats2 tumor suppressors prevents tetraploidization. *Genes Dev.* 20, 2687–2700.
- Babalola, I.T., Shode, F.O., 2013. Ubiquitous Ursolic Acid: A Potential Pentacyclic Triterpene Natural Product. *J. Pharmacogn. Phytochem. Ubiquitous* 2, 214–222.
- Baek, J.H., Lee, Y.S., Kang, C.M., Kim, J.A., Kwon, K.S., Son, H.C., Kim, K.W., 1997. Intracellular Ca²⁺ release mediates ursolic acid-induced apoptosis in human leukemic HL-60 cells. *Int. J. Cancer* 73, 725–8.
- Banik, R.M., Pandey, D.K., 2008. Optimizing conditions for oleanolic acid extraction from *Lantana camara* roots using response surface methodology. *Ind. Crops Prod.* 27, 241–248.

- Bartek, J., Lukas, C., Lukas, J., 2004. Checking on DNA damage in S phase. *Nat. Rev. Mol. Cell Biol.* 5, 792–804.
- Bartek, J., Lukas, J., 2001. Mammalian G1- and S-phase checkpoints in response to DNA damage. *Curr. Opin. Cell Biol.* 13, 738–747.
- Bartek, J., Lukas, J., 2001. Cell cycle. Order from destruction. *Science* 294, 66–67.
- Bassett, M.T., Chokunonga, E., Mauchaza, B., Levy, L., Ferlay, J., Parkin, D.M., 1995. Cancer in the African population of Harare, Zimbabwe, 1990-1992. *Int. J. Cancer* 63, 29–36.
- Beckerman, R., Prives, C., 2010. Transcriptional Regulation by P53. *Cold Spring Harb. Perspect. Biol.* 2, a000935–a000935.
- Bell, E.L., Emerling, B.M., Ricoult, S.J.H., Guarente, L., 2011. SirT3 suppresses hypoxia inducible factor 1 α and tumor growth by inhibiting mitochondrial ROS production. *Oncogene* 30, 2986–2996.
- Ben-Yehoyada, M., Gautier, J., Dupré, A., 2007. The DNA damage response during an unperturbed S-phase. *DNA Repair (Amst)*. 6, 914–922.
- Berry, D.L., Baehrecke, E.H., 2008. Autophagy functions in programmed cell death. *Autophagy* 4, 359–360.
- Besson, A., Dowdy, S.F., Roberts, J.M., 2008. CDK inhibitors: cell cycle regulators and beyond. *Dev. Cell* 14, 159–69.
- Beukes, N., Levendal, R.-A., Frost, C.L., 2014. Selected terpenoids from medicinal plants modulate endoplasmic reticulum stress in metabolic disorders. *J. Pharm. Pharmacol.* 66, 1505–1525.
- Biondi, E.G., Reisinger, S.J., Skerker, J.M., Arif, M., Perchuk, B.S., Ryan, K.R., Laub, M.T., 2006. Regulation of the bacterial cell cycle by an integrated genetic circuit. *Nature* 444, 899–904.
- Bloom, J., Cross, F.R., 2007. Multiple levels of cyclin specificity in cell-cycle control. *Nat. Rev. Mol. Cell Biol.* 8, 149–160.
- Bononi, A., Agnoletto, C., De Marchi, E., Marchi, S., Patergnani, S., Bonora, M., Giorgi, C., Missiroli, S., Poletti, F., Rimessi, A., Pinton, P., 2011. Protein kinases and phosphatases in the control of cell fate. *Enzyme Res.* 2011, 329098.
- Bonora, M., Bononi, A., De Marchi, E., Giorgi, C., Lebiezinska, M., Marchi, S., Patergnani, S., Rimessi, A., Suski, J.M., Wojtala, A., Wieckowski, M.R., Kroemer, G., Galluzzi, L., Pinton, P., 2013. Role of the c subunit of the FO ATP synthase in mitochondrial permeability transition. *Cell Cycle* 12, 674–683.
- Boutros, R., Mondesert, O., Lorenzo, C., Astuti, P., McArthur, G., Chircop, M., Ducommun, B., Gabrielli, B., 2013. CDC25B Overexpression Stabilises Centrin 2 and Promotes the Formation of Excess Centriolar Foci. *PLoS One* 8, 1–13.
- Boya, P., González-Polo, R., Gonzalez-Polo, Rosa-Ana Casares, N., Perfettini, J.-L., Dessen, P., Larochette, N., Métiévier, D., Meley, D., Souquere, S., Yoshimori, T., Pierron, G., Codogno, P., Kroemer, G., 2005. Inhibition of macroautophagy triggers apoptosis. *Cell. Biol.* 25, 1025–1040.
- Brahmkshatriya, P.P., Brahmkshatriya, P.S., 2013. Terpenes: Chemistry, Biological Role, and Therapeutic Applications. In: *Natural Products*. Springer Berlin Heidelberg, Berlin, Heidelberg, pp. 2665–2691.

- Bravo-Sagua, R., Rodriguez, A.E., Kuzmicic, J., Gutierrez, T., Lopez-Crisosto, C., Quiroga, C., Díaz-Elizondo, J., Chiong, M., Gillette, T.G., Rothermel, B.A., Lavandero, S., 2013. Cell death and survival through the endoplasmic reticulum-mitochondrial axis. *Curr. Mol. Med.* 13, 317–29.
- Brawek, B., Löffler, M., Wagner, K., Huppertz, H.J., Wendling, A.S., Weyerbrock, A., Jackisch, R., Feuerstein, T.J., 2010. Reactive oxygen species (ROS) in the human neocortex: Role of aging and cognition. *Brain Res. Bull.* 81, 484–490.
- Brendolise, C., Yauk, Y.K., Eberhard, E.D., Wang, M., Chagne, D., Andre, C., Greenwood, D.R., Beuning, L.L., 2011. An unusual plant triterpene synthase with predominant β -amyrin-producing activity identified by characterizing oxidosqualene cyclases from *Malus domestica*. *FEBS J.* 278, 2485–2499.
- Brentnall, M., Rodriguez-Menocal, L., De Guevara, R.L., Cepero, E., Boise, L.H., 2013. Caspase-9, caspase-3 and caspase-7 have distinct roles during intrinsic apoptosis. *BMC Cell Biol.* 14, 32.
- Bröker, L.E., Kruyt, F.A.E., Giaccone, G., 2005. Cell Death Independent of Caspases: A Review. *Clin. Cancer Res.* 11, 3155–3162.
- Brookes, P.S., Yoon, Y., Robotham, J.L., Anders, M.W., Sheu, S.-S., 2004. Calcium, ATP, and ROS: a mitochondrial love-hate triangle. *Am. J. Physiol. Cell Physiol.* 287, C817–C833.
- Burns, T.F., Fei, P., Scata, K.A., Dicker, D.T., El-Deiry, W.S., 2003. Silencing of the novel p53 target gene Snk/Plk2 leads to mitotic catastrophe in paclitaxel (taxol)-exposed cells. *Mol. Cell. Biol.* 23, 5556–71.
- Büttner, S., Habernig, L., Broeskamp, F., Ruli, D., Vögtle, F.N., Vlachos, M., Macchi, F., Küttner, V., Carmona-Gutierrez, D., Eisenberg, T., Ring, J., Markaki, M., Taskin, A.A., Benke, S., Ruckstuhl, C., Braun, R., Van den Haute, C., Bammens, T., van der Perren, A., Fröhlich, K.-U., Winderickx, J., Kroemer, G., Baekelandt, V., Tavernarakis, N., Kovacs, G.G., Dengjel, J., Meisinger, C., Sigrist, S.J., Madeo, F., 2013. Endonuclease G mediates α -synuclein cytotoxicity during Parkinson's disease. *EMBO J.* 32, 3041–3054.
- Cammareri, M., Consiglio, M.F., Pecchia, P., Corea, G., Lanzotti, V., Ibeas, J.I., Tava, A., Conicella, C., 2008. Molecular characterization of β -amyrin synthase from *Aster sedifolius* L. and triterpenoid saponin analysis. *Plant Sci.* 175, 255–261.
- Cao, S.S., Kaufman, R.J., 2012. Unfolded protein response. *Curr. Biol.* 22, R622–6.
- Carelli, M., Biazzini, E., Panara, F., Tava, A., Scaramelli, L., Porceddu, A., Graham, N., Odoardi, M., Piano, E., Arcioni, S., May, S., Scotti, C., Calderini, O., 2011. *Medicago truncatula* CYP716A12 is a multifunctional oxidase involved in the biosynthesis of hemolytic saponins. *Plant Cell* 23, 3070–81.
- Carew, J.S.D., Zhou, Y., Albitar, M., Carew, J.S.D., Keating, M.J., Huang, P., 2003. Mitochondrial DNA mutations in primary leukemia cells after chemotherapy: clinical significance and therapeutic implications. *Leukemia* 17, 1437–1447.
- Castedo, M., Perfettini, J.-L., Roumier, T., Andreau, K., Medema, R., Kroemer, G., 2004a. Cell death by mitotic catastrophe: a molecular definition. *Oncogene* 23, 2825–2837.
- Castedo, M., Perfettini, J.-L., Roumier, T., Yakushijin, K., Horne, D., Medema, R., Kroemer, G., 2004b. The cell cycle checkpoint kinase Chk2 is a negative regulator of mitotic catastrophe. *Oncogene* 23, 4353–4361.

- Chan, E.Y.W., Longatti, A., McKnight, N.C., Tooze, S.A., 2009. Kinase-inactivated ULK proteins inhibit autophagy via their conserved C-terminal domains using an Atg13-independent mechanism. *Mol. Cell. Biol.* 29, 157–71.
- Chao, C., Wu, Z., Mazur, S.J., Borges, H., Rossi, M., Lin, T., Wang, J.Y.J., Anderson, C.W., Appella, E., Xu, Y., 2006. Acetylation of Mouse p53 at Lysine 317 Negatively Regulates p53 Apoptotic Activities after DNA Damage. *Mol. Cell. Biol.* 26, 6859–6869.
- Chen, H., Gao, Y., Wang, A., Zhou, X., Zheng, Y., Zhou, J., 2015. Evolution in medicinal chemistry of ursolic acid derivatives as anticancer agents. *Eur. J. Med. Chem.* 92C, 648–655.
- Chen, Y., Klionsky, D.J., 2011. The regulation of autophagy - unanswered questions. *J. Cell Sci.* 124, 161–70.
- Chia, S.K., Speers, C.H., D'yachkova, Y., Kang, A., Malfair-Taylor, S., Barnett, J., Coldman, A., Gelmon, K.A., O'reilly, S.E., Olivotto, I.A., 2007. The impact of new chemotherapeutic and hormone agents on survival in a population-based cohort of women with metastatic breast cancer. *Cancer* 110, 973–979.
- Chung, Y.M., Bae, Y.S., Lee, S.Y., 2003. Molecular ordering of ROS production, mitochondrial changes, and caspase activation during sodium salicylate-induced apoptosis. *Free Radic. Biol. Med.* 34, 434–442.
- Ciechomska, I. a, Goemans, C.G., Tolkovsky, A.M., 2008. Molecular links between autophagy and apoptosis. *Methods Mol. Biol.* 445, 175–93.
- Cieślak-Pobuda, A., Saenko, Y., Rzeszowska-Wolny, J., 2012. PARP-1 inhibition induces a late increase in the level of reactive oxygen species in cells after ionizing radiation. *Mutat. Res.* 732, 9–15.
- Circu, M.L., Aw, T.Y., 2010. Reactive oxygen species, cellular redox systems, and apoptosis. *Free Radic. Biol. Med.* 48, 749–762.
- Cohen, I., 2004. Endometrial pathologies associated with postmenopausal tamoxifen treatment. *Gynecol. Oncol.* 94, 256–66.
- Coleman, M.P., Quresma, M., Berrino, F., Lutz, J.-M., De Angelis, R., Capocaccia, R., Baili, P., Rachet, B., Gatta, G., Hakulinen, T., Micheli, A., Sant, M., Weir, H.K., Elwood, J.M., Tsukuma, H., Koifman, S., E Silva, G.A., Francisci, S., Santaquilani, M., Verdecchia, A., Storm, H.H., Young, J.L., 2008. Cancer survival in five continents: a worldwide population-based study (CONCORD). *Lancet Oncol.* 9, 730–56.
- Coley, H.M., 2008. Mechanisms and strategies to overcome chemotherapy resistance in metastatic breast cancer. *Cancer Treat. Rev.* 34, 378–90.
- Conley, S.J., Gheordunescu, E., Kakarala, P., Newman, B., Korkaya, H., Heath, A.N., Clouthier, S.G., Wicha, M.S., 2012. Antiangiogenic agents increase breast cancer stem cells via the generation of tumor hypoxia. *Proc. Natl. Acad. Sci. U. S. A.* 109, 2784–9.
- Cortez, D., Glick, G., Elledge, S.J., 2004. From The Cover: Minichromosome maintenance proteins are direct targets of the ATM and ATR checkpoint kinases. *Proc. Natl. Acad. Sci.* 101, 10078–10083.
- Cullen, S.P., Brunet, M., Martin, S.J., 2010. Granzymes in cancer and immunity. *Cell Death Differ.* 17, 616–623.

- Cummings, S.R., Tice, J.A., Bauer, S., Browner, W.S., Cuzick, J., Ziv, E., Vogel, V., Shepherd, J., Vachon, C., Smith-Bindman, R., Kerlikowske, K., 2009. Prevention of Breast Cancer in Postmenopausal Women: Approaches to Estimating and Reducing Risk. *JNCI J. Natl. Cancer Inst.* 101, 384–398.
- Czabotar, P.E., Lessene, G., Strasser, A., Adams, J.M., 2014. Control of apoptosis by the BCL-2 protein family: implications for physiology and therapy. *Nat. Rev. Mol. Cell Biol.* 15, 49–63.
- Das, B.B., Huang, S.N., Murai, J., Rehman, I., Amé, J.C., Sengupta, S., Das, S.K., Majumdar, P., Zhang, H., Biard, D., Majumder, H.K., Schreiber, V., Pommier, Y., 2014. PARP1-TDPI coupling for the repair of topoisomerase I-induced DNA damage. *Nucleic Acids Res.* 42, 4435–4449.
- Dasika, G.K., Lin, S.C., Zhao, S., Sung, P., Tomkinson, A., Lee, E.Y., 1999. DNA damage-induced cell cycle checkpoints and DNA strand break repair in development and tumorigenesis. *Oncogene* 18, 7883–99.
- Debnath, S., Mohanta, B.C., Harigaya, Y., Tripura, S., 2010. Naturally Occurring Triterpenoid Saponins. *Chem. biodiversity* 7, 2327–2580.
- Demidova, A.R., Aau, M.Y., Zhuang, L., Yu, Q., 2009. Dual regulation of Cdc25A by Chk1 and p53-ATF3 in DNA replication checkpoint control. *J. Biol. Chem.* 284, 4132–4139.
- Deretic, V., Levine, B., 2009. Autophagy, immunity, and microbial adaptations. *Cell Host Microbe* 5, 527–49.
- DeSantis, C., Siegel, R., Bandi, P., Jemal, A., 2011. Breast cancer statistics, 2011. *CA. Cancer J. Clin.* 61, 409–418.
- Dewick, P.M., 2009. *Medicinal Natural Products, Medicinal Natural Products: A Biosynthetic Approach: Third Edition.* John Wiley & Sons, Ltd, Chichester, UK.
- Diaz-Moralli, S., Tarrado-Castellarnau, M., Miranda, A., Cascante, M., 2013. Targeting cell cycle regulation in cancer therapy. *Pharmacol. Ther.* 138, 255–71.
- Dixon, S.J., Stockwell, B.R., 2014. The role of iron and reactive oxygen species in cell death. *Nat. Chem. Biol.* 10, 9–17.
- Domingo, V., Arteaga, J.F., López Pérez, J.L., Peláez, R., Quílez del Moral, J.F., Barrero, A.F., 2012. Total synthesis of (+)-seco-C-oleanane via stepwise controlled radical cascade cyclization. *J. Org. Chem.* 77, 341–50.
- Domingues, R., Guerra, A., Duarte, M., Freire, C., Neto, C., Silva, C., Silvestre, A., 2014. Bioactive Triterpenic Acids: From Agroforestry Biomass Residues to Promising Therapeutic Tools. *Mini. Rev. Org. Chem.* 11, 382–399.
- Doonan, F., Cotter, T.G., 2008. Morphological assessment of apoptosis. *Methods* 44, 200–204.
- Durfee, T., Becherer, K., Chen, P.L., Yeh, S.H., Yang, Y., Kilburn, A.E., Lee, W.H., Elledge, S.J., 1993. The retinoblastoma protein associates with the protein phosphatase type 1 catalytic subunit. *Genes Dev.* 7, 555–69.
- Eckerdt, F., Yuan, J., Strebhardt, K., 2005. Polo-like kinases and oncogenesis. *Oncogene* 24, 267–276.
- Eguchi, Y., Shimizu, S., Tsujimoto, Y., 1997. Intracellular ATP levels determine cell death fate by apoptosis or necrosis. *Cancer Res.* 57, 1835–1840.

- Ekholm, S. V, Reed, S.I., 2000. Regulation of G1 cyclin-dependent kinases in the mammalian cell cycle. *Curr. Opin. Cell Biol.* 12, 676–684.
- El-Khoury, R., Dufour, E., Rak, M., Ramanantsoa, N., Grandchamp, N., Csaba, Z., Duvillié, B., Bénit, P., Gallego, J., Gressens, P., Sarkis, C., Jacobs, H.T., Rustin, P., 2013. Alternative Oxidase Expression in the Mouse Enables Bypassing Cytochrome c Oxidase Blockade and Limits Mitochondrial ROS Overproduction. *PLoS Genet.* 9, e1003182.
- Evan, G.I., Vousden, K.H., 2001. progress Proliferation, cell cycle and apoptosis in cancer. *Nature* 411, 342–348.
- Feissner, R.F., Skalska, J., Gaum, W.E., Sheu, S.-S., 2009. Crosstalk signaling between mitochondrial Ca²⁺ and ROS. *Front. Biosci.* 14, 1197–1218.
- Feng, Y., Cheung, K.-F., Wang, N., Liu, P., Nagamatsu, T., Tong, Y., 2009. Chinese medicines as a resource for liver fibrosis treatment. *Chin. Med.* 4, 16.
- Feng, Y., He, D., Yao, Z., Klionsky, D.J., 2014. The machinery of macroautophagy. *Cell Res.* 24, 24–41.
- Ferlay, J., Shin, H.-R.R., Bray, F., Forman, D., Mathers, C., Parkin, D.M., 2010. Estimates of worldwide burden of cancer in 2008: GLOBOCAN 2008. *Int. J. Cancer* 127, 2893–917.
- Fimia, G.M., Di Bartolomeo, S., Piacentini, M., Cecconi, F., 2014. Unleashing the Ambra1-Beclin 1 complex from dynein chains: Ulk1 sets Ambra1 free to induce autophagy. *Autophagy* 7, 115–117.
- Fontanay, S., Grare, M., Mayer, J., Finance, C., Duval, R.E., 2008. Ursolic, oleanolic and betulinic acids: Antibacterial spectra and selectivity indexes. *J. Ethnopharmacol.* 120, 272–276.
- Frenzel, A., Grespi, F., Chmelewskij, W., Villunger, A., 2009. Bcl2 family proteins in carcinogenesis and the treatment of cancer. *Apoptosis* 14, 584–96.
- Fujikura, D., Ito, M., Chiba, S., Harada, T., Perez, F., Reed, J.C., Uede, T., Miyazaki, T., 2012. CLIPR-59 regulates TNF- α -induced apoptosis by controlling ubiquitination of RIP1. *Cell Death Dis.* 3, e264.
- Fulda, S., 2012. Autophagy and cell death. *Autophagy* 8, 1250–1251.
- Gao, X., Deeb, D., Jiang, H., Liu, Y., Dulchavsky, S.A., Gautam, S.C., 2007. Synthetic triterpenoids inhibit growth and induce apoptosis in human glioblastoma and neuroblastoma cells through inhibition of prosurvival Akt, NF-kappaB and Notch1 signaling. *J. Neurooncol.* 84, 147–57.
- Gillies, R.J., Didier, N., Denton, M., 1986. Determination of cell number in monolayer cultures. *Anal. Biochem.* 159, 109–13.
- Golstein, P., Kroemer, G., 2007. Cell death by necrosis: towards a molecular definition. *Trends Biochem. Sci.* 32, 37–43.
- Gomes, L.C., Di Benedetto, G., Scorrano, L., 2011. During autophagy mitochondria elongate, are spared from degradation and sustain cell viability. *Nat. Cell Biol.* 13, 589–598.
- Gonçalves, A.P., Máximo, V., Lima, J., Singh, K.K., Soares, P., Videira, A., 2011. Involvement of p53 in cell death following cell cycle arrest and mitotic catastrophe induced by rotenone. *Biochim. Biophys. Acta - Mol. Cell Res.* 1813, 492–499.

- Gonzalez-Angulo, A.M., Morales-Vasquez, F., Hortobagyi, G.N., 2007. Overview of Resistance to Systemic Therapy in Patients with Breast Cancer. In: *Advances in Experimental Medicine and Biology*. pp. 1–22.
- Gordy, C., He, Y.-W., 2012. The crosstalk between autophagy and apoptosis: where does this lead? *Protein Cell* 3, 17–27.
- Gozuacik, D., Kimchi, A., 2004. Autophagy as a cell death and tumor suppressor mechanism. *Oncogene* 23, 2891–2906.
- Green, D.R., Ferguson, T., Zitvogel, L., Kroemer, G., 2009. Immunogenic and tolerogenic cell death. *Nat. Rev. Immunol.* 9, 353–63.
- Ha, H.C., Snyder, S.H., 1999. Poly(ADP-ribose) polymerase is a mediator of necrotic cell death by ATP depletion. *Proc. Natl. Acad. Sci. U. S. A.* 96, 13978–13982.
- Han, J.-Y.Y., Kim, M.-J.J., Ban, Y.W., Hwang, H.-S.S., Choi, Y.E., 2013. The involvement of β -amyrin 28-oxidase (cyp716a52v2) in oleanane-type ginsenoside biosynthesis in panax ginseng. *Plant Cell Physiol.* 54, 2034–2046.
- Hao, C., Song, J.H., Vilimanovich, U., Kneteman, N.M., 2004. Modulation of TRAIL Signaling Complex. In: *Vitamins & Hormones*. pp. 81–99.
- Hardie, D.G., Ross, F.A., Hawley, S.A., 2012. AMPK: a nutrient and energy sensor that maintains energy homeostasis. *Nat. Rev. Mol. Cell Biol.*
- Harmand, P.-O., Duval, R., Delage, C., Simon, A., 2005. Ursolic acid induces apoptosis through mitochondrial intrinsic pathway and caspase-3 activation in M4Beu melanoma cells. *Int. J. Cancer* 114, 1–11.
- Harmand, P.-O., Duval, R., Liagre, B., Jayat-Vignoles, C., Beneytout, J.-L., Delage, C., Simon, A., 2003. Ursolic acid induces apoptosis through caspase-3 activation and cell cycle arrest in HaCat cells. *Int. J. Oncol.* 23, 105–12.
- Hassan, B., Akcakanat, A., Holder, A.M., Meric-Bernstam, F., 2013. Targeting the PI3-kinase/Akt/mTOR signaling pathway. *Surg. Oncol. Clin. N. Am.* 22, 641–64.
- Henley, S.A., Dick, F.A., 2012. The retinoblastoma family of proteins and their regulatory functions in the mammalian cell division cycle. *Cell Div.* 7, 10.
- Hill, B.G., Dranka, B.P., Zou, L., Chatham, J.C., Darley-USmar, V.M., 2009. Importance of the bioenergetic reserve capacity in response to cardiomyocyte stress induced by 4-hydroxynonenal. *Biochem. J.* 424, 99–107.
- Holanda Pinto, S.A., Pinto, L.M.S., Guedes, M.A., Cunha, G.M.A., Chaves, M.H., Santos, F.A., Rao, V.S., 2008. Antinoceptive effect of triterpenoid α,β -amyrin in rats on orofacial pain induced by formalin and capsaicin. *Phytomedicine* 15, 630–634.
- Hotchkiss, R.S., Strasser, A., McDunn, J.E., Swanson, P.E., 2009. Cell Death. *N. Engl. J. Med.* 361, 1570–1583.
- Hsu, Y.L., Kuo, P.L., Lin, C.C., 2004. The proliferative inhibition and apoptotic mechanism of Saikosaponin D in human non-small cell lung cancer A549 cells. *Life Sci.* 75, 1231–1242.
- Hsu, Y.-L.L., Kuo, P.-L.L., Lin, C.-C.C., 2004. Proliferative inhibition, cell-cycle dysregulation, and induction of apoptosis by ursolic acid in human non-small cell lung cancer A549 cells. *Life Sci.* 75, 2303–16.
- Huang, J., Klionsky, D.J., 2007. Autophagy and Human Disease. *Cell Cycle* 6, 1837–1849.

- Huang, L., Li, J., Ye, H., Li, C., Wang, H., Liu, B., Zhang, Y., 2012. Molecular characterization of the pentacyclic triterpenoid biosynthetic pathway in *Catharanthus roseus*. *Planta* 236, 1571–1581.
- Hustedt, N., Gasser, S.M., Shimada, K., 2013. Replication checkpoint: tuning and coordination of replication forks in S phase. *Genes (Basel)*. 4, 388–434.
- Hwang, Y.-J., Song, J., Kim, H.-R., Hwang, K.-A., 2014. Oleanolic acid regulates NF- κ B signaling by suppressing MafK expression in RAW 264.7 cells. *BMB Rep.* 47, 524–9.
- Ikeda, Y., Murakami, A., Ohigashi, H., 2008. Ursolic acid: An anti- and pro-inflammatory triterpenoid. *Mol. Nutr. Food Res.* 52, 26–42.
- Indran, I.R., Hande, M.P., Pervaiz, S., 2011. hTERT overexpression alleviates intracellular ROS production, improves mitochondrial function, and inhibits ROS-mediated apoptosis in cancer cells. *Cancer Res.* 71, 266–276.
- Inzé, D., De Veylder, L., 2006. Cell cycle regulation in plant development. *Annu. Rev. Genet.* 40, 77–105.
- Irrcher, I., Ljubcic, V., Hood, D.A., 2009. Interactions between ROS and AMP kinase activity in the regulation of PGC-1 α transcription in skeletal muscle cells. *Am. J. Physiol. Cell Physiol.* 296, C116–C123.
- Itagaki, H., Hagino, S., Kato, S., Kobayashi, T., Umeda, M., 1991. An in vitro alternative to the Draize eye-irritation test: Evaluation of the crystal violet staining method. *Toxicol. In Vitro* 5, 139–43.
- Iwasaki, M., Tsugane, S., 2011. Risk factors for breast cancer: epidemiological evidence from Japanese studies. *Cancer Sci.* 102, 1607–14.
- Jackson, P.K., 2008. The hunt for cyclin. *Cell* 134, 199–202.
- Jayapal, S.R., Kaldis, P., 2014. p57Kip2 regulates T-cell development and lymphoma. *Blood* 123, 3370–1.
- Jelezcova, E., Trivedi, R.N., Wang, X. hong, Tang, J. b., Brown, A.R., Goellner, E.M., Schamus, S., Fornaglio, J.L., Sobol, R.W., 2010. Parp1 activation in mouse embryonic fibroblasts promotes Pol γ -dependent cellular hypersensitivity to alkylation damage. *Mutat. Res. - Fundam. Mol. Mech. Mutagen.* 686, 57–67.
- Jemal, A., Bray, F., Center, M.M., Ferlay, J., Ward, E., Forman, D., 2011. Global cancer statistics. *CA Cancer J Clin* 61, 69–90.
- Jiang, 2011. Aberrant expression and function of death receptor-3 and death decoy receptor-3 in human cancer (Review). *Exp. Ther. Med.* 2, 167–172.
- Jiang, P., Mizushima, N., 2014. LC3- and p62-based biochemical methods for the analysis of autophagy progression in mammalian cells. *Methods* 75, 13–18.
- Johnson, D.G., Walker, C.L., 1999. Cyclins and cell cycle checkpoints. *Annu. Rev. Pharmacol. Toxicol.* 39, 295–312.
- Johnstone, R.W., Ruefli, A.A., Lowe, S.W., 2002. Apoptosis: a link between cancer genetics and chemotherapy. *Cell* 108, 153–64.
- Jones, R.M.M., Petermann, E., 2012. Replication fork dynamics and the DNA damage response. *Biochem. J.* 443, 13–26.
- Jossen, R., Bermejo, R., 2013. The DNA damage checkpoint response to replication stress:

A Game of Forks. *Front. Genet.* 4, 26.

- Kabeya, Y., 2000. LC3, a mammalian homologue of yeast Apg8p, is localized in autophagosomal membranes after processing. *EMBO J.* 19, 5720–5728.
- Kahán, Z., 2014. Breast cancer surveillance: nothing has changed in the past decades (?). memo - *Mag. Eur. Med. Oncol.* 7, 22–26.
- Kang, R., Livesey, K.M., Zeh, H.J., Lotze, M.T., Tang, D., Loze, M.T., Tang, D., 2010. HMGB1: A novel Beclin 1-binding protein active in autophagy. *Autophagy* 6, 1209–11.
- Kang, R., Zeh, H.J., Lotze, M.T., Tang, D., 2011. The Beclin 1 network regulates autophagy and apoptosis. *Cell Death Differ.* 18, 571–80.
- Karanasios, E., Stapleton, E., Manifava, M., Kaizuka, T., Mizushima, N., Walker, S. a, Ktistakis, N.T., 2013. Dynamic association of the ULK1 complex with omegasomes during autophagy induction. *J. Cell Sci.* 126, 5224–38.
- Kassi, E., Papoutsis, Z., Pratsinis, H., Aligiannis, N., Manoussakis, M., Moutsatsou, P., 2007. Ursolic acid, a naturally occurring triterpenoid, demonstrates anticancer activity on human prostate cancer cells. *J. Cancer Res. Clin. Oncol.* 133, 493–500.
- Kassi, E., Sourlingas, T.G., Spiliotaki, M., Papoutsis, Z., Pratsinis, H., Aligiannis, N., Moutsatsou, P., 2009. Ursolic Acid Triggers Apoptosis and Bcl-2 Downregulation in MCF-7 Breast Cancer Cells. *Cancer Invest.* 27, 723–733.
- Katzenellenbogen, B.S., Choi, I., Delage-Mourroux, R., Ediger, T.R., Martini, P.G. V, Montano, M., Sun, J., Weis, K., Katzenellenbogen, J. a., 2000. Molecular mechanisms of estrogen action: Selective ligands and receptor pharmacology. *J. Steroid Biochem. Mol. Biol.* 74, 279–285.
- Keaton, M.A., 2007. Review of “The Cell Cycle: Principles of Control” by David O. Morgan. *Cell Div.* 2, 27.
- Kerr, J.F.R., Wyllie, A.H., Currie, A.R., 1972. Apoptosis: A Basic Biological Phenomenon with Widespread Implications in Tissue Kinetics. *Br. J. Cancer* 26, 239–57.
- Kim, D.K., Baek, J.H., Kang, C.M., Yoo, M.A., Sung, J.W., Chung, H.Y., Kim, N.D., Choi, Y.H., Lee, S.H., Kim, K.W., 2000. Apoptotic activity of ursolic acid may correlate with the inhibition of initiation of DNA replication. *Int. J. Cancer* 87, 629–36.
- Kim, J.-H., Yoo, H.-I., Kang, H.S., Ro, J., Yoon, S., 2012. Salinomycin sensitizes antimetabolic drugs-treated cancer cells by increasing apoptosis via the prevention of G2 arrest. *Biochem. Biophys. Res. Commun.* 418, 98–103.
- Kim, S., Sun, H., Ball, H.L., Wassmann, K., Luo, X., Yu, H., 2010. Phosphorylation of the spindle checkpoint protein Mad2 regulates its conformational transition. *Proc. Natl. Acad. Sci. U. S. A.* 107, 19772–19777.
- Kimura, M., Yoshioka, T., Saio, M., Banno, Y., Nagaoka, H., Okano, Y., 2013. Mitotic catastrophe and cell death induced by depletion of centrosomal proteins. *Cell Death Dis.* 4, e603.
- Klionsky, D.J., Cuervo, A.M., Seglen, P.O., 2007. Methods for monitoring autophagy from yeast to human. *Autophagy* 3, 181–206.
- Kohn, K.W., 1999. Molecular interaction map of the mammalian cell cycle control and DNA repair systems. *Mol. Biol. Cell* 10, 2703–34.

- Kokoszka, J.E., Waymire, K.G., Levy, S.E., Sligh, J.E., Cai, J., Jones, D.P., MacGregor, G.R., Wallace, D.C., 2004. The ADP/ATP translocator is not essential for the mitochondrial permeability transition pore. *Nature* 427, 461–465.
- Kong, B., Qia, C., Erkan, M., Kleeff, J., Michalski, C.W., 2013. Overview on how oncogenic Kras promotes pancreatic carcinogenesis by inducing low intracellular ROS levels. *Front. Physiol.* 4, 246.
- Kook, S., Gurevich, V. V, Gurevich, E. V, 2014. Arrestins in Apoptosis. In: *Handbook of Experimental Pharmacology*. pp. 309–339.
- Kroemer, G., Mariño, G., Levine, B., 2010. Autophagy and the Integrated Stress Response. *Mol. Cell* 40, 280–293.
- Kroemer, G., Pouyssegur, J., 2008. Tumor Cell Metabolism: Cancer's Achilles' Heel. *Cancer Cell* 13, 472–482.
- Kruiswijk, F., Labuschagne, C.F., Vousden, K.H., 2015. p53 in survival, death and metabolic health: a lifeguard with a licence to kill. *Nat. Rev. Mol. Cell Biol.* 16, 393–405.
- Krukiewicz, K., Jarosz, T., Zak, J.K., Lapkowski, M., Ruszkowski, P., Bobkiewicz-Kozłowska, T., Bednarczyk-Cwynar, B., 2015. Advancing the delivery of anticancer drugs: Conjugated polymer/triterpenoid composite. *Acta Biomater.* 19, 158–165.
- Kushiro, T., Shibuya, M., Ebizuka, Y., 1998. Beta-amyrin synthase--cloning of oxidosqualene cyclase that catalyzes the formation of the most popular triterpene among higher plants. *Eur. J. Biochem.* 256, 238–44.
- Kusuzaki, K., Murata, H., Takeshita, H., Hashiguchi, S., Nozaki, T., Emoto, K., Ashihara, T., Hirasawa, Y., 2000. Intracellular binding sites of acridine orange in living osteosarcoma cells. *Anticancer Res.* 20, 971–5.
- Lambert, S., Carr, A.M., 2005. Checkpoint responses to replication fork barriers. *Biochimie* 87, 591–602.
- Langerak, P., Russell, P., 2011. Regulatory networks integrating cell cycle control with DNA damage checkpoints and double-strand break repair. *Philos. Trans. R. Soc. Lond. B. Biol. Sci.* 366, 3562–71.
- Laplante, M., Sabatini, D.M., 2012. mTOR signaling in growth control and disease. *Cell* 149, 274–93.
- Lappano, R., Pisano, A., Maggiolini, M., 2014. GPER function in breast cancer: An overview. *Front. Endocrinol. (Lausanne)*. 5, 1–6.
- Lara-Gonzalez, P., Westhorpe, F.G., Taylor, S.S., 2012. The spindle assembly checkpoint. *Curr. Biol.* 22, R966–80.
- Laszczyk, M.N., 2009. Pentacyclic triterpenes of the lupane, oleanane and ursane group as tools in cancer therapy. *Planta Med.* 75, 1549–1560.
- Latt, S.A., Stetten, G., Juergens, L.A., Willard, H.F., Scher, C.D., 1975. Recent developments in the detection of deoxyribonucleic acid synthesis by 33258 Hoechst fluorescence. *J. Histochem. Cytochem.* 23, 493–505.
- Latta, M., Künstle, G., Lucas, R., Hentze, H., Wendel, A., 2007. ATP-depleting carbohydrates prevent tumor necrosis factor receptor 1-dependent apoptotic and necrotic liver injury in mice. *J. Pharmacol. Exp. Ther.* 321, 875–883.

- Lau, A.T.Y., Wang, Y., Chiu, J.-F., 2008. Reactive oxygen species: Current knowledge and applications in cancer research and therapeutic. *J. Cell. Biochem.* 104, 657–667.
- Lauthier, F., Taillet, L., Trouillas, P., Delage, C., Simon, A., 2000. Ursolic acid triggers calcium-dependent apoptosis in human Daudi cells. *Anticancer. Drugs* 11, 737–45.
- Leadsham, J.E., Sanders, G., Giannaki, S., Bastow, E.L., Hutton, R., Naeimi, W.R., Breitenbach, M., Gourlay, C.W., 2013. Loss of cytochrome c oxidase promotes ras-dependent ros production from the er resident nadph oxidase, yno1p, in yeast. *Cell Metab.* 18, 279–286.
- Lee, H.-C., Wei, Y.-H., 2007. Oxidative stress, mitochondrial DNA mutation, and apoptosis in aging. *Exp. Biol. Med. (Maywood)*. 232, 592–606.
- Lee, J.S., Collins, K.M., Brown, A.L., Lee, C.H., Chung, J.H., 2000. hCds1-mediated phosphorylation of BRCA1 regulates the DNA damage response. *Nature* 404, 201–4.
- Lee, J.S., Ha, T.K., Park, J.H., Lee, G.M., 2013. Anti-cell death engineering of CHO cells: Co-overexpression of Bcl-2 for apoptosis inhibition, Beclin-1 for autophagy induction. *Biotechnol. Bioeng.* 110, 2195–2207.
- Leipold, D., Wünsch, G., Schmidt, M., Bart, H.-J., Bley, T., Ekkehard Neuhaus, H., Bergmann, H., Richling, E., Muffler, K., Ulber, R., 2010. Biosynthesis of ursolic acid derivatives by microbial metabolism of ursolic acid with *Nocardia* sp. strains—Proposal of new biosynthetic pathways. *Process Biochem.* 45, 1043–1051.
- Leist, M., Single, B., Castoldi, a F., Kühnle, S., Nicotera, P., 1997. Intracellular adenosine triphosphate (ATP) concentration: a switch in the decision between apoptosis and necrosis. *J. Exp. Med.* 185, 1481–1486.
- Leist, M., Single, B., Naumann, H., Fava, E., Simon, B., Kühnle, S., Nicotera, P., 1999. Inhibition of mitochondrial ATP generation by nitric oxide switches apoptosis to necrosis. *Exp. Cell Res.* 249, 396–403.
- Li, L.-L., Xue, A.-M., Li, B.-X., Shen, Y.-W., Li, Y.-H., Luo, C.-L., Zhang, M.-C., Jiang, J.-Q., Xu, Z.-D., Xie, J.-H., Zhao, Z.-Q., 2014. JMJD2A contributes to breast cancer progression through transcriptional repression of the tumor suppressor ARHI. *Breast Cancer Res.* 16, R56.
- Li, Q., Ye, Z., Wen, J., Ma, L., He, Y., Lian, G., Wang, Z., Wei, L., Wu, D., Jiang, B., 2009. Gelsolin, but not its cleavage, is required for TNF-induced ROS generation and apoptosis in MCF-7 cells. *Biochem. Biophys. Res. Commun.* 385, 284–289.
- Li, Y., Birnbaumer, L., Teng, C.T., 2010. Regulation of ERRalpha gene expression by estrogen receptor agonists and antagonists in SKBR3 breast cancer cells: differential molecular mechanisms mediated by g protein-coupled receptor GPR30/GPER-1. *Mol. Endocrinol.* 24, 969–980.
- Lim, S., Kaldis, P., 2013. Cdks, cyclins and CKIs: roles beyond cell cycle regulation. *Development* 140, 3079–93.
- Liou, G.-Y., Storz, P., 2010. Reactive oxygen species in cancer. *Free Radic. Res.* 44, 479–96.
- Liu, J., 2005. Oleanolic acid and ursolic acid: Research perspectives. *J. Ethnopharmacol.* 100, 92–4.
- Liu, X.-S., Jiang, J., 2007. Induction of apoptosis and regulation of the MAPK pathway by ursolic acid in human leukemia K562 cells. *Planta Med.* 73, 1192–4.

- Liu, Y., Xiong, Y., Bassham, D.C., 2009. Autophagy is required for tolerance of drought and salt stress in plants. *Autophagy* 5, 954–963.
- Loor, G., Kondapalli, J., Schriewer, J.M., Chandel, N.S., Vanden Hoek, T.L., Schumacker, P.T., 2010. Menadione triggers cell death through ROS-dependent mechanisms involving PARP activation without requiring apoptosis. *Free Radic. Biol. Med.* 49, 1925–1936.
- Lopes, M., Cotta-Ramusino, C., Pelliccioli, A., Liberi, G., Plevani, P., Muzi-Falconi, M., Newlon, C.S., Foiani, M., 2001. The DNA replication checkpoint response stabilizes stalled replication forks. *Nature* 412, 557–561.
- Lúcio, K.A., Rocha, G. da G., Monção-Ribeiro, L.C., Fernandes, J., Takiya, C.M., Gattass, C.R., 2011. Oleanolic acid initiates apoptosis in non-small cell lung cancer cell lines and reduces metastasis of a B16F10 melanoma model in vivo. *PLoS One* 6, e28596.
- Lukas, J., Lukas, C., Bartek, J., 2001. Mammalian G1- and S-phase checkpoints in response to DNA damage. *Curr. Opin. Cell Biol.* 13, 738–747.
- Lum, J.J., Bauer, D.E., Kong, M., Harris, M.H., Li, C., Lindsten, T., Thompson, C.B., 2005. Growth factor regulation of autophagy and cell survival in the absence of apoptosis. *Cell* 120, 237–48.
- Luo, S., Rubinsztein, D.C., 2007. Atg5 and Bcl-2 provide novel insights into the interplay between apoptosis and autophagy. *Cell Death Differ.* 14, 1247–1250.
- Macip, S., Igarashi, M., Berggren, P., Yu, J., Lee, S.W., Aaronson, S.A., 2003. Influence of induced reactive oxygen species in p53-mediated cell fate decisions. *Mol. Cell Biol.* 23, 8576–8585.
- Maddika, S., Ande, S.R., Panigrahi, S., Paranjothy, T., Weglarczyk, K., Zuse, A., Eshraghi, M., Manda, K.D., Wiechec, E., Lös, M., 2007. Cell survival, cell death and cell cycle pathways are interconnected: Implications for cancer therapy. *Drug Resist. Updat.* 10, 13–29.
- Madhok, B.M., Yeluri, S., Perry, S.L., Hughes, T.A., Jayne, D.G., 2010. Dichloroacetate induces apoptosis and cell-cycle arrest in colorectal cancer cells. *Br. J. Cancer* 102, 1746–1752.
- Mah, L.Y., Ryan, K.M., 2012. Autophagy and Cancer. *Cold Spring Harb. Perspect. Biol.* 4, a008821–a008821.
- Mahmood, Z., Shukla, Y., 2010. Death receptors: targets for cancer therapy. *Exp. Cell Res.* 316, 887–99.
- Mahmoudi, M., Rabe, S.Z.T., Balali-Mood, M., Karimi, G., Tabasi, N., Riahi-Zanjani, B., 2015. Ursolic acid induced apoptotic cell death following activation of caspases in isolated human melanoma cells. *Cell Biol. Int.* 39, 230–236.
- Mailand, N., Podtelejnikov, A. V, Groth, A., Mann, M., Bartek, J., Lukas, J., 2002. Regulation of G(2)/M events by Cdc25A through phosphorylation-dependent modulation of its stability. *EMBO J.* 21, 5911–20.
- Maiuri, M.C., Criollo, A., Kroemer, G., 2010. Crosstalk between apoptosis and autophagy within the Beclin 1 interactome. *EMBO J.* 29, 515–516.
- Maiuri, M.C., Criollo, A., Tasdemir, E., Vicencio, J.M., Tajeddine, N., Hickman, J.A., Geneste, O., Kroemer, G., 2007. BH3-only proteins and BH3 mimetics induce autophagy by competitively disrupting the interaction between Beclin 1 and Bcl-

2/Bcl-XL. *Autophagy* 3, 374–376.

- Malhotra, J.D., Kaufman, R.J., 2011. ER stress and its functional link to mitochondria: role in cell survival and death. *Cold Spring Harb. Perspect. Biol.* 3, a004424.
- Malumbres, M., Barbacid, M., 2007. Cell cycle kinases in cancer. *Curr. Opin. Genet. Dev.* 17, 60–65.
- Man, D.K.W., Casettari, L., Cespi, M., Bonacucina, G., Palmieri, G.F., Sze, S.C.W., Leung, G.P.H., Lam, J.K.W., Kwok, P.C.L., 2015. Oleanolic Acid Loaded PEGylated PLA and PLGA Nanoparticles with Enhanced Cytotoxic Activity against Cancer Cells. *Mol. Pharm.* 12, 2112–2125.
- Manning, G., Whyte, D.B., Martinez, R., Hunter, T., Sudarsanam, S., 2002. The protein kinase complement of the human genome. *Science* 298, 1912–34.
- Mannuss, A., Trapp, O., Puchta, H., 2012. Gene regulation in response to DNA damage. *Biochim. Biophys. Acta* 1819, 154–65.
- Mansilla, S., Priebe, W., Portugal, J., 2006. Mitotic Catastrophe Results in Cell Death by Caspase-Dependent and Caspase-Independent Mechanisms. *Cell Cycle* 5, 53–60.
- Mantovani, A., Allavena, P., Sica, A., Balkwill, F., 2008. Cancer-related inflammation. *Nature* 454, 436–44.
- Mao, Z., Hine, C., Tian, X., Van Meter, M., Au, M., Vaidya, A., Seluanov, A., Gorbunova, V., 2011. SIRT6 promotes DNA repair under stress by activating PARP1. *Science* 332, 1443–1446.
- Marchese, S., Silva, E., 2012. Disruption of 3D MCF-12A Breast Cell Cultures by Estrogens - An In Vitro Model for ER-Mediated Changes Indicative of Hormonal Carcinogenesis. *PLoS One* 7, 1–11.
- Marchi, S., Giorgi, C., Suski, J.M., Agnoletto, C., Bononi, A., Bonora, M., De Marchi, E., Missiroli, S., Patergnani, S., Poletti, F., Rimessi, A., Duszynski, J., Wieckowski, M.R., Pinton, P., 2012. Mitochondria-Ros Crosstalk in the Control of Cell Death and Aging. *J. Signal Transduct.*
- Mariño, G., Niso-Santano, M., Baehrecke, E.H., Kroemer, G., 2014. Self-consumption: the interplay of autophagy and apoptosis. *Nat. Rev. Mol. Cell Biol.* 15, 81–94.
- Martin, K.R., Barrett, J.C., 2002. Reactive oxygen species as double-edged swords in cellular processes: low-dose cell signaling versus high-dose toxicity. *Hum. Exp. Toxicol.* 21, 71–75.
- Martins, I., Wang, Y., Michaud, M., Ma, Y., Sukkurwala, A.Q., Shen, S., Kepp, O., Métivier, D., Galluzzi, L., Perfettini, J.-L., Zitvogel, L., Kroemer, G., 2013. Molecular mechanisms of ATP secretion during immunogenic cell death. *Cell Death Differ.* 21, 79–91.
- Matsen, C.B., Neumayer, L. a, 2013. Breast cancer: a review for the general surgeon. *JAMA Surg.* 148, 971–9.
- Mazars, C., Thuleau, P., Lamotte, O., Bourque, S., 2010. Cross-talk between ROS and calcium in regulation of nuclear activities. *Mol. Plant* 3, 706–718.
- McTiernan, A., Porter, P., Potter, J.D., 2008. Breast cancer prevention in countries with diverse resources. *Cancer* 113, 2325–30.
- Medema, R.H., Macurek, L., 2012. Checkpoint control and cancer. *Oncogene* 31, 2601–

2613.

- Mérino, D., Lalaoui, N., Morizot, A., Schneider, P., Solary, E., Micheau, O., 2006. Differential inhibition of TRAIL-mediated DR5-DISC formation by decoy receptors 1 and 2. *Mol. Cell. Biol.* 26, 7046–7055.
- Mikolcevic, P., Sigl, R., Rauch, V., Hess, M.W., Pfaller, K., Barisic, M., Pelliniemi, L.J., Boesl, M., Geley, S., 2012. Cyclin-dependent kinase 16/PCTAIRE kinase 1 is activated by cyclin Y and is essential for spermatogenesis. *Mol. Cell. Biol.* 32, 868–79.
- Misra, R.C., Maiti, P., Chanotiya, C.S., Shanker, K., Ghosh, S., 2014. Methyl jasmonate-elicited transcriptional responses and pentacyclic triterpene biosynthesis in sweet basil. *Plant Physiol.* 164, 1028–44.
- Mitsuda, S., Yokomichi, T., Yokoigawa, J., Kataoka, T., 2014. Ursolic acid, a natural pentacyclic triterpenoid, inhibits intracellular trafficking of proteins and induces accumulation of intercellular adhesion molecule-1 linked to high-mannose-type glycans in the endoplasmic reticulum. *FEBS Open Bio* 4, 229–239.
- Mizushima, N., Komatsu, M., 2011. Autophagy: Renovation of cells and tissues. *Cell* 147, 728–741.
- Mizushima, N., Yoshimori, T., Levine, B., 2010. Methods in Mammalian Autophagy Research. *Cell* 140, 313–326.
- Mizushima, N., Yoshimori, T., Ohsumi, Y., 2011. The role of Atg proteins in autophagosome formation. *Annu. Rev. Cell Dev. Biol.* 27, 107–132.
- Mohammed, H., Russell, I.A., Stark, R., Rueda, O.M., Hickey, T.E., Tarulli, G.A., Serandour, A.A.A., Birrell, S.N., Bruna, A., Saadi, A., Menon, S., Hadfield, J., Pugh, M., Raj, G. V, Brown, G.D., D’Santos, C., Robinson, J.L.L., Silva, G., Launchbury, R., Perou, C.M., Stingl, J., Caldas, C., Tilley, W.D., Carroll, J.S., 2015. Progesterone receptor modulates ER α action in breast cancer. *Nature* 523, 313–317.
- Moongkarndi, P., Kosem, N., Kaslungka, S., Luanratana, O., Pongpan, N., Neungton, N., 2004. Antiproliferation, antioxidation and induction of apoptosis by *Garcinia mangostana* (mangosteen) on SKBR3 human breast cancer cell line. *J. Ethnopharmacol.* 90, 161–166.
- Morikawa, T., Nakamura, S., Kato, Y., Muraoka, O., Matsuda, H., Yoshikawa, M., 2007. Bioactive saponins and glycosides. XXVIII. New triterpene saponins, foliatheasaponins I, II, III, IV, and V, from Tencha (the leaves of *Camellia sinensis*). *Chem Pharm Bull* 55, 293–298.
- Muffler, K., Leipold, D., Scheller, M.-C., Haas, C., Steingroewer, J., Bley, T., Neuhaus, H.E., Mirata, M.A., Schrader, J., Ulber, R., 2011. Biotransformation of triterpenes. *Process Biochem.* 46, 1–15.
- Musgrove, E. a, Swarbrick, A., Lee, C.S.L., Cornish, A.L., Sutherland, R.L., 1998. Mechanisms of Cyclin-Dependent Kinase Inactivation by Progestins. *Mol. Cell. Biol.* 18, 1812–1825.
- Nair, P., Lu, M., Petersen, S., Ashkenazi, A., 2014. Apoptosis Initiation Through the Cell-Extrinsic Pathway. In: *Methods in Enzymology*. pp. 99–128.
- Nakatogawa, H., 2013. Two ubiquitin-like conjugation systems that mediate membrane formation during autophagy. *Essays Biochem.* 55, 39–50.

- Nataraju, A., Saini, D., Ramachandran, S., Benschhoff, N., Liu, W., Chapman, W., Mohanakumar, T., 2009. Oleanolic Acid, a plant triterpenoid, significantly improves survival and function of islet allograft. *Transplantation* 88, 987–94.
- Nelson, D.M., Ye, X., Hall, C., Santos, H., Ma, T., Kao, G.D., Yen, T.J., Harper, J.W., Adams, P.D., 2002. Coupling of DNA synthesis and histone synthesis in S phase independent of cyclin/cdk2 activity. *Mol. Cell. Biol.* 22, 7459–7472.
- Neto, C.C., 2011. Ursolic acid and other pentacyclic triterpenoids: anticancer activities and occurrence in berries. In: Seeram, N.P., Stoner, G.D. (Eds.), *Berries and Cancer Prevention*. Springer New York, pp. 41–50.
- Nicotera, P., Leist, M., Ferrando-May, E., 1998. Intracellular ATP, a switch in the decision between apoptosis and necrosis. *Toxicol. Lett.* 102-103, 139–142.
- Nikoletopoulou, V., Markaki, M., Palikaras, K., Tavernarakis, N., 2013. Crosstalk between apoptosis, necrosis and autophagy. *Biochim. Biophys. Acta* 1833, 3448–59.
- Okamoto, K., Kashima, K., Pereg, Y., Ishida, M., Yamazaki, S., Nota, A., Teunisse, A., Migliorini, D., Kitabayashi, I., Marine, J.-C., Prives, C., Shiloh, Y., Jochemsen, A.G., Taya, Y., 2005. DNA damage-induced phosphorylation of MdmX at serine 367 activates p53 by targeting MdmX for Mdm2-dependent degradation. *Mol. Cell. Biol.* 25, 9608–20.
- Ola, M.S., Nawaz, M., Ahsan, H., 2011. Role of Bcl-2 family proteins and caspases in the regulation of apoptosis. *Mol. Cell. Biochem.* 351, 41–58.
- Orford, K.W., Scadden, D.T., 2008. Deconstructing stem cell self-renewal: genetic insights into cell-cycle regulation. *Nat. Rev. Genet.* 9, 115–128.
- Orrenius, S., Gogvadze, V., Zhivotovsky, B., 2007. Mitochondrial oxidative stress: implications for cell death. *Annu. Rev. Pharmacol. Toxicol.* 47, 143–183.
- Ouyang, L., Shi, Z., Zhao, S., Wang, F.T., Zhou, T.T., Liu, B., Bao, J.K., 2012. Programmed cell death pathways in cancer: A review of apoptosis, autophagy and programmed necrosis. *Cell Prolif.* 45, 487–498.
- Ovesná, Z., Kozics, K., Slaménová, D., 2006. Protective effects of ursolic acid and oleanolic acid in leukemic cells. *Mutat. Res.* 600, 131–7.
- Pagani, O., Senkus, E., Wood, W., Colleoni, M., Cufer, T., Kyriakides, S., Costa, A., Winer, E.P., Cardoso, F., 2010. International guidelines for management of metastatic breast cancer: can metastatic breast cancer be cured? *J. Natl. Cancer Inst.* 102, 456–463.
- Paravicini, T., Touyz, R., 2006. Redox signaling in hypertension. *Cardiovasc. Res.* 71, 247–258.
- Park, M.S., Koff, A., 2001. Overview of the cell cycle. *Curr. Protoc. Cell Biol.* Chapter 8, Unit 8.1.
- Paull, T.T., Rogakou, E.P., Yamazaki, V., Kirchgessner, C.U., Gellert, M., Bonner, W.M., 2000. A critical role for histone H2AX in recruitment of repair factors to nuclear foci after DNA damage. *Curr. Biol.* 10, 886–895.
- Pearce, L.R., Alton, G.R., Richter, D.T., Kath, J.C., Lingardo, L., Chapman, J., Hwang, C., Alessi, D.R., 2010. Characterization of PF-4708671, a novel and highly specific inhibitor of p70 ribosomal S6 kinase (S6K1). *Biochem. J.* 431, 245–255.
- Pertino, M.W., Lopez, C., Theoduloz, C., Schmeda-Hirschmann, G., 2013. 1,2,3-triazole-

- substituted oleanolic Acid derivatives: synthesis and antiproliferative activity. *Molecules* 18, 7661–74.
- Peters, J.-M., 2006. The anaphase promoting complex/cyclosome: a machine designed to destroy. *Nat. Rev. Mol. Cell Biol.* 7, 644–56.
- Pietenpol, J., Stewart, Z., 2002. Cell cycle checkpoint signaling: Toxicology 181-182, 475–481.
- Platini, F., Pérez-Tomás, R., Ambrosio, S., Tessitore, L., 2010. Understanding autophagy in cell death control. *Curr. Pharm. Des.* 16, 101–113.
- Polager, S., Ginsberg, D., 2009. p53 and E2f: partners in life and death. *Nat. Rev. Cancer* 9, 738–748.
- Pollier, J., Goossens, A., 2012. Oleanolic acid. *Phytochemistry* 77, 10–5.
- Portugal, J., Mansilla, S., Bataller, M., 2010. Mechanisms of drug-induced mitotic catastrophe in cancer cells. *Curr. Pharm. Des.* 16, 69–78.
- Pua, H.H., Dzhagalov, I., Chuck, M., Mizushima, N., He, Y.-W., 2007. A critical role for the autophagy gene Atg5 in T cell survival and proliferation. *J. Exp. Med.* 204, 25–31.
- Pulido, P., Perello, C., Rodriguez-Concepcion, M., 2012. New insights into plant Isoprenoid metabolism. *Mol. Plant* 5, 964–967.
- Ragaz, J., Olivotto, I.A., Spinelli, J.J., Phillips, N., Jackson, S.M., Wilson, K.S., Knowling, M.A., Coppin, C.M.L., Weir, L., Gelmon, K., Le, N., Durand, R., Coldman, A.J., Manji, M., 2005. Locoregional radiation therapy in patients with high-risk breast cancer receiving adjuvant chemotherapy: 20-year results of the British Columbia randomized trial. *J. Natl. Cancer Inst.* 97, 116–126.
- Raphael, T.J., Kuttan, G., 2003. Effect of naturally occurring triterpenoids glycyrrhizic acid, ursolic acid, oleanolic acid and nomilin on the immune system. *Phytomedicine* 10, 483–489.
- Reggiori, F., Klionsky, D.J., 2005. Autophagosomes: biogenesis from scratch? *Curr. Opin. Cell Biol.* 17, 415–22.
- Reinhardt, H.C., Aslanian, A.S., Lees, J.A., Yaffe, M.B., 2007. p53-deficient cells rely on ATM- and ATR-mediated checkpoint signaling through the p38MAPK/MK2 pathway for survival after DNA damage. *Cancer Cell* 11, 175–189.
- Reisman, S.A., Aleksunes, L.M., Klaassen, C.D., 2009. Oleanolic acid activates Nrf2 and protects from acetaminophen hepatotoxicity via Nrf2-dependent and Nrf2-independent processes. *Biochem. Pharmacol.* 77, 1273–82.
- Rodier, G., Coulombe, P., Tanguay, P.-L., Boutonnet, C., Meloche, S., 2008. Phosphorylation of Skp2 regulated by CDK2 and Cdc14B protects it from degradation by APC(Cdh1) in G1 phase. *EMBO J.* 27, 679–691.
- Romagosa, C., Simonetti, S., López-Vicente, L., Mazo, A., Leonart, M.E., Castellvi, J., Ramon y Cajal, S., 2011. p16(Ink4a) overexpression in cancer: a tumor suppressor gene associated with senescence and high-grade tumors. *Oncogene* 30, 2087–97.
- Roque, T., Haton, C., Etienne, O., Chicheportiche, A., Rousseau, L., Martin, L., Mouthon, M.-A., Boussin, F.D., 2012. Lack of a p21waf1/cip -dependent G1/S checkpoint in neural stem and progenitor cells after DNA damage in vivo. *Stem Cells* 30, 537–47.

- Ruzinova, M.B., Benezra, R., 2003. Id proteins in development, cell cycle and cancer. *Trends Cell Biol.*
- Ryabokon, N.I., Goncharova, R.I., Duburs, G., Hancock, R., Rzeszowska-Wolny, J., 2008. Changes in poly(ADP-ribose) level modulate the kinetics of DNA strand break rejoining. *Mutat. Res.* 637, 173–81.
- Ryter, S.W., Mizumura, K., Choi, A.M.K., 2014. The Impact of Autophagy on Cell Death Modalities. *Int. J. Cell Biol.* 2014, 1–12.
- Sancar, A., Lindsey-Boltz, L.A., Unsal-Kacmaz, K., Linn, S., 2004. Molecular mechanisms of mammalian DNA repair and the DNA damage checkpoints. *Annu Rev Biochem* 73, 39–85.
- Santiago, C., Bashaw, G.J., 2014. Transcription factors and effectors that regulate neuronal morphology. *Development* 141, 4667–4680.
- Santos, F., Frota, J., Arruda, B., de Melo, T., da Silva, A.A. de C.A., Brito, G.A. de C., Chaves, M., Rao, V., 2012. Antihyperglycemic and hypolipidemic effects of α , β -amyryn, a triterpenoid mixture from *Protium heptaphyllum* in mice. *Lipids Health Dis.* 11, 98.
- Saotome, K., Morita, H., Umeda, M., 1989. Cytotoxicity test with simplified crystal violet staining method using microtitre plates and its application to injection drugs. *Toxicol. In Vitro* 3, 317–21.
- Scarbath-Evers, L.K., Hunt, P.A., Kirchner, B., MacFarlane, D.R., Zahn, S., 2015. Molecular features contributing to the lower viscosity of phosphonium ionic liquids compared to their ammonium analogues. *Phys. Chem. Chem. Phys.* 17, 20205–16.
- Scarlett, J.L., Murphy, M.P., 1997. Release of apoptogenic proteins from the mitochondrial intermembrane space during the mitochondrial permeability transition. *FEBS Lett.* 418, 282–286.
- Schlebusch, C.M., Dreyer, G., Sluiter, M.D., Yawitch, T.M., van den Berg, H.J., van Rensburg, E.J., 2010. Cancer prevalence in 129 breast-ovarian cancer families tested for BRCA1 and BRCA2 mutations. *S. Afr. Med. J.* 100, 113–7.
- Scorah, J., McGowan, C.H., 2010. Regulation of Cell Cycle Progression. In: *Handbook of Cell Signaling*. Elsevier, pp. 2545–2553.
- Sevrioukova, I.F., 2011. Apoptosis-inducing factor: structure, function, and redox regulation. *Antioxid. Redox Signal.* 14, 2545–2579.
- Shalaeva, D.N., Dibrova, D. V, Galperin, M.Y., Mulkidjanian, A.Y., 2015. Modeling of interaction between cytochrome c and the WD domains of Apaf-1: bifurcated salt bridges underlying apoptosome assembly. *Biol. Direct* 10, 29.
- Shan, J.-Z., Xuan, Y.-Y., Ruan, S.-Q., Sun, M., 2011. Proliferation-inhibiting and apoptosis-inducing effects of ursolic acid and oleanolic acid on multi-drug resistance cancer cells in vitro. *Chin. J. Integr. Med.* 17, 607–611.
- Shangary, S., Wang, S., 2008. Targeting the MDM2-p53 interaction for cancer therapy. *Clin. Cancer Res.* 14, 5318–5324.
- Shanmugam, M.K., Dai, X., Kumar, A.P., Tan, B.K.H., Sethi, G., Bishayee, A., 2013. Ursolic acid in cancer prevention and treatment: molecular targets, pharmacokinetics and clinical studies. *Biochem. Pharmacol.* 85, 1579–87.
- Shanmugam, M.K., Nguyen, A.H., Kumar, A.P., Tan, B.K.H.H., Sethi, G., 2012. Targeted

- inhibition of tumor proliferation, survival, and metastasis by pentacyclic triterpenoids: Potential role in prevention and therapy of cancer. *Cancer Lett.* 320, 158–170.
- Shen, G.X., 2010. Oxidative stress and diabetic cardiovascular disorders: roles of mitochondria and NADPH oxidase. *Can. J. Physiol. Pharmacol.* 88, 241–248.
- Shen, H.-M., Codogno, P., 2012. Autophagy is a survival force via suppression of necrotic cell death. *Exp. Cell Res.* 318, 1304–1308.
- Sherr, C.J., Roberts, J.M., 1999. CDK inhibitors: positive and negative regulators of G1-phase progression. *Genes Dev.* 13, 1501–1512.
- Shibata, A., Barton, O., Noon, A.T., Dahm, K., Deckbar, D., Goodarzi, A.A., Löbrich, M., Jeggo, P.A., 2010. Role of ATM and the damage response mediator proteins 53BP1 and MDC1 in the maintenance of G(2)/M checkpoint arrest. *Mol. Cell. Biol.* 30, 3371–83.
- Shimizu, S., Kanaseki, T., Mizushima, N., Mizuta, T., Arakawa-Kobayashi, S., Thompson, C.B., Tsujimoto, Y., 2004. Role of Bcl-2 family proteins in a non-apoptotic programmed cell death dependent on autophagy genes. *Nat. Cell Biol.* 6, 1221–1228.
- Shin, S.W., Park, J.-W., 2013. Ursolic acid sensitizes prostate cancer cells to TRAIL-mediated apoptosis. *Biochim. Biophys. Acta* 1833, 723–30.
- Shishodia, S., Majumdar, S., Banerjee, S., Aggarwal, B.B., 2003. Ursolic acid inhibits nuclear factor-kappaB activation induced by carcinogenic agents through suppression of IkappaBalpha kinase and p65 phosphorylation: correlation with down-regulation of cyclooxygenase 2, matrix metalloproteinase 9, and cyclin D1. *Cancer Res.* 63, 4375–83.
- Shyu, M.H., Kao, T.C., Yen, G.C., 2010. Oleanolic acid and ursolic acid induce apoptosis in Huh7 human hepatocellular carcinoma cells through a mitochondrial-dependent pathway and downregulation of XIAP. *J. Agric. Food Chem.* 58, 6110–6118.
- Siewert, B., Pianowski, E., Obernauer, A., Csuk, R., 2014. Towards cytotoxic and selective derivatives of maslinic acid. *Bioorg. Med. Chem.* 22, 594–615.
- Simic, P.M., Weiland, A.J., 2003. Fractures of the distal aspect of the radius: changes in treatment over the past two decades. *Instr. Course Lect.* 52, 185–195.
- Sjögren, C., Nasmyth, K., 2001. Sister chromatid cohesion is required for postreplicative double-strand break repair in *Saccharomyces cerevisiae*. *Curr. Biol.* 11, 991–995.
- Sjögren, C., Ström, L., 2010. S-phase and DNA damage activated establishment of sister chromatid cohesion--importance for DNA repair. *Exp. Cell Res.* 316, 1445–53.
- Soule, H.D., Maloney, T.M., Wolman, S.R., Peterson, W.D., Brenz, R., McGrath, C.M., Russo, J., Pauley, R.J., Jones, R.F., Brooks, S.C., 1990. Isolation and characterization of a spontaneously immortalized human breast epithelial cell line, MCF-10. *Cancer Res.* 50, 6075–86.
- Spink, B.C., Cole, R.W., Katz, B.H., Gierthy, J.F., Bradley, L.M., Spink, D.C., 2006. Inhibition of MCF-7 breast cancer cell proliferation by MCF-10A breast epithelial cells in coculture. *Cell Biol. Int.* 30, 227–238.
- Spinner, J.L., Seo, K.S., O'Loughlin, J.L., Cundiff, J.A., Minnich, S.A., Bohach, G.A., Kobayashi, S.D., 2010. Neutrophils are resistant to *Yersinia YopJ/P*-induced apoptosis and are protected from ROS-mediated cell death by the type III secretion

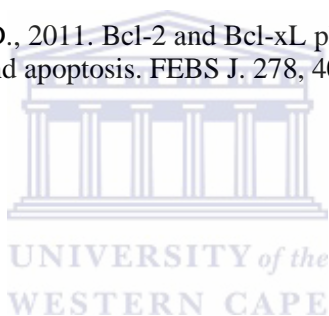
system. *PLoS One* 5.

- Starostina, N.G., Simpliciano, J.M., McGuirk, M.A., Kipreos, E.T., 2010. CRL2(LRR-1) targets a CDK inhibitor for cell cycle control in *C. elegans* and actin-based motility regulation in human cells. *Dev. Cell* 19, 753–64.
- Steigenberger, G., Herm, C., 2011. Natural resins and balsams from an eighteenth-century pharmaceutical collection analysed by gas chromatography/mass spectrometry. *Anal. Bioanal. Chem.* 401, 1771–1784.
- Steigerová, J., Okleštková, J., Levková, M., Rárová, L., Kolář, Z., Strnad, M., 2010. Brassinosteroids cause cell cycle arrest and apoptosis of human breast cancer cells. *Chem. Biol. Interact.* 188, 487–496.
- Sultana, N., 2011. Clinically useful anticancer, antitumor, and antiwrinkle agent, ursolic acid and related derivatives as medicinally important natural product. *J. Enzyme Inhib. Med. Chem.* 26, 616–642.
- Sultana, N., Ata, A., 2008. Oleanolic acid and related derivatives as medicinally important compounds. *J. Enzyme Inhib. Med. Chem.* 23, 739–756.
- Surova, O., Zhivotovsky, B., 2013. Various modes of cell death induced by DNA damage. *Oncogene* 32, 3789–3797.
- Tait, L., Soule, H.D., Russo, J., 1990. Ultrastructural and immunocytochemical characterization of an immortalized human breast epithelial cell line, MCF-10. *Cancer Res* 50, 6087–94.
- Tait, S.W.G., Green, D.R., 2008. Caspase-independent cell death: leaving the set without the final cut. *Oncogene* 27, 6452–6461.
- Tait, S.W.G., Green, D.R., 2012. Mitochondria and cell signalling. *J. Cell Sci.* 125, 807–815.
- Takahashi, P., Polson, A., Reisman, D., 2011. Elevated transcription of the p53 gene in early S-phase leads to a rapid DNA-damage response during S-phase of the cell cycle. *Apoptosis* 16, 950–8.
- Takahashi, Y., Coppola, D., Matsushita, N., Cualing, H.D., Sun, M., Sato, Y., Liang, C., Jung, J.U., Cheng, J.Q., Mulé, J.J., Pledger, W.J., Wang, H.-G., 2007. Bif-1 interacts with Beclin 1 through UVRAG and regulates autophagy and tumorigenesis. *Nat. Cell Biol.* 9, 1142–51.
- Tang, J.Y., Fang, Y.Y., Edward, H., Huang, Y.C., Hsu, N.C.H., Yang, W.C., Chang, H.W., Chai, C.Y., Chu, P.Y., 2013. Immunopositivity of Beclin-1 and ATG5 as indicators of survival and disease recurrence in oral squamous cell carcinoma. *Anticancer Res.* 33, 5611–5616.
- Timofeev, O., Cizmecioglu, O., Settele, F., Kempf, T., Hoffmann, I., 2010. Cdc25 Phosphatases Are Required for Timely Assembly of CDK1-Cyclin B at the G2/M Transition. *J. Biol. Chem.* 285, 16978–16990.
- Todde, V., Veenhuis, M., van der Klei, I.J., 2009. Autophagy: principles and significance in health and disease. *Biochim. Biophys. Acta* 1792, 3–13.
- Tominaga, Y., Wang, A., Wang, R.-H., Wang, X., Cao, L., Deng, C.-X., 2006. Genistein inhibits Brca1 mutant tumor growth through activation of DNA damage checkpoints, cell cycle arrest, and mitotic catastrophe. *Cell Death Differ.* 14, 472–479.
- Torres, M.A., 2010. ROS in biotic interactions. *Physiol. Plant.* 138, 414–29.

- Trachootham, D., Alexandre, J., Huang, P., 2009. Targeting cancer cells by ROS-mediated mechanisms: a radical therapeutic approach? *Nat. Rev. Drug Discov.* 8, 579–91.
- Trigka, E.A., Levidou, G., Saetta, A.A., Chatziandreu, I., Tomos, P., Thalassinou, N., Anastasiou, N., Spartalis, E., Kavantzias, N., Patsouris, E., Korkolopoulou, P., 2013. A detailed immunohistochemical analysis of the PI3K/AKT/mTOR pathway in lung cancer: correlation with PIK3CA, AKT1, K-RAS or PTEN mutational status and clinicopathological features. *Oncol. Rep.* 30, 623–36.
- Tsai, C.-F., Hsu, Y.-W., Chen, W.-K., Ho, Y.-C., Lu, F.-J., 2009. Enhanced induction of mitochondrial damage and apoptosis in human leukemia HL-60 cells due to electrolyzed-reduced water and glutathione. *Biosci. Biotechnol. Biochem.* 73, 280–287.
- Tsai, S.J., Yin, M.C., 2008. Antioxidative and anti-inflammatory protection of oleanolic acid and ursolic acid in PC12 cells. *J. Food Sci.* 73.
- Tsujimoto, Y., 1997. Apoptosis and necrosis: intracellular ATP level as a determinant for cell death modes. *Cell Death Differ.* 4, 429–434.
- Tsujimoto, Y., Shimizu, S., 2007. Role of the mitochondrial membrane permeability transition in cell death. *Apoptosis.*
- Turk, B., Stoka, V., 2007. Protease signalling in cell death: caspases versus cysteine cathepsins. *FEBS Lett.* 581, 2761–2767.
- Tury, A., Mairet-Coello, G., DiCicco-Bloom, E., 2012. The multiple roles of the cyclin-dependent kinase inhibitory protein p57(KIP2) in cerebral cortical neurogenesis. *Dev. Neurobiol.* 72, 821–42.
- Urlacher, V.B., Girhard, M., 2012. Cytochrome P450 monooxygenases: an update on perspectives for synthetic application. *Trends Biotechnol.* 30, 26–36.
- Vakifahmetoglu, H., Olsson, M., Zhivotovsky, B., 2008. Death through a tragedy: mitotic catastrophe. *Cell Death Differ.* 15, 1153–62.
- van den Heuvel, S., 2005. Cell-cycle regulation. *WormBook* 1–16.
- Vande Walle, L., Van Damme, P., Lamkanfi, M., Saelens, X., Vandekerckhove, J., Gevaert, K., Vandenabeele, P., 2007. Proteome-wide Identification of HtrA2/Omi Substrates. *J. Proteome Res.* 6, 1006–1015.
- Vanlangenakker, N., Bertrand, M.J.M., Bogaert, P., Vandenabeele, P., Vanden Berghe, T., 2011. TNF-induced necroptosis in L929 cells is tightly regulated by multiple TNFR1 complex I and II members. *Cell Death Dis.* 2, e230.
- Virshup, D.M., Shenolikar, S., 2009. From promiscuity to precision: protein phosphatases get a makeover. *Mol. Cell* 33, 537–45.
- Visagie, M.H., Joubert, A.M., 2011. 2-Methoxyestradiol-bis-sulfamate induces apoptosis and autophagy in a tumorigenic breast epithelial cell line. *Mol. Cell. Biochem.* 357, 343–52.
- Vogelstein, B., Kinzler, K.W., 2004. Cancer genes and the pathways they control. *Nat. Med.* 10, 789–799.
- Vorobiof, D.A., Sitas, F., Vorobiof, G., 2001. Breast cancer incidence in South Africa. *J. Clin. Oncol.* 19, 125S–127S.
- Vucic, D., Dixit, V.M., Wertz, I.E., 2011. Ubiquitylation in apoptosis: a post-translational

- modification at the edge of life and death. *Nat. Rev. Mol. Cell Biol.* 12, 439–452.
- Wang, W., Zhao, C., Jou, D., Lü, J., Zhang, C., Lin, L., Lin, J., 2013. Ursolic acid inhibits the growth of colon cancer-initiating cells by targeting STAT3. *Anticancer Res.* 33, 4279–84.
- Wang, X., Ye, X., Liu, R., Chen, H.-L., Bai, H., Liang, X., Zhang, X.-D., Wang, Z., Li, W., Hai, C.-X., 2010. Antioxidant activities of oleanolic acid in vitro: possible role of Nrf2 and MAP kinases. *Chem. Biol. Interact.* 184, 328–37.
- Wang, X., Zhang, F., Yang, L., Mei, Y., Long, H., Zhang, X., Zhang, J., Qimuge-Suyila, Su, X., 2011. Ursolic Acid Inhibits Proliferation and Induces Apoptosis of Cancer Cells In Vitro and In Vivo. *J. Biomed. Biotechnol.* 2011, 1–8.
- Wang, Z., Hsu, C., Huang, C., Yin, M., 2010. Anti-glycative effects of oleanolic acid and ursolic acid in kidney of diabetic mice. *Eur. J. Pharmacol.* 628, 255–60.
- Wangersky, P.J., 1993. Introduction to marine biogeochemistry. *Mar. Chem.* 42, 253–254.
- Watanabe, K., Pacher, M., Dukowic, S., Schubert, V., Puchta, H., Schubert, I., 2009. The STRUCTURAL MAINTENANCE OF CHROMOSOMES 5/6 Complex Promotes Sister Chromatid Alignment and Homologous Recombination after DNA Damage in *Arabidopsis thaliana*. *PLANT CELL ONLINE* 21, 2688–2699.
- Weinberg, R.A., 1995. The retinoblastoma protein and cell cycle control. *Cell* 81, 323–330.
- Weng, H., Tan, Z.-J., Hu, Y.-P., Shu, Y.-J., Bao, R.-F., Jiang, L., Wu, X.-S., Li, M.-L., Ding, Q., Wang, X.-A., Xiang, S.-S., Li, H.-F., Cao, Y., Tao, F., Liu, Y.-B., 2014. Ursolic acid induces cell cycle arrest and apoptosis of gallbladder carcinoma cells. *Cancer Cell Int.* 14, 96.
- Williams, G.H., Stoeber, K., 2012. The cell cycle and cancer. *J. Pathol.* 226, 352–364.
- Willis, N., Rhind, N., 2009. Mus81, Rhp51(Rad51), and Rqh1 form an epistatic pathway required for the S-phase DNA damage checkpoint. *Mol. Biol. Cell* 20, 819–33.
- Wójciak-Kosior, M., Paduch, R., Matysik-Woźniak, A., Niedziela, P., Donica, H., 2011. The effect of ursolic and oleanolic acids on human skin fibroblast cells. *Folia Histochem. Cytobiol.* 49, 664–9.
- Wu, W.-S., 2006. The signaling mechanism of ROS in tumor progression. *Cancer Metastasis Rev.* 25, 695–705.
- Xiao, B., Sanders, M.J., Underwood, E., Heath, R., Mayer, F. V., Carmena, D., Jing, C., Walker, P.A., Eccleston, J.F., Haire, L.F., Saiu, P., Howell, S.A., Aasland, R., Martin, S.R., Carling, D., Gamblin, S.J., 2011. Structure of mammalian AMPK and its regulation by ADP. *Nature* 472, 230–3.
- Xie, Z., Klionsky, D.J., 2007. Autophagosome formation: core machinery and adaptations. *Nat. Cell Biol.* 9, 1102–1109.
- Xue, Z., Duan, L., Liu, D., Guo, J., Ge, S., Dicks, J., ÓMáille, P., Osbourn, A., Qi, X., 2012. Divergent evolution of oxidosqualene cyclases in plants. *New Phytol.* 193, 1022–38.
- Yagata, H., Kajiura, Y., Yamauchi, H., 2011. Current strategy for triple-negative breast cancer: Appropriate combination of surgery, radiation, and chemotherapy. *Breast Cancer* 18, 165–173.
- Ye, X., Franco, A.A., Santos, H., Nelson, D.M., Kaufman, P.D., Adams, P.D., 2003.

- Defective S phase chromatin assembly causes DNA damage, activation of the S phase checkpoint, and S phase arrest. *Mol. Cell* 11, 341–351.
- Yin, M.-C., Chan, K.-C., 2007. Nonenzymatic antioxidative and antiglycative effects of oleanolic acid and ursolic acid. *J. Agric. Food Chem.* 55, 7177–81.
- Yuan, J., Kroemer, G., 2010. Alternative cell death mechanisms in development and beyond. *Genes Dev.* 24, 2592–2602.
- Yusuf, R., Frenkel, K., 2010. Morphologic transformation of human breast epithelial cells MCF-10A: dependence on an oxidative microenvironment and estrogen/epidermal growth factor receptors. *Cancer Cell Int.* 10, 30.
- Zhai, D., Jin, C., Huang, Z., Satterthwait, A.C., Reed, J.C., 2008. Differential regulation of Bax and Bak by anti-apoptotic Bcl-2 family proteins Bcl-B and Mcl-1. *J. Biol. Chem.* 283, 9580–9586.
- Zhang, G.-P., Lu, Y.-Y., Lv, J.-C., Ou, H.-J., 2006. Effect of ursolic acid on caspase-3 and PARP expression of human MCF-7 cells. *Zhongguo Zhong Yao Za Zhi* 31, 141–144.
- Zhong, Y., Wang, Q.J., Li, X., Yan, Y., Backer, J.M., Chait, B.T., Heintz, N., Yue, Z., 2009. Distinct regulation of autophagic activity by Atg14L and Rubicon associated with Beclin 1-phosphatidylinositol-3-kinase complex. *Nat. Cell Biol.* 11, 468–76.
- Zhou, F., Yang, Y., Xing, D., 2011. Bcl-2 and Bcl-xL play important roles in the crosstalk between autophagy and apoptosis. *FEBS J.* 278, 403–413.



6 Appendix I (WESTERN BLOT RECIPES)

<p>PBS 10X</p> <p>40 g NaCl 1 g KCl 13.4 g Na₂HPO₄-7H₂O 1.2 g H₂O</p> <p>Adjust the pH at 7.4 with HCl. Complete to 500 mL with distilled water.</p>	<p>Lysis Buffer</p> <p>580 µL Nonidet P40 0.58 g CHAPS 0.150 g HEPES 0.508 g NaCl 9.93 g Saccharose 0.022 g Na₂EDTA</p> <p>Adjust the pH to 8.0. Complete to 50 mL with distilled water.</p>
<p>Laemmli buffer samples 5X</p> <p>1 mL Glycerol 1 g SDS 10% 6.25 mL Tris HCl 0.5M pH 6.8 2.5 mL β-mercaptoethanol 1 mL Bromophenol 0.5%</p> <p>Complete to 10 mL with distilled water.</p>	<p>Acrylis bis 30%</p> <p>29.2 g Acrylamide (29.2%) 0.8 g N-N'-methylene-bisacrylamide (0.8%)</p> <p>Complete to 100 mL with distilled water.</p>
<p>SDS 10%</p> <p>100 g Sodium Dodecyl Sulfate 1000 mL distilled H₂O</p>	<p>APS 10%</p> <p>1 g Ammonium Persulfate 10 mL distilled H₂O</p> <p>Prepare it fresh.</p>
<p>Running Buffer 1.5 M, pH 8.8</p> <p>90.75 g Tris 500 mL distilled H₂O</p> <p>Adjust the pH at 8.8 with HCl.</p>	<p>Stacking Buffer 0.5 M, pH 6.8</p> <p>6 g Tris 100 mL distilled H₂O</p> <p>Adjust the pH at 6.8 with HCl.</p>

<p>TANK Buffer 10X</p> <p>15 g Tris 72 g Glycine 50 mL SDS 10% Heat for. Complete to 500 mL with distilled water.</p>	<p>TANK Buffer 1X</p> <p>100 mL Tank 10X 900 mL distilled H₂O</p>
<p>Transfer buffer 1X</p> <p>3.03 g Tris HCl 14.4 g Glycine 200 mL Methanol 1 mL SDS 10%</p> <p>Complete to 1 liter with distilled water.</p>	<p>TBS 10X</p> <p>24.2 g Tris 84 g NaCl</p> <p>Adjust the pH to 7.6 with HCl. Complete to 1 liter with distilled water.</p>
<p>T-TBS 1X</p> <p>To 1 liter of TBS 1X, add 1 mL of Tween 20.</p>	<p>Blocking Buffer</p> <p>To 10 mL of T-TBS 1X, add 0.5 g of non-fat dry milk.</p>
<p>Coomassie blue R-250 0.5%</p> <p>0.5 g Coomassie blue R-250 (Biorad, 161-0400) 40 mL Methanol 10 mL Acetic acid</p> <p>Complete to 100 mL with distilled water. Shaking with magnet for some hours. It is possible to recuperate the dye for 3-4 gels.</p>	<p>Decoloration solution</p> <p>25 mL Methanol 50 mL Glacial acetic acid</p> <p>Complete to 1 liter with distilled water.</p>
<p>Stripping Buffer</p> <p>10 mL β-mercaptoethanol 200 mL SDS 10% 137 mL Tris-HCl 0.5 M, pH 6.8 Complete to 1 liter with distilled water.</p>	

7 Appendix II (QPCR)

Table1: Nanodrop measurements of MCF10 samples. The samples highlighted in red failed the QC requirements. This is indicated by A_{260}/A_{230} ratios less than 1.5, which indicates poor RNA purity.

Sample ID	Concentration	A260	A280	260/280	260/230
10UA_1	29.88	0.747	0.382	1.96	2.58
10UA_2	38.6	0.965	0.437	2.21	1.9
10UA_3	90.14	2.253	1.164	1.94	2.73
100A_1	88.8	2.22	1.16	1.91	2.37
100A_2	55.86	1.396	0.755	1.85	2.31
100A_3	65.62	1.64	0.822	2	2.29
20UA_1	39.64	0.991	0.494	2.01	2.59
20UA_2	100.54	2.513	1.286	1.95	2.48
20UA_3	21.02	0.526	0.257	2.05	2.44
200A_1	23.91	0.598	0.299	2	1.79
200A_2	52.89	1.322	0.649	2.04	2.17
200A_3	47.41	1.185	0.604	1.96	1.96
500A_1	33.38	0.835	0.429	1.95	2.18
500A_2	20.56	0.514	0.271	1.9	1.03
500A_3	19.72	0.493	0.245	2.01	1.72
50UA_1	39.61	0.99	0.512	1.93	1.92
50UA_2	56.23	1.406	0.736	1.91	2.13
50UA_3	22.86	0.571	0.3	1.9	1.61
100UA_1	39.85	0.996	0.586	1.7	1.09
100UA_2	8.49	0.212	0.186	1.14	0.32
100UA_3	14.86	0.371	0.257	1.44	0.67
1000A_1	21.99	0.55	0.362	1.52	0.64
1000A_2	29.52	0.738	0.455	1.62	0.84
1000A_3	12.02	0.301	0.214	1.4	0.66
Control1	42.96	1.074	0.555	1.94	2.3
Control2	49.01	1.225	0.655	1.87	2.22
Control3	61.63	1.541	0.794	1.94	2.01
Control4	15.01	0.375	0.218	1.72	1.49
Control5	11.92	0.298	0.152	1.97	1.51
Control6	15.28	0.382	0.197	1.94	2.42

Table2: Nanodrop measurements of MCF7samples.

Sample ID	Concentration (ng/ μ l)	A260	A280	260/280	260/230
100A_1	1629.91	40.748	20.269	2.01	2
100A_2	1256.56	31.414	15.811	1.99	2.18
100A_3	768.52	19.213	9.477	2.03	1.5
10UA_1	351.64	8.791	4.643	1.89	2.12
10UA_2	452.02	11.301	5.881	1.92	1.76
10UA_3	500.39	12.51	6.337	1.97	2.27
20UA_1	210.96	5.274	2.772	1.9	1.82
20UA_2	200.83	5.021	2.528	1.99	2.43
20UA_3	175.05	4.376	2.28	1.92	2
200A_1	443.71	11.093	5.8	1.91	1.82
200A_2	1367.76	34.194	16.765	2.04	2.39
200A_3	964.72	24.118	12.054	2	2.2
50UA_1	1342.31	33.558	16.868	1.99	2.21
50UA_2	292.26	7.306	3.804	1.92	2.19
50UA_3	291.85	7.296	3.682	1.98	2.4
500A_1	683	17.075	8.53	2	2.1
500A_2	234.88	5.872	3.096	1.9	2.04
500A_3	857.53	21.438	10.62	2.02	1.58
100UA_1	599.61	14.99	6.916	2.17	1.96
100UA_2	291.11	7.278	3.353	2.17	1.74
100UA_3	126.62	3.166	1.594	1.99	2.28
1000A_1	376.39	9.41	4.839	1.94	2.4
1000A_2	104.01	2.6	1.254	2.07	1.03
1000A_3	124.2	3.105	1.599	1.94	2.32
ControlOA_1	1016.12	25.403	12.773	1.99	2.33
ControlOA_2	1126.03	28.151	13.634	2.06	2.46
ControlOA_3	972.46	24.312	11.871	2.05	2.38
ControlUA_1	314.65	7.866	4.002	1.97	2.17
ControlUA_2	324.55	8.114	4.309	1.88	1.76
ControlUA_3	381.1	9.527	5.014	1.9	2.18

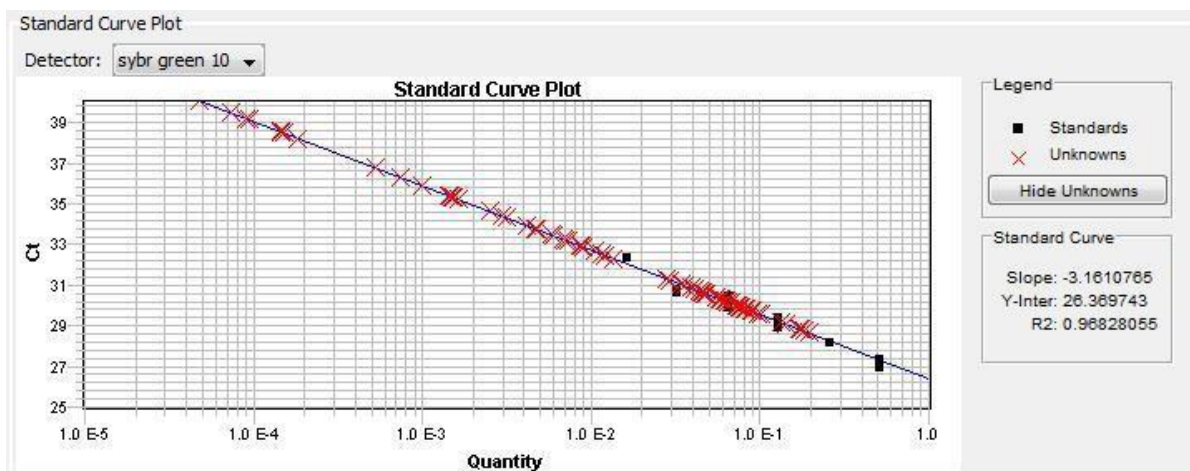


Figure 1: Standard curve of ATG6 in MCF7 samples

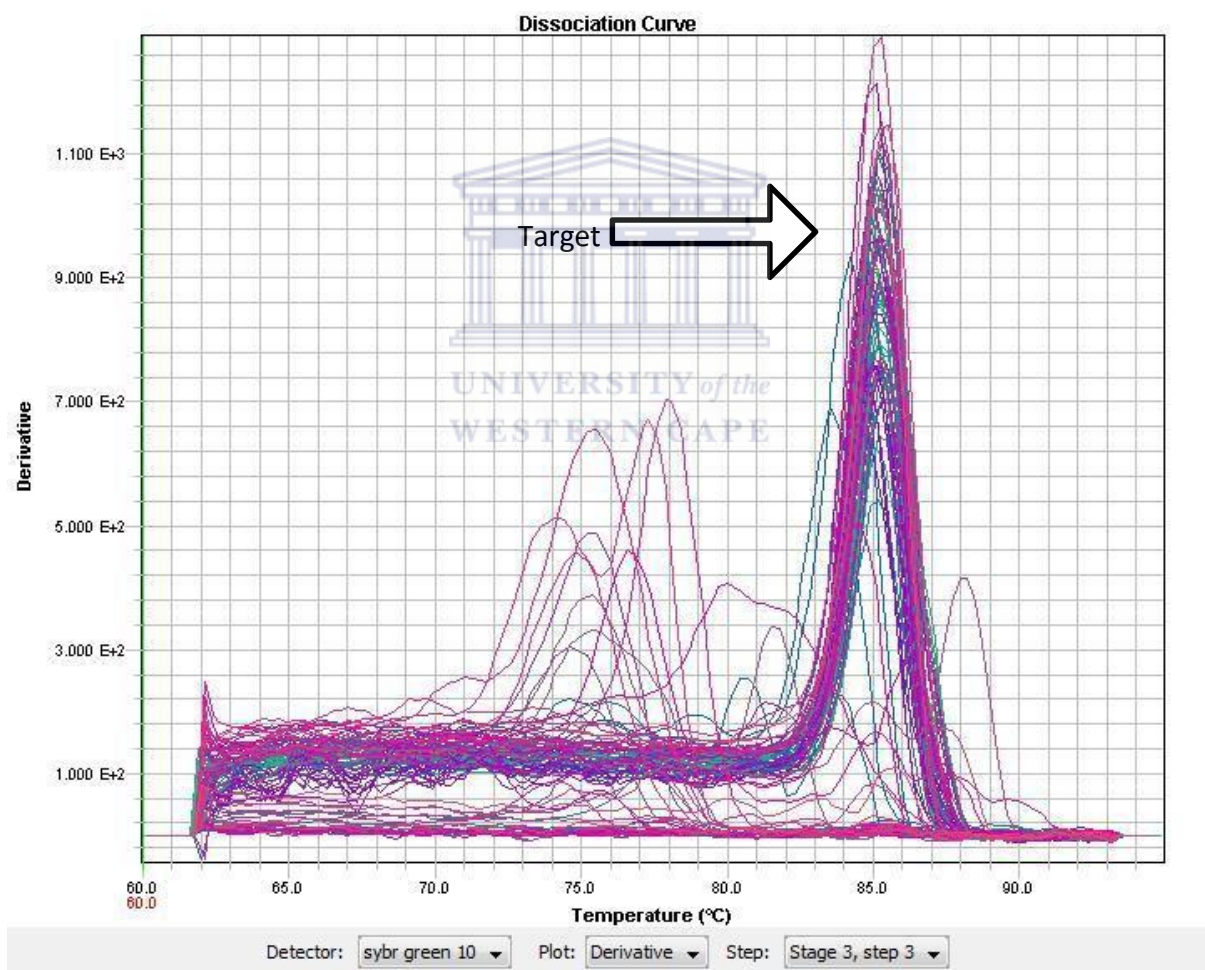


Figure2: Disassociation curve of ATG6 in MCF7 samples

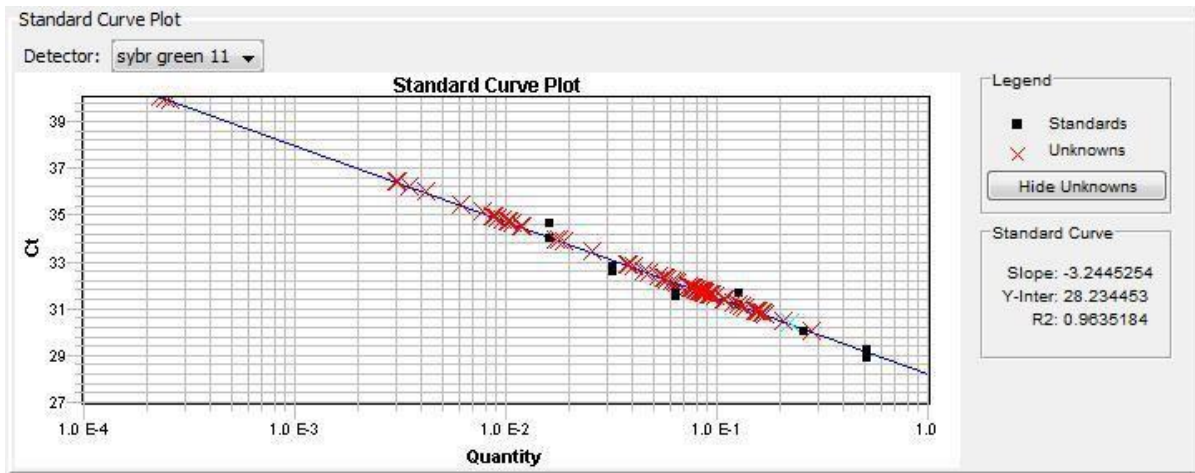


Figure3: Standard curve of *ATG6* in MCF10 samples

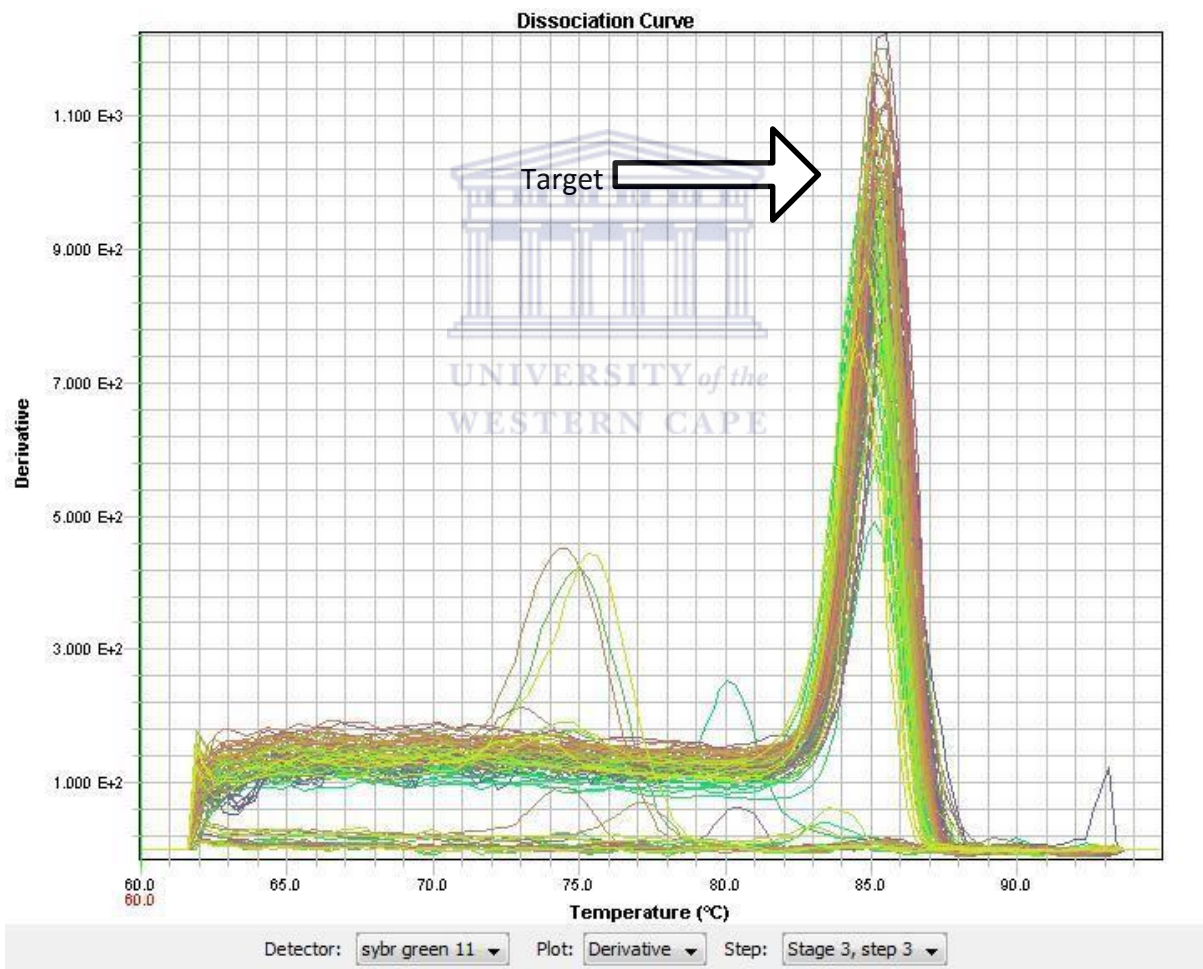


Figure 4: Disassociation curve of *ATG6* in MCF10 samples

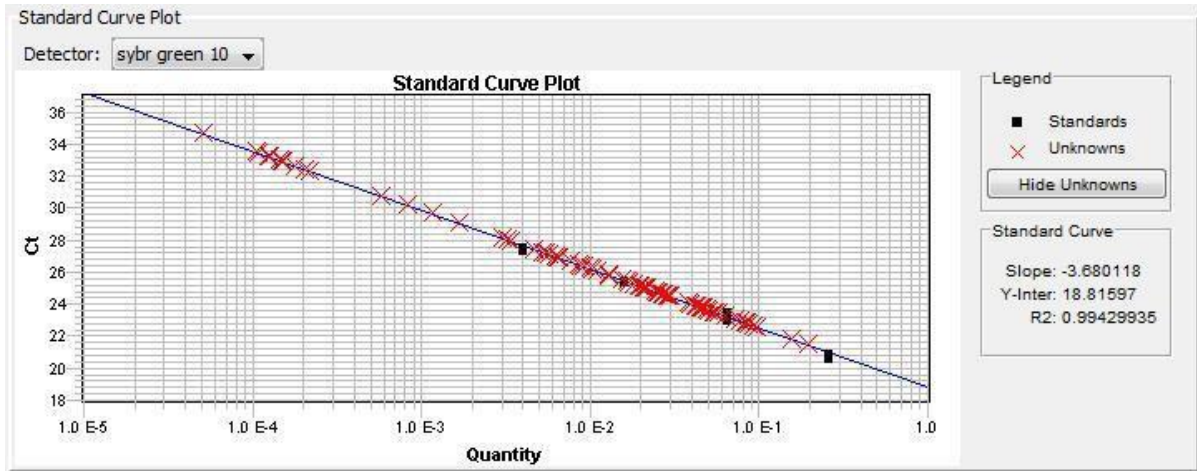


Figure 5: Standard curve of *GAPDH* in MCF7 samples

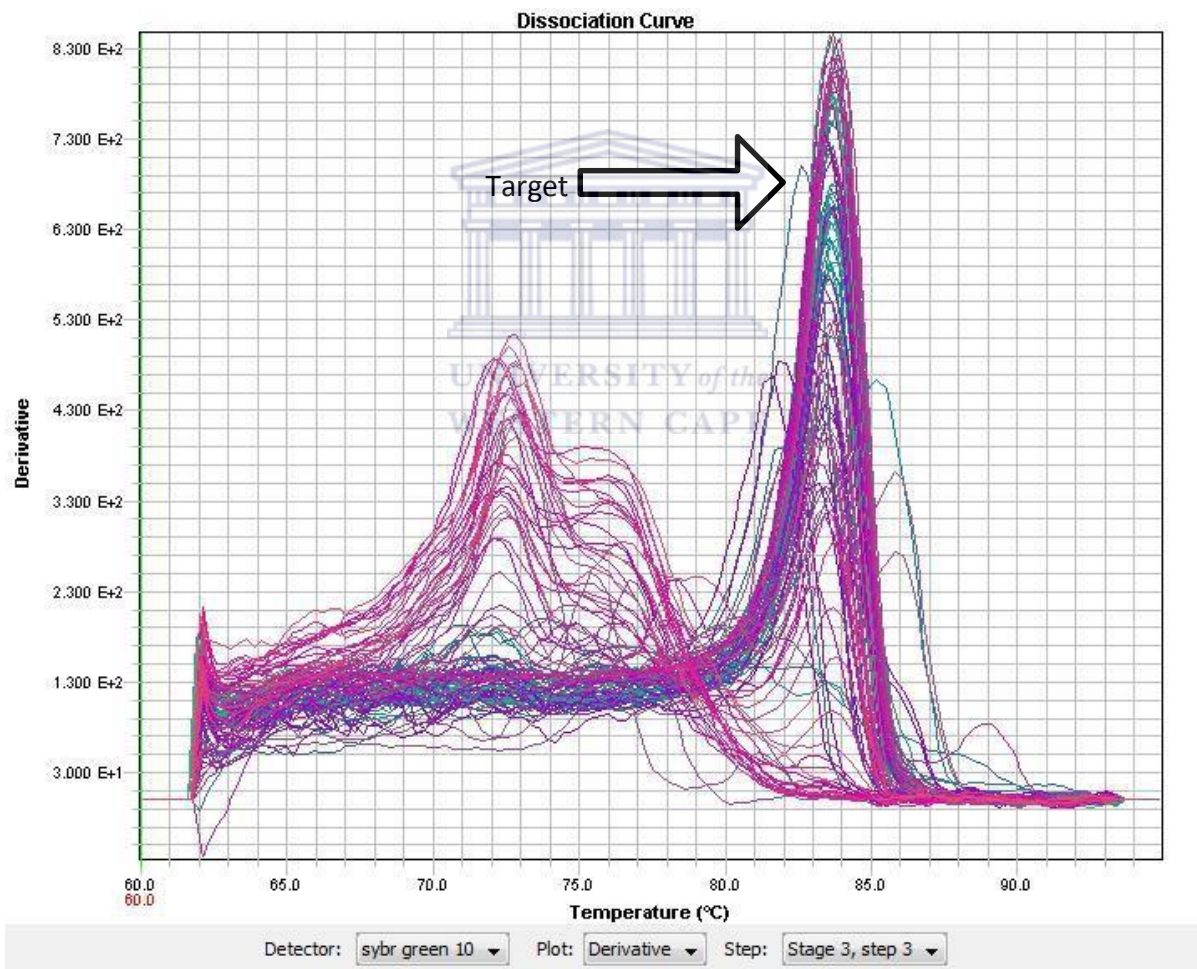


Figure 6: Disassociation curve of *GAPDH* in MCF7 samples

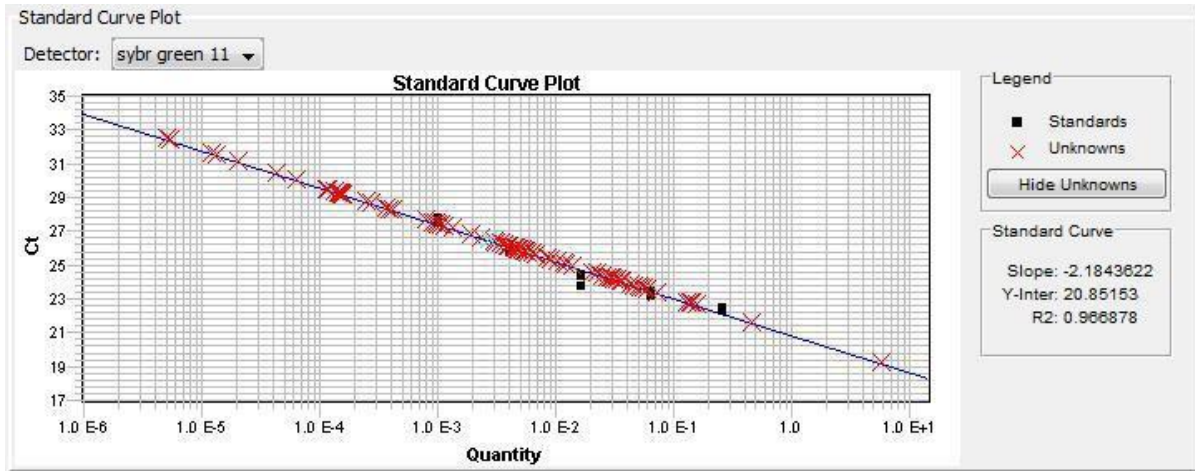


Figure 7: Standard curve of *GAPDH* in MCF10 samples

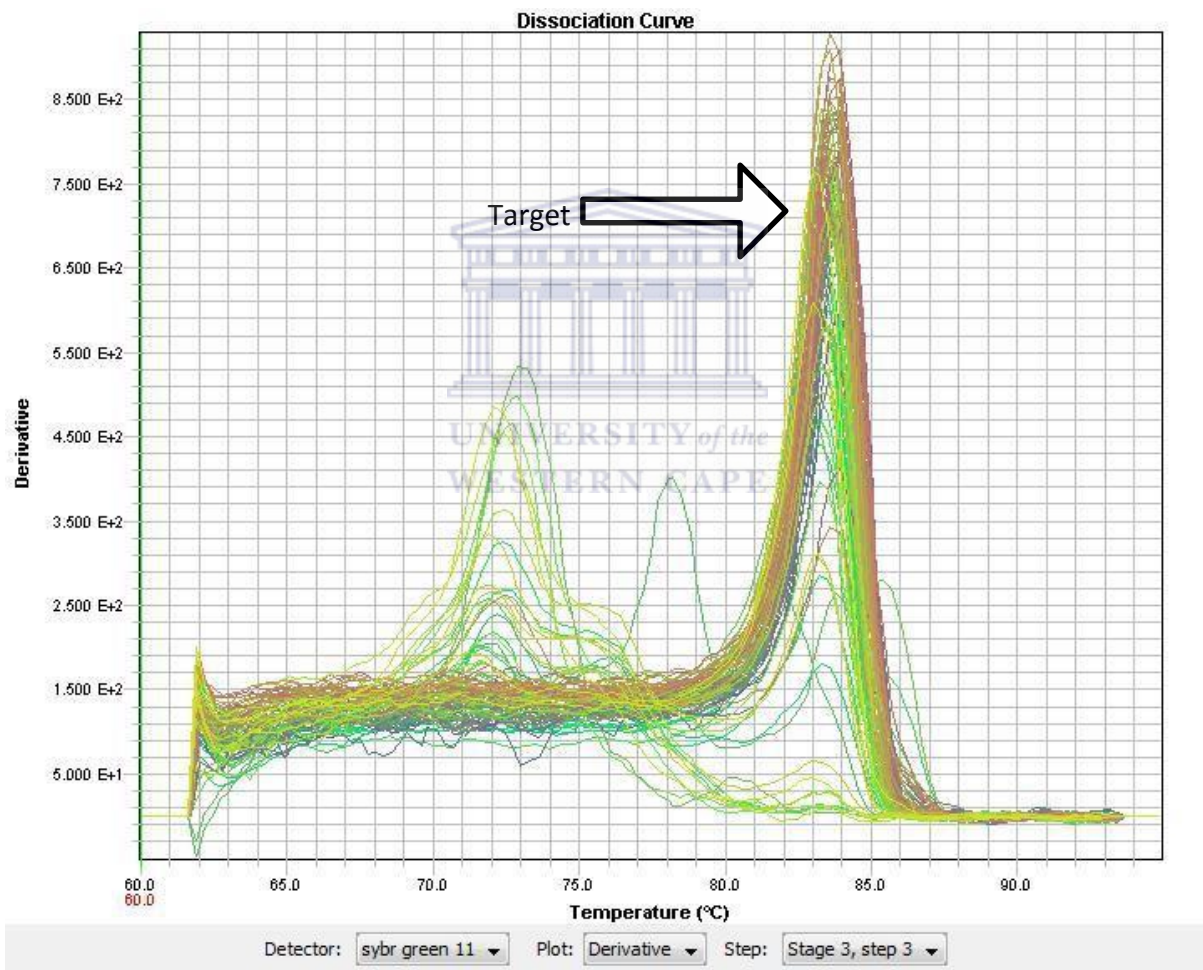


Figure 8: Disassociation curve of *GAPDH* in MCF10 samples

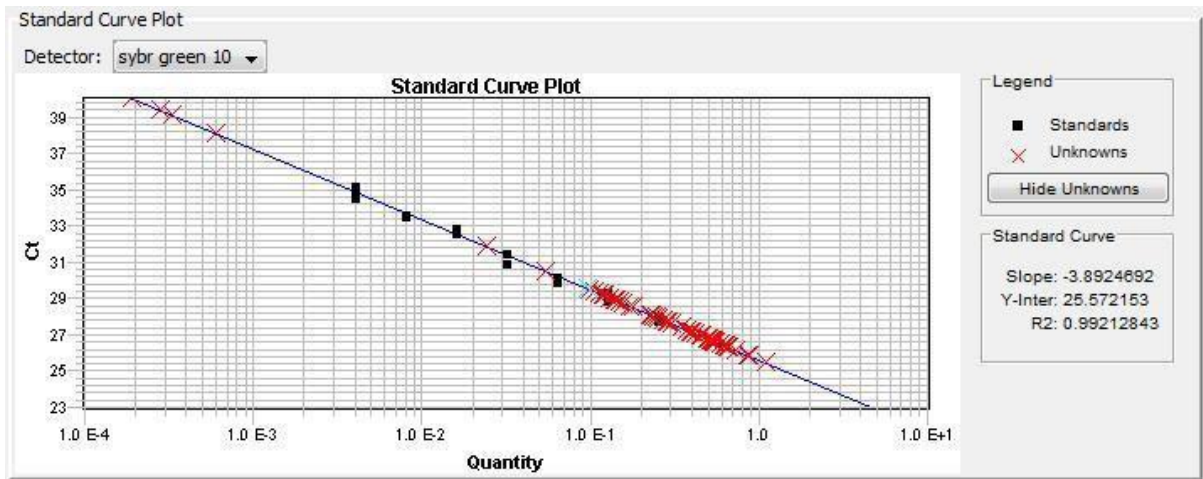


Figure 9: Standard curve *RAB7A* in MCF7

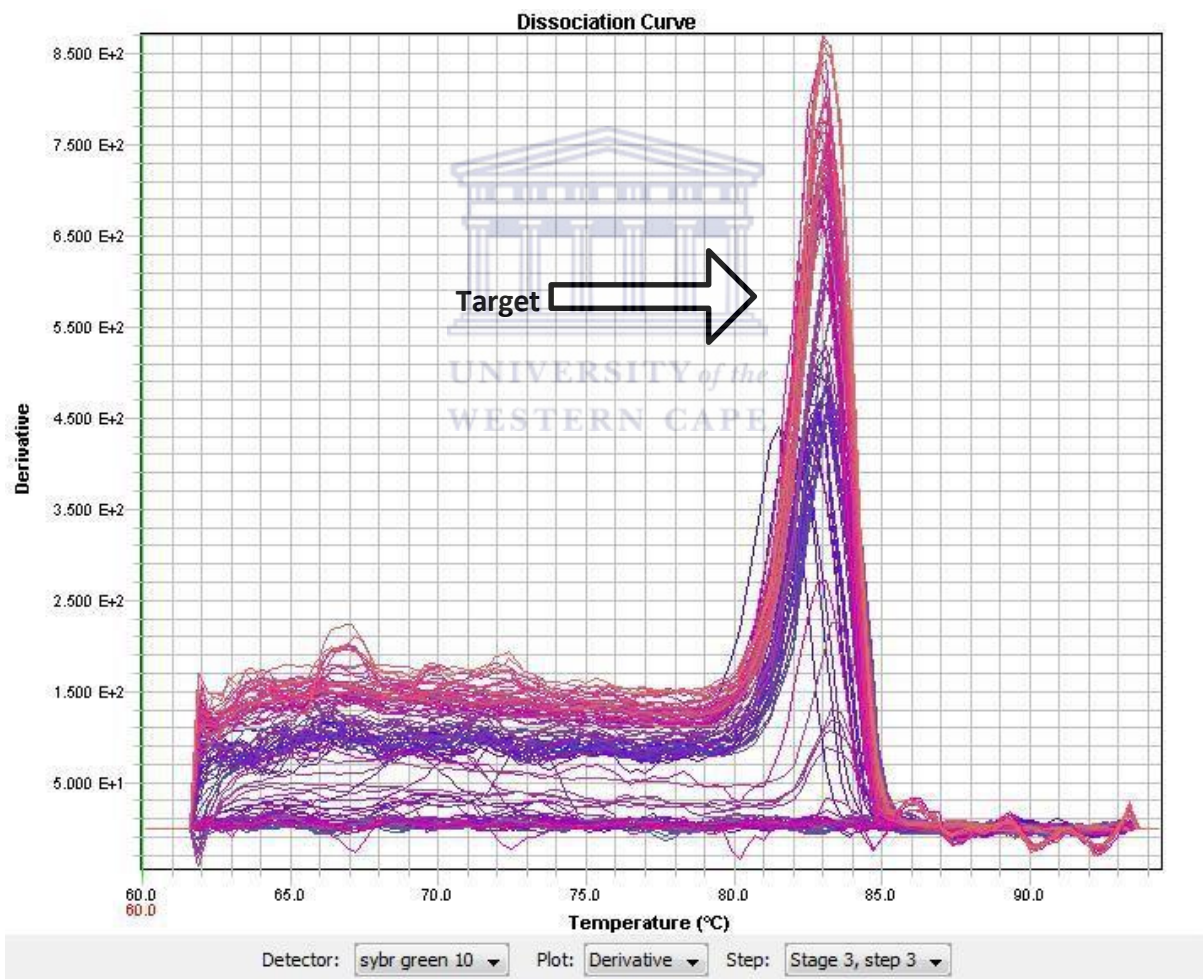


Figure 10: Disassociation curve of *RAB7A* in MCF7 samples

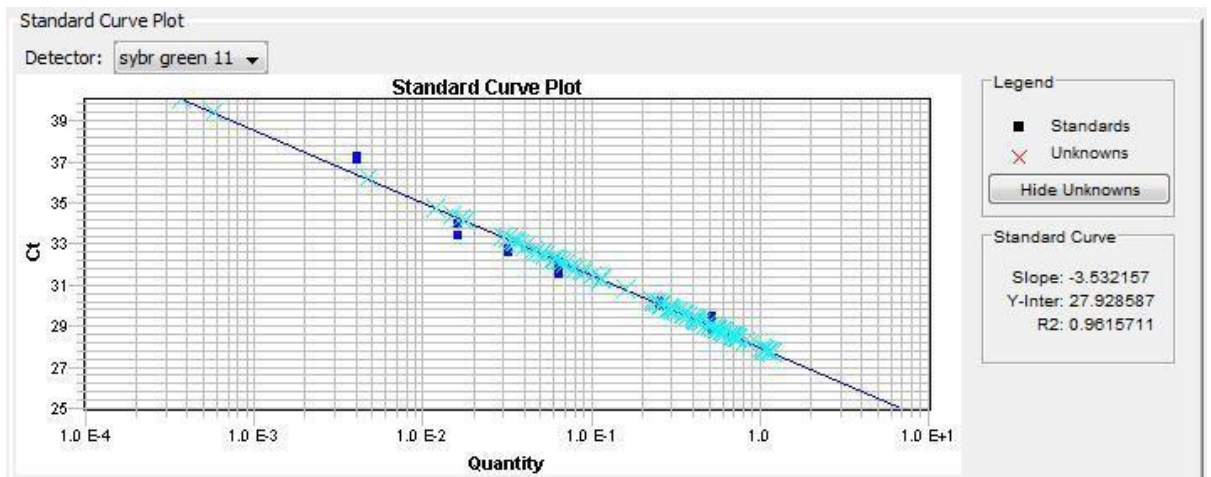


Figure 11: Standard curve of *RAB7A* in MCF10 samples

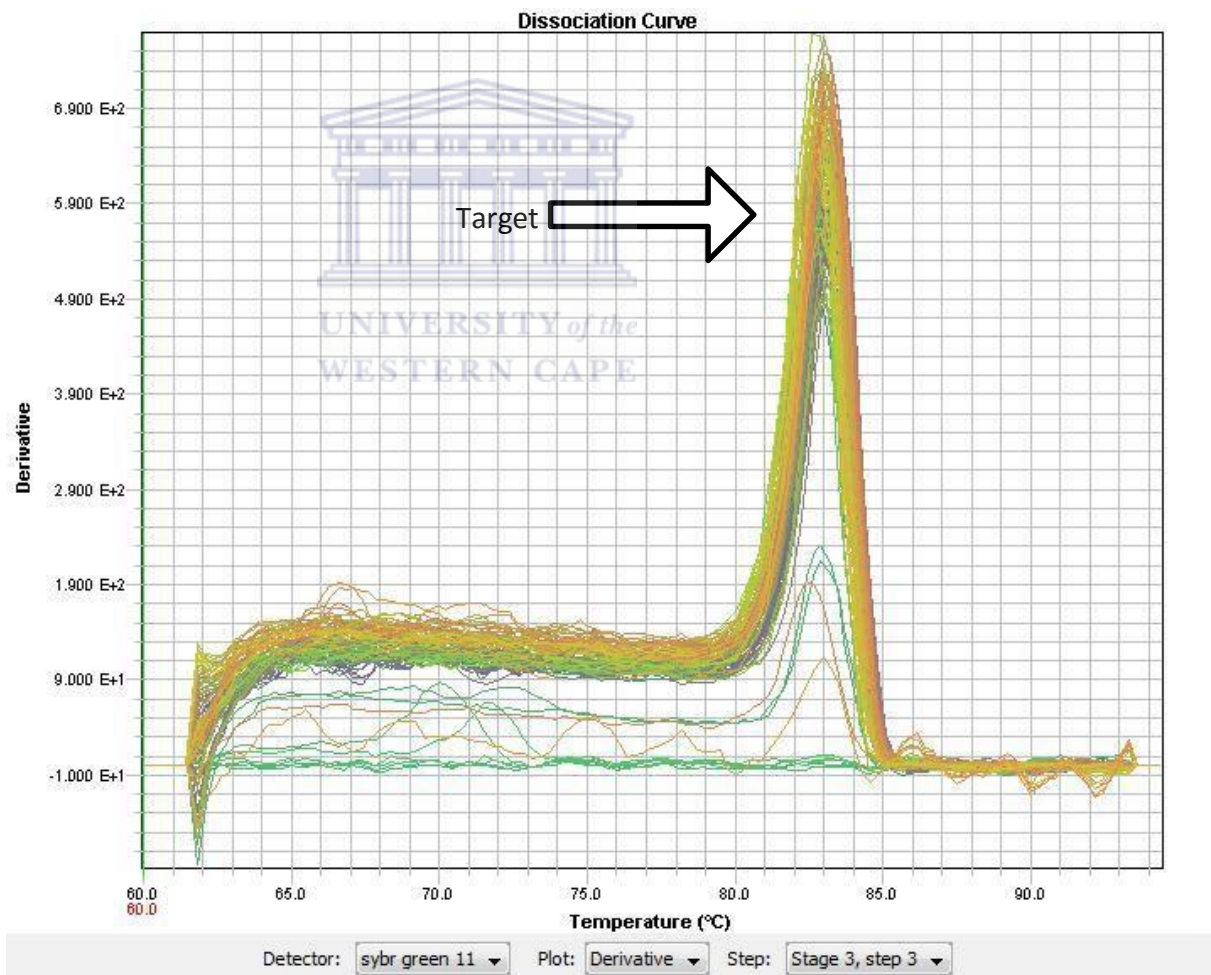


Figure 12: Disassociation curve of *RAB7A* in MCF10 samples